



Durham E-Theses

Novel P-alkene and pincer-type POCOP ligands: synthesis, coordination chemistry, and reactivity

TUXWORTH, LUKE, WILLIAM

How to cite:

TUXWORTH, LUKE, WILLIAM (2014) *Novel P-alkene and pincer-type POCOP ligands: synthesis, coordination chemistry, and reactivity*, Durham theses, Durham University. Available at Durham E-Theses Online: <http://etheses.dur.ac.uk/10582/>

Use policy

The full-text may be used and/or reproduced, and given to third parties in any format or medium, without prior permission or charge, for personal research or study, educational, or not-for-profit purposes provided that:

- a full bibliographic reference is made to the original source
- a [link](#) is made to the metadata record in Durham E-Theses
- the full-text is not changed in any way

The full-text must not be sold in any format or medium without the formal permission of the copyright holders.

Please consult the [full Durham E-Theses policy](#) for further details.

**Novel P-alkene and pincer-type POCOP ligands:
synthesis, coordination chemistry, and reactivity**

**Thesis submitted for the Degree of
Doctor of Philosophy**

By

Luke William Tuxworth, MChem (Dunelm)

**Work undertaken in the Department of Chemistry
at
Durham University**

January 2014

Statement

This thesis is based on work conducted by the author, in the Department of Chemistry at Durham University, during the period October 2010 to December 2013.

All the work described in this thesis is original, unless otherwise acknowledged in the text or in the references. None of this work has been submitted for another degree in this or any other University.

Signed: _____

Date: _____

Luke William Tuxworth

Abstract

Title: Novel P-alkene and pincer-type POCOP ligands: synthesis, coordination chemistry, and reactivity

This thesis describes the development of a range of polydentate phosphorus-containing ligands relevant to catalysis. The focus is on developing a fundamental understanding of how changes to the substituents on a ligand impact on the environment at a coordinated metal centre.

Chapter 2 reports the synthesis and coordination chemistry of the phosphine-alkene ligands *N*-R₂P-7-aza-benzobicyclo[2.2.1]hept-2-ene, R = Ph (**2-1**) and ^tPr (**2-2**). The electronic properties of **2-1** and **2-2** are probed by a variety of methods, which reveals them to be electron deficient. The coordination chemistry of **2-1** to various transition metal fragments is then explored, exhibiting a range of coordination geometries including tetrahedral ([Ni(κ²-P,C-**2-1**)₂] (**2-6**)), square based pyramidal ([RhCl(κ²-P,C-**2-1**)₂] (**2-7**)) and trigonal bipyramidal ([IrCl(κ²-P,C-**2-1**)₂] (**2-8**)).

Chapter 3 introduces the problem of slow reductive elimination in some palladium-catalysed catalytic transformations along with methods of promoting this process, before describing the application of the electron deficient **2-1** in enhancing reductive elimination reactions. A detailed study of the formation of ethane by reductive elimination from a palladium dimethyl complex of phosphine-alkene ligand **2-1** has been undertaken. The mechanism of this process has been probed by a combination of experimental and computational studies and revealed that the mechanism proceeded *via* an associative mechanism through a 5-coordinate intermediate.

Chapter 4 describes the synthesis and systematic study of the steric and electronic impact of a range of POCOP pincer ligands 1,3-{{^tBu₂PO}₂C₆H₄} (**4-1**) and 1,3-{{(R₂PO)₂C₁₄H₂₀}}, R = ^tBu (**4-7**), ⁱPr (**4-8**), NEt₂ (**4-9**), morpholine (**4-10**) and pyrrole (**4-12**). The coordination chemistry of these ligands is then appraised to probe the steric impact of the ligand crystallographically. Subsequently, the electronic impact of the ligands are assessed by ³¹P{¹H} NMR and infrared spectroscopy of the corresponding phosphine selenide compounds and palladium carbonyl complexes.

Chapter 5 reports exploratory reactions of a novel palladium hydride complex [PdH(κ³-P,C,P-**4-1**)] (**5-1**). The insertion of C=C (ethylene) and C=O (acetone, CO₂) bonds into the Pd-H bond of **5-1** is attempted, notably showing facile insertion of CO₂ to form the metal formate complex [Pd(OC(H)O)(κ³-P,C,P-**4-1**)] (**5-4**). Complex **5-1** is shown to be a catalyst for palladium-catalysed alkene isomerisation and aldehyde hydrosilylation, but the activity in both reactions is low.

Acknowledgements

First of all I would like to thank my supervisor Dr Philip Dyer for his guidance throughout this project, once again it really is appreciated!

I also extend my gratitude to Prof. Paul Low, Dr Alan Kenwright, and Dr Keith Dillon for their advice over the years. Dr Karinne Miqueu, Dr Jean-Marc Sotiropoulos, and Dr Laura Estevez (Université de Pau) and Dr Mark Fox (Durham) are thanked for their computational calculations. Dr Andrei Batsanov is thanked for X-ray crystallography.

I must also acknowledge the outstanding work done by the following analytical services in Durham: solution-state NMR spectroscopy, solid-state NMR spectroscopy, mass spectrometry, and elemental analysis, without who this thesis would not have been possible.

I express thanks to all the fantastic technical staff (glass blowers, electrical workshop, mechanical workshop, waste and solvent stores, and general stores) for keeping me supplied with equipment.

Durham University are thanked for funding (Durham doctoral studentship).

I express gratitude to all those who have worked in lab 101 past and present, it has been a pleasure to work with you all.

Finally, all my friends and family are thanked for their support.

Contents

CHAPTER 1: GENERAL INTRODUCTION	13
1.1 Phosphorus-based ligands	13
1.1.1 The bonding of phosphine ligands to metal centres	13
1.1.2 Quantifying the steric impact of phosphine ligands	15
1.1.3 Quantifying the electronic impact of phosphine ligands	18
1.2 Aminophosphine ligands, $(R_2N)_xPR^{i}_{3-x}$	20
1.3 Binding of alkene ligands to metal centres	22
1.4 Aims and objectives	24
1.5 References	26
2 SYNTHESIS AND COORDINATION CHEMISTRY OF NOVEL PHOSPHINE-ALKENE LIGANDS	28
2.1 Introduction	28
2.1.1 P-alkene ligands	28
2.1.2 Synthesis and structure of P-alkene ligands	29
2.1.2.1 TROPP-type P-alkene ligands	29
2.1.2.2 5 <i>H</i> -dibenz[<i>b,f</i>]azepine-type P-alkene ligands	30
2.1.2.3 Norbornene-type P-alkene ligands	31
2.1.2.4 Vinyl-type P-alkene ligands	32
2.1.3 Recent developments in the application of P-alkene ligands in catalysis	32
2.2 Synthesis and coordination chemistry of <i>N</i>-R_2P-7-aza-benzobicyclo[2.2.1]hept-2-ene, $R = Ph, ^iPr$	37
2.2.1 Key features of <i>N</i> - R_2 P-7-aza-benzobicyclo[2.2.1]hept-2-ene as a ligand	38
2.2.2 Synthesis of diphenylphosphino- and diisopropylphosphino-substituted P-alkene ligands (2-1 and 2-2)	39
2.2.3 Assessment of the electronic character of P-alkene ligands 2-1 and 2-2	41
2.2.3.1 Synthesis of phosphine selenides 2-1.Se and 2-2.Se	41
2.2.3.2 Synthesis of a rhodium carbonyl complex of 2-1	42
2.2.3.3 Synthesis of chromium carbonyl complexes $[Cr(CO)_4(\kappa^2\text{-P,C-2-1})]$ (2-4) and $[Cr(CO)_4(\kappa^2\text{-P,C-2-2})]$ (2-5)	42
2.2.3.3.1 X-Ray crystallographic study of $[Cr(CO)_4(\kappa^2\text{-P,C-2-1})]$ (2-4)	44
2.2.4 Synthesis of $[Ni(\kappa^2\text{-P,C-2-1})_2]$ (2-6)	45
2.2.4.1 X-Ray crystallographic study of $[Ni(\kappa^2\text{-P,C-2-1})_2]$ (2-6)	47
2.2.4.2 Stability and reactivity of $[Ni(\kappa^2\text{-P,C-2-1})_2]$ (2-6)	48
2.2.5 Coordination chemistry of 2-1 with rhodium and iridium metal fragments	49

2.2.5.1	X-Ray crystallographic study of $[\text{RhCl}(\kappa^2\text{-P,C-2-1})_2]$ (2-7)	50
2.2.5.2	X-Ray crystallographic study of $[\text{IrCl}(\kappa^2\text{-P,C-2-1})_2]$ (2-8)	50
2.3	Synthesis and coordination chemistry of a potentially tridentate P-dialkene ligand, <i>N</i>-PPh-<i>bis</i>-7-<i>aza</i>-benzobicyclo[2.2.1]hept-2-ene (2-9)	52
2.1.1.	Coordination chemistry of <i>N</i> -PPh- <i>bis</i> -7- <i>aza</i> -benzobicyclo[2.2.1]hept-2-ene (2-9) with a chromium carbonyl metal fragment	53
2.3.1.1	X-Ray crystallographic study of $[\text{Cr}(\text{CO})_4(\kappa^2\text{-P,C-2-9})]$ (2-10)	55
2.4	Chapter 2 summary and conclusions	56
2.5	References	57
3	PHOSPHINE-ALKENE LIGANDS: PROMOTION OF REDUCTIVE ELIMINATION FROM PALLADIUM(II) COMPLEXES	61
3.1	Introduction	61
3.1.1	Promotion of reductive elimination from 4-coordinate square-planar complexes	62
3.1.1.1	The impact of the steric bulk of the ancillary ligands on the rates of reductive elimination in 4-coordinate square planar complexes	62
3.1.1.2	The impact of the electronic properties of the ancillary ligands on the rates of reductive elimination in 4-coordinate square planar complexes	64
3.1.1.3	The impact of the addition of an alkene co-ligand on the rates of reductive elimination in 4-coordinate square planar complexes	64
3.1.1.3.1	The proposed associative mechanism of reductive elimination from 4-coordinate square planar complexes upon addition of alkenes	67
3.1.2	Using P-alkene ligands to promote reductive elimination in palladium-catalysed reactions	68
3.1.2.1	Palladium-catalysed $\text{C}_{\text{sp}}\text{-C}_{\text{sp}}$ cross-coupling	69
3.1.2.2	Palladium-catalysed Negishi cross-coupling	71
3.2	Using ligand 2-1 to promote reductive elimination of ethane from Pd(II) dimethyl complexes	73
3.2.1	Coordination of P-alkene ligand 2-1 to a PdMe_2 fragment	74
3.2.1.1	X-Ray crystallographic study of <i>cis</i> - $[\text{PdMe}_2(\kappa^2\text{-P,C-2-1})]$ (3-1)	76
3.2.2	Reaction of two equivalents of P-alkene ligand 2-1 with a PdMe_2 fragment	77
3.2.2.1	X-Ray crystallographic study of $[\text{Pd}(\kappa^2\text{-P,C-2-1})_2]$ (3-2).	78
3.2.3	Investigating the mechanism of ethane reductive elimination promoted by P-alkene ligand 2-1	79
3.2.3.1	Accelerated ethane reductive elimination from <i>cis</i> - $[\text{PdMe}_2(\kappa^2\text{-P,C-2-1})]$ (3-1) by the addition of PPh_3 or propene	79
3.2.3.2	Attempts to trap the proposed 5-coordinate intermediate: variable temperature NMR studies	80

3.2.3.3	Theoretical investigation of the interaction of P-alkene ligand 2-1 with <i>cis</i> -[PdMe ₂ (κ ² -P,C- 2-1)] (3-1)	82
3.3	Stability and reactivity of complex [Pd(κ²-P,C-2-1)₂] (3-2)	85
3.3.1	Utilising P-alkene ligand 2-1 in palladium-catalysed reactions	87
3.3.1.1	Suzuki-Miyaura cross-coupling	87
3.3.1.2	Negishi cross-coupling	89
3.4	Coordination chemistry of P-alkene 2-1 with a PdCl(Me) fragment	90
3.4.1	Investigating the mechanism of the reaction between P-alkene 2-1 and [PdCl(Me)(COD)]	92
3.5	Synthesis and coordination chemistry of <i>N</i>-PPh₂-3-pyrroline – a less rigid and bulky analogue of P-alkene 2-1	96
3.5.1	Synthesis of <i>N</i> -PPh ₂ - 3 -pyrroline (3-4)	97
3.5.2	Synthesis of <i>N</i> -PPh ₂ -pyrrolidine (3-5)	98
3.5.3	Exploring the coordination chemistry of monocyclic P-alkene 3-4 with PdMe ₂ fragments	99
3.5.3.1	Ethane elimination from complex [PdMe ₂ (κ ¹ -P- 3-4) ₂] (3-6)	101
3.5.3.1.1	X-Ray crystallographic study of [Pd(κ ¹ -P- 3-4) ₃] (3-7)	103
3.5.3.1.2	Investigating the mechanism of ethane reductive elimination from [PdMe ₂ (κ ¹ -P- 3-4) ₂] (3-6)	103
3.5.4	Synthesis of [Pd(κ ¹ -P- 3-4) ₄] (3-8)	106
3.5.5	Coordination chemistry of P-alkene 3-4 and P-alkane 3-5 with PdCl(Me) fragment	106
3.5.5.1	X-Ray crystallographic study of <i>trans</i> -[PdCl(Me)(κ ¹ -P- 3-4) ₂] (3-9) and <i>trans</i> -[PdCl(Me)(κ ¹ -P- 3-5) ₂] (3-10)	109
3.6	Chapter 3 summary and conclusions	111
3.7	Future work	112
3.8	References	113
4	CHAPTER 4: SYNTHESIS AND COORDINATION CHEMISTRY OF NOVEL POCOP Pincer Ligands	115
4.1	Introduction	115
4.1.1	Pincer ligand nomenclature	116
4.1.2	Synthesis of POCOP ligands	117
4.1.3	Application of POCOP pincer ligands in catalysis	119
4.2	Synthesis of [PdCl(κ³-P,C,P-4-1)] (4-2)	123
4.2.1	X-Ray crystallographic study of [PdCl(κ ³ -P,C,P- 4-1)] (4-2)	125

4.3 Synthesis of POCOP pincer compounds and the assessment of their electronic and steric properties	126
4.3.1 Development of a new synthetic route to POCOP pincer ligands	127
4.3.1.1 Synthesis of 1,3- $\{(\text{Cl}_2\text{PO})_2\text{C}_6\text{H}_4\}$ (4-3)	128
4.3.1.1.1 <i>In situ</i> synthesis of 1,3- $\{(\text{Cl}_2\text{PO})_2\text{C}_6\text{H}_4\}$ (4-3) via 1,3- $\{(\text{iPr}_2\text{N})_2\text{PO}\}_2\text{C}_6\text{H}_4\}$ (4-4)	130
4.3.1.1.2 Synthesis of 1,3- $\{(\text{Cl}_2\text{PO})_2\text{C}_6\text{H}_4\}$ (4-3) from 1,3- $\{(\text{iPr}_2\text{N})_2\text{PO}\}_2\text{C}_6\text{H}_4\}$ (4-4)	131
4.3.1.2 Synthesis of 1,3- $\{(\text{iPrO})_2\text{PO}\}_2\text{C}_6\text{H}_4\}$ (4-5)	132
4.3.2 Synthesis of a range of novel POCOP pincer compounds	133
4.3.2.1 Synthesis of 1,3- $\{(\text{tBu}_2\text{PO})_2\text{C}_{14}\text{H}_{20}\}$ (4-7)	134
4.3.2.2 Synthesis of 1,3- $\{(\text{R}_2\text{PO})_2\text{C}_{14}\text{H}_{20}\}$, R = O ⁱ Pr (4-8), NEt ₂ (4-9), and morpholine (4-10)	135
4.3.2.3 Attempted synthesis of 1,3- $\{(\text{R}_2\text{PO})_2\text{C}_{14}\text{H}_{20}\}$, R = N ⁱ Pr ₂	136
4.3.2.3.1 Further attempts to synthesise 1,3- $\{(\text{R}_2\text{PO})_2\text{C}_{14}\text{H}_{20}\}$, R = N ⁱ Pr ₂	137
4.3.2.4 Synthesis of 1,3- $\{(\text{R}_2\text{PO})_2\text{C}_{14}\text{H}_{20}\}$, R = pyrrole, (4-12)	139
4.3.3 Quantification of the electronic and steric properties of POCOP ligands 4-1 , 4-7 to 4-10 , and 4-12	139
4.3.3.1 Synthesis of palladium chloride complexes [PdCl(κ^3 -P,C,P-L)], L = 4-7 to 4-10 , and 4-12	140
4.3.3.1.1 X-Ray crystallographic study of complexes [PdCl(κ^3 -P,C,P-L)], L = 4-7 to 4-10 , and 4-12	141
4.3.3.2 Assessment of the steric properties of POCOP ligands	143
4.3.3.3 Assessment of the electronic properties of POCOP ligands	145
4.4 Chapter 4 summary and conclusions	150
4.5 Future work	151
4.6 References	152
5 CHAPTER 5: EXPLORATORY REACTIONS INTO A NOVEL PALLADIUM HYDRIDE COMPLEX	155
5.1 Introduction	155
5.2 Synthesis of [PdH(κ^3-P,C,P-4-1)] (5-1)	156
5.2.1 Reactivity of the palladium hydride complex [PdH(κ^3 -P,C,P-4-1)] (5-1)	156
5.2.1.1 Attempted reaction of ethylene with [PdH(κ^3 -P,C,P-4-1)] (5-1)	157
5.2.1.1.1 Synthesis of [PdMe(κ^3 -P,C,P-4-1)] (5-2)	160
5.2.1.1.2 X-Ray crystallographic study of [PdMe(κ^3 -P,C,P-4-1)] (5-2)	161
5.2.1.2 Attempted reaction of acetone with [PdH(κ^3 -P,C,P-4-1)] (5-1)	162
5.2.1.2.1 X-Ray crystallographic study of [μ -(4-1)Pd] ₂ (5-3)	163
5.2.1.2.2 Proposed mechanism for the formation of [μ -(4-1)Pd] ₂ (5-3)	163

5.2.1.3	Reversible insertion of carbon dioxide into palladium hydride bond of [PdH(κ^3 -P,C,P-4-1)] (5-1)	165
5.2.1.3.1	X-Ray crystallographic study of [Pd(OC(H)O)(κ^3 -P,C,P-4-1)] (5-4)	167
5.2.1.3.2	Attempted further reactivity of complex 5-4	168
5.2.1.4	Isomerisation of <i>cis</i> -stilbene catalysed by 5-1	169
5.2.1.5	Hydrosilylation of benzaldehyde with phenylsilane catalysed by 5-1	172
5.3	Chapter 5 summary and conclusions	174
5.4	References	175
6	CHAPTER 6: SUMMARY AND OUTLOOK	177
7	CHAPTER 7: EXPERIMENTAL	180
7.1	General considerations	180
7.2	Chapter 2 experimental	182
7.3	Chapter 3 experimental	194
7.4	Chapter 4 experimental	211
7.5	Chapter 5 experimental	229
7.6	References	235
8	APPENDIX	236
8.1	Appendix 1: List of compound numbers	236
8.1.1	Chapter 2	236
8.1.2	Chapter 3	237
8.1.3	Chapter 4	238
8.1.4	Chapter 5	239
8.2	Appendix 2: Crystallographic data	240
8.3	Appendix 3: Example percent buried volume (% V_{bur}) calculation	247
8.4	Appendix 4: Seminars attended	252
8.5	Appendix 5: Conferences attended	257

General abbreviations

ASAP	=	Atmospheric solids analysis probe
BOC	=	<i>tert</i> -Butyloxycarbonyl
Bp	=	Boiling point
^t Bu	=	<i>tert</i> -Butyl
COD	=	<i>cis,cis</i> -1,5-Cyclooctadiene
CSD	=	Cambridge Structural Database
DCE	=	1,2-Dichloroethane
DCM	=	Dichloromethane
DME	=	1,2-Dimethoxyethane
DMF	=	Dimethylformamide
Dmpe	=	1,2- <i>bis</i> (Dimethylphosphino)ethane
Dppe	=	1,2- <i>bis</i> (Diphenylphosphino)ethane
Dppm	=	1,1- <i>bis</i> (Diphenylphosphino)methane
equiv	=	Equivalent(s)
ESI	=	Electrospray ionisation
Et	=	Ethyl
FWHM	=	Full Width at Half Maximum
GC-FID	=	Gas Chromatography-Flame ionization detector
GC-MS	=	Gas Chromatography-Mass spectrometry
h	=	Hour
IR	=	Infrared spectroscopy
L	=	Generic 2-electron donor ligand
M	=	Generic transition metal, unless stated otherwise
Me	=	Methyl
Mp	=	Melting point
MS	=	Mass spectrometry
<i>m/z</i>	=	Mass/charge ratio
NMR	=	Nuclear Magnetic Resonance

Ph	=	Phenyl
ppm	=	Parts per million
<i>i</i> Pr	=	<i>iso</i> -Propyl
R	=	Generic substituent
RBF	=	Round-bottomed flask
RT	=	Room Temperature
TCE	=	1,1,2,2-Tetrachloroethane
Temp	=	Temperature
THF	=	Tetrahydrofuran
Tmeda	=	<i>N,N,N',N'</i> -Tetramethylethylenediamine
VT	=	Variable Temperature
X	=	Generic 1-electron donor ligand
XRD	=	X-Ray diffraction
Xs	=	Excess

NMR spectroscopy abbreviations

δ	=	Chemical shift (in ppm)
$\Delta\delta$	=	Coordination chemical shift (ppm)
b	=	broad signal
s	=	singlet
d	=	doublet
t	=	triplet
m	=	multiplet
<i>ps</i> -	=	<i>psuedo</i> - (prefixing multiplicity)

Phosphorus-containing compounds terminology

PR ₃	=	General phosphine
R ₂ POR'	=	General phosphinite
RP(OR') ₂	=	General phosphonite

$P(OR')_3$	=	General phosphite
$(R_2N)P(OR')_2$	=	General aminophosponite
$(R_2N)_2POR'$	=	General diaminophosphinite

Chapter 1: General introduction

Over the last 40 years the design of new ligands for late transition metals has become a significant area of research.^{1, 2} In particular, there is a push for ligands that give greater activity and/or selectivity in homogeneously-catalysed processes especially involving organic substrates.³ However, prediction of the effects of small changes to the ligand framework on the overall catalysed transformation remains difficult. Therefore, there is a need to synthesise new ligands with tuneable steric and electronic properties and to use them to develop better understanding of the mechanism of homogeneously-catalysed processes, and thus to help predict structure-reactivity relationships.

One important area where very notable achievements have been made in recent years is the design and application of new polydentate ligands in preference to monodentate ligands. This has been driven, in part, by the observations that polydentate ligands are less labile than their monodentate counterparts and generally form complexes that show longer catalytic lifetimes as a result. At a simplistic level, these two features are interlinked with the longer catalytic lifetimes exhibited by systems that incorporate polydentate ligands often attributed to their better retention within a metal's coordination sphere as a result of the *chelate effect*.⁴

Chapter 1 will introduce basic aspects of coordination and phosphorus chemistry relevant to the design and evaluation of new polydentate phosphorus-containing ligands which are presented in this thesis.

1.1 Phosphorus-based ligands

Phosphorus-containing ligands are ubiquitous in homogeneous catalysis due to their comparative ease of synthesis, something that makes their steric and electronic properties highly tuneable often in a systematic fashion.² In order that the best ligand for a particular metal-mediated transformation can be chosen or, in order to understand the performance of a particular metal phosphine combination, the quantification of the steric and electronic properties is required and is detailed below.

1.1.1 The bonding of phosphine ligands to metal centres

Phosphine-metal bonding is generally regarded as comprising of two components. The phosphorus lone pair of electrons donates into an empty metal orbital of appropriate σ -symmetry, which is also accompanied by an additional π -back-bonding component from a filled metal d orbital to the phosphine (Figure 1.1). The identity of the π -accepting orbital on phosphorus was debated for some time, but is now generally

believed to be one of the doubly degenerate orbitals formed from the combination of a P-R σ^* orbital and a P 3d orbital (Figure 1.2).^{5, 6} Orpen *et al.* showed crystallographically that there is a lengthening of the P-R bond upon a shortening of the M-P bond, consistent with back-donation into a P-R antibonding orbital in the coordination sphere of a metal.⁵

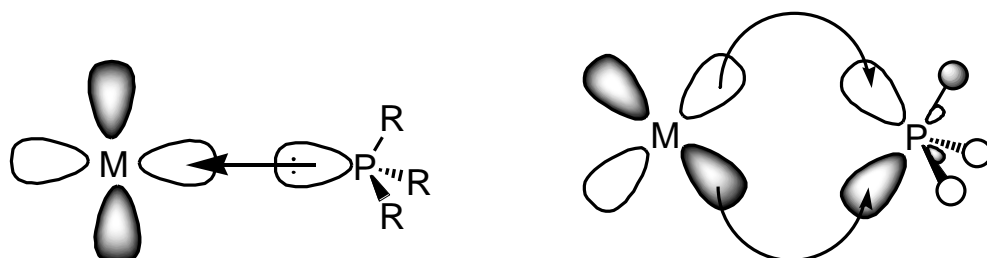


Figure 1.1: σ -Bonding (left) and π -bonding (right) components of a phosphine binding to a metal. The π -accepting orbital on the phosphine is one of the doubly degenerate orbitals formed from the combination of a P-R σ^* orbital and a P 3d orbital (Figure 1.2).

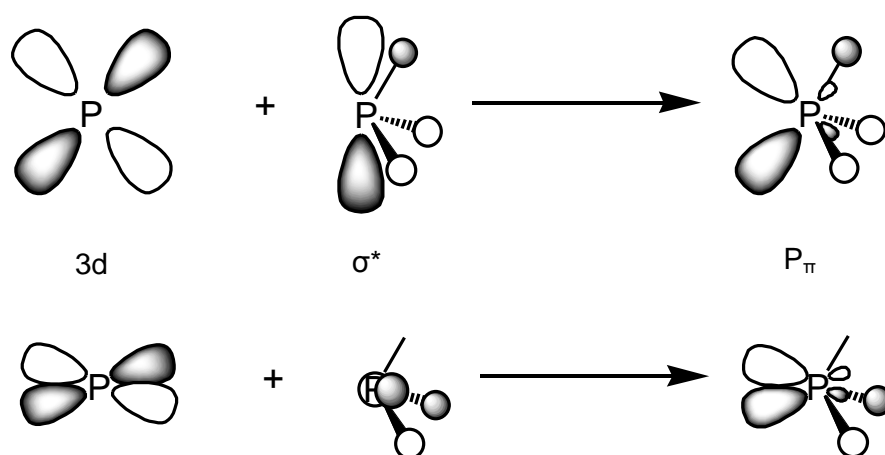


Figure 1.2: Degenerate orbitals formed from the combination of a P-R σ^* orbital and a P 3d orbital, modified from Orpen *et al.*⁵

As would be expected, the extent of both σ -donation to and π -back-acceptance from the metal can be modified depending on the substituents on phosphorus. In general terms, the extent of back-donation increases with higher electronegativity of the substituents, due to a lowering of the energy of the phosphorus accepting orbital (Figure 1.3).⁷

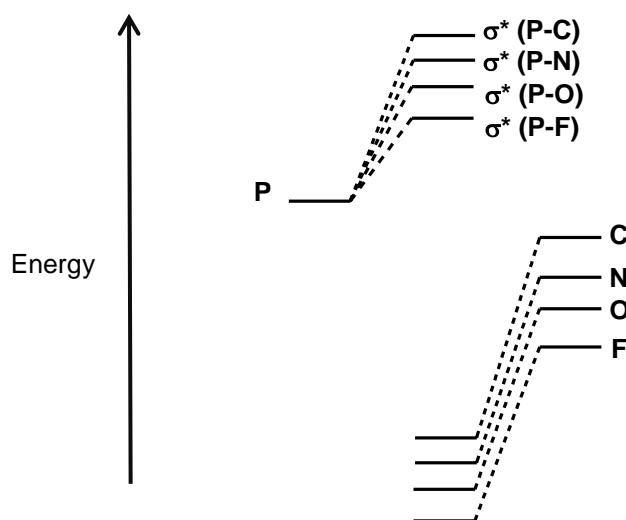


Figure 1.3: The P-R σ^* orbital lowers in energy as the electronegativity of the R group increases, adapted from Dyer.⁸

1.1.2 Quantifying the steric impact of phosphine ligands

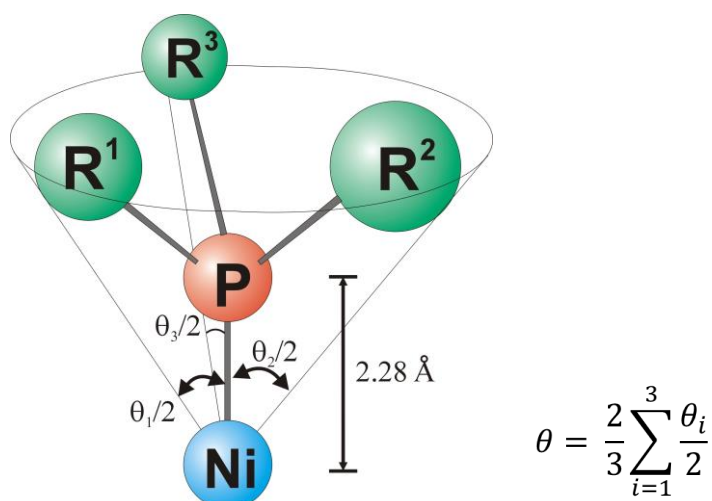


Figure 1.4: Determination of the Tolman cone angle for an unsymmetrical phosphine; the circles represent the van der Waals radii of the substituents, adapted from Dyer.^{8,9}

The steric bulk of a phosphine is one of the key factors in determining the reactivity of metal-phosphine complexes as, at the most basic level, it determines the size and number of other species that can bind to the metal-phosphine fragment. Perhaps the most common method of quantifying the steric bulk of a phosphine is to measure the Tolman cone angle, θ .^{9, 10} Using empirical bond data and the van der Waals radii for the phosphorus substituents, a model for the phosphine binding to a metal can be built. If the phosphine is rotated about the nickel-phosphorus bond, a conical region in space

is carved out, with the angle at the point of the cone being called the Tolman cone angle (Figure 1.4). Some representative Tolman cone angles are shown in Table 1.1 and show a 95° variation in the cone angle between PH₃ and P^tBu₃.

PR ₃	Cone angle, $\theta / ^\circ$
PH ₃	87
PMe ₃	118
PEt ₂	132
PPh ₃	145
P ⁱ Pr ₃	160
P ^t Bu ₃	182
P(OMe) ₃	107
P(OEt) ₃	109

Table 1.1: Representative Tolman cone angles.⁹

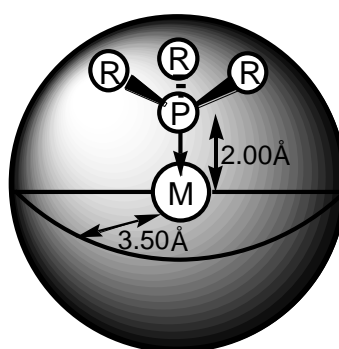


Figure 1.5: Depiction of the percentage buried volume ($\%V_{bur}$) of a phosphine, PR₃, with a fixed M–P bond distance of 2.00 Å and a sphere radius of 3.50 Å.¹¹

Whilst the Tolman cone angle works well for symmetrical and asymmetrical (using a weighted average angle, Figure 1.4) phosphines, it cannot easily be applied to bidentate phosphines.¹² Hence, there has been continual development of new methods of measuring the steric bulk of a ligand. One recently developed approach to measuring steric bulk is to calculate the ‘percentage buried volume’ ($\%V_{bur}$) of a ligand. The $\%V_{bur}$ concept was originally developed for N-heterocyclic carbene ligands, but has since been applied to mono- and bi-dentate phosphines (with some modification).^{11, 13} The percentage buried volume of a ligand is measured using crystallographic data and is defined as the percentage of the total volume of a sphere (radius 3.50 Å) occupied by a ligand with a fixed metal-ligand bond distance. Figure 1.5

gives a pictorial representation for a generic phosphine, PR_3 and representative values of $\%V_{\text{bur}}$ for symmetrical phosphines calculated by Nolan *et al.* are given in Table 1.2.¹³ The buried volume, $\%V_{\text{bur}}$ gives an easily calculable measure of the space occupied by an organometallic ligand in the first coordination sphere of the metal centre based on experimental data that can be used to help rationalise structure-activity relationships. The percent buried volume method shows good correlation with the Tolman cone angle with good positive correlation between the Tolman cone angles of various phosphines (PR_3) and the $\%V_{\text{bur}}$ calculated for the $[\text{AuCl}(\text{PR}_3)]$ complexes of the same ligands, with one notable exception (Figure 1.6). The $\%V_{\text{bur}}$ value of triphenylphosphite was higher than predicted based upon the Tolman cone angle, thus it is suggested that the simple molecular model approach used to estimate the Tolman cone angle might underestimate the steric parameters of more flexible phosphite ligands.¹³

PR_3	Percentage buried volume ($\%V_{\text{bur}}$) / %
PMe_3	22
PEt_3	28
P^nPr_3	26
P^nBu_3	26
PPh_3	30
$\text{P}(\rho\text{-Tol})_3$	28
P^iPr_3	32
PCy_3	32
P^tBu_3	27
$\text{P}(\text{C}_6\text{F}_5)_3$	37
$\text{P}(o\text{-Tol})_3$	41
PMes_3	48
$\text{P}(\text{OPh})_3$	31

Table 1.2: Representative percentage buried volume ($\%V_{\text{bur}}$) values for phosphines, calculated for $[\text{AuCl}(\text{PR}_3)]$ complexes with a fixed Au–P bond distance of 2.00 Å.¹³

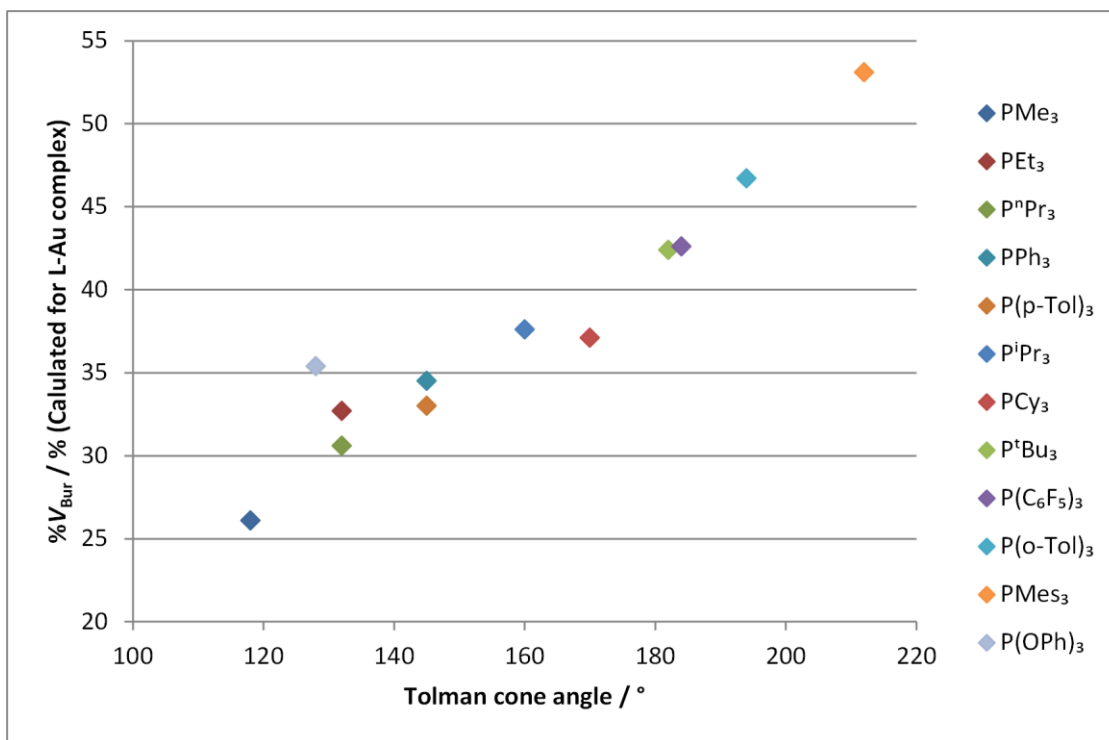


Figure 1.6: Correlation of the Tolman cone angle with the percent buried volume ($\%V_{bur}$) calculated for $[AuCl(PR_3)]$ complexes with a fixed Au–P bond distance of 2.00 \AA , modified from Nolan et al.¹³

1.1.3 Quantifying the electronic impact of phosphine ligands

As previously stated the bonding of a phosphine to metal has two components, σ -donation and π -back-donation. One method for determining the overall net electronic contribution of the phosphine (combination of σ -donation and π -back-donation effects) is through its coordination to a metal carbonyl fragment and subsequent measurement of the carbonyl stretching frequency by infrared (IR) spectroscopy.^{9, 14, 15} Initially, studies were undertaken using $[Ni(CO)_3(PR_3)]$ complexes, to measure the so-called Tolman electronic parameter ν ; representative values shown in Table 1.3. However, due to the high toxicity of the necessary $[Ni(CO)_4]$ precursor, the use of *trans*- $[RhCl(CO)(PR_3)_2]$ complexes has become more widespread, with an established correlation between values obtained using $[RhCl(CO)]$ and $[Ni(CO)_3]$ metal fragments.¹⁶ A further advantage of using the rhodium system is its utility in studying the electronic impact of bidentate ligands, by the formation of $[RhCl(CO)(P^{\wedge}L)]$ complexes (where $P^{\wedge}L$ is a bidentate phosphorus-containing ligand).¹⁷⁻¹⁹ For both the nickel and rhodium carbonyl complexes, a greater electron donation ability of the phosphine leads to an increase in back-bonding from a filled metal orbital into a carbonyl antibonding orbital, resulting in a weakening and consequently lowering of the carbonyl IR stretching frequency.⁷

PR_3	ν / cm^{-1}
PF_3	2111
PCl_3	2097
P(OMe)_3	2080
P(OEt)_3	2076
PPh_3	2069
PMe_3	2064
PEt_3	2062
$\text{P(NMe}_2)_3$	2062
P^iPr_3	2059
P^tBu_3	2056

Table 1.3: Stretching frequencies (A_1 band, DCM solution) for $[\text{Ni}(\text{CO})_3(\text{PR}_3)]$ complexes.^{9, 15}

Both of the now well-established IR-based protocols involving the formation of nickel or rhodium carbonyl complexes provide a method for assessing the net electron donation by the phosphine to the metal, *i.e.* the sum of the σ -donor and π -acceptor contributions. However, it is desirable to have a complementary technique that only assesses one of these two contributions. In an attempt to accomplish this target Allen *et al.* demonstrated the use of an NMR spectroscopy-based technique involving phosphine selenide compounds (R_3PSe) in order to “measure” the σ -donor strength of a particular phosphine.^{20, 21} Since ^{77}Se has a nuclear spin of $1/2$ and a natural abundance of 7.5%, the ^{31}P NMR spectroscopic resonance for a phosphine selenide compound exhibits satellites resulting from a $^1J_{\text{SeP}}$ coupling. It has been demonstrated that the larger the $|^1J_{\text{SeP}}|$ coupling constants, the greater the s-character of the phosphorus lone-pair on the parent phosphine. Therefore, poorly donating (poorly Lewis basic) phosphines exhibit $^1J_{\text{SeP}}$ coupling constant whose magnitude is greater than those for more electron rich (more basic) systems. Table 1.4 shows some representative values for the $^1J_{\text{SeP}}$ coupling constants for various phosphines, and demonstrates the large difference between the couplings for poorly basic F_2HP (1046 Hz) and the highly basic PMe_3 (684 Hz), as expected. Moreover, the preparation of phosphine-selenides is generally straightforward, necessitating only reaction of the parent phosphine with elemental grey selenium in an appropriate solvent (*e.g.* CDCl_3). Accordingly, the measurement of the $|^1J_{\text{SeP}}|$ coupling for phosphine selenides is a simple and effective method of estimating the basicity of a phosphine.

PR_3	$ ^1J_{\text{SeP}} / \text{Hz}$
F_2HP	1046
$\text{P}(\text{OMe})_3$	963
$\text{P}(\text{NMe}_2)_3$	805
PPh_3	736
PMe_3	684

Table 1.4: Representative $^1J_{\text{SeP}}$ coupling constants.²²

1.2 Aminophosphine ligands, $(\text{R}_2\text{N})_x\text{PR}'_{3-x}$

The coordination chemistry of aminophosphines, $(\text{R}_2\text{N})_x\text{PR}'_{3-x}$, is relatively poorly studied compared to that for phosphines and phosphites, $(\text{RO})_x\text{PR}'_{3-x}$.²³ A major advantage of aminophosphines when compared to phosphites, is that they can be very bulky as twice the steric bulk can be incorporated onto each heteroatom at phosphorus and they have more widely variable electronic properties.²⁴ Aminophosphines can be considered both strongly and poorly donating ligands, depending on the nature of the amino substituent. To rationalise this electronic variation a more detailed description of the bonding of aminophosphines to metals is needed. Replacing carbon-based substituents of alkyl and aryl phosphines by more electronegative amino groups reduces the electron density at phosphorus by a σ -inductive effect. However, there is some multiple bond character to a P-N bond resulting from partial π -donation from the nitrogen lone pair into an empty phosphorus-based orbital of appropriate symmetry (Figure 1.7). Depending on the nature of the amino substituent, this π -donation outweighs the inductive effects and leads to an electron-rich phosphorus centre. Hence, aminophosphine ligands can even be highly electron donating. For example, the data presented in Table 1.3 indicate that $\text{P}(\text{NMe}_2)_3$ is highly electron donating, giving rise to a carbonyl stretching frequency of 2062 cm^{-1} for its nickel carbonyl complex $[\text{Ni}(\text{CO})_3(\text{P}(\text{NMe}_2)_3)]$, which is comparable to that determined for $[\text{Ni}(\text{CO})_3(\text{PMe}_3)]$ (2064 cm^{-1}) containing the highly electron rich PMe_3 ligand.^{9, 15}

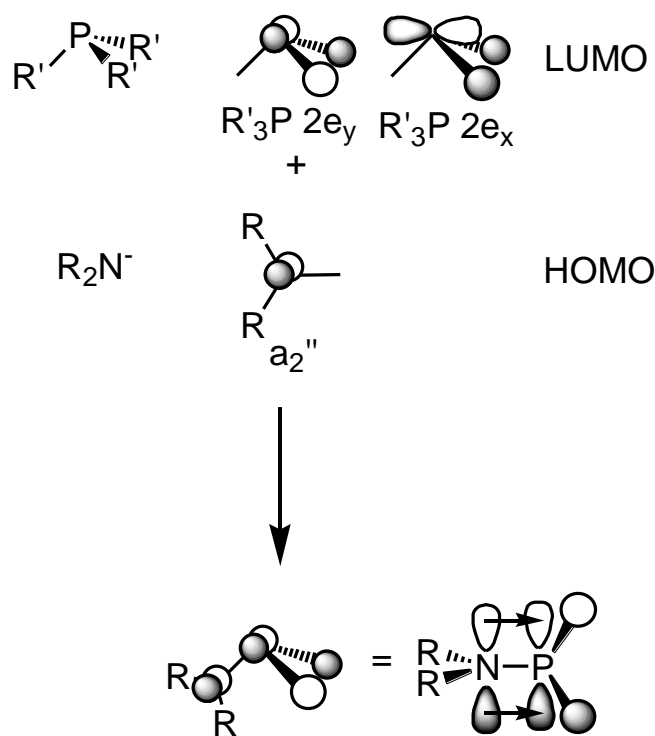


Figure 1.7: π -Donation of the nitrogen lone pair into an acceptor orbital on phosphorus in an aminophosphine.^{6, 8}

While there are many aminophosphines, which may be regarded as being strongly donating, the flexibility surrounding both the structure and the nature of the amino substituents R, means that it is possible to significantly alter the donor character of aminophosphines, to the extent that comparatively electron-poor aminophosphine systems may also be prepared. For example, pyrrolyl phosphines are a very electron poor class of ligand, something that arises as the lone pair on nitrogen can be delocalised into the 5-membered ring of the pyrrole substituent making it less available for π -donation to phosphorus (Figure 1.8). In addition, the nitrogen develops a partial positive charge next to the phosphorus atom, resulting in a large electronic induction effect through the P-N σ -bond. As the nitrogen lone pair is unavailable to donate to the phosphorus centre and due to the presence of an electron deficient nitrogen substituent, the phosphorus centre of pyrrolyl-phosphines is highly electron deficient and accordingly make these poorly donating ligands.²⁵

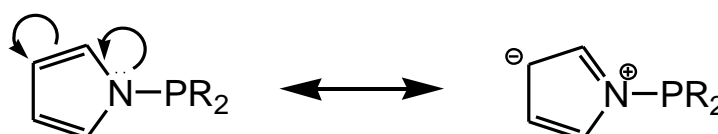


Figure 1.8: Delocalisation of the nitrogen lone pair onto the pyrrole ring.

1.3 Binding of alkene ligands to metal centres

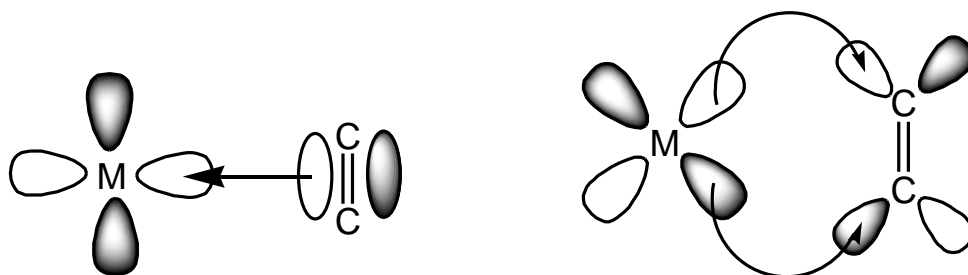


Figure 1.9: Dewar, Chatt, Duncanson model of an alkene binding to a metal centre, σ -donation (left) and π -back-bonding (right).

An alkene group is formally a two electron donor, but also has the potential to act as a π -acid as best described by the Dewar, Chatt, Duncanson binding model (Figure 1.9).²⁶ The back-bonding lengthens the olefin carbon-carbon bond and, consequently, increases the 'sp³' character of the carbon atoms (pyramidalisation).⁷ The extent of back-bonding from the metal centre is dependent on both the identity of the metal and of the alkene. Weakly π -basic metal ions such as Pt(II) and Pd(II) exhibit little back-bonding whereas strongly π -basic metals such as Pt(0) and Pd(0) exhibit more extensive back-bonding. There are many factors that impact on the extent of back-bonding from a metal to an alkene. Firstly, an alkene with electron withdrawing substituents will be susceptible to more back-bonding from the metal as the LUMO is lower in energy. However, there are additional factors that impact on the extent of back-bonding, including steric effects, with large alkene substituents hindering alkene coordination (Figure 1.10). A final factor to consider is the ring strain experienced by the alkene-containing scaffold: highly strained scaffolds experience very large amounts of back-bonding from metal centres due to the reduction in ring strain caused by the pyramidalisation of the alkene carbon atoms (Figure 1.11).²⁷ Thus, rigid and strained alkene ligands form strong metal alkene bonds and are highly π -accepting.

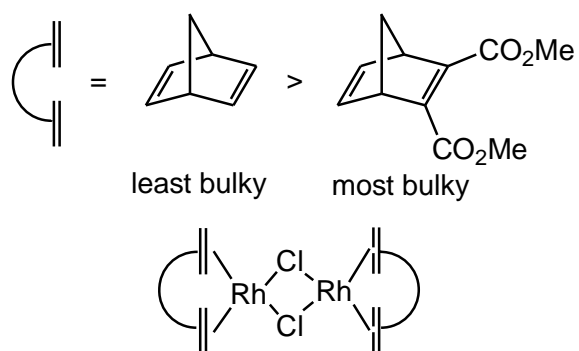


Figure 1.10: The relative stabilities of rhodium–diene complexes containing norbornadiene-based ligands with different amount of steric bulk on alkene substituent.²⁷

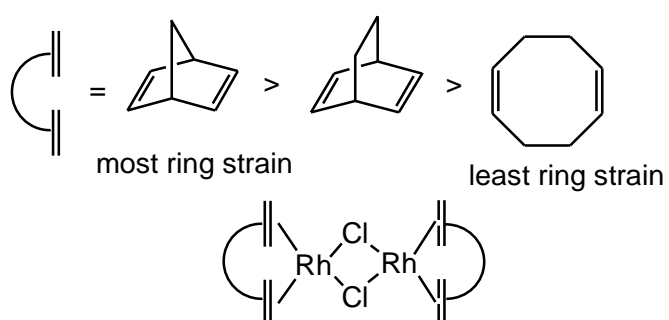


Figure 1.11: The relative stabilities of rhodium–diene complexes containing diene ligands with different amounts of ring strain.²⁷

1.4 Aims and objectives

General thesis objectives: To prepare a range of polydentate phosphorus-containing ligands relevant to catalysis and to develop a fundamental understanding of how changes to the ligands' structure and substituents impact on the coordination environment and behaviour of a bound metal centre.

Chapter 2

- Preparation of the potentially electron-deficient and bidentate phosphine-alkene ligands, *N*-R₂P-7-aza-benzobicyclo[2.2.1]hept-2-ene, R = Ph (**2-1**) and ⁱPr (**2-2**).
- To probe the electronic properties of compounds **2-1** and **2-2** by the synthesis and subsequent analysis of their phosphine-selenide compounds and metal carbonyl complexes.
- Exploration of the coordination chemistry of compound **2-1** with nickel-, rhodium- and iridium-containing fragments.

Chapter 3

- To explore the utility of phosphine-alkene compound **2-1** in facilitating the reductive elimination step in palladium-catalysed cross-coupling reactions, where slow reductive elimination is a known problem in some reactions.
- Determination of the mechanism of ethane reductive elimination from dimethyl palladium metal fragments promoted by compound **2-1** by a combination of experimental and theoretical experiments.
- Probe the utility of phosphine-alkene compound **2-1** in palladium-catalysed Suzuki and Negishi cross-coupling reactions.
- Assessment of the utility of compound **2-1** to promote known difficult reductive elimination processes from Pd(II), e.g. chloromethane from a PdCl(Me) complex.
- To synthesise, the less bulky and rigid P-alkene ligand *N*-PPh₂-3-pyrroline (**3-4**) and to study its reactivity with the PdMe₂ metal fragment.

Chapter 4

- Systematically study the synthesis and steric and electronic impact of a range of POCOP pincer ligands with different heteroatom substituents at phosphorus.

- To study the coordination chemistry of these ligands to a palladium chloride metal fragment and, subsequently, to probe the steric impact of the ligands by the percent buried volume ($\% V_{\text{bur}}$) method from the obtained molecular structures.
- Carry out an assessment of the electronic impact of the variously-substituted POCOP pincer ligands by two methods: i) measurement of the $|^1J_{\text{SeP}}|$ coupling constants of the relevant phosphine-selenide compounds and ii) by infrared spectroscopic analysis of their palladium carbonyl complexes.

Chapter 5

- Undertake the synthesis and characterisation of the novel palladium hydride complex $[\text{PdH}(\kappa^3\text{-P,C,P-4-1})]$ (**5-1**).
- Gauge the reactivity of the palladium hydride bond of complex **5-1** through reactions with ethylene (insertion of C=C) and acetone and CO_2 (C=O insertion).
- To assess the ability of complex **5-1** to catalyse alkene isomerisation and the hydrosilylation of an aldehyde.

1.5 References

1. B. Cornils and W. A. Herrmann, *Applied Homogeneous Catalysis with Organometallic Compounds*, 2nd edn., Wiley-VCH Verlag GmbH, Weinheim, 2002.
2. P. C. J. Kamer and P. N. W. Van Leeuwen, *Phosphorus(III) Ligands in Homogeneous Catalysis: Design and Synthesis*, John Wiley & Sons, Ltd, Chichester, 2012.
3. P. N. W. Van Leeuwen, *Homogeneous Catalysis: Understanding the art*, Kluwer Academic Publishers, Dordrecht, 2004.
4. P. Atkins, T. Overton, J. Rourke, M. Weller and F. Armstrong, *Inorganic Chemistry*, 4th edn., Oxford University Press, Oxford, 2006.
5. A. G. Orpen and N. G. Connelly, *J. Chem. Soc., Chem. Commun.*, 1985, 1310-1311.
6. D. G. Gilheany, *Chem. Rev.*, 1994, **94**, 1339-1374.
7. R. Crabtree, *The Organometallic Chemistry of the transition metals*, John Wiley, New York, 1988.
8. P. W. Dyer, *Unpublished work*.
9. C. A. Tolman, *Chem. Rev.*, 1977, **77**, 313-348.
10. C. A. Tolman, *J. Am. Chem. Soc.*, 1970, **92**, 2956-2965.
11. A. Poater, B. Cosenza, A. Correa, S. Giudice, F. Ragone, V. Scarano and L. Cavallo, *Eur. J. Inorg. Chem.*, 2009, 1759-1766.
12. C. A. Tolman, W. C. Seidel and L. W. Gosser, *J. Am. Chem. Soc.*, 1974, **96**, 53-60.
13. H. Clavier and S. P. Nolan, *Chem. Commun.*, 2010, **46**, 841-861.
14. W. Strohmeier and F.-J. Müller, *Chem. Ber.*, 1967, **100**, 2812-2821.
15. C. A. Tolman, *J. Am. Chem. Soc.*, 1970, **92**, 2953-2956.
16. S. Vastag, B. Heil and L. Markó, *J. Mol. Catal.*, 1979, **5**, 189-195.
17. D. A. Smith, A. S. Batsanov, K. Miqueu, J.-M. Sotiropoulos, D. C. Apperley, J. A. K. Howard and P. W. Dyer, *Angew. Chem. Int. Ed.*, 2008, **47**, 8674-8677.
18. J. Cipot, R. McDonald, M. J. Ferguson, G. Schatte and M. Stradiotto, *Organometallics*, 2007, **26**, 594-608.
19. S. Burling, L. D. Field, B. A. Messerle, K. Q. Vuong and P. Turner, *Dalton Trans.*, 2003, 4181-4191.
20. D. W. Allen and B. F. Taylor, *J. Chem. Res., Synop.* 1981, 220-221.
21. D. W. Allen and B. F. Taylor, *J. Chem. Soc., Dalton Trans.*, 1982, 51-54.
22. McFarlan.W and D. S. Rycroft, *J. Chem. Soc., Dalton Trans.*, 1973, 2162-2166.

23. M. Alajarin, C. Lopez-Leonardo and P. Llamas-Lorente, in *New Aspects in Phosphorus Chemistry V*, ed. J. P. Majoral, Springer-Verlag Berlin, Berlin, Editon edn., 2005, vol. 250, pp. 77-106.
24. T. J. Clark, J. M. Rodezno, S. B. Clendenning, S. Aouba, P. M. Brodersen, A. J. Lough, H. E. Ruda and I. Manners, *Chem. Eur. J.*, 2005, **11**, 4526-4534.
25. K. G. Moloy and J. L. Petersen, *J. Am. Chem. Soc.*, 1995, **117**, 7696-7710.
26. J. Chatt and L. A. Duncanson, *J. Chem. Soc.*, 1953, 2939-2947.
27. C. Defieber, H. Grutzmacher and E. M. Carreira, *Angew. Chem. Int. Ed.*, 2008, **47**, 4482-4502.

2 Synthesis and coordination chemistry of novel phosphine-alkene ligands

2.1 Introduction

Bidentate ligands with differing donor moieties, often termed *heteroditopic ligands*, have been employed widely in homogeneous catalysis. The electronic and steric disparity between the two different donor sites (L1 vs L2, Figure 2.1) of such heteroditopic ligands can be used to provide control and selectivity in reactions occurring at the metal centre. For example, bidentate P^N ligands have brought notable benefits to a range of reactions including transfer hydrogenation,¹ hydroboration,² olefin polymerisation,³ co-polymerisation,^{4, 5} and coupling reactions.^{6, 7} The most dramatic enhancements are achieved on maximising the difference between the π -acidity/Lewis basicity at P and the degree of σ -donor character at N.^{8, 9}

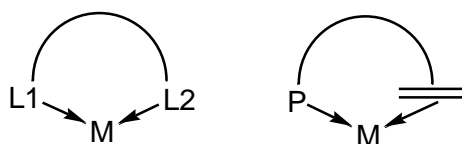


Figure 2.1: Schematic representation of a generic heteroditopic ligand (left) and P-alkene ligand (right).

2.1.1 P-alkene ligands

Phosphine-alkene (P-alkene) ligands are a class of heteroditopic compounds that bind to a metal centre in a bidentate fashion through both a phosphine and an alkene moiety (Figure 2.1). These P-alkene frameworks provide a highly sterically and electronically unsymmetrical coordination environment between the two donor components by virtue of the differing binding modes of each fragment to metal centres. Whilst phosphine-donor ligands are ubiquitous in catalysis due to their highly tuneable steric and electronic properties, alkenes have somewhat been ignored as ligands to control catalytic reactions. The limited use of alkenes here is sometimes attributed to the general notion that alkenes are both reactive and labile and so easily dissociate in the course of a catalytic cycle, thereby giving poor control over the environment at the metal.¹⁰ However, there are examples of chiral diene ligands that produce good asymmetric induction, by tightly controlling the environment of the metal centre (Figure 2.2).¹⁰⁻¹²

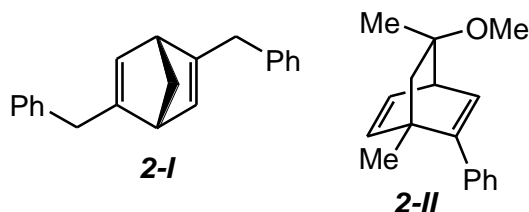


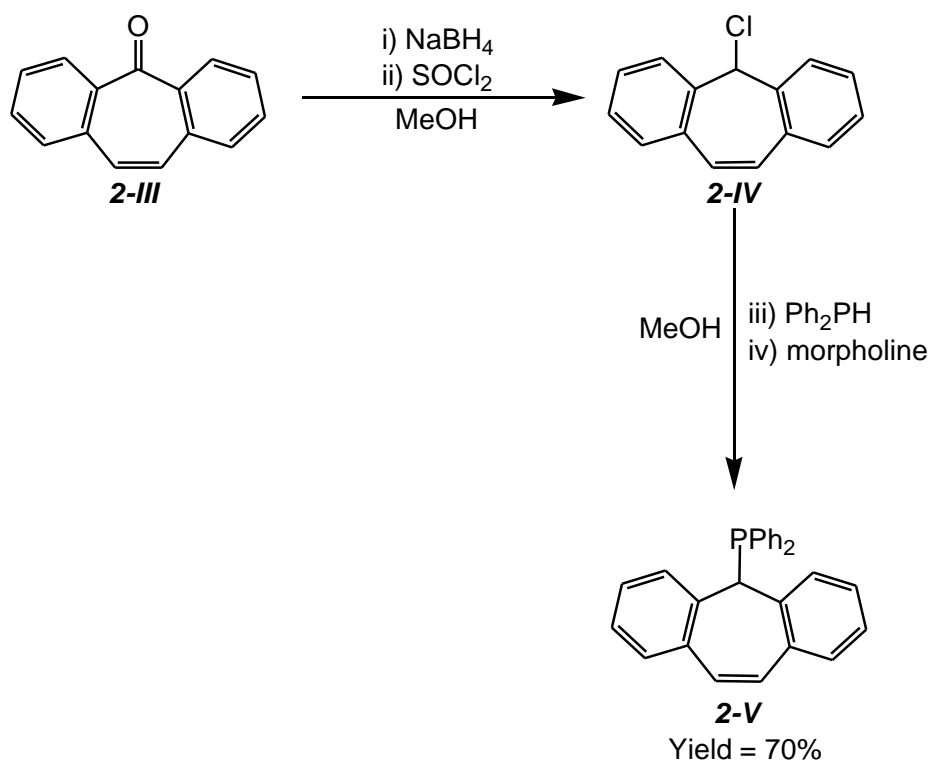
Figure 2.2: Chiral diene ligands **2-I** and **2-II** give good enantioselectivities in metal-catalysed reactions.^{11, 12}

2.1.2 Synthesis and structure of P-alkene ligands

Although examples of P-alkene ligands have been known for 35 years, they remain a relatively poorly studied class of ligand, whose unique steric and electronic properties have not been fully exploited to this date. There are a number of different strategies that have been employed to synthesise P-alkene ligands, which allow the identity and nature of the alkene-containing moiety to be varied, something that is critical in the design of strongly chelating ligands (to circumvent the perceived lability of the alkene-containing unit). The following section details the structure of some key P-alkene frameworks and describes their synthesis.

2.1.2.1 TROPP-type P-alkene ligands

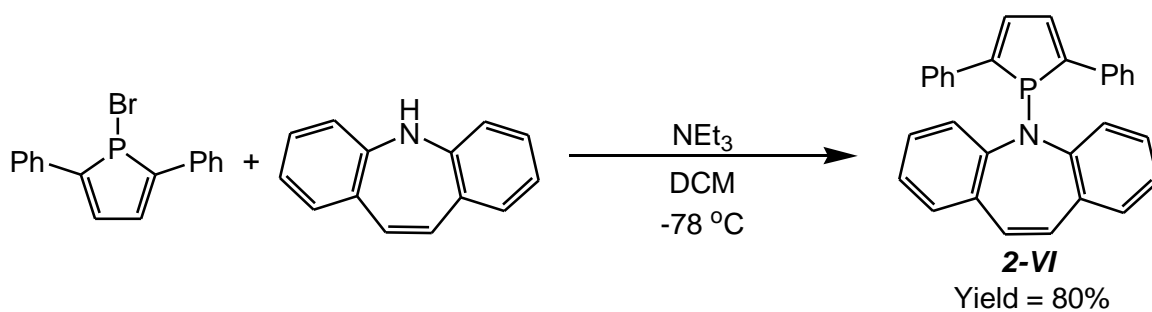
Among the types of P-alkene ligand that have been explored, one particular framework that has received considerable attention is that containing the dibenzocycloheptatrienyl phosphine (TROPP) (**2-V**) motif, which is synthesised by the reduction of the commercially available ketone **2-III** to the corresponding alcohol followed by chlorination to give **2-IV**; the phosphorus donor is introduced by substitution with HPPH_2 (Scheme 2.1).¹³ The dibenzocycloheptatrienyl moiety adopts a rigid boat conformation with an inversion barrier of $\sim 120 \text{ kJ mol}^{-1}$ and forms a stereochemically well-defined concave pocket, which is pre-organised for metal coordination, leading to strong alkene-metal bonding. In an extension to the work on TROPP ligands, chiral variants have been developed for use in asymmetric catalysis, something achieved by functionalising the alkene moiety; however, very little modification of the phosphorus donor component has been undertaken.¹⁴⁻¹⁶



Scheme 2.1: Dibenzocycloheptatrienyl phosphine ligand **2-V** (TROPP), developed by Grützmacher and co-workers.¹³

2.1.2.2 5*H*-dibenz[*b,f*]azepine-type P-alkene ligands

In contrast to the TROPP-type ligands described above (Section 2.1.2.1) there has been significant variation of the phosphorus substituents in ligands containing the structurally similar 5*H*-dibenz[*b,f*]azepine moiety facilitated by the relative synthetic ease of formation of a P-N bond. The first example of this type of P-alkene ligand (**2-VI**) was synthesised from commercially available 5*H*-dibenz[*b,f*]azepine and a bromophosphole by Le Floch and co-workers in 2005 (Scheme 2.2).¹⁶ Since this initial report many P-chiral derivatives have been synthesised. Moreover, studies have shown that the alkene group can bind to a metal centre in a hemilabile manner (Figure 2.3), thus indicating that the alkene group is not strongly bound to the metal.¹⁷⁻¹⁹



Scheme 2.2: Synthesis of ligand **2-VI**, containing a 5H-dibenz[b,f]azepine moiety, developed by Le Floch and co-workers.²⁰

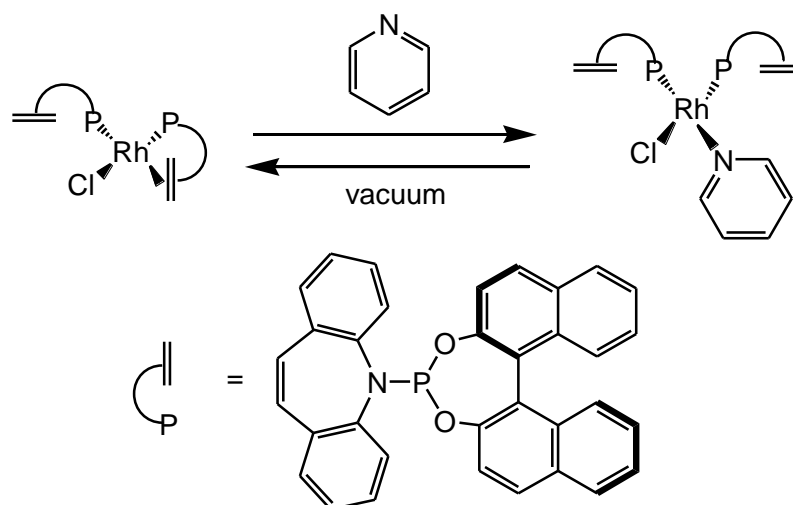


Figure 2.3: A 5H-dibenz[b,f]azepine-type P-alkene ligand behaving in a hemilabile manner, as reported by Dorta and co-workers.¹⁸

2.1.2.3 Norbornene-type P-alkene ligands

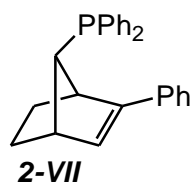
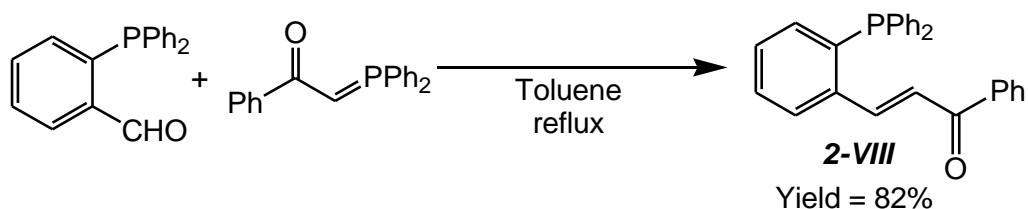


Figure 2.4: P-alkene ligand **2-VII** based on norbornene moiety, developed by Hayashi and co-workers.²¹

In order to impose a high level of control at metal centres, ligands that bind strongly to a metal are required. To this end, Hayashi developed the highly rigid P-alkene ligand **2-**

VII, containing a strained alkene group. The highly strained alkene containing moiety of **2-VII** experiences a very large amount of back-bonding from metal centres due to the reduction in ring strain caused by the pyramidalisation of the alkene carbon atoms (Section 1.3). The synthesis of the ligand **2-VII** (Figure 2.4) from norbornene is non-trivial, with multiple steps involving the separation of enantiomeric intermediates by chiral HPLC being required. As a result of this complex synthesis very little change in the functionality on the ligand has been reported or is indeed possible, something that has and continues to limit the utility of such systems.²¹

2.1.2.4 Vinyl-type P-alkene ligands



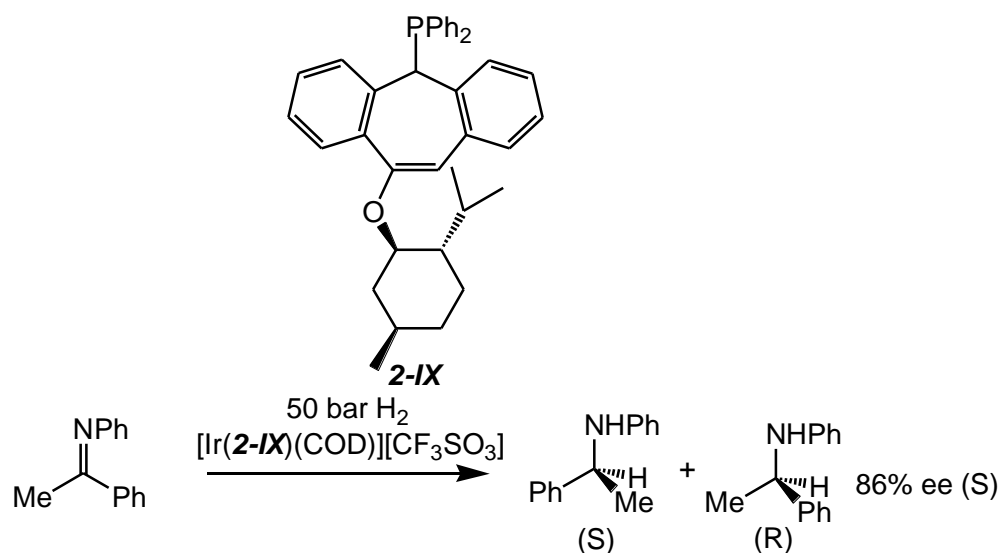
Scheme 2.3: Synthesis of ligand **2-VIII**, containing an electron deficient alkene moiety, developed by Lei and co-workers.²²

Whilst the use of a strained alkene group has been used by Hayashi (Section 2.1.2.3) to achieve strong alkene metal coordination to impose good stereocontrol over a metal centre, an alternative approach to achieving strong alkene metal bonding has been used by Lei and co-workers. They synthesised ligand **2-VIII** by the Wittig reaction shown in Scheme 2.3.²² Ligand **2-VIII** contains an electron-deficient alkene group which promotes strong metal back-bonding when bound to a metal centre.

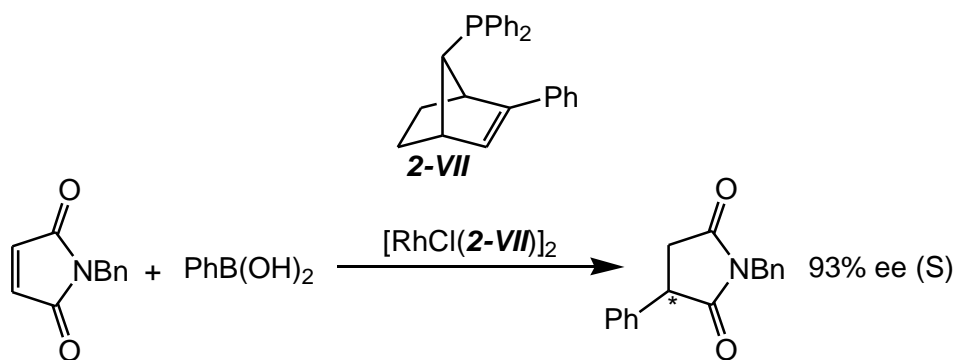
2.1.3 Recent developments in the application of P-alkene ligands in catalysis

Although examples of P-alkene ligands have been known for 35 years, the first reported use of a P-alkene metal scaffold in catalysis was not shown until 2004, when Grützmacher *et al.* achieved 86% ee for the hydrogenation of an imine using an iridium catalyst containing a TROPP-based P-alkene ligand (**2-IX**) (Scheme 2.4).¹⁴ At the same time as Grützmacher was developing chiral TROPP-based P-alkene ligands Hayashi *et al.* independently developed a different chiral P-alkene ligand (**2-VII**) based

on a norbornene framework. It was shown that Rh(I) complexes of ligand **2-VII** mediated asymmetric 1,4-addition of arylboronic acid to maleimides with up to 93% ee (Scheme 2.5).²¹ However, the complex synthesis of ligand **2-VII** precludes the tuning of the steric and electronic properties of the ligand to increase catalytic performance.

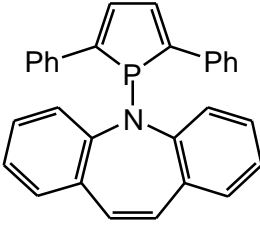
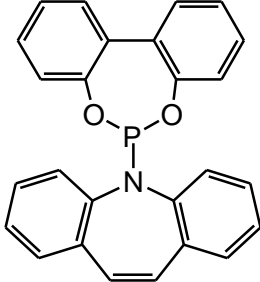
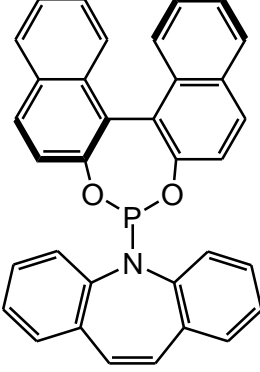
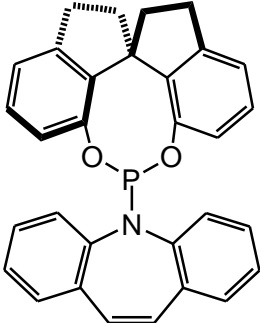


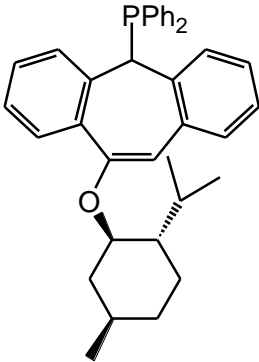
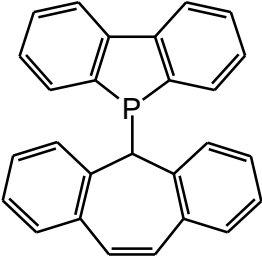
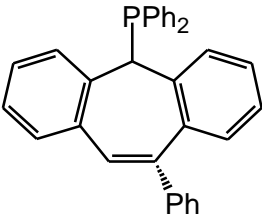
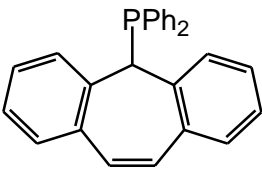
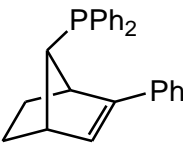
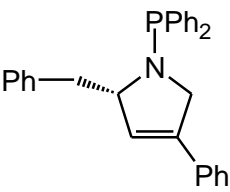
Scheme 2.4: Iridium-catalysed hydrogenation of an imine utilising a TROP-based P-alkene ligand (**2-IX**).¹⁴



Scheme 2.5: Rhodium-catalysed asymmetric 1,4-addition of phenylboronic acid to a maleimide utilising a P-alkene ligand (**2-VII**).²¹

Since the initial reports by Grützmacher and Hayashi of the use of P-alkene ligands in catalysis, a variety of different chiral and non-chiral bidentate phosphine-alkene ligands have been described and employed in a range of different transition metal-mediated catalytic reactions. Table 2.1 shows a selection of such ligands from 2004 to 2013 and indicates their applications in catalysis that have been developed.

Entry	Ligand	Catalysed reaction	Author
1		Rhodium-catalysed hydroformylation	Le Floch <i>et al.</i> ²⁰
2		Iridium-catalysed synthesis of allylic amines from allylic alcohols	Carreira <i>et al.</i> ¹⁷
3		<p>Rhodium-catalysed 1,4-addition of phenylboronic acid to α,β-unsaturated carbonyl compounds</p> <p>Iridium-catalysed allylic etherification</p> <p>Iridium-catalysed allylic thioetherification</p> <p>Iridium-catalysed allylic amination of allylic alcohols</p> <p>Iridium-catalysed allylic vinylation</p>	<p>Dorta <i>et al.</i>^{18, 23}</p> <p>Carreira <i>et al.</i>²⁴</p> <p>Carreira <i>et al.</i>²⁵</p> <p>Carreira <i>et al.</i>²⁶</p> <p>Carreira <i>et al.</i>²⁷</p>
4		Rhodium-catalysed intramolecular hydroacylation	Carreira <i>et al.</i> ¹⁹

5		Rhodium-catalysed hydrogenation	Grützmacher <i>et al.</i> ¹⁴
6		Palladium-catalysed Suzuki-Miyaura cross-coupling Palladium-catalysed allylation of amines	Le Floch <i>et al.</i> ¹⁶ Le Floch <i>et al.</i> ²⁸
7		Rhodium-catalysed 1,4-addition of phenylboronic acid to α,β -unsaturated carbonyl compounds Iridium-catalysed hydrogenation	Grützmacher <i>et al.</i> ¹⁵ Grützmacher <i>et al.</i> ¹⁵
8		Palladium-catalysed Methoxycarbonylation of terminal alkynes	Oberhauser <i>et al.</i> ²⁹
9		Rhodium-catalysed 1,4-addition of phenylboronic acid to α,β -unsaturated carbonyl compounds Palladium-catalysed allylic alkylation	Hayashi <i>et al.</i> ^{21, 30} Hayashi <i>et al.</i> ³¹
10		Rhodium-catalysed addition of organoboroxines to <i>N</i> -sulfonyl imines Rhodium-catalysed 1,4-addition of phenylboronic acid to α,β -unsaturated carbonyl compounds	Hayashi <i>et al.</i> ³² Hayashi <i>et al.</i> ³³

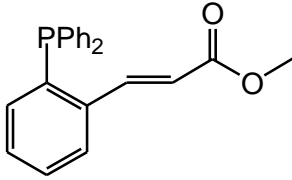
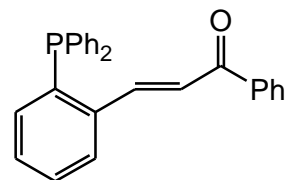
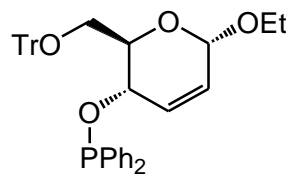
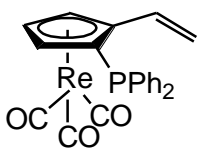
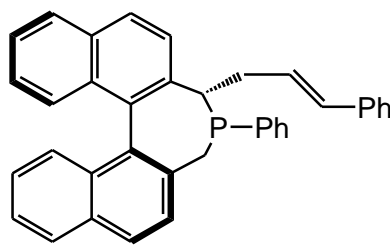
11		Palladium-catalysed Suzuki-Miyaura cross-coupling Platinum-catalysed Hydroformylation	Williams <i>et al.</i> ³⁴ Williams <i>et al.</i> ³⁵
12		Palladium-catalysed Negishi cross-coupling	Lei <i>et al.</i> ²²
13		Palladium-catalysed allylic alkylation Rhodium-catalysed 1,4-addition of phenylboronic acid to α,β -unsaturated carbonyl compounds	Boysen <i>et al.</i> ³⁶ Boysen <i>et al.</i> ^{36, 37}
14		Rhodium-catalysed 1,4-addition of phenylboronic acid to α,β -unsaturated carbonyl compounds	Bolm <i>et al.</i> ³⁸
15		Rhodium-catalysed 1,4-addition of phenylboronic acid to α,β -unsaturated carbonyl compounds	Widhalm <i>et al.</i> ³⁹

Table 2.1: Selected applications of P-alkene ligands in transition metal-mediated catalysis for the period 2004 to 2013.

Following the work done to date (summarised in Table 2.1), it is clear that there is scope to significantly extend the role of P-alkene ligands in catalysis, through developing new ligand frameworks. This chapter details the development of a new rigid

P-alkene ligand for application in a variety of transition metal-catalysed transformations.

2.2 Synthesis and coordination chemistry of $N\text{-R}_2\text{P-7-aza-benzobicyclo[2.2.1]hept-2-ene}$, $\text{R} = \text{Ph}, \text{tPr}$

This PhD project sought to develop a new class of P-alkene ligand that would marry the norbornene-like alkene moiety of **2-VII** (strong alkene-metal binding) with the ease of modifying the phosphorus donor moiety of aminophosphine-based ligand **2-VI**, first developed by Le Floch (Figure 2.5).^{20, 21} Since the difference in the donor/acceptor properties of the two Lewis basic components of heteroditopic ligands are known to control their selectivity in catalysis, a study probing the characteristics of the phosphorus and alkene moieties was undertaken (Section 2.2.3). The new class of P-alkene ligands was also coordinated to a variety of late transition metal fragments and the reactivity of subsequent complexes studied.

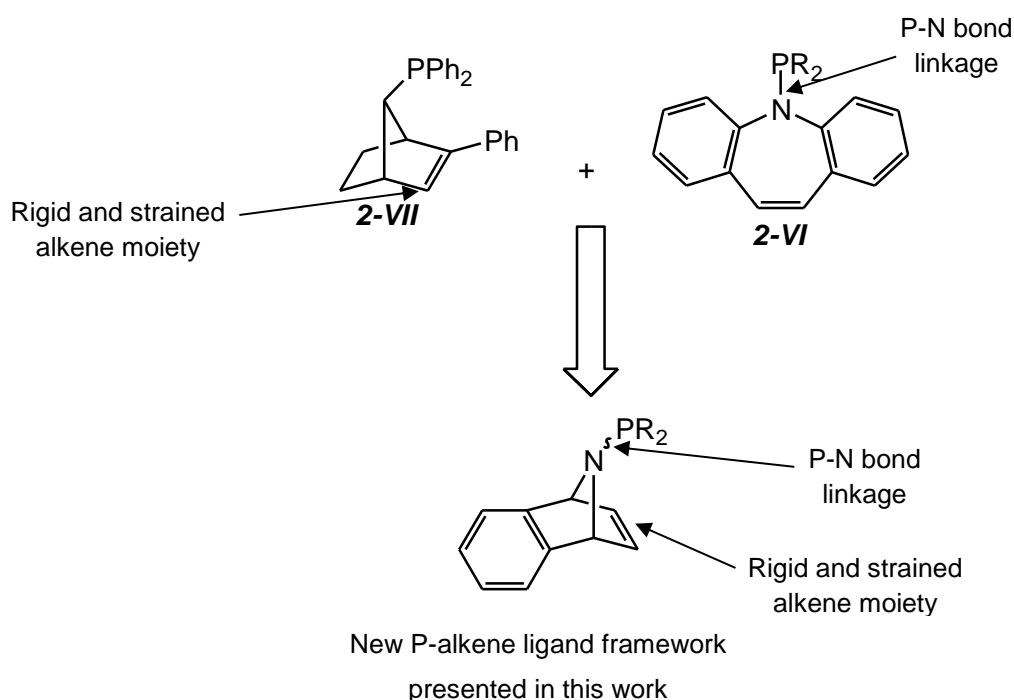


Figure 2.5: Structure and design ideas for new P-alkene ligands described in this thesis.

2.2.1 Key features of *N*-R₂P-7-aza-benzobicyclo[2.2.1]hept-2-ene as a ligand

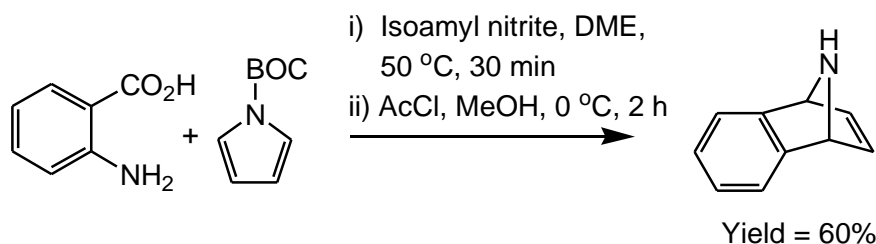
The key features of the new family of P-alkene ligands introduced in Figure 2.5 (*N*-R₂P-7-aza-benzobicyclo[2.2.1]hept-2-ene) include:

- A P-N linkage:
 - the ease of synthesis of P-N bonds should allow facile introduction of a range of different phosphorus moieties that will allow tuning of the steric and electronic properties of the ligand.
- Alkene group located within a 5-membered ring as part of a rigid 7-aza-norbornene structure:
 - encourages strong alkene-metal coordination due to a reduction in ring strain experienced upon alkene coordination to a metal (an increase in the sp³ character of the alkene carbon atoms as a result of M→alkene retrodonation).
- Bulky aromatic backbone:
 - adds steric bulk;
 - makes the synthesis more straight forward.

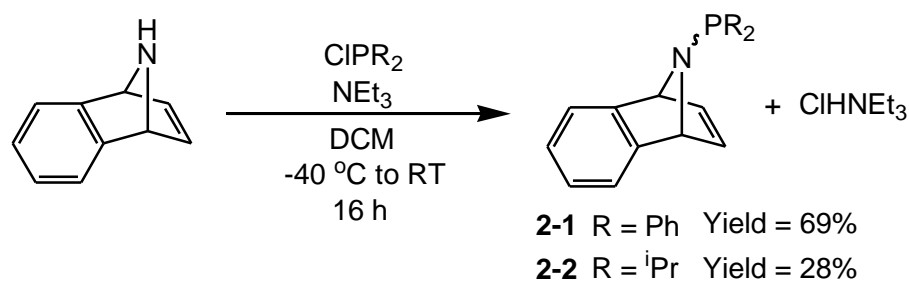
This work builds on initial studies made previously in the Dyer group by Dr Lise Baiget (PDRA in the Dyer group 2007-2008), who prepared a number of P-alkene ligands based on the motif shown in Figure 2.5, where R = Ph (**2-1**), ⁱPr (**2-2**), OEt, and probed their coordination to the PdCl₂ fragment. Additionally she studied the reaction of *N*-Ph₂P-7-aza-benzobicyclo[2.2.1]hept-2-ene (**2-1**) with [Rh(CO)₂Cl], which is included here for completeness (Section 2.2.3.2).

The work presented in this thesis gives an improved, higher-yielding synthesis for **2-1** (R = Ph) and **2-2** (R = ⁱPr), and explores the coordination chemistry of **2-1** and **2-2** with a range of transition metals.

2.2.2 Synthesis of diphenylphosphino- and diisopropylphosphino-substituted P-alkene ligands (2-1 and 2-2)



Scheme 2.6: Synthesis of 7-aza-benzobicyclo[2.2.1]hept-2-ene, developed by Lautens and Maison.^{40, 41}



Scheme 2.7: Synthesis of P-alkene ligands **2-1** and **2-2**.

The synthesis of 7-aza-benzobicyclo[2.2.1]hept-2-ene has been reported previously, and involves the [4 + 2] Diels-Alder cycloaddition of benzyne (generated *in situ*) and *N*-BOC-pyrrole. Subsequent deprotection of the BOC-protected species results in the formation of the desired amine in good yield (Scheme 2.6).^{40, 41} The relative ease of the synthesis of 7-aza-benzobicyclo[2.2.1]hept-2-ene over 7-aza-norbornene was a major factor for the inclusion of the aromatic ring in the ligand design.⁴²

Ligand **2-1** was prepared in 69% yield from 7-aza-benzobicyclo[2.2.1]hept-2-ene, *via* the addition of chlorodiphenylphosphine in the presence of an amine base (Scheme 2.7). Purification of **2-1** is achieved by recrystallisation from a hot hexane solution, resulting in its isolation as a pale orange solid.

Compound **2-1** was characterised by multinuclear NMR spectroscopy and CHN analyses. A singlet resonance at δ ³¹P 41.6 ppm is exhibited by ³¹P{¹H} NMR spectroscopy, typical of other diphenylaminophosphines such as P(ⁱPr)₂Ph₂ (δ ³¹P 36.7 ppm) and P(NEt₂)Ph₂ (δ ³¹P 66.8 ppm).⁴³ The alkene CH groups appear as a complex multiplet between 6.77 and 6.78 ppm in the ¹H NMR spectrum due to coupling to both the bridgehead protons and the phosphorus atom, and as a doublet at 143.0

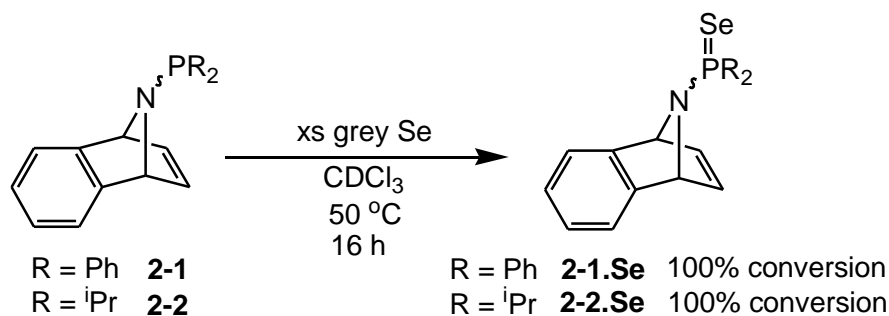
ppm ($^3J_{PC} = 4$ Hz) by $^{13}\text{C}\{^1\text{H}\}$ NMR spectroscopy. The barrier to inversion at nitrogen has been calculated computationally (B3LYP/6-31G*) (by Dr Mark A. Fox) to be very low, ~ 3 kcal mol $^{-1}$, which should permit compound **2-1** to adopt the necessary conformation for κ^2 -P,C metal binding, *i.e.* with the phosphine unit lying above the alkene moiety.

In an extension to this work, the ligand *N*- $^i\text{Pr}_2\text{P}$ -7-aza-benzobicyclo[2.2.1]hept-2-ene (**2-2**) has been prepared to include the more Lewis basic diisopropylphosphino group and was synthesised in an analogous fashion to that used to access **2-1** (Scheme 2.7). Compound **2-2** was isolated as a colourless oil in 28% yield following purification by vacuum distillation. Upon cooling to -20 °C, compound **2-2** solidifies into a white solid that does not melt upon warming to room temperature. Compound **2-2** was characterised by multinuclear NMR spectroscopy, exhibiting a singlet resonance at δ $^{31}\text{P}\{^1\text{H}\}$ 62.7 ppm, with the alkene CH resonances being similar to those of **2-1** according to ^1H and $^{13}\text{C}\{^1\text{H}\}$ NMR spectroscopy, signifying that there is no communication between the two donor sites.

Notably, it proved impossible to synthesise *N*- $^t\text{Bu}_2\text{P}$ -7-aza-benzobicyclo[2.2.1]hept-2-ene using the nucleophilic substitution strategy described in Scheme 2.7; no reaction was observed between di-*tert*-butylchlorophosphine and 7-aza-benzobicyclo[2.2.1]hept-2-ene in the presence of triethylamine, with unreacted di-*tert*-butylchlorophosphine being recovered. Increasing the reaction temperature to 80 °C in DCE solvent did not lead to formation of the expected product, with starting materials again being recovered. We postulate that di-*tert*-butylchlorophosphine is too bulky to react with 7-aza-benzobicyclo[2.2.1]hept-2-ene.

2.2.3 Assessment of the electronic character of P-alkene ligands **2-1** and **2-2**

2.2.3.1 Synthesis of phosphine selenides **2-1.Se** and **2-2.Se**

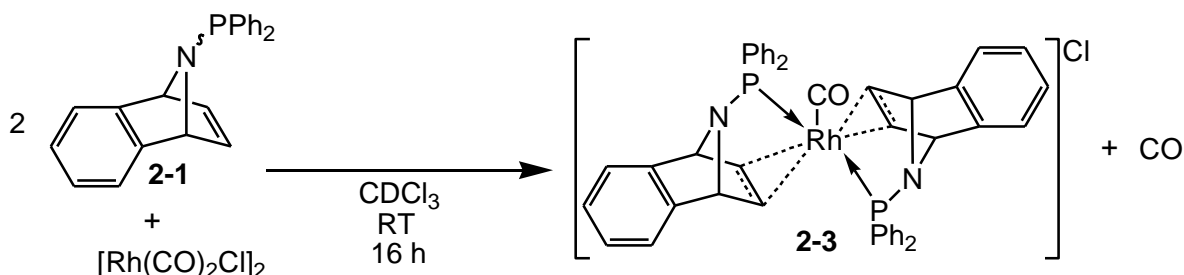


Scheme 2.8: Synthesis of phosphine selenides **2-1.Se** and **2-2.Se**.

Comparison of the magnitudes of the $^1J_{\text{SeP}}$ coupling constants of phosphine selenides is an established method for assessing the basicity of the lone pair on the parent phosphine (see Section 1.1.3).^{44, 45} With this in mind, the selenides **2-1.Se** and **2-2.Se** of phosphine-alkenes **2-1** and **2-2** were synthesised through reaction of the parental phosphine with elemental grey selenium with quantitative conversion (Scheme 2.8). The values of $|^1J_{\text{SeP}}|$ for **2-1.Se** and **2-2.Se** of 792 Hz and 734 Hz, respectively, indicate that the P-donor components of **2-1** and **2-2** are both weakly basic when compared to trialkylphosphines, for example PMe_3 ($^1J_{\text{SeP}} = 684$ Hz), and akin to triarylphosphines for example PPh_3 ($^1J_{\text{SeP}} = 736$ Hz).⁴⁶ The magnitude of the $^1J_{\text{SeP}}$ for **2-2.Se** shows that the phosphorus donor moiety of **2-2** is more basic than **2-1**, which is consistent with alkylphosphines being more electron rich than arylphosphines, nevertheless the P-donor component of both **2-1** and **2-2** should be considered weakly basic.

Since a comparison of the $|^1J_{\text{SeP}}|$ values only assesses the electronic character of the lone pair on the phosphorus component of the P-alkene framework, a complementary technique was required in order to probe the cumulative electronic character of each half of the P-alkene ligands as a whole. To this end, two indirect approaches that use the spectroscopic study of metal-carbonyls are detailed.

2.2.3.2 Synthesis of a rhodium carbonyl complex of **2-1**



Scheme 2.9: Synthesis of $[\text{Rh}(\text{CO})(\kappa^2\text{-P,C-2-1})_2]\text{Cl}$ (**2-3**).

Chapter 1 introduced the use of rhodium carbonyl complexes, specifically $[\text{RhCl}(\text{CO})(\text{P}^\wedge\text{L})]$ (where P^\wedgeL is a bidentate ligand containing a phosphorus donor), to assess the electronic character of a bidentate ligand. Therefore, we attempted to synthesise the necessary complex $[\text{RhCl}(\text{CO})(\kappa^2\text{-P,C-2-1})]$. However, addition of either one or two equivalents of P-alkene **2-1** ($\text{Rh}:\text{P} = 1:1$ or $1:2$) to a chloroform solution of $[\text{RhCl}(\text{CO})_2]_2$ resulted in the formation of $[\text{Rh}(\text{CO})(\kappa^2\text{-P,C-2-1})_2]\text{Cl}$ (**2-3**). Complex **2-3** was characterised by multinuclear NMR spectroscopy ($\delta^{31}\text{P}$ 91.4 ppm, $^1J_{\text{RhP}} = 89$ Hz) and infrared spectroscopy; the infrared spectrum of **2-3** (deuterated chloroform solution) revealed a single band in the expected carbonyl region at 1993 cm^{-1} . This gives **2-3** the highest carbonyl stretching frequency of all known 5-coordinate rhodium-carbonyl complexes, (for example $[\text{Rh}(\text{CO})(\text{dppm})_2]\text{BF}_4$ (ν_{CO} (Nujol) 1948 cm^{-1}) and $[\text{Rh}(\text{CO})(\text{dppp})]\text{BF}_4$ (ν_{CO} (Nujol) 1930 cm^{-1}).⁴⁷ As **2-3** exhibits a higher carbonyl stretching frequency than $[\text{Rh}(\text{CO})(\text{dppm})_2]\text{BF}_4$ and $[\text{Rh}(\text{CO})(\text{dppp})_2]\text{BF}_4$ we suggest that overall **2-1** is more electron withdrawing than the bidentate diphosphines dppm and dppp , something resulting from the coordination of the electron-accepting alkene moiety. To confirm the electron deficient nature of **2-1** an alternative method of assessing the electronic properties of the P-alkene ligands **2-1** and **2-2** was sought.

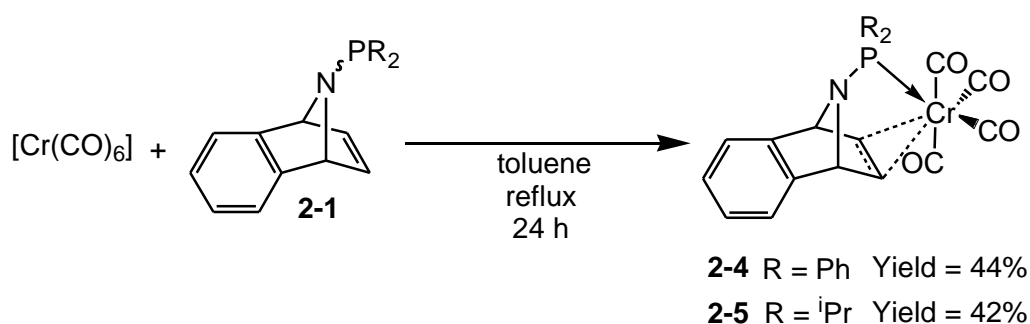
2.2.3.3 Synthesis of chromium carbonyl complexes $[\text{Cr}(\text{CO})_4(\kappa^2\text{-P,C-2-1})]$ (**2-4**) and $[\text{Cr}(\text{CO})_4(\kappa^2\text{-P,C-2-2})]$ (**2-5**)

The synthesis of chromium carbonyl complexes of the type $[\text{Cr}(\text{CO})_4(\kappa^2\text{-(L}^1\wedge\text{L}^2))]$ is an established method for estimating the electron-withdrawing/-donating ability of a bidentate ligand by infrared spectroscopic analysis of the metal carbonyl units. However, the results tend to be less definitive and more descriptive than in the use of rhodium carbonyl complexes as there are multiple carbonyl stretching bands and small

changes in geometry around the metal alter the stretching frequencies observed. For example, the diphosphine ligands presented in Table 2.2 all have a similar electronic character, but there is slight variation in the carbonyl stretching frequencies.

Complex	$\nu_{(\text{CO})}$ (toluene) / cm^{-1}
$[\text{Cr}(\text{CO})_4(\text{dppm})]$	2012, 1922, 1903, 1891
$[\text{Cr}(\text{CO})_4(\text{dppe})]$	2020, 1929, 1917, 1897
$[\text{Cr}(\text{CO})_4(\text{dppp})]$	2015, 1935, 1907, 1890

Table 2.2: Chromium carbonyl stretching frequencies for diphosphine chromium carbonyl complexes.⁴⁸



Scheme 2.10: Synthesis of $[\text{Cr}(\text{CO})_4(\kappa^2\text{-P,C-2-1})]$ (**2-4**) and $[\text{Cr}(\text{CO})_4(\kappa^2\text{-P,C-2-2})]$ (**2-5**).

From the reaction of equimolar quantities of either **2-1** or **2-2** with $[\text{Cr}(\text{CO})_6]$ in toluene at reflux for 24 h (Scheme 2.10), followed by subsequent precipitation, the complexes $[\text{Cr}(\text{CO})_4(\kappa^2\text{-P,C-2-1})]$ (**2-4**) and $[\text{Cr}(\text{CO})_4(\kappa^2\text{-P,C-2-2})]$ (**2-5**), respectively, were isolated in moderate yields. Complex **2-4** was characterised by multinuclear NMR spectroscopy and mass spectrometry (ASAP+). Its $^{31}\text{P}\{^1\text{H}\}$ NMR spectrum presented a singlet resonance at 131.7 ppm, with a coordination chemical shift ($\Delta\delta$) of 90.1 ppm relative to **2-1**; ^{13}C NMR spectroscopy showed a $\Delta\delta$ of -59.8 ppm for the alkene carbon atoms and that there were three metal-bound carbonyl environments, consistent with a $[\text{Cr}(\text{CO})_4(\text{L}^1\wedge\text{L}^2)]$ system.⁴⁹ Infrared spectroscopy was performed in the solid state (Nujol mull) and revealed four carbonyl stretching bands at 2017, 1952, 1915 and 1884 cm^{-1} , as expected for a **2-4**, which has C_{2v} symmetry. Overall, the carbonyl bands for **2-4** are at higher frequency than those for $[\text{Cr}(\text{CO})_4(\text{dppe})]$ ($\nu_{(\text{CO})}$ (Nujol) 2001, 1907, 1883 and, 1865 cm^{-1})⁵⁰, which suggests that **2-1** is significantly more electron withdrawing than dppe, as would be expected.

Complex **2-5** was characterised by multinuclear NMR spectroscopy and CHN analyses, with ^1H and ^{13}C NMR spectroscopic data for the alkene-containing moiety closely resembling those of **2-4**. The infrared spectrum of **2-5** (Nujol mull) revealed only three distinct carbonyl stretching bands at 1911(broad), 1921 and 2015 cm^{-1} . As a result of these overlapping bands, it is difficult to draw any conclusions from the comparison of the carbonyl stretching frequencies of **2-4** and **2-5**.

2.2.3.3.1 X-Ray crystallographic study of $[\text{Cr}(\text{CO})_4(\kappa^2\text{-P,C-2-1})]$ (**2-4**)

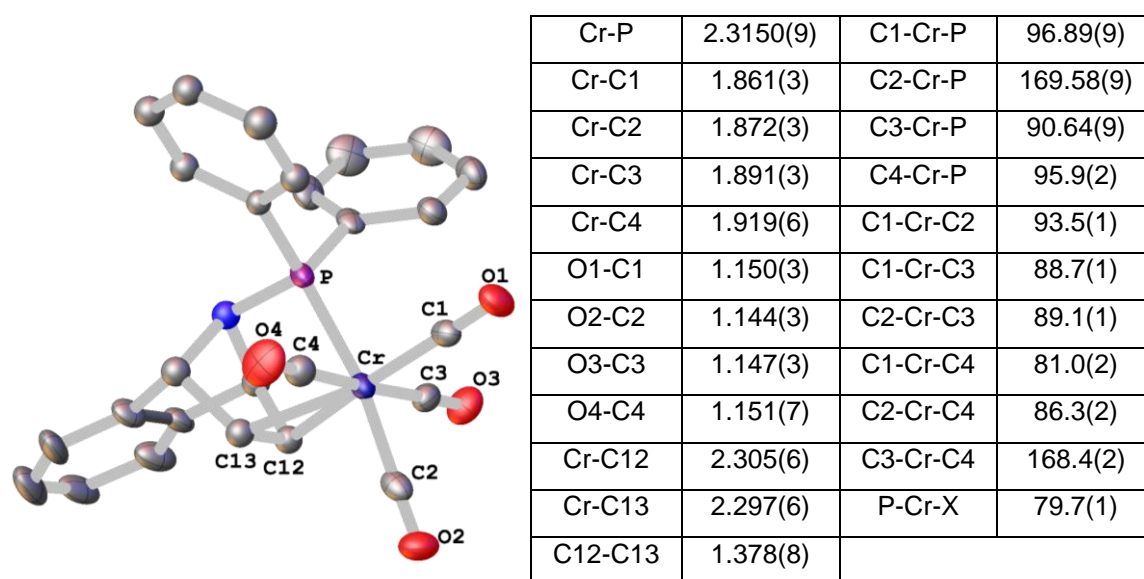


Figure 2.6: Molecular structure of $[\text{Cr}(\text{CO})_4(\kappa^2\text{-P,C-2-1})]$ (**2-4**) with selected bond lengths (Å) and angles ($^\circ$). X is the midpoint of C(12)=C(13), (thermal ellipsoids set at 50% level).

Single crystals of complex **2-4** were grown by layering a concentrated DCM solution with methanol. Subsequent X-ray diffraction analysis shows that complex **2-4** presents a distorted octahedral structure about chromium, with the bite-angle of **2-1**, measured by the P-Cr-X angle (where X is the midpoint of C(12)=C(13)), being 79.7(1) $^\circ$ (cf. $\angle\text{P-Cr-P} = 83.48(8)^\circ$ in $[\text{Cr}(\text{CO})_4(\text{dppe})]$)⁵¹ (Figure 2.6). The chromium carbonyl bond distances (Cr-C) are identical for carbonyl groups located *trans* to the alkene (1.861(3) Å) and the phosphorus group (1.872(3) Å), surprisingly showing that there is little difference in the *trans*-influence between the two donor moieties of **2-1**. In line with moderate metal $\rightarrow\pi^*(\text{C}=\text{C})$ retro-donation, the C(12)=C(13) alkene bond in **2-4** (1.378(8) Å) is longer than the corresponding bond in an uncoordinated 7-aza-benzobicyclo[2.2.1]hept-2-ene fragment in complex **2-10** (1.331(2) Å) (Figure 2.7).

Unfortunately, despite repeated attempts, single crystals of **2-5** suitable for X-ray diffraction could not be grown to compare the solid state structure of **2-4** and **2-5**.

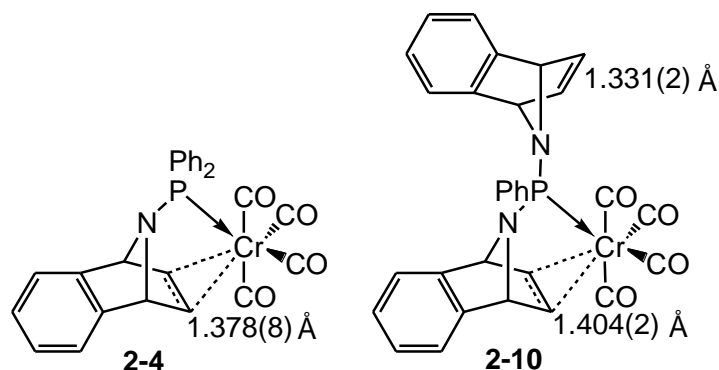
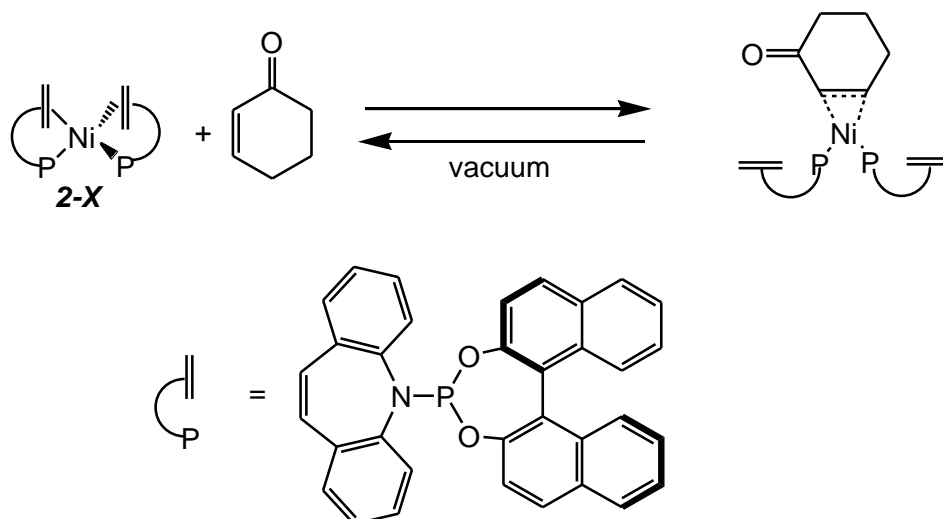


Figure 2.7: Comparison of the C–C alkene bond lengths in complexes **2-4** and **2-10** determined by single crystal X-ray diffraction.

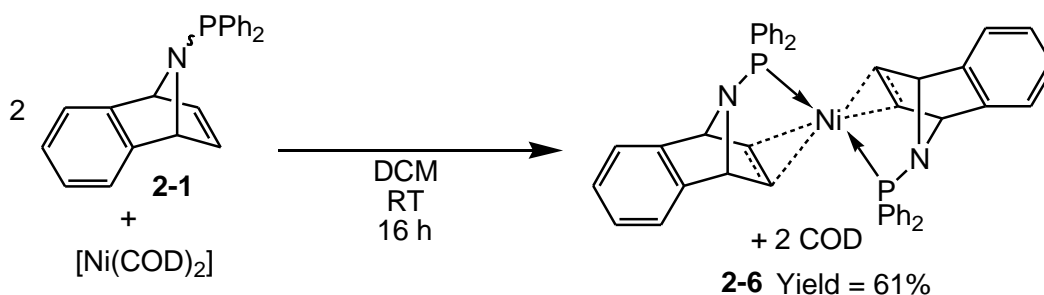
2.2.4 Synthesis of $[\text{Ni}(\kappa^2\text{-P,C-2-1})_2]$ (**2-6**)

There are numerous organic reactions which are catalysed by Ni(0) complexes,⁵² including cross-couplings,^{53, 54} hydrocyanation of alkenes,⁵⁵ hydroamination of dienes⁵⁶ and the carbonylation of dienes.⁵⁷ However, to the best of our knowledge there are no known nickel-catalysed processes involving P-alkene ligands. It was therefore of interest to synthesise a nickel(0) complex of ligand **2-1** and to test it as a homogeneous catalyst. Whilst there are no known nickel-catalysed transformations involving P-alkene ligands, Dorta *et al.* have recently shown that complex **2-X** containing a P-alkene ligand forms a 18ve, Ni(0)L₄ complex that can reversibly bind α,β -unsaturated carbonyl compounds, upon alkene dissociation (Scheme 2.11), a feature that could have applications in catalysis.⁵⁸

Given that the P-alkene ligand in complex **2-X** (Scheme 2.11) showed hemilabile properties it was of interest to synthesise the analogous nickel(0) complex $[\text{Ni}(\kappa^2\text{-P,C-2-1})_2]$ (**2-6**), to compare the reactivity between the two nickel(0) complexes. It was predicted that the alkene group of **2-1** would bind more strongly to a nickel(0) centre than that of the P-alkene ligand in **2-X**, by virtue of the alkene group being located within a strained 5-membered ring, something that could lead to significantly different reactivity.



Scheme 2.11: *P*-alkene-containing nickel(0) complex **2-X**, developed by Dorta and co-workers, can reversibly add α,β -unsaturated carbonyl compounds.⁵⁸



Scheme 2.12: Synthesis of $[\text{Ni}(\kappa^2\text{-P,C-2-1})_2]$ (**2-6**).

Complex **2-6** was synthesised in moderate yield (61%) by treating two equivalents of **2-1** with $[\text{Ni}(\text{COD})_2]$ in DCM overnight (Scheme 2.12). Subsequent recrystallization afforded **2-6** as a bright yellow crystalline solid (MS-ASAP+ m/z 712). $^{31}\text{P}\{^1\text{H}\}$ NMR spectroscopy revealed a singlet resonance at 99.9 ppm ($\Delta\delta$ +58 ppm). As expected, each carbon nucleus of the alkene group of Ni-bound **2-1** is in a slightly different chemical environment in tetrahedral **2-6** (the tetrahedral geometry is confirmed by a single crystal X-ray diffraction study described later), leading to two resonances for the alkene group in both its ^1H (3.91-3.92 and 3.95-3.99 ppm) and $^{13}\text{C}\{^1\text{H}\}$ (68.8 and 72.1 ppm) NMR spectra, presenting a coupling pattern consistent with the 'AB' part of an 'ABX' system. The $^{13}\text{C}\{^1\text{H}\}$ NMR spectrum of **2-6** shows that the alkene carbons have a significantly different chemical shift (68.9 and 72.1 ppm) compared to those of the free ligand (**2-1**) (143.0 ppm), something that has been attributed to a large π -back-bonding component for the alkene-nickel bond, consistent with a reduction of the double bond character (*i.e.* the alkene group is now significantly more 'alkane like').

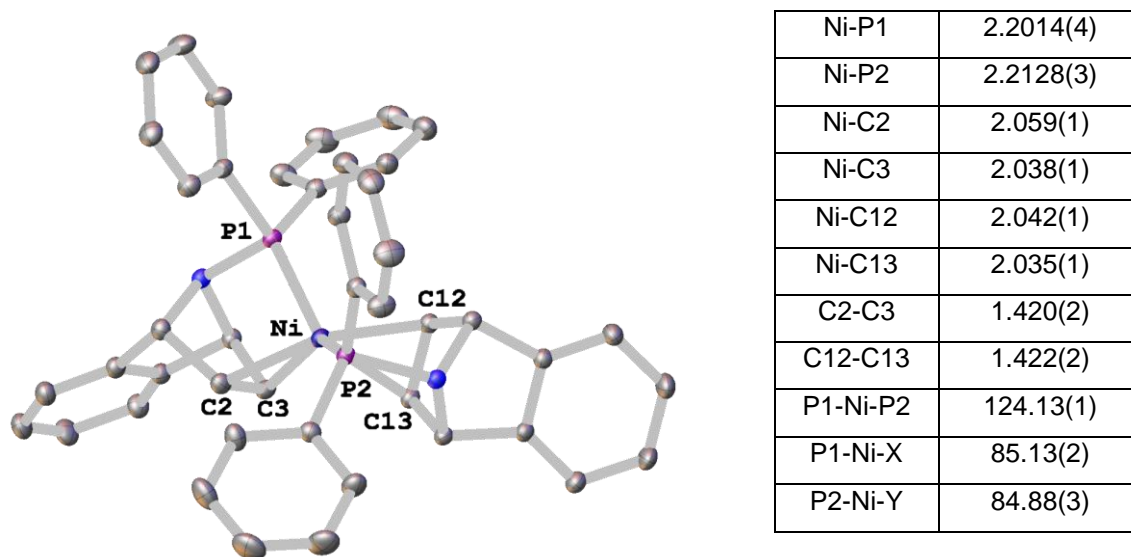
2.2.4.1 X-Ray crystallographic study of $[\text{Ni}(\kappa^2\text{-P,C-2-1})_2]$ (**2-6**)

Figure 2.8: Molecular structure of $[\text{Ni}(\kappa^2\text{-P,C-2-1})_2]$ (**2-6**) with selected bond lengths (Å) and angles (°). X is the midpoint of C(12)=C(13), Y is the midpoint of C(2)=C(3), (thermal ellipsoids set at 50% level).

Single crystals of complex **2-6** suitable for X-ray diffraction were grown by slow diffusion of hexane into a concentrated toluene solution. The resulting molecular structure is shown in Figure 2.8 and confirms that ligand **2-1** is indeed bound in a bidentate $\kappa^2\text{-P,C}$ fashion. The nickel centre of **2-6** presents a distorted tetrahedral structure with a P1-Pd-P2 angle of $124.13(1)^\circ$ and an angle between the two planes defined by the atoms P1-Pd-X and P2-Pd-Y of $90.91(3)^\circ$. The P1-Ni-X and P2-Ni-Y bite-angles of **2-1** are $85.13(2)^\circ$ and $84.88(3)^\circ$, respectively, which are significantly larger than that of complex $[\text{Cr}(\text{CO})_4(\kappa^1\text{-P,C-2-1})]$ **2-4** ($79.7(1)^\circ$). The mean Ni-P and Ni-C distances for **2-6** are $2.2071(5)$ and $2.0435(13)$, respectively, which are comparable with those determined for **2-XI** (Figure 2.9) of $2.199(1)$ and $2.041(5)$.⁵⁹

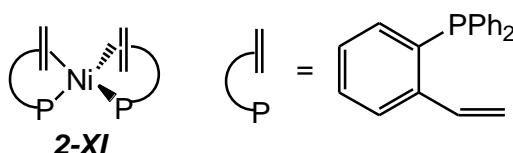
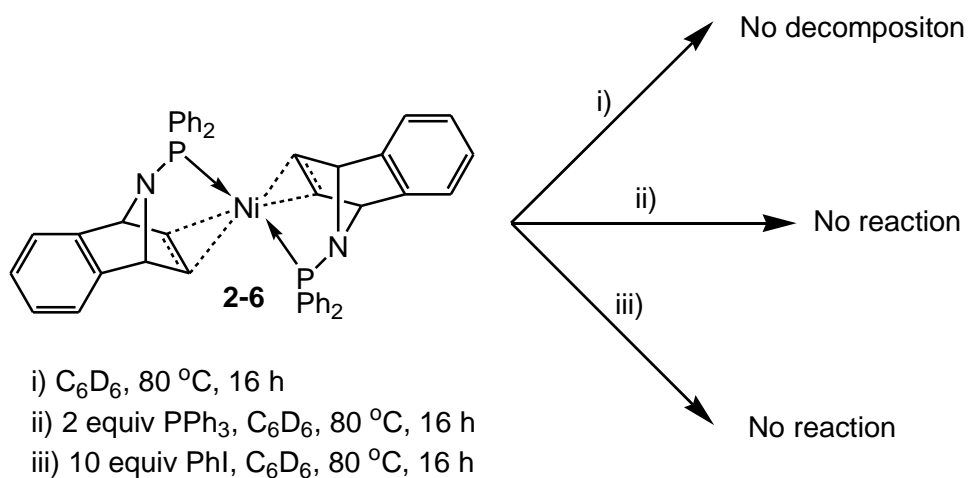


Figure 2.9: $[\text{Ni}(\text{P-alkene})_2]$ **2-XI** complex developed by Bennett and co-workers.⁵⁹

2.2.4.2 Stability and reactivity of $[\text{Ni}(\kappa^2\text{-P,C-2-1})_2]$ (**2-6**)



Scheme 2.13: $[\text{Ni}(\kappa^2\text{-P,C-2-1})_2]$ (**2-6**), a remarkably stable and unreactive $\text{Ni}(0)$ complex.

Remarkably, complex **2-6** is stable in moist air and solution (under air in non-dried solvent) for several days, in contrast to Bennett's $[\text{Ni}(\text{P-alkene})_2]$ complex **2-XI**, which is reported to be air-sensitive.⁵⁹ Furthermore, complex **2-6** is highly thermally stable in the solid state and in solution, with the onset of decomposition of **2-6** being 190 °C in the solid state, while a C_6D_6 solution of complex **2-6** could be heated at 80 °C for 16 h with no decomposition detected by $^{31}\text{P}\{^1\text{H}\}$ NMR spectroscopy^a (Scheme 2.13). The stability of **2-6** is further exemplified by its lack of reaction with chlorinated solvents (e.g. d_2 -DCM and CDCl_3). In contrast, all other known $[\text{Ni}(\text{P-alkene})_2]$ complexes are reported to react with such chlorinated solvents leading to decomposition.^{58, 59} Indeed, not only is complex **2-6** stable in d_2 -DCM for days, but it also doesn't react with iodobenzene, even when heated to 80 °C for 16 h (Scheme 2.13).

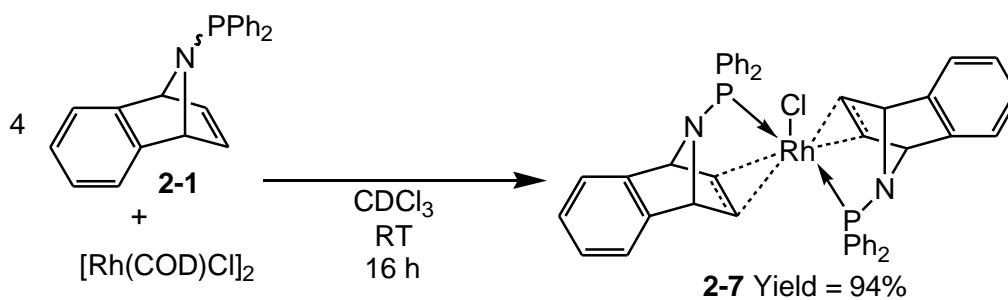
In order to probe the strength with which the alkene moieties of **2-1** are bound to the nickel centre an additional phosphine ligand was added to a solution of **2-6** in an attempt to displace the alkene groups. Specifically, the addition of two equivalents of triphenylphosphine to **2-6** did not lead to the displacement of the alkene groups, even after heating at 80 °C for 16 h, analysis by $^{31}\text{P}\{^1\text{H}\}$ NMR spectroscopy revealed only resonances for **2-6** and free PPh_3 . Together these observations suggest that the alkene moieties are strongly bound in **2-6** and that **2-1** is not a hemilabile ligand with $\text{Ni}(0)$.

^a With reference to an internal phosphorus-containing standard (PPh_3) located within a sealed capillary

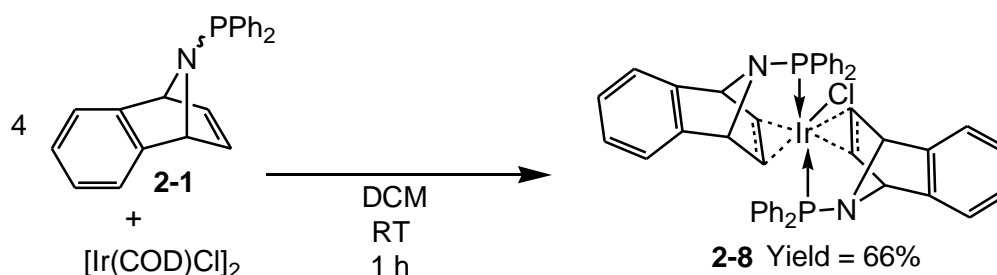
The high thermal and chemical stability of **2-6** can be related to the highly electron-withdrawing nature of **2-1**, which stabilises the electron rich nickel centre and the strong nickel-alkene bond keeps **2-6** coordinatively saturated. However, the high affinity of **2-1** for nickel(0) will limit its application as a homogeneous catalyst, hence a different metal centre with a lower affinity for alkenes or a different geometry is required.

2.2.5 Coordination chemistry of **2-1** with rhodium and iridium metal fragments

It was of interest to synthesise the group 9 complexes of ligand **2-1**, namely $[\text{RhCl}(\kappa^2\text{-P,C-2-1})_2]$ (**2-7**) and $[\text{IrCl}(\kappa^2\text{-P,C-2-1})_2]$ (**2-8**), as chloride abstraction would leave a free coordination site at a highly Lewis acidic metal centre.



Scheme 2.14: Synthesis of $[\text{RhCl}(\kappa^2\text{-P,C-2-1})_2]$ (**2-7**).



Scheme 2.15: Synthesis of $[\text{IrCl}(\kappa^2\text{-P,C-2-1})_2]$ (**2-8**).

To this end, $[\text{RhCl}(\text{COD})]_2$ and $[\text{IrCl}(\text{COD})]_2$ were treated with four equivalents of **2-1**, which resulted in the formation of the monomeric 5-coordinate complexes $[\text{RhCl}(\kappa^2\text{-P,C-2-1})_2]$ (**2-7**) and $[\text{IrCl}(\kappa^2\text{-P,C-2-1})_2]$ (**2-8**) in good yield (Scheme 2.14 and Scheme 2.15). Both complexes have been characterised by multinuclear NMR spectroscopy.

Complex **2-7** exhibits a single doublet resonance at δ ^{31}P 90.9 ppm with a $^1J_{\text{RhP}}$ coupling of 103 Hz ($\Delta\delta$ +49.3 ppm), while **2-8** displays a singlet resonance at δ ^{31}P 61.2 ppm ($\Delta\delta$ +19.6 ppm).

2.2.5.1 X-Ray crystallographic study of $[\text{RhCl}(\kappa^2\text{-P,C-2-1})_2]$ (**2-7**)

Crystals of **2-7** suitable for single crystal X-ray diffraction were grown by layering a concentrated DCM solution with hexane. Complex **2-7** was subsequently found to have a distorted square-based pyramidal geometry about rhodium, with the chloride ligand occupying an axial site with a Rh-Cl bond distance of 2.4744(5) Å (Figure 2.10). This bond is significantly shorter than the equivalent bond distance in $[\text{RhCl}(\text{dppm})_2]$, 2.615(2) Å.⁶⁰ The short Rh-Cl bond of complex **2-7** is believed to be due to the electron poor nature of the rhodium centre, resulting from the presence of the electron-withdrawing alkene moiety, creating a strong ionic component to the Rh-Cl bond.

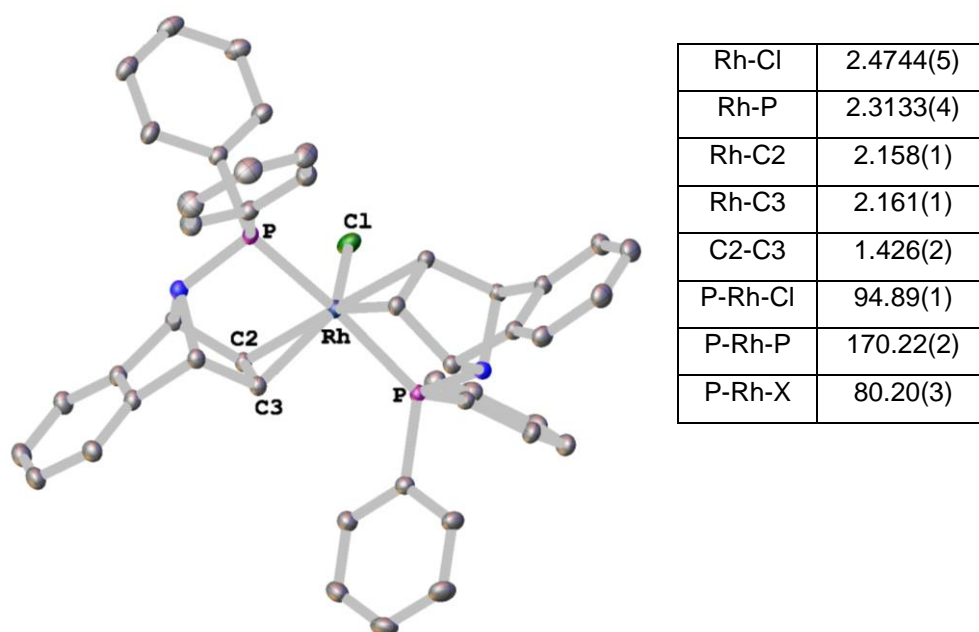


Figure 2.10: Molecular structure of $[\text{RhCl}(\kappa^2\text{-P,C-2-1})_2]$, **2-7**, with selected bond lengths (Å) and angles (°). X is the midpoint of C(2)=C(3). The molecular structure contains a molecule of DCM that is omitted for clarity, (thermal ellipsoids set at 50% level).

2.2.5.2 X-Ray crystallographic study of $[\text{IrCl}(\kappa^2\text{-P,C-2-1})_2]$ (**2-8**)

Unlike $[\text{RhCl}(\kappa^2\text{-P,C-2-1})_2]$ (**2-7**) the analogous iridium complex was found to have a distorted trigonal bipyramidal geometry about its metal centre with the phosphine

moieties occupying the axial sites with an Ir-P bond distance of 2.3128(9) Å (Figure 2.11). There are examples of 5-coordinate iridium chloride complexes containing two bidentate ligands that adopt both a distorted trigonal bipyramidal and a distorted square-based pyramidal geometry (Figure 2.12).^{61, 62} We postulate that the distorted trigonal bipyramidal geometry is observed in **2-8** to avoid placing the highly *trans*-influencing alkene moieties in a *trans*-orientation.

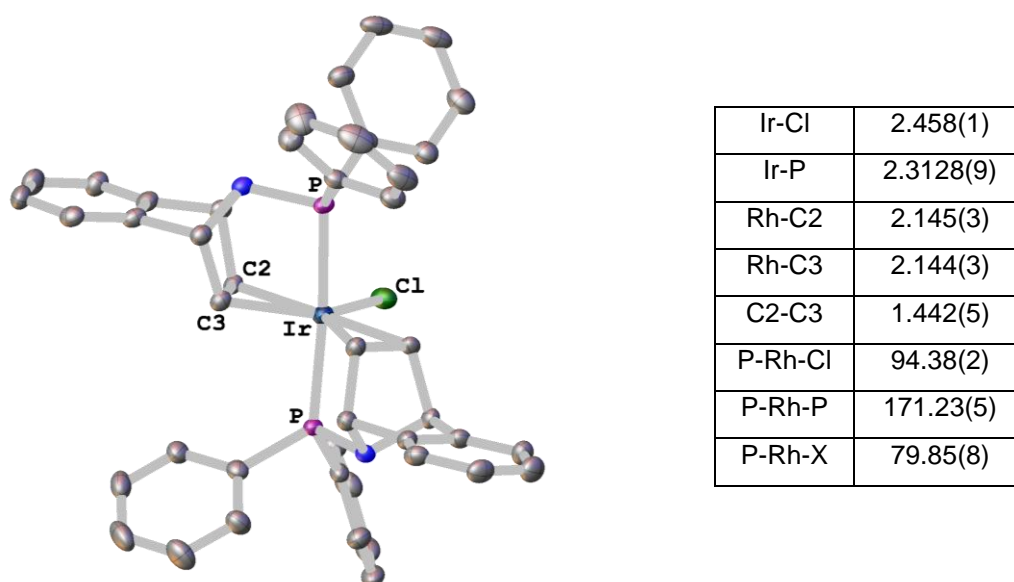


Figure 2.11: Molecular structure of $[\text{IrCl}(\kappa^2\text{-P,C-2-1})_2]$, **2-8**, with selected bond lengths (Å) and angles (°). X is the midpoint of C(2)=C(3), (thermal ellipsoids set at 50% level).

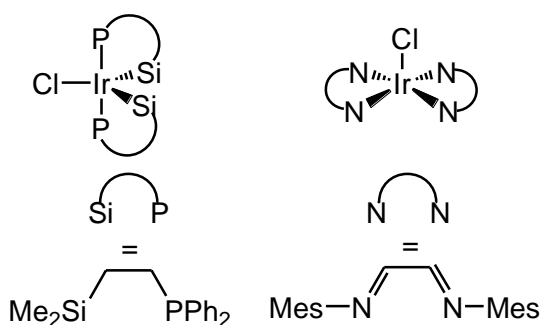


Figure 2.12: Structurally characterised 5-coordinate iridium(III) and iridium(I) chloride complexes containing two bidentate ligands.^{61, 62}

2.3 Synthesis and coordination chemistry of a potentially tridentate P-dialkene ligand, *N*-PPh-*bis*-7-aza-benzobicyclo[2.2.1]hept-2-ene (**2-9**)

Ligands that contain a phosphine and two alkene donors (P-dialkenes) are comparatively rare compared to P-alkene ligands. Yet, complexes bearing tridentate (κ^3 -P,C,C)P-dialkene ligands are known, based on flexible alkene-containing moieties including TROPP,⁶³ and allyloxy-based systems (Figure 2.13).⁶⁴ Hence, it was of interest to synthesise a P-dialkene compound based on the 7-aza-benzobicyclo[2.2.1]hept-2-ene alkene moiety, to see if it could act as a tridentate ligand. It was anticipated that the alkene group of 7-aza-benzobicyclo[2.2.1]hept-2-ene would bind more strongly to a metal centre than known P-dialkene ligands due to its rigid structure, giving greater control over the environment at the metal centre.

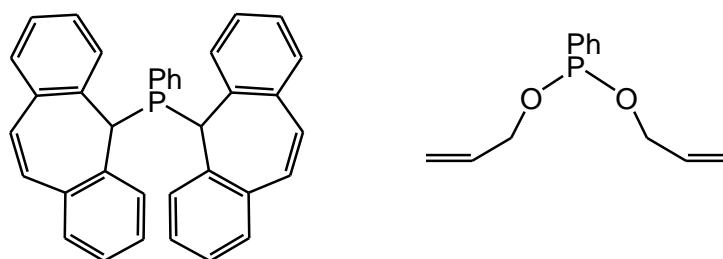
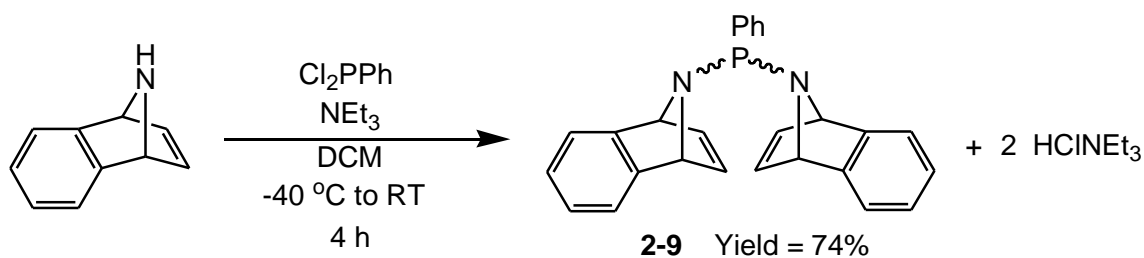


Figure 2.13: Known P-dialkene ligands.^{63, 64}

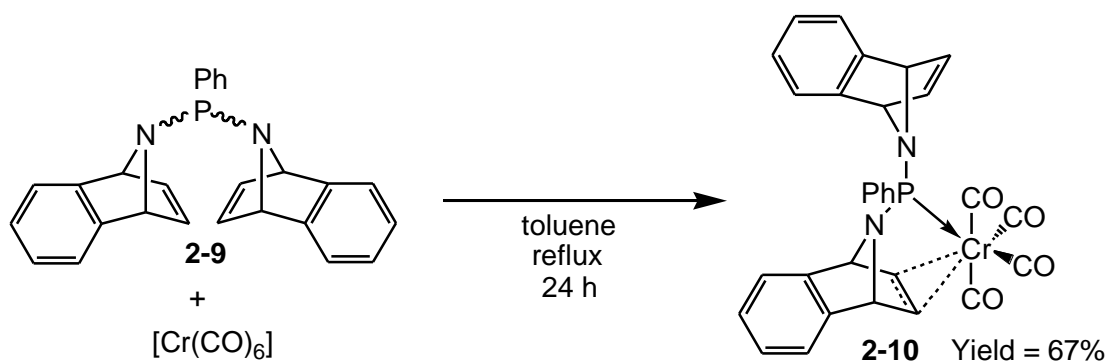
To this end, the compound *N*-PPh-*bis*-7-aza-benzobicyclo[2.2.1]hept-2-ene (**2-9**) was prepared in good yield from 7-aza-benzobicyclo[2.2.1]hept-2-ene *via* the addition of dichlorophenylphosphine in the presence of an amine base (Scheme 2.16). Purification of **2-9** is achieved by recrystallisation from a hot hexane solution affording complex **2-9** as a pale orange solid. The $^{31}\text{P}\{^1\text{H}\}$ NMR spectrum of **2-9** exhibits a singlet resonance at 56.9 ppm, consistent with known diamminophosphines, e.g. $\text{P}(\text{N}^i\text{Pr}_2)_2\text{Ph}$ δ ^{31}P 59.2 ppm.⁴³ The ^1H and $^{13}\text{C}\{^1\text{H}\}$ NMR spectra of **2-9** show two resonances for every proton and carbon atom in each 7-aza-benzobicyclo[2.2.1]hept-2-ene moiety, which is presumed to result from hindered rotation around the P-N bonds, which removes the mirror plane passing through the middle of the alkene group.



Scheme 2.16: Synthesis of compound **2-9**.

Subsequently, compound **2-9** was coordinated to a chromium carbonyl fragment; this was done for two reasons. Firstly, its coordination was used to assess the preference of **2-9** to bind in a bidentate or tridentate manner. Secondly, the carbonyl stretching frequencies can be measured by infrared spectroscopy, which provides a means of assessing the electronic nature of the ligand.

2.1.1. Coordination chemistry of *N*-PPH-*bis*-7-aza-benzobicyclo[2.2.1]hept-2-ene (**2-9**) with a chromium carbonyl metal fragment



Scheme 2.17: Synthesis of $[\text{Cr}(\text{CO})_4(\kappa^2\text{-P,C-2-9})]$ (**2-10**).

Heating a mixture of **2-9** and $[\text{Cr}(\text{CO})_6]$ in toluene at reflux for 24 h (Scheme 2.17), followed by induced precipitation of the subsequent complex from a concentrated DCM solution by addition of methanol, afforded $[\text{Cr}(\text{CO})_4(\kappa^2\text{-P,C-2-9})]$ (**2-10**) in moderate yield (67%). Complex **2-10** was characterised by multinuclear NMR spectroscopy ($^{31}\text{P}\{^1\text{H}\}$: 156.9 ppm; $\Delta\delta = +100.0$ ppm). Analysis of the complex by $^{13}\text{C}\{^1\text{H}\}$ NMR spectroscopy revealed that only one of the two alkene groups of **2-9** was bound to the chromium centre, with resonances for the alkene groups of **2-9** being found at 83.6 and

141.9 ppm, $\Delta\delta$ -60.6 and -2.3 ppm, respectively. It is proposed that the inflexible ligand **2-9** cannot adopt the correct geometry to adopt tridentate coordination and hence reacts with $[\text{Cr}(\text{CO})_6]$ to give only κ^2 -P,C coordination in **2-10**.

The only known example of a structurally characterised chromium tricarbonyl complex containing a tridentate ligand (with at least one of the donors being P), which forms two 5-membered chelate rings is with the triphos ligand (Figure 2.14).^{65, b} Triphos is a significantly more flexible ligand than **2-9** and thus can bind to the chromium centre in a *fac* orientation.

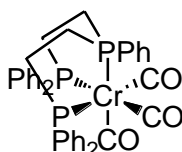


Figure 2.14: The structure of previously reported $[\text{Cr}(\text{CO})_3(\kappa^3\text{-P,P,P-triphos})]$.⁶⁵

The infrared spectrum of complex **2-10** displayed the expected four carbonyl stretching bands at 2016, 1952, 1919, 1890 cm^{-1} , which are very similar to those of complex **2-4**, $[\text{Cr}(\text{CO})_4(\kappa^2\text{-P,C-2-1})]$, (2017, 1952, 1915 and 1884 cm^{-1}). This suggests that the metal-bound P-alkene fragments in complexes **2-4** and **2-9** both have a comparable electronic character, as would be expected.

^b CSD search 29/11/13

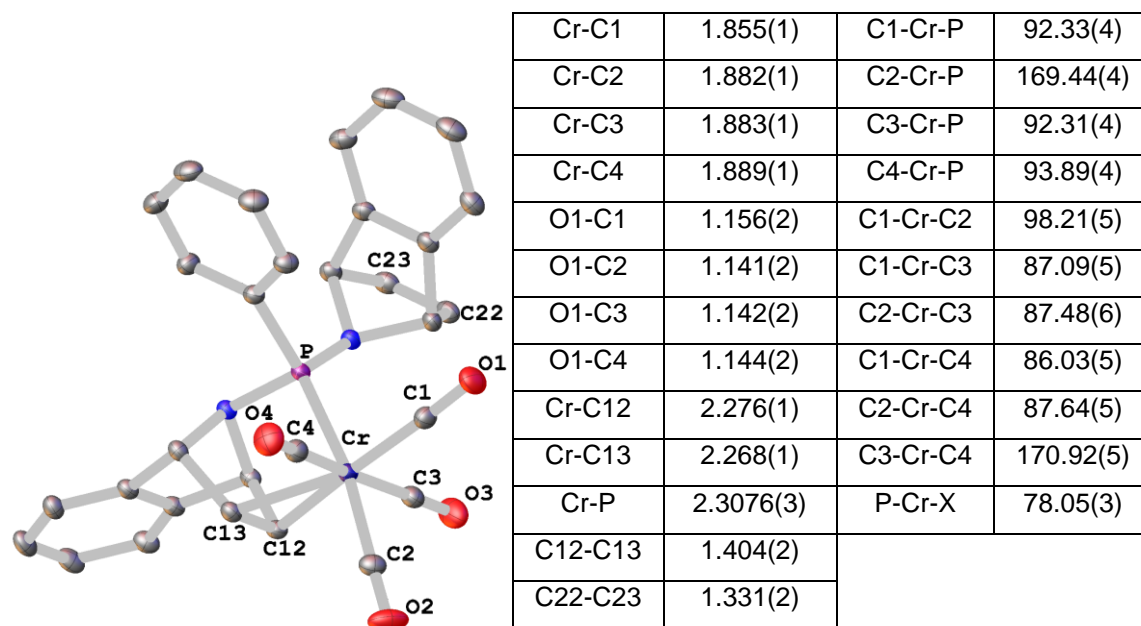
2.3.1.1 X-Ray crystallographic study of $[\text{Cr}(\text{CO})_4(\kappa^2\text{-P,C-2-9})]$ (**2-10**)

Figure 2.15: Molecular structure of $[\text{Cr}(\text{CO})_4(\kappa^2\text{-P,C-2-9})]$ (**2-10**) with selected bond lengths (Å) and angles (°). X is defined as the midpoint of C(12)=C(13), (thermal ellipsoids set at 50% level).

Following growth of single crystals of complex **2-10** by layering a concentrated DCM solution with methanol, an X-ray crystallographic study was undertaken. Subsequently, the chromium centre of **2-10** was found to have a distorted octahedral geometry; all the bond distances and angles about chromium are similar to those determined for **2-4** (Figure 2.15). The molecular structure confirms $\kappa^2\text{-P,C}$ coordination of **2-9** to chromium, consistent with the inferences made from solution-state NMR spectroscopy, with both the unbound alkene moiety and the P-bound Ph group pointing away from the chromium centre, presumably to minimise steric repulsion. The metal-bound and uncoordinated alkene groups have considerably different bond lengths (1.404(2) and 1.331(2) Å, respectively), as expected, highlighting the impact of metal $\rightarrow\pi^*(\text{C}=\text{C})$ retro-donation leading to bond lengthening.

2.4 Chapter 2 summary and conclusions

Two novel phosphine-alkene ligands, **2-1** and **2-2**, both based around a 7-aza-benzobicyclo[2.2.1]hept-2-ene moiety, have been synthesised. The modular synthesis and the ease of making a P-N bond allows facile modification of the steric and electronic properties of the phosphine moiety. The structure of the ligand locates the alkene moiety in a constrained, rigid 5-membered ring, which encourages strong alkene metal binding in order to relieve ring strain.

As proposed, the diphenylphosphino-substituted bidentate P-alkene ligand **2-1** is more electron-withdrawing than bidentate diphosphines such as dppe, based upon interpretation of infrared stretching frequencies of rhodium (**2-3**) and chromium (**2-4**) carbonyl complexes. Based upon consideration of the values of $|^1J_{\text{SeP}}|$ for the corresponding phosphine selenides of **2-1** and **2-2**, the basicity of the phosphine moiety of **2-1** is less than that of triphenylphosphine, something that also makes a significant contribution to the overall electron-withdrawing effect of the ligand. Moreover, ligand **2-2** is less electron-withdrawing than **2-1**, with the basicity of the phosphine moiety being greater.

The coordination chemistry of **2-1** to various transition metal fragments was accomplished. The electron-withdrawing properties of **2-1** are exemplified in the tetrahedral nickel(0) complex **2-6** which is remarkably stable, being resistant to the addition of iodobenzene, reaction with chlorinated solvents and phosphines such as PPh_3 . Rhodium(I) (**2-7**) and iridium(I) (**2-8**) complexes of **2-1** were synthesised in a facile manner from $[\text{MCl}(\text{COD})]_2$ ($\text{M} = \text{Rh}, \text{Ir}$) precursors and interestingly exhibited different coordination geometries about their metal centres, squared based pyramid and trigonal bipyramidal respectively, as determined by single crystal X-ray diffraction.

To further probe the chemistry and coordination of phosphine-alkene ligands, the synthesis of a ligand with potentially one phosphine and two alkene donor sites was achieved (**2-9**). However, ligand **2-9** was shown to bind in a bidentate (P-alkene) fashion to a chromium carbonyl fragment, with the rigid structure of the backbone not allowing the adoption of the *fac* coordination geometry.

Building on these preliminary coordination studies, the utility of ligand **2-1** in Pd-mediated catalytic transformations will be looked at in chapter 3. We will attempt to exploit the proven electron-deficient nature of **2-1** to promote and develop fundamental understanding into the process of reductive elimination.

2.5 References

1. M. S. Rahman, P. D. Prince, J. W. Steed and K. K. Hii, *Organometallics*, 2002, **21**, 4927-4933.
2. A. Schnyder, A. Togni and U. Wiesli, *Organometallics*, 1997, **16**, 255-260.
3. F. Speiser, P. Braunstein and L. Saussine, *Organometallics*, 2004, **23**, 2625-2632.
4. A. D. Burrows, M. F. Mahon and M. Varrone, *Dalton Trans.*, 2003, 4718-4730.
5. P. W. Dyer, J. Fawcett and M. J. Hanton, *J. Organomet. Chem.*, 2005, **690**, 5264-5281.
6. E. K. van den Beuken, B. L. Feringa, W. J. J. Smeets and A. L. Spek, *Chem. Commun.*, 1998, 223-224.
7. K. R. Reddy, K. Surekha, G.-H. Lee, S.-M. Peng and S.-T. Liu, *Organometallics*, 2000, **19**, 2637-2639.
8. F. Fache, E. Schulz, M. L. Tommasino and M. Lemaire, *Chem. Rev.*, 2000, **100**, 2159-2232.
9. A. Schnyder, L. Hintermann and A. Togni, *Angew. Chem. Int. Ed.*, 1995, **34**, 931-933.
10. C. Defieber, H. Grutzmacher and E. M. Carreira, *Angew. Chem. Int. Ed.*, 2008, **47**, 4482-4502.
11. T. Hayashi, K. Ueyama, N. Tokunaga and K. Yoshida, *J. Am. Chem. Soc.*, 2003, **125**, 11508-11509.
12. C. Fischer, C. Defieber, T. Suzuki and E. M. Carreira, *J. Am. Chem. Soc.*, 2004, **126**, 1628-1629.
13. J. Thomaier, S. Boulmaaz, H. Schonberg, H. Ruegger, A. Currao, H. Grutzmacher, H. Hillebrecht and H. Pritzkow, *New J. Chem.*, 1998, **22**, 947-958.
14. P. Maire, S. Deblon, F. Breher, J. Geier, C. Bohler, H. Ruegger, H. Schonberg and H. Grutzmacher, *Chem. Eur. J.*, 2004, **10**, 4198-4205.
15. E. Piras, F. Lang, H. Ruegger, D. Stein, M. Worle and H. Grutzmacher, *Chem. Eur. J.*, 2006, **12**, 5849-5858.
16. C. Thoumazet, L. Ricard, H. Grutzmacher and P. Le Floch, *Chem. Commun.*, 2005, 1592-1594.
17. C. Defieber, M. A. Ariger, P. Moriel and E. M. Carreira, *Angew. Chem. Int. Ed.*, 2007, **46**, 3139-3143.
18. E. Drinkel, A. Briceño, R. Dorta and R. Dorta, *Organometallics*, 2010, **29**, 2503-2514.
19. T. J. Hoffman and E. M. Carreira, *Angew. Chem. Int. Ed.*, 2011, **50**, 10670-10674.

20. G. Mora, S. van Zutphen, C. Thoumazet, X. F. Le Goff, L. Ricard, H. Grutzmacher and P. Le Floch, *Organometallics*, 2006, **25**, 5528-5532.
21. R. Shintani, W. L. Duan, T. Nagano, A. Okada and T. Hayashi, *Angew. Chem. Int. Ed.*, 2005, **44**, 4611-4614.
22. X. C. Luo, H. Zhang, H. Duan, O. Liu, W. Zhu, T. Zhang and A. Lei, *Org. Lett.*, 2007, **9**, 4571-4574.
23. R. Mariz, A. Briceno and R. Dorta, *Organometallics*, 2008, **27**, 6605-6613.
24. M. Roggen and E. M. Carreira, *Angew. Chem. Int. Ed.*, 2011, **50**, 5568-5571.
25. M. Roggen and E. M. Carreira, *Angew. Chem. Int. Ed.*, 2012, **51**, 8652-8655.
26. M. Lafrance, M. Roggen and E. M. Carreira, *Angew. Chem. Int. Ed.*, 2012, **51**, 3470-3473.
27. J. Y. Hamilton, D. Sarlah and E. M. Carreira, *J. Am. Chem. Soc.*, 2012, **135**, 994-997.
28. C. Thoumazet, H. Grützmacher, B. Deschamps, L. Ricard and P. le Floch, *Eur. J. Inorg. Chem.*, 2006, **2006**, 3911-3922.
29. L. Bettucci, C. Bianchini, W. Oberhauser, M. Vogt and H. Grutzmacher, *Dalton Trans.*, 2010, **39**, 6509-6517.
30. W. L. Duan, H. Iwamura, R. Shintani and T. Hayashi, *J. Am. Chem. Soc.*, 2007, **129**, 2130-2138.
31. R. Shintani, W. L. Duan, K. Okamoto and T. Hayashi, *Tetrahedron: Asymmetry*, 2005, **16**, 3400-3405.
32. R. Shintani, R. Narui, Y. Tsutsumi, S. Hayashi and T. Hayashi, *Chem. Commun.*, 2011, **47**, 6123-6125.
33. R. Narui, S. Hayashi, H. Otomo, R. Shintani and T. Hayashi, *Tetrahedron: Asymmetry*, 2012, **23**, 284-293.
34. D. B. G. Williams and M. L. Shaw, *Tetrahedron*, 2007, **63**, 1624-1629.
35. P. Pongrácz, G. Petőcz, M. Shaw, D. B. G. Williams and L. Kollár, *J. Organomet. Chem.*, 2010, **695**, 2381-2384.
36. T. Minuth and M. M. K. Boysen, *Org. Lett.*, 2009, **11**, 4212-4215.
37. H. Grugel, F. Albrecht, T. Minuth and M. M. K. Boysen, *Org. Lett.*, 2012, **14**, 3780-3783.
38. R. T. Stemmler and C. Bolm, *Synlett*, 2007, 1365-1370.
39. P. Kasak, V. B. Arion and M. Widhalm, *Tetrahedron: Asymmetry*, 2006, **17**, 3084-3090.
40. M. Lautens, K. Fagnou and V. Zunic, *Org. Lett.*, 2002, **4**, 3465-3468.
41. A. Prenzel, N. Deppermann and W. Maison, *Org. Lett.*, 2006, **8**, 1681-1684.

42. A. P. Marchand and R. W. Allen, *J. Org. Chem.*, 1975, **40**, 2551-2552.
43. P. W. Dyer, J. Fawcett, M. J. Hanton, R. D. W. Kemmitt, R. Padda and N. Singh, *Dalton Trans.*, 2003, 104-113.
44. D. W. Allen and B. F. Taylor, *J. Chem. Res., Synop.* 1981, 220-221.
45. D. W. Allen and B. F. Taylor, *J. Chem. Soc., Dalton Trans.*, 1982, 51-54.
46. McFarlan.W and D. S. Rycroft, *J. Chem. Soc., Dalton Trans.*, 1973, 2162-2166.
47. B. R. James and D. Mahajan, *Can. J. Chem.*, 1980, **58**, 996-1004.
48. A. Tekkaya and S. Özkar, *J. Organomet. Chem.*, 1999, **590**, 208-216.
49. M. A. Sierra, I. Fernández, M. J. Mancheño, M. Gómez-Gallego, M. R. Torres, F. P. Cossío, A. Arrieta, B. Lecea, A. Poveda and J. Jiménez-Barbero, *J. Am. Chem. Soc.*, 2003, **125**, 9572-9573.
50. J. A. Iggo and B. L. Shaw, *J. Chem. Soc., Dalton Trans.*, 1985, 1009-1013.
51. K. Maitra and J. H. Nelson, *Polyhedron*, 1998, **18**, 203-210.
52. Y. Tamaru, *Modern Organonickel Chemistry*, WILEY-VCH Verlag GmbH & Co., Weinheim, 2005.
53. J. Zhou and G. C. Fu, *J. Am. Chem. Soc.*, 2003, **125**, 14726-14727.
54. G. Y. Li and W. J. Marshall, *Organometallics*, 2002, **21**, 590-591.
55. J. E. Backvall and O. S. Andell, *Organometallics*, 1986, **5**, 2350-2355.
56. J. Pawlas, Y. Nakao, M. Kawatsura and J. F. Hartwig, *J. Am. Chem. Soc.*, 2002, **124**, 3669-3679.
57. H. Hoberg, S. Gross and A. Milchereit, *Angew. Chem. Int. Ed.*, 1987, **26**, 571-572.
58. A. Linden, L. Llovera, J. Herrera, R. Dorta, G. Agrifoglio and R. Dorta, *Organometallics*, 2012, **31**, 6162-6171.
59. M. A. Bennett, C. Chiraratvatana, G. B. Robertson and U. Tooptakong, *Organometallics*, 1988, **7**, 1394-1402.
60. C.-P. Shao, G.-B. Cheng, J.-Y. Wang and H. F. Guo, *Jeigou Huaxue (Chin. J. Struct. Chem.)*, 1993, **12**, 343.
61. M. J. Auburn, R. D. Holmes-Smith, S. R. Stobart, P. K. Bakshi and T. S. Cameron, *Organometallics*, 1996, **15**, 3032-3036.
62. J. Langer and H. Görls, *Inorg. Chem. Commun.*, 2011, **14**, 1612-1615.
63. F. F. Puschmann, H. Grützmacher and B. d. Bruin, *J. Am. Chem. Soc.*, 2009, **132**, 73-75.
64. H. L. Ji, J. H. Nelson, A. De Cian and J. Fischer, *Organometallics*, 1992, **11**, 1618-1626.

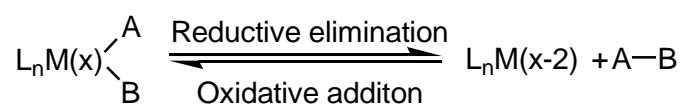
65. M. C. Favas, D. L. Kepert, B. W. Skelton and A. H. White, *J. Chem. Soc., Dalton Trans.*, 1980, 447-453.

3 Phosphine-alkene ligands: promotion of reductive elimination from palladium(II) complexes

3.1 Introduction

The use of palladium complexes as catalysts for cross-coupling reactions is a large and important field of research, with the significance of palladium-catalysed cross-coupling reactions being recognised in 2010 by the award of the Nobel prize to Heck, Negishi and Suzuki for their development and study of ‘palladium-catalysed cross-couplings in organic synthesis’. The generally accepted mechanism for palladium-catalysed cross-coupling reactions proceeds *via* three steps: (1) oxidative addition, (2) transmetalation and (3) reductive elimination. The process of reductive elimination is the final step in all cross-coupling catalytic cycles during which the metal centre reduces its oxidation state and coordination number by two units *via* formation of a new bond between two mutually *cis* ligands (Scheme 3.1). This reductive elimination reaction is the critical product-forming step in the catalytic cycle and, as a result, there have been several comprehensive theoretical and experimental studies on how the nature of the ancillary ligands impacts on this reductive elimination process; these studies are detailed in Section 3.1.1.

The design of ligands that can accelerate reductive elimination is essential as slow reductive elimination has been shown to be problematic in some palladium-catalysed cross-coupling reactions, often leading to poorly selective processes; key examples presenting these problems are summarised in Section 3.1.2.



Scheme 3.1: A schematic representation of reductive elimination and oxidative addition.

The following sections of this thesis seek to identify some of the major elements that can be used to enhance the rate of reductive elimination in 4-coordinate square-planar complexes and will later describe the use of P-alkene ligands for this purpose. The discussion will involve the application of the three major proposed mechanisms (direct, dissociative and associative) of reductive elimination from d^8 square planar complexes (Figure 3.1). As reductive elimination is a concerted process it is a prerequisite that the groups to be eliminated must lie in a *cis*-orientation.

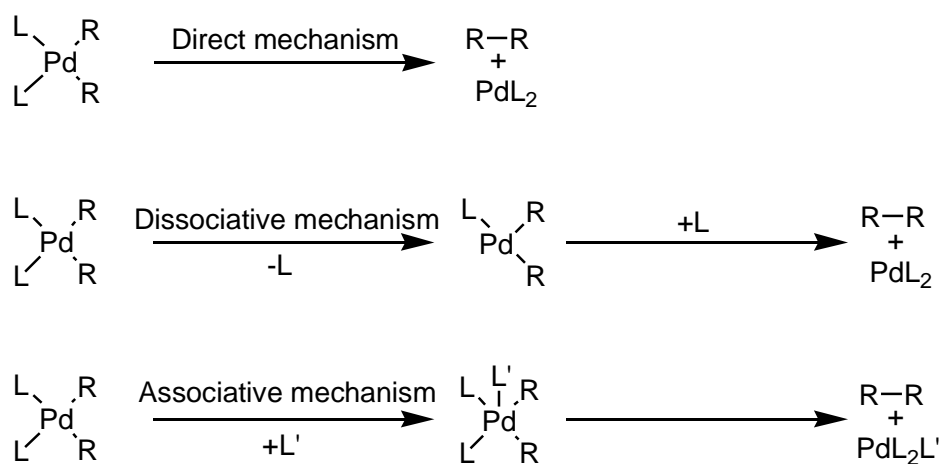


Figure 3.1: Three proposed mechanisms of reductive elimination from d^8 square planar complexes.

3.1.1 Promotion of reductive elimination from 4-coordinate square-planar complexes

There are many factors that can influence the rate of reductive elimination from 4-coordinate square-planar complexes. The following discussion reveals a rather complex picture of reductive elimination, with a strong dependence on the number and nature of the ancillary ligands.

3.1.1.1 The impact of the steric bulk of the ancillary ligands on the rates of reductive elimination in 4-coordinate square planar complexes

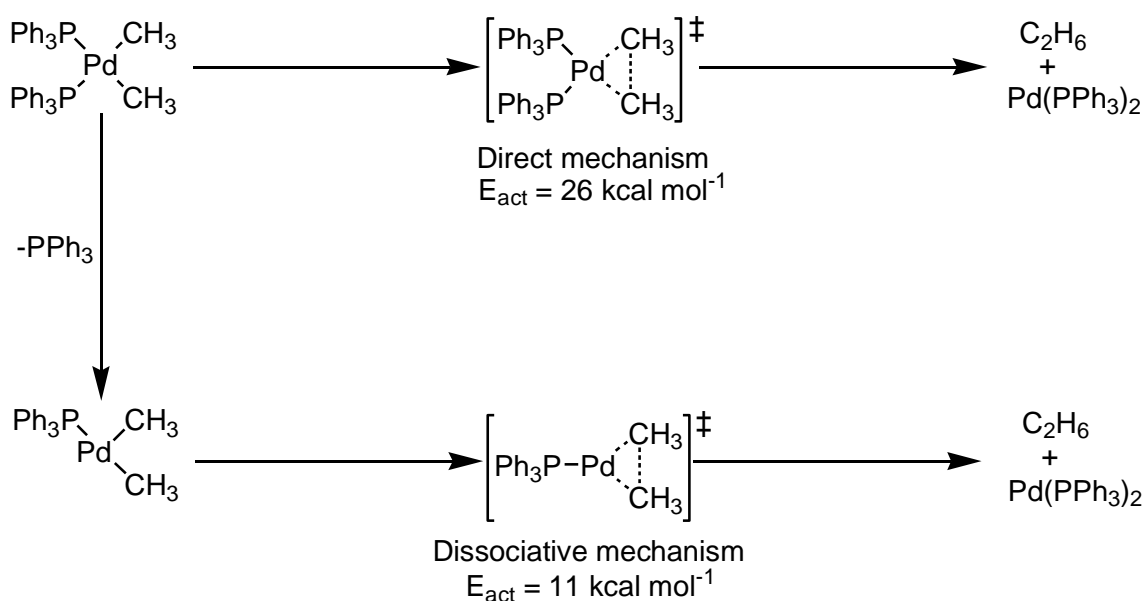
Complexes that contain ancillary ligands with large steric bulk tend to undergo faster reductive elimination than complexes containing less bulky ancillary ligands.¹ The origins of this effect are attributed to a relief of steric congestion upon forming a product with a coordination number two less than that of the starting complex.

Along with varying the steric bulk of a bidentate ancillary ligand it is also possible to alter the rate of reductive elimination by using chelating ligands with different natural bite angles; a larger natural bite angle leading to higher rates of reductive elimination.^c For example, Moloy and co-workers investigated the rate of reductive elimination of $R-CN$ from $cis-[Pd(CN)(R)(\kappa^2-P,P\text{-diphosphine})]$ ($R = CH_2TMS$) experimentally.² They found that as the bite angle of the chelating diphosphine was increased, the rate of reductive elimination of $R-CN$ increased significantly. This effect has been explained by the increase in bite angle of the diphosphine causing a contraction in the $R-Pd-CN$

^c The *cis*-orientation of the groups to be eliminated must be maintained.

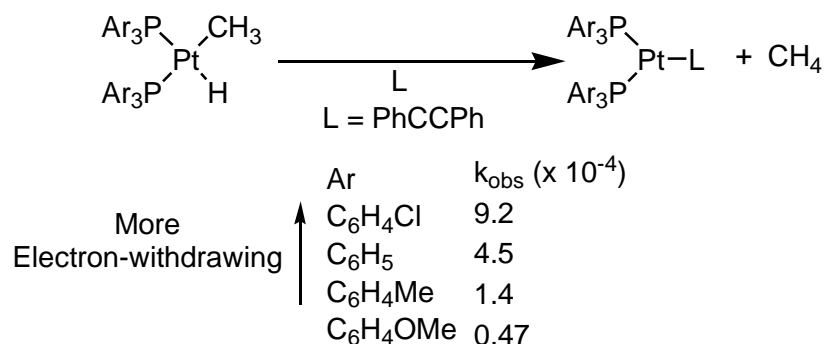
angle, which facilitates orbital overlap between the two carbon atoms to be coupled, resulting in a decrease in the activation barrier for reductive elimination.³

In contrast to the mechanisms discussed so far, square planar complexes possessing monodentate ligands offer different mechanistic pathways. The barrier to reductive elimination from a complex containing two bulky monodentate ancillary ligands can be lower than in an analogous complex containing a bidentate ancillary ligand of equivalent total steric bulk, as a dissociative pathway becomes the favoured reductive elimination route. As a consequence of the chelate effect a dissociative mechanism for reductive elimination from complexes containing bidentate ancillary ligands is unlikely and direct reductive elimination from a 4-coordinate species is more favoured. Reductive elimination through a dissociative pathway, by pre-dissociation of one of the bound ligands to relieve steric congestion in the starting complex, often has a lower energy barrier than by direct reductive elimination from a 4-coordinate complex.⁴ For example, the activation barrier to the formation of ethane *via* reductive elimination from *cis*-[PdMe₂(PPh₃)₂] by a dissociative pathway has been calculated computationally by Suresh and co-workers to be significantly lower (11 kcal mol⁻¹) than through a direct reductive elimination pathway (26 kcal mol⁻¹) (Scheme 3.2).⁵ Further evidence in support of a dissociative pathway for reductive elimination of ethane from *cis*-[PdMe₂(PPh₃)₂] is provided experimentally by the observation that the rate of ethane reductive elimination is significantly slower in the presence of additional PPh₃ (one equivalent). This observation indicates that pre-dissociation of a PPh₃ ligand from *cis*-[PdMe₂(PPh₃)₂] is an important step.⁶



Scheme 3.2: Formation of ethane via reductive elimination of ethane from *cis*-[PdMe₂(PPh₃)₂] by direct and dissociative mechanisms, modified from Suresh et al.⁵

3.1.1.2 The impact of the electronic properties of the ancillary ligands on the rates of reductive elimination in 4-coordinate square planar complexes



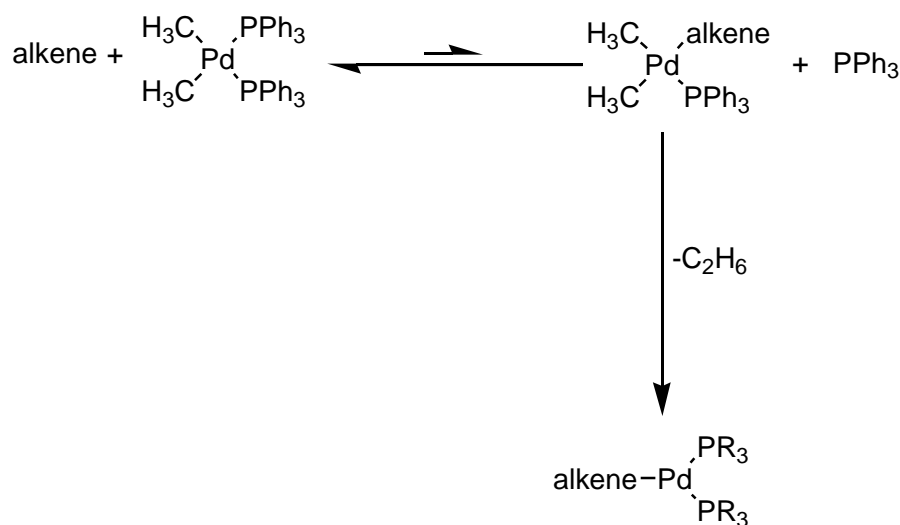
Scheme 3.3: Alteration of the rate of formation of methane by reductive elimination from platinum methyl hydride complexes on changing the electronic properties of the ancillary ligands.^{1, 7}

It is now well established that reductive elimination occurs faster from more electron-poor metal centres than it does from electron-rich metal centres with similar steric properties. This results from a destabilisation of the higher oxidation state starting complex by the electron-withdrawing ligand. One example of where this effect has been verified is through the work of Halpern and co-workers, who have demonstrated that the formation of methane *via* reductive elimination from platinum methyl hydride complexes bearing substituted triarylphosphine ligands is faster when electron-withdrawing groups are incorporated (Scheme 3.3).^{1, 7} With the rate of methane reductive elimination being approximately 20 times faster when the electron deficient P(C₆H₄Cl)₃ ancillary ligand is used compared to P(C₆H₄OMe)₃. Consequently, the electronic character of an ancillary ligand is a highly important factor to consider when designing a ligand to promote reductive elimination.

3.1.1.3 The impact of the addition of an alkene co-ligand on the rates of reductive elimination in 4-coordinate square planar complexes

In the field of metal-catalysed reactions, alkenes are often seen as reagents. However, there is a well-developed body of work that exemplifies the use of alkene-based additives to influence both the rate and selectivity of reactions, which has been summarised in a recent review.⁸

The rationale behind the use of alkene ligand additives to promote reductive elimination is that they are good π -acceptors which can influence the electron density experienced at the metal centre. The coordination of an electron-withdrawing alkene to a metal centre results in a reduction in the electron density at the metal centre (due to the high π -basicity of alkenes), enhancing the rate of reductive elimination (see Section 3.1.1.2). It has been demonstrated by Álvarez and Espinet that the addition of an electron withdrawing alkene (e.g. maleic anhydride) to *cis*-[PdMe₂(PPh₃)₂] results in a significant enhancement in the rate of reductive elimination of ethane, but, the addition of more electron rich alkenes (e.g. 1-hexene) has minimal effect on the rate.⁶

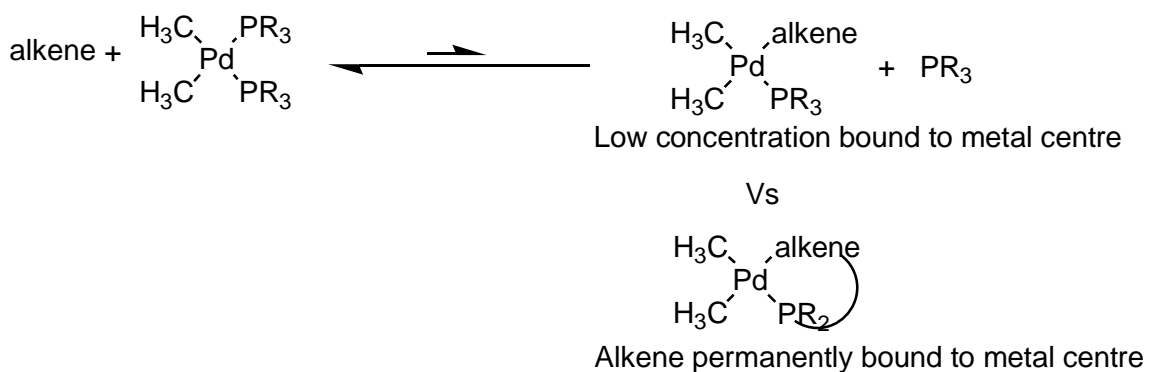


Scheme 3.4: Formation of small amounts of *cis*-[PdMe₂(PPh₃)(alkene)] enhances the rate of reductive elimination of ethane from *cis*-[PdMe₂(PPh₃)₂].

Álvarez and Espinet postulated that as a result of the equilibrium process described in Scheme 3.4, the formation of a small, but vital proportion of *cis*-[PdMe₂(PPh₃)(alkene)] occurs when the alkene is electron withdrawing. The barrier to reductive elimination of ethane from the resulting *cis*-[PdMe₂(PPh₃)(alkene)] complex is significantly lower than that from *cis*-[PdMe₂(PPh₃)₂] due to the presence of the electron withdrawing alkene, which reduces the electron density at the metal centre.⁶ The greatest rates of reductive elimination are experienced when the alkene is more strongly bound to the metal centre as the concentration of *cis*-[PdMe₂(PPh₃)(alkene)] is increased.

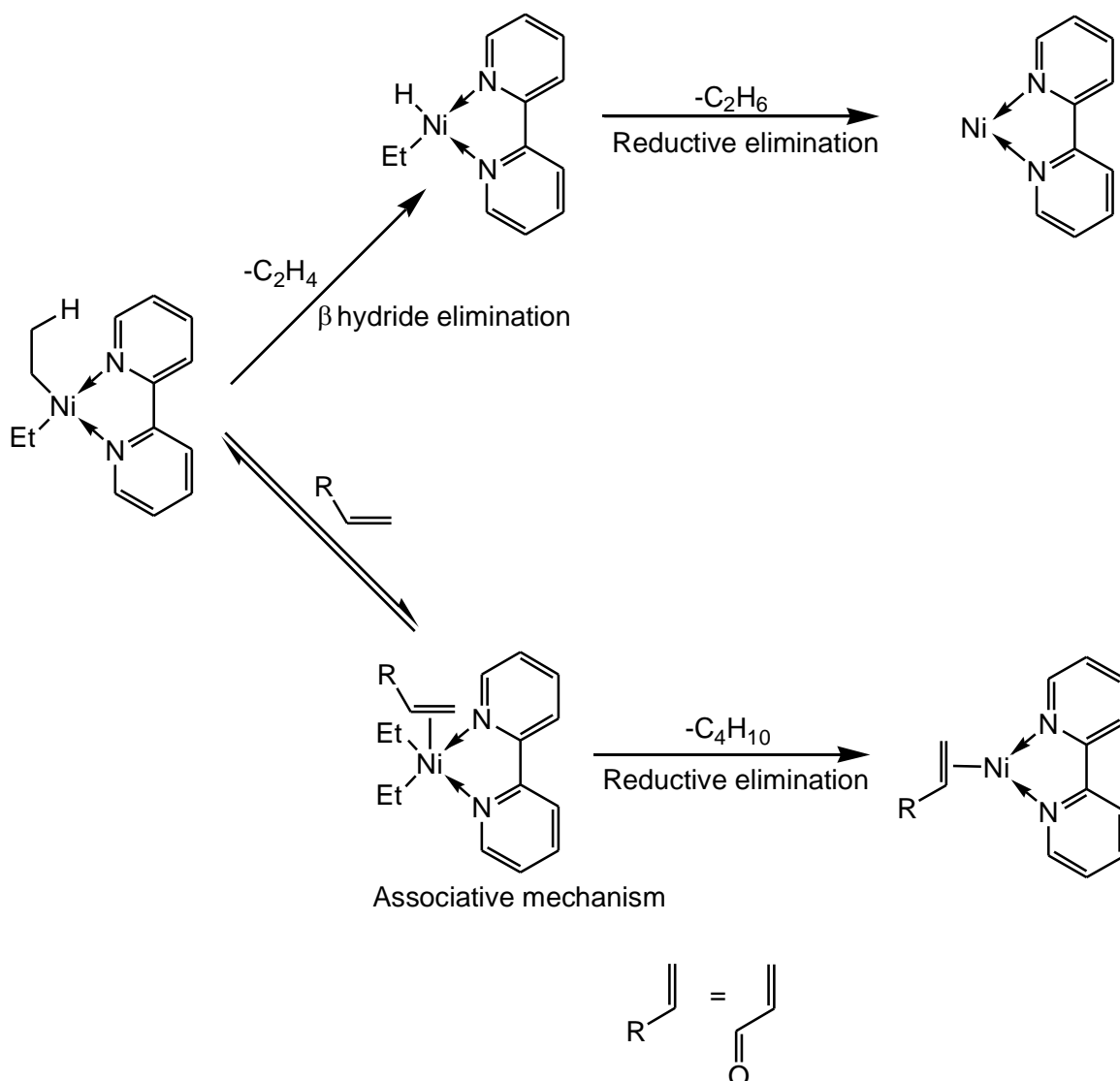
In an extension to the work described above, and in order to maximise the impact of a metal bound alkene group upon reductive elimination, there have been reports of bidentate P-alkene ligands being used in this type of process. These P-alkene ligands contain both phosphine and electron-deficient alkene metal-coordinating moieties, and

have led to dramatic improvements in selectivity in palladium catalysed reactions (detailed in Section 3.1.2).⁹⁻¹¹ The chelating nature of the bidentate P-alkene ligand enforces a *cis* orientation (a prerequisite for reductive elimination) at the metal centre and results in a significantly higher concentration of a metal-alkene complex (Scheme 3.5).



Scheme 3.5: Increase in the effective concentration of alkene-bound complex upon utilising a bidentate P-alkene ligand.

3.1.1.3.1 The proposed associative mechanism of reductive elimination from 4-coordinate square planar complexes upon addition of alkenes



Scheme 3.6: Two possible pathways for the decomposition of $[\text{NiEt}_2(\text{bipy})]$ via reductive elimination, modified from Rovis et al.^{8, 12, 13}

In contrast to the mechanism described above (Section 3.1.1.3), it is also proposed that the addition of an alkene co-ligand can promote the process of reductive elimination by an associative mechanism. Yamamoto and co-workers reported that the complex $[\text{NiEt}_2(\text{bipy})]$ (bipy = bipyridine) decomposes by a β -hydride/reductive elimination pathway to form a mixture of ethene and ethane (Scheme 3.6). However, upon addition of an electron deficient alkene the rate of decomposition is significantly enhanced, and butane is formed (Scheme 3.6). The displacement of bipyridine by a monodentate alkene (as depicted for a phosphine ligand in Scheme 3.4) is unlikely due to the chelate

effect. Thus, Yamamoto proposes an associative mechanism, in which the alkene binds to $[\text{NiEt}_2(\text{bipy})]$ to form a square-based pyramidal intermediate in which the barrier to reductive elimination of butane is significantly reduced compared to that from the square planar complex $[\text{NiEt}_2(\text{bipy})]$.^{12, 13}

3.1.2 Using P-alkene ligands to promote reductive elimination in palladium-catalysed reactions

A recently-developed approach to promoting the reductive elimination step in palladium-catalysed reactions where slow reductive elimination is problematic, is the use of phosphine-alkene ligands such as **3-1**, containing an electron-deficient alkene moiety (Figure 3.2).^{10, 11} It is proposed that the π -acidic alkene fragment of **3-1** accelerates reductive elimination by reducing the electron density at the metal centre. Two examples of palladium-catalysed reactions where P-alkene ligand **3-1** has been shown to reduce the formation of by-products formed by pathways competitive to slow reductive elimination are presented in the following sections.

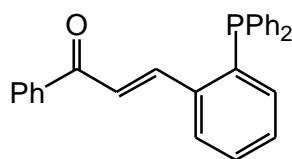
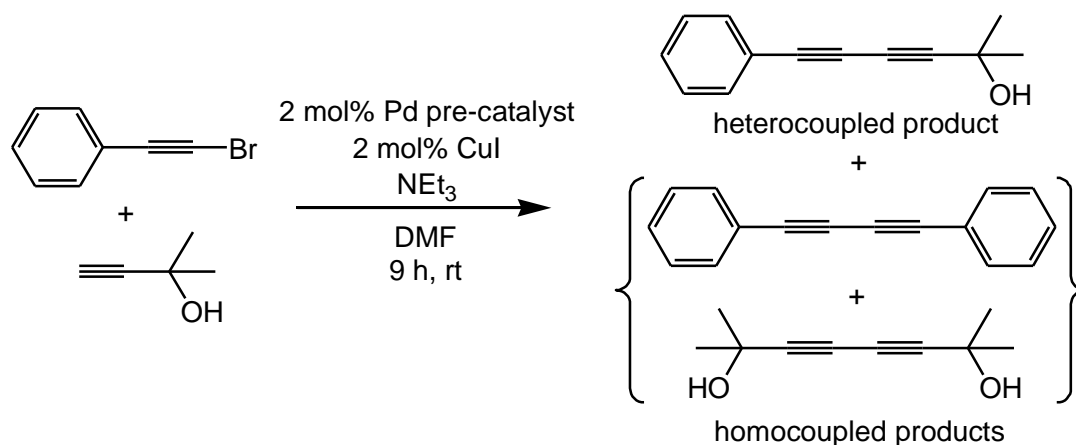


Figure 3.2: P-alkene ligand **3-1**, containing an electron-deficient alkene moiety, developed by Lei.¹⁰

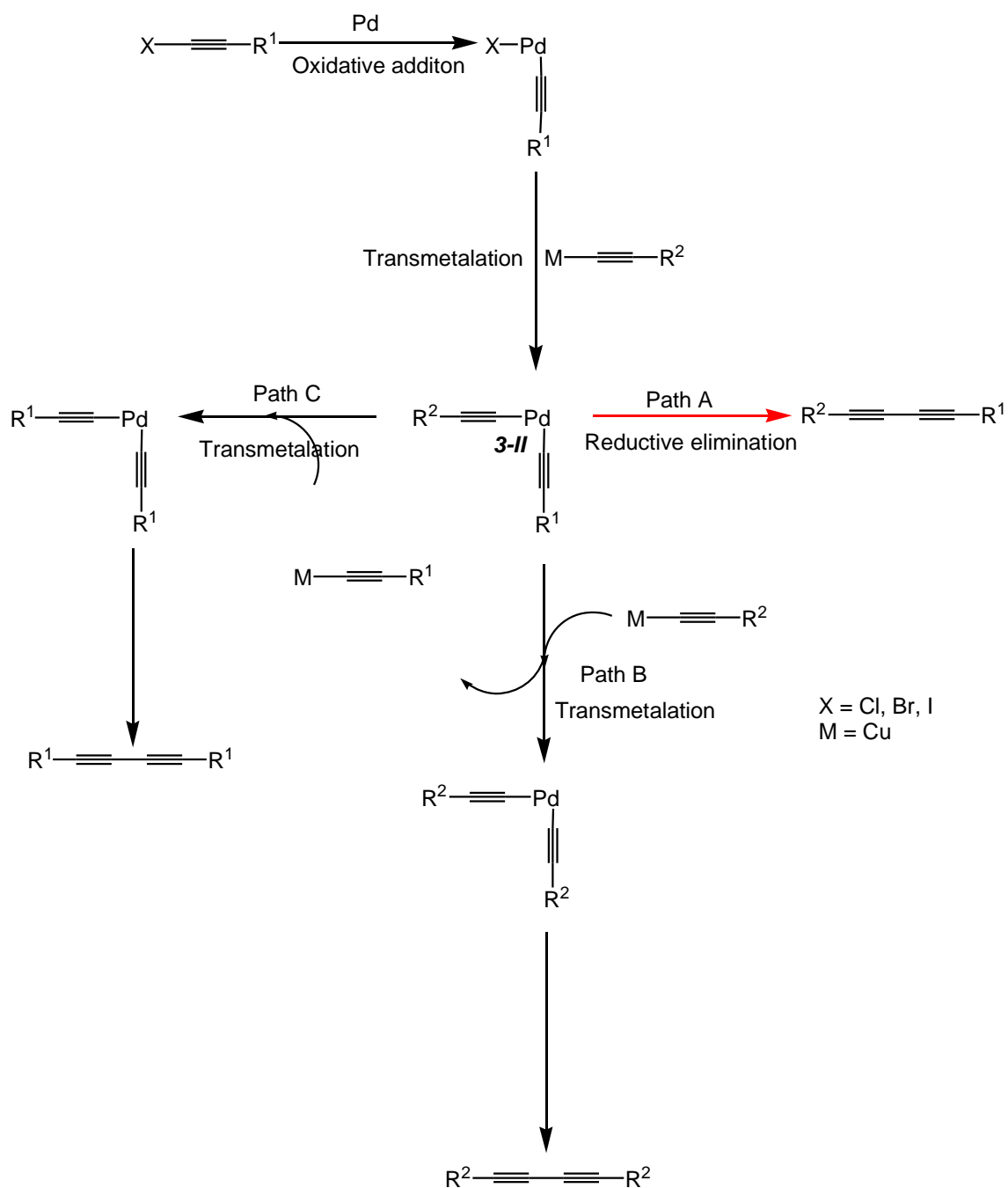
3.1.2.1 Palladium-catalysed C_{sp}-C_{sp} cross-coupling



Pd pre-catalyst	Selectivity (heterocoupled products : homocoupled products)
[PdCl ₂ (PPh ₃) ₂]	69:31
[Pd(dba) ₂]: 3-I (1:1)	91:9

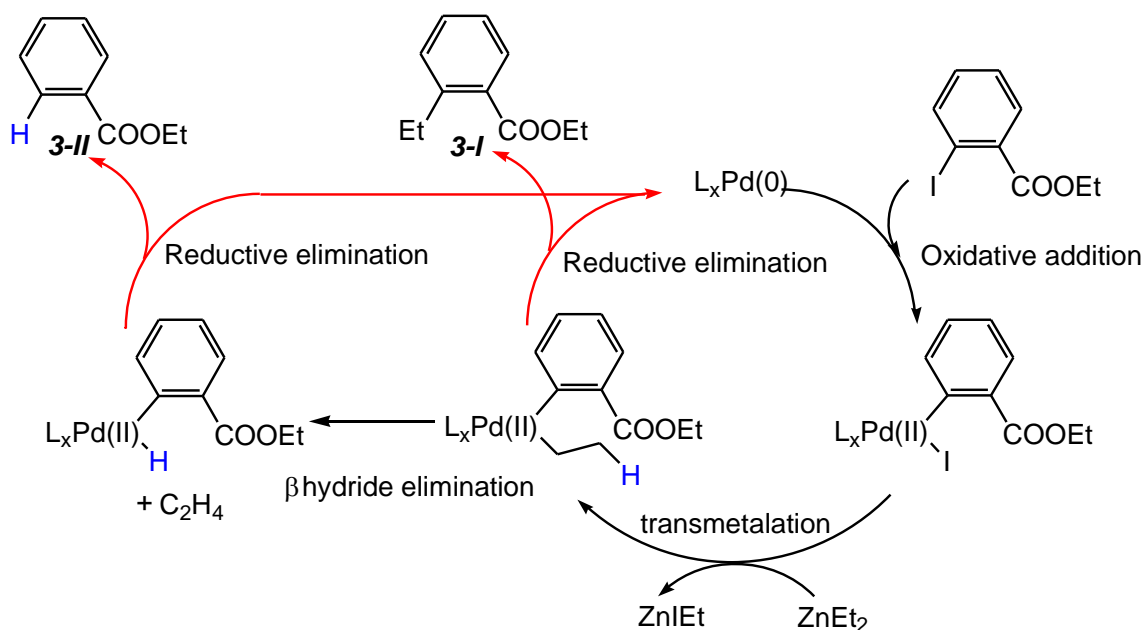
Scheme 3.7: Mixture of *P*-alkene ligand **3-I** and [Pd(dba)₂] gives increased selectivity for the heterocoupled product during palladium-catalysed C_{sp}-C_{sp} cross-coupling compared to [PdCl₂(PPh₃)₂].

During palladium-catalysed C_{sp}-C_{sp} cross-coupling reactions there is a significant problem with the formation of homocoupled by-products, resulting in poor yields of the desired heterocoupled product.¹⁴ For example, for the reaction presented in Scheme 3.7 the selectivity for heterocoupled over homocoupled products is 69:31 when [PdCl₂(PPh₃)₂] is used as the pre-catalyst; a proposed mechanism for this process is presented in Scheme 3.8. After formation of the intermediate **3-II** by oxidative addition and transmetallation the desired heterocoupled product is formed by direct reductive elimination (path A). However, if this reductive elimination step is slow, then further transmetallation can occur with the alkynylmetal reagents in the reaction system forming undesired homocoupled side products (paths B and C). Thus, in order to improve the selectivity for path A, it is necessary to speed up reductive elimination from intermediate **3-II**. To this end, Lei and co-workers have shown that using the *P*-alkene ligand **3-I** they were able to increase the selectivity for heterocoupled to homocoupled products to 91:9 ([Pd(dba)₂]:**3-I** (1:1)).



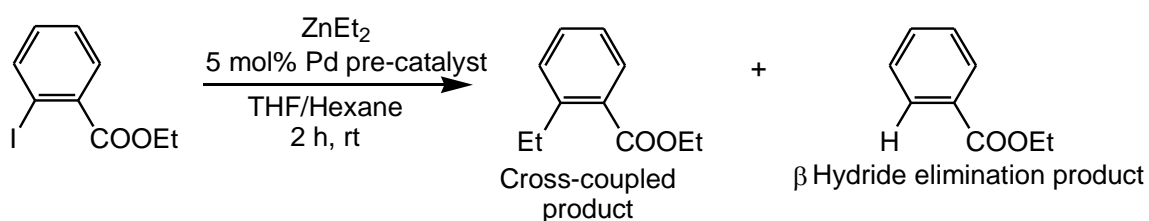
Scheme 3.8: Simplified mechanism of palladium-catalysed $C_{sp}-C_{sp}$ cross-coupling reaction, adapted from Lei et al.¹¹

3.1.2.2 Palladium-catalysed Negishi cross-coupling



Scheme 3.9: Proposed mechanism for the formation of an undesired by-product formed by β -hydride elimination/reductive elimination during the Negishi cross-coupling of ethyl 2-iodobenzoate and diethylzinc.

The problems of slow reductive elimination in palladium-catalysed cross-coupling reactions are especially evident for reactions involving alkyl reagents, where the presence of β -hydrogens can lead to the formation of undesired by-products by β -hydride elimination (Scheme 3.9). For example, during the Negishi cross-coupling of ethyl 2-iodobenzoate and diethylzinc the selectivity for the desired cross-coupled product over the β -hydride elimination product when using $[\text{PdCl}_2(\text{PPh}_3)_2]$ as a pre-catalyst is 39:61 (Scheme 3.10).¹⁰ When undertaking the coupling of alkyl reagents increased selectivity for the desired cross-coupled product will be seen upon increasing the rate of reductive elimination pathway with respect to the β -hydride elimination/reductive elimination pathway (Scheme 3.9). Accordingly, the use of P-alkene ligand **3-I** increases the selectivity to the cross-coupled product over the product from β -hydride elimination to 94:6.



Pd pre-catalyst	Selectivity
	(cross-coupled product : β -hydride elimination product)
$[\text{PdCl}_2(\text{PPh}_3)_2]$	39:61
$[\text{PdCl}_2(\text{MeCN})_2]$: 3-1 (1:1)	94:6

Scheme 3.10: Mixture of P-alkene ligand **3-1** and $[\text{PdCl}_2(\text{MeCN})_2]$ gives increased selectivity for the cross-coupled product during palladium-catalysed Negishi cross-coupling compared to $[\text{PdCl}_2(\text{PPh}_3)_2]$.¹⁰

The above two examples (Sections 3.1.2.1 and 3.1.2.2) show that P-alkene ligands containing an electron-deficient alkene moiety have tangible benefits during palladium-catalysed cross-coupling reactions. In order to exploit this beneficial effect, it was of interest to probe the use of the P-alkene ligand **2-1** introduced in chapter 2, which contains a strained and rigid alkene moiety, to see whether it could give similar/improved benefits in analogous palladium-catalysed reactions. The more rigid structure of **2-1**, coupled with the preferential olefin coordination resulting from a relief of ring-strain, should offer increased control and hence increased selectivity in reactions where slow reductive elimination is problematic. Thus, firstly, a study of comparatively simple ethane reductive elimination from palladium(II) dimethyl complexes promoted by ligand **2-1** was undertaken in order to gain a greater understanding of its chemistry, before applying ligand **2-1** to more complex catalytic systems.

3.2 Using ligand **2-1** to promote reductive elimination of ethane from Pd(II) dimethyl complexes

Compound **2-1** contains several key features in its design that would favour its bidentate (κ^2 -P,C) coordination, which should result in a promotion of reductive elimination in palladium-catalysed cross-coupling reactions.

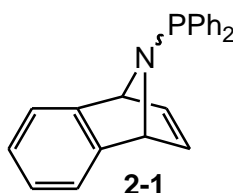
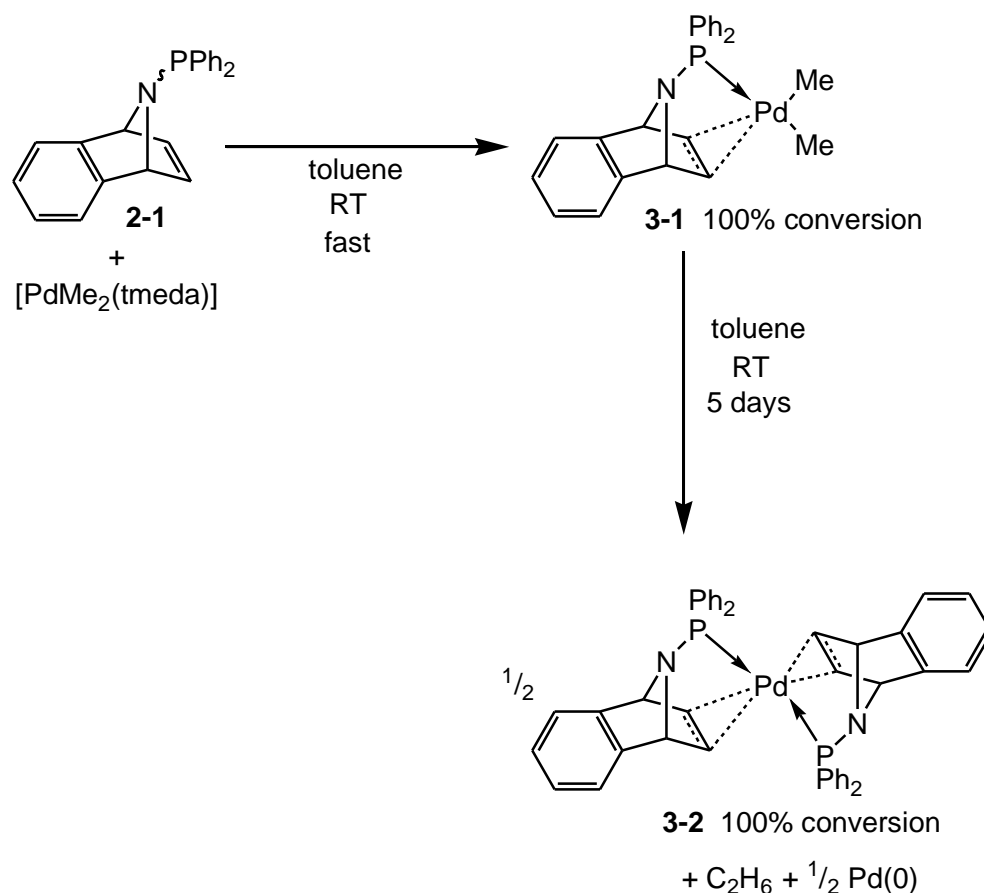


Figure 3.3: Ligand **2-1**.

Features of ligand **2-1**

- Ligand **2-1** contains a π -accepting alkene group and thus should be electron-withdrawing in nature:
 - Strong metal to alkene back-bonding encouraged as the alkene moiety is located within a strained 5-membered ring.
 - The magnitude of the $^1J_{\text{SeP}}$ (792 Hz) coupling constant for the phosphine-selenide **2-1** shows that the phosphorus donor moiety of **2-1** is weakly basic, which is consistent with an overall electron withdrawing nature of the entire ligand.
- Ligand **2-1** is sterically bulky, therefore steric crowding will be relieved upon reductive elimination from a 4-coordinate square planar complex, thus favouring the lower oxidation state.

The electron deficient and sterically-demanding nature of **2-1** makes it an ideal candidate as a ligand to promote the reductive elimination step in palladium-catalysed transformations where slow reductive elimination is problematic (Section 3.1.2). The use of a strained alkene within a P-alkene framework to achieve strong alkene back-bonding and promote reductive elimination is in contrast with the use of an electron deficient alkene (**3-1**) by Lei and co-workers to achieve the same effect.¹⁰ Firstly, the ability of ligand **2-1** to promote the reductive elimination of two methyl groups to form ethane will be tested before **2-1** will be applied to potentially catalytic systems.

3.2.1 Coordination of P-alkene ligand 2-1 to a PdMe₂ fragment

Scheme 3.11: Reaction of **2-1** with one equivalent $[\text{PdMe}_2(\text{tmeda})]$.

Treating a d_8 -toluene solution of $[\text{PdMe}_2(\text{tmeda})]$ with one equivalent of ligand **2-1** afforded $\text{cis-}[\text{PdMe}_2(\kappa^2\text{-P,C-2-1})]$ (**3-1**) in 100% conversion (according to $^{31}\text{P}\{^1\text{H}\}$ NMR spectroscopy) (Scheme 3.11). Complex **3-1** exhibits a singlet resonance at 81.3 ppm by $^{31}\text{P}\{^1\text{H}\}$ NMR spectroscopy ($\Delta\delta$ +39.7 ppm), with the alkene carbons displaying a broad singlet resonance at 119.2 ppm ($\Delta\delta$ -23.8 ppm). The magnitudes of the coordination chemical shifts observed for both the phosphine and the alkene functionalities are indicative of bidentate coordination of **2-1**. The anticipated two inequivalent methyl groups are indeed observed by ^1H NMR spectroscopy, 0.97 (d, $^3J_{\text{PH}} = 7.7$ Hz) and 1.69 (d, $^3J_{\text{PH}} = 7.5$ Hz), consistent with their *cis* orientation in **3-1**.

Complex **3-1** is thermally unstable in solution at room temperature and after 5 days evolves smoothly to afford half an equivalent of the palladium(0) complex $[\text{Pd}(\kappa^2\text{-P,C-2-1})_2]$ (**3-2**) (δ $^{31}\text{P}\{^1\text{H}\}$ 82.2 ppm) and >0.9 equivalents of ethane (δ ^1H 0.80 ppm) as the only products,^d together with a quantity of elemental palladium precipitated from

^d With reference to an internal standard (PPh_3) housed within a sealed capillary tube.

solution (Scheme 3.11). Alternatively if the reaction temperature is increased to 80 °C then complex **3-1** fully eliminates ethane in <5 mins. In contrast, complete reductive elimination of ethane from [PdMe₂(dppe)] requires heating at 80 °C for 20 days to eliminate ethane.¹⁵ This difference in the rate of reductive elimination from **3-1** compared with that from [PdMe₂(dppe)] is attributed to the palladium centre of **3-1** being considerably more electron poor than that in [PdMe₂(dppe)] due to the presence of the electron withdrawing ligand **2-1**.

It should be noted that during the thermolysis of **3-1** no methane was detected (δ ¹H 0.16 ppm), suggesting that 1,1-reductive elimination of ethane is the dominant process taking place, enhanced by electron withdrawing ligand **2-1**. In contrast, methane is seen in significant amounts during the thermolysis of some palladium dimethyl complexes and is believed to form as a result of solvent C-H activation or α -elimination, followed by methane reductive elimination (Figure 3.4).¹⁶ For example, complete conversion of [PdMe₂(dmpe)] requires thermolysis at 90 °C for one week and liberates a 3:1 mixture of methane and ethane.¹⁶

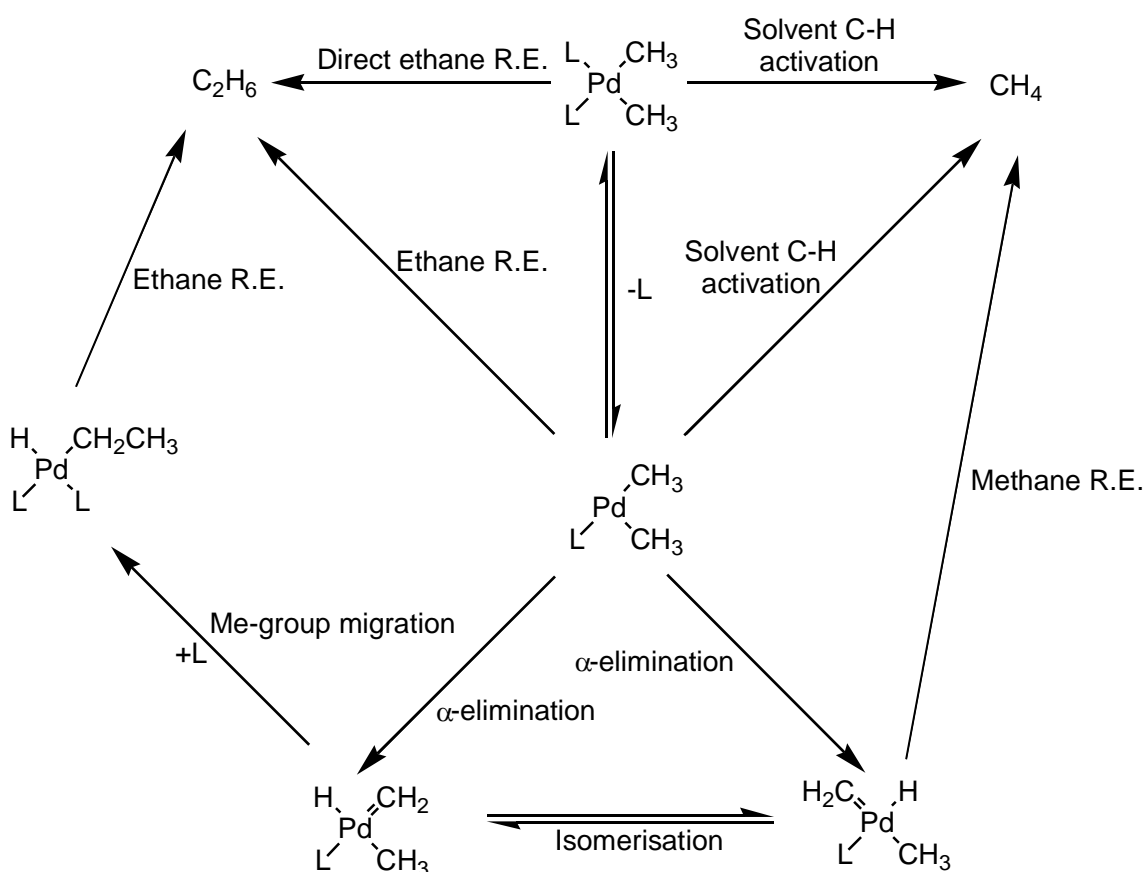


Figure 3.4: Pathways for the thermal decomposition of dimethylpalladium species, adapted from van Koten et al.¹⁶ (R.E. = reductive elimination)

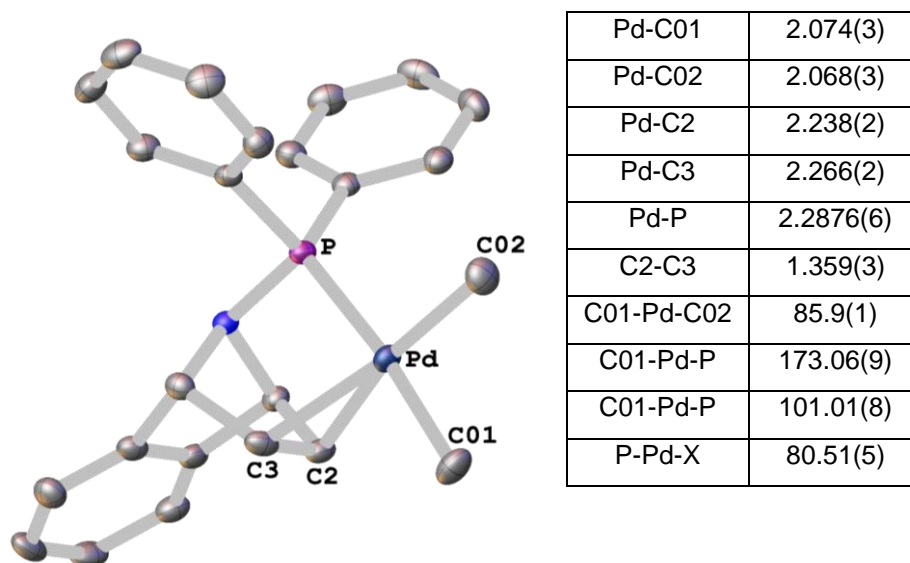
3.2.1.1 X-Ray crystallographic study of *cis*-[PdMe₂(κ²-P,C-2-1)] (**3-1**)

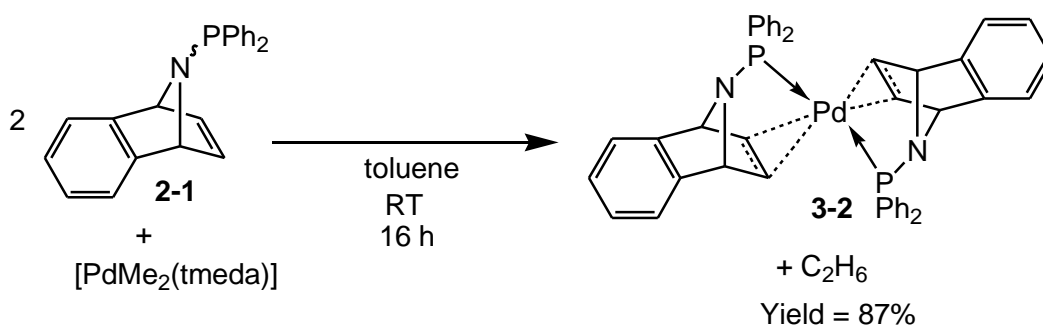
Figure 3.5: Molecular structure of *cis*-[PdMe₂(κ²-P,C-2-1)] (**3-1**) with selected bond lengths (Å) and angles (°). X is defined as the midpoint of C(2)=C(3), (thermal ellipsoids set at 50% level).

Single crystals of complex **3-1** were grown by cooling a concentrated toluene solution, with the ensuing X-ray crystallographic study confirming the proposed structure of *cis*-[PdMe₂(κ²-P,C-2-1)] (Figure 3.5). Complex **3-1** presents a distorted square planar structure about palladium; the angle between the two planes defined by the atoms P,Pd,X and C01,Pd,C02 is 0.57(1)°, while the P-Pd-X bite-angle of **2-1** in complex **3-1** is 80.51(5)°, where X is the mid-point between C(2)=C(3).

The molecular structure of [PdMe₂(dppe)] is not known, hence a direct structural comparison with **3-1** cannot be made, something that precludes any comparison of geometric effects that could impact on the differences in rate of reductive elimination of the dppe complex with **3-1**. The nearest analogues that have been structurally characterised are [PdMe₂(tmeda)] and [PdMe₂(dmpe)]. The angle between the two palladium bound methyl groups of **3-1** (85.9(1)°) is slightly smaller than that for either [PdMe₂(tmeda)] (87.4(1)°) or [PdMe₂(dmpe)] (88.8(2)°).¹⁶ The Pd–C bond distances for the two methyl ligands in **3-1** are identical, despite being located *trans* to the alkene (2.068(3) Å) and *trans* to a phosphine moieties (2.074(3) Å), suggesting there is little difference in the *trans* influence between these two donor moieties. The P–CH₃ bond lengths of **3-1** are identical (within error) to those for [PdMe₂(dmpe)] (mean = 2.087(4) Å), but slightly longer than those determined for [PdMe₂(tmeda)] (mean = 2.028(4) Å).¹⁶

In conclusion, it is proposed that reductive elimination is facilitated from complex **3-1** by the small angle between its two palladium-bound methyl groups, which is assumed to result from the tight coordination of P-alkene **2-1**. A small angle between the two palladium-bound methyl groups facilitates orbital overlap between the two methyl carbon atoms to be coupled, resulting in a decrease in the activation barrier for reductive elimination (Section 3.1.1.1).

3.2.2 Reaction of two equivalents of P-alkene ligand **2-1** with a PdMe₂ fragment



Scheme 3-12: Synthesis of $[\text{Pd}(\kappa^2\text{-P,C-2-1})_2]$ (**3-2**).

With a view to achieving the direct synthesis of the palladium(0) complex $[\text{Pd}(\kappa^2\text{-P,C-2-1})_2]$ (**3-2**) the reaction of $[\text{PdMe}_2(\text{tmeda})]$ with two equivalents of **2-1** was undertaken (Scheme 3.12). A detailed NMR-scale study of this reaction revealed that complete conversion to **3-2** was achieved in just 5 h (*cf.* 5 days when a Pd:**2-1** ratio of 1:1 was used).

Characterisation of **3-2** was achieved by multinuclear NMR spectroscopy, with complex **3-2** exhibiting a singlet resonance at $\delta^{31\text{P}}$ 82.2 ppm ($\Delta\delta$ +40.6 ppm), consistent with a single phosphorus environment. Due to the pseudo-tetrahedral geometry of complex **3-2** (confirmed by single crystal X-ray diffraction), there is no mirror plane running through the alkene bond and so each half of the two **2-1** ligands is in a different environment, exactly as is observed for $[\text{Ni}(\kappa^2\text{-P,C-2-1})_2]$ (**2-6**), Section 2.2.4.

3.2.2.1 X-Ray crystallographic study of $[\text{Pd}(\kappa^2\text{-P,C-2-1})_2]$ (**3-2**).

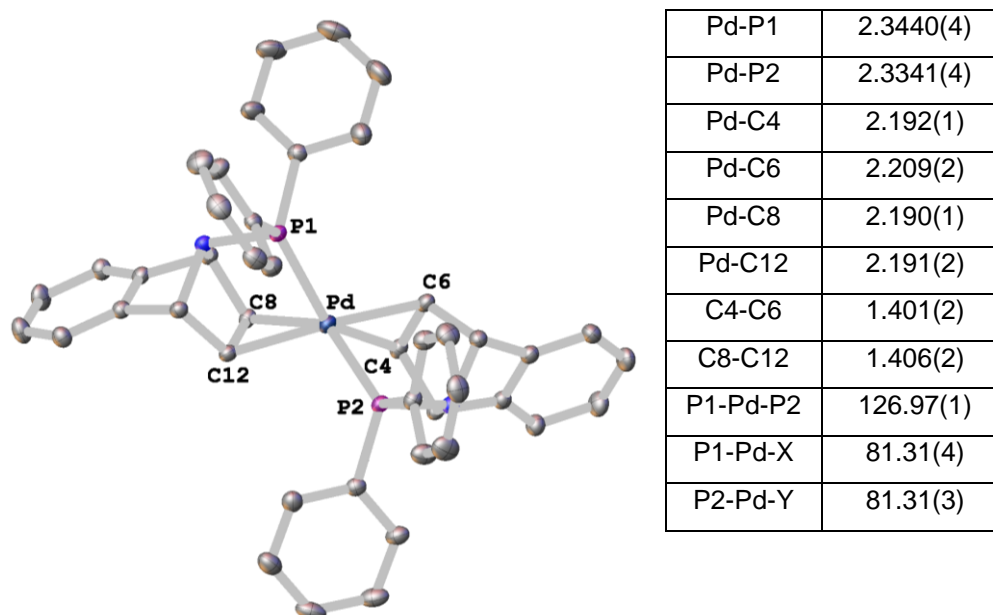


Figure 3.6: Molecular structure of $[\text{Pd}(\kappa^2\text{-P,C-2-1})_2]$ (**3-2**), with selected bond lengths (Å) and angles (°). X is defined as the midpoint of C(4)=C(6) and Y as the midpoint of C(8)=C(12), (thermal ellipsoids set at 50% level).

A single crystal X-ray diffraction study of complex **3-2** revealed a distorted tetrahedral structure about palladium (Figure 3.6). We postulate that **3-2** adopts a tetrahedral geometry to minimise steric interaction between the bulky **2-1** ligands. This contrasts with the only other example of a structurally characterised *bis*(P-alkene)palladium(0) complex, **3-III** (Figure 3.7), reported by Lei and co-workers, which contains a much less bulky P-alkene ligand and adopts a geometry in which the palladium centre is in an intermediate geometry between that of a square-planar and a tetrahedral structure.¹⁷

The C–C bond distances of the η^2 -coordinated alkene moieties in **3-2** are longer (mean = 1.404(3) Å) than that determined for dimethyl complex **3-1** (1.359(3) Å), which is consistent with increased $\text{Pd} \rightarrow \pi^*(\text{C}=\text{C})$ retro-donation from the more electron-rich Pd(0) centre. Compared to the analogous nickel(0) complex **2-6** (see Section 2.2.4), the phosphine and alkene groups of **3-2** exhibit longer bond distances to the metal centre, consistent with binding to a metal centre with a larger covalent radius (Ni: 1.24 Å; Pd: 1.39 Å).¹⁸ The P1-Pd-X and P2-Pd-Y bite angles for ligand **2-1** in complex **3-2** are 81.31(4)° and 81.31(3)°, respectively, showing a less than 1% difference in bite angle compared to those found for complex **3-1**, suggestive that ligand **2-1** is quite rigid in its mode and geometry of coordination.

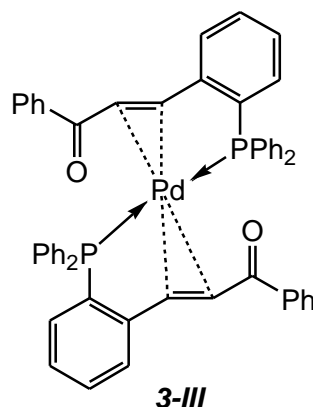


Figure 3.7: Bis(*P*-Alkene)palladium(0) complex **3-III** as described by Lei and co-workers.¹⁷

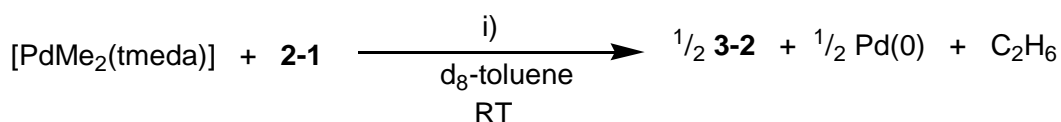
3.2.3 Investigating the mechanism of ethane reductive elimination promoted by *P*-alkene ligand **2-1**

In Section 3.2.2 a discussion of the observations made following the addition of two equivalents of **2-1** to [PdMe₂(tmeda)], which resulted in complete elimination of ethane in 5 h at RT with formation of the palladium(0) complex **3-2**, was presented. The following section describes experiments and computational calculations carried out to determine the mechanism of this unusually facile process.

3.2.3.1 Accelerated ethane reductive elimination from *cis*-[PdMe₂(κ²-*P,C*-**2-1**)] (**3-1**) by the addition of PPh₃ or propene

The experiments in Section 3.2.3.1 were carried out by Andreas Phanopoulos (MChem student in the Dyer group 2010-2011).

The addition of one equivalent of **2-1** to [PdMe₂(tmeda)] resulted in complete elimination of ethane in 5 days at RT with formation of equimolar quantities of **3-2** and palladium metal (Section 3.2.1). It was found that it was possible to speed up this reaction significantly by the addition of small amounts of either PPh₃ or propene.



Conditions i)	Complete elimination of ethane / h
No additive	120
9 mol% PPh ₃	12
4 mol% propene	36

Scheme 3.13: The effect of the addition of sub-stoichiometric quantities of PPh₃ or propene on the rate of reductive elimination of ethane from complex **3-1** at room temperature.

The addition of sub-stoichiometric quantities of either PPh₃ or propene to the reaction between one equivalent of **2-1** and [PdMe₂(tmeda)] resulted in a significant enhancement in the rate of reductive elimination of ethane, with complete elimination of ethane achieved in 12 and 36 h, respectively (*cf.* 120 h in the absence of an additional L-donor ligand), Scheme 3.13. In the presence of an L-donor the formation of a 5-coordinate intermediate is proposed (Figure 3.8), from which the barrier to ethane reductive elimination is lower than from complex **3-1** itself.

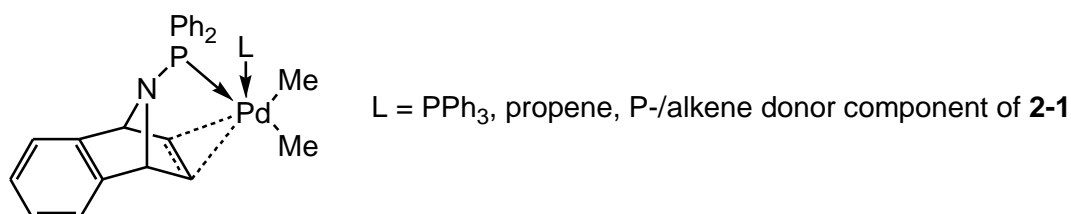
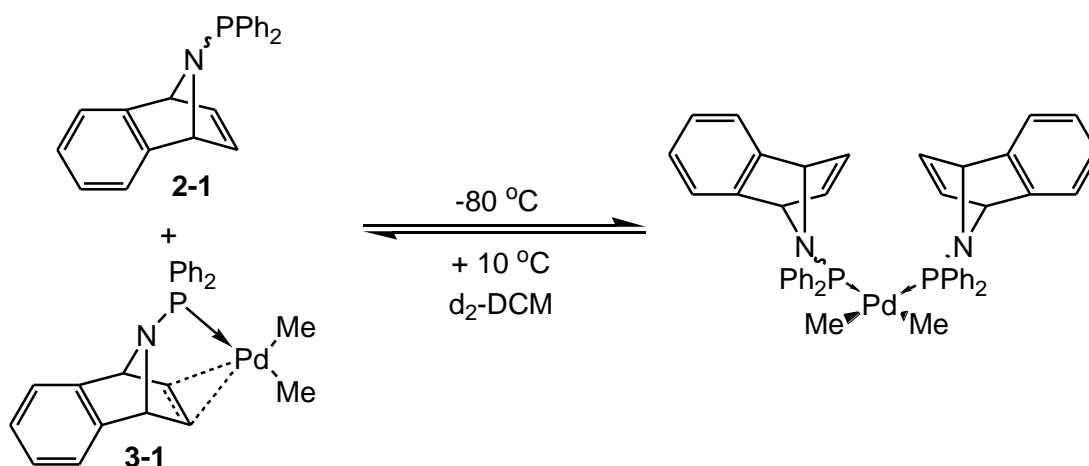


Figure 3.8: Proposed 5-coordinate intermediate from which reductive elimination of ethane takes place.

3.2.3.2 Attempts to trap the proposed 5-coordinate intermediate: variable temperature NMR studies

Following the addition of two equivalents of **2-1** to [PdMe₂(tmeda)] we have proposed the formation of a 5-coordinate intermediate, where **2-1** is acting as the donor L (through either its phosphine or alkene moieties), from which ethane reductive elimination takes place (Figure 3.8). In an attempt to identify or trap this proposed 5-coordinate intermediate, a variable temperature NMR spectroscopic study of the reaction between **2-1** and *cis*-[PdMe₂(κ²-P,C-**2-1**)] (**3-1**) was performed.

The reagents were mixed at 0 °C immediately prior to loading the NMR tube into the spectrometer with the probe pre-cooled to +10 °C.^e At +10 °C the $^{31}\text{P}\{^1\text{H}\}$ NMR spectrum presented two very broad (FWHM = 850 Hz) resonances, at 41.3 and 81.3 ppm, which can be ascribed to **2-1** and **3-1**, respectively. Upon cooling the solution to –80 °C, these two very broad resonances were replaced by a comparatively sharp resonance (FWHM = 35 Hz) at 59.4 ppm, accompanied by a broad (FWHM = 9 Hz) singlet resonance at 0.15 ppm in the ^1H NMR spectrum.^f Together, the observation of a single phosphorus and a single methyl environment suggests that the new species formed at –80 °C could be *cis*-[PdMe₂(κ¹-P-**2-1**)₂] (Scheme 3.14). The presence of a 5-coordinate species was not detected, which would show two resonances by $^{31}\text{P}\{^1\text{H}\}$ NMR spectroscopy. In order to help determine from which species ethane reductive elimination takes place a computational study on the reaction of **2-1** with *cis*-[PdMe₂(κ²-P,C-**2-1**)] (**3-1**) was performed, and is detailed in the next section.



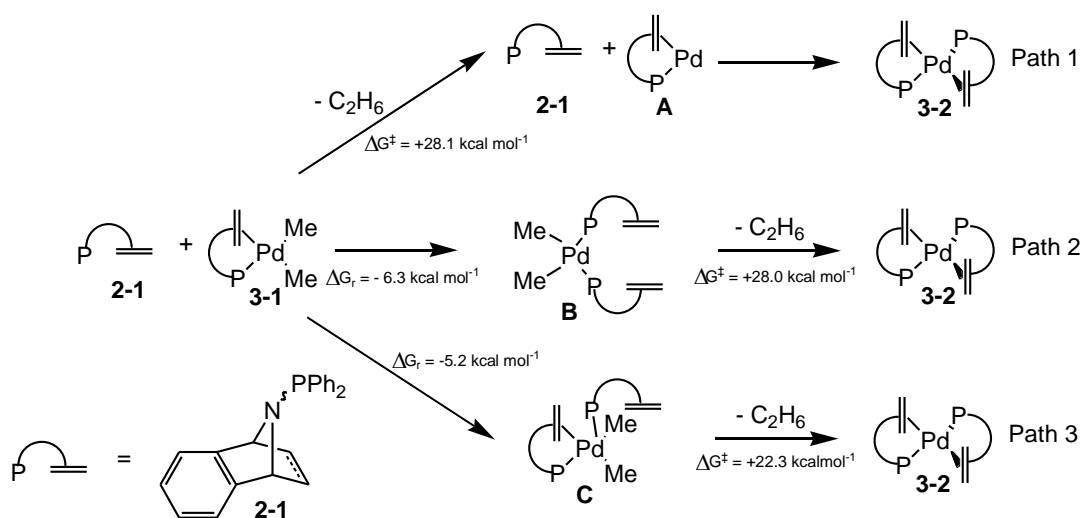
Scheme 3.14: Proposed complex *cis*-[PdMe₂(κ¹-P-**2-1**)₂] (right), to which were attributed the signals $\delta^{31}\text{P}\{^1\text{H}\}$ 59.4 ppm and $\delta^1\text{H}$ 0.15 ppm observed by NMR spectroscopy at –80 °C.

^e The reaction mixture was kept cool (+10 °C) to minimise the formation of complex **3-2**, which would complicate the spectra.

^f Slowly warming back to +20 °C resulted in the re-formation of the two very broad resonances at 41.3 and 81.3 ppm.

3.2.3.3 Theoretical investigation of the interaction of P-alkene ligand **2-1** with *cis*-[PdMe₂(κ²-P,C-**2-1**)] (**3-1**)

Three possible pathways for the interaction of P-alkene **2-1** with dimethyl complex **3-1** were investigated by a computational analysis (Scheme 3.15) and will be discussed in turn below. Computational studies were performed by Karinne Miqueu, Jean-Marc Sotiropoulos, and Laura Estevez (Université de Pau), and were performed *in vacuo* at the B3LYP/SDD+f(Pd), 631G** (other atoms) level of theory.



Scheme 3.15: Three possible pathways for the reductive elimination of ethane from 3-1 + 2-1, investigated by a computational analysis.

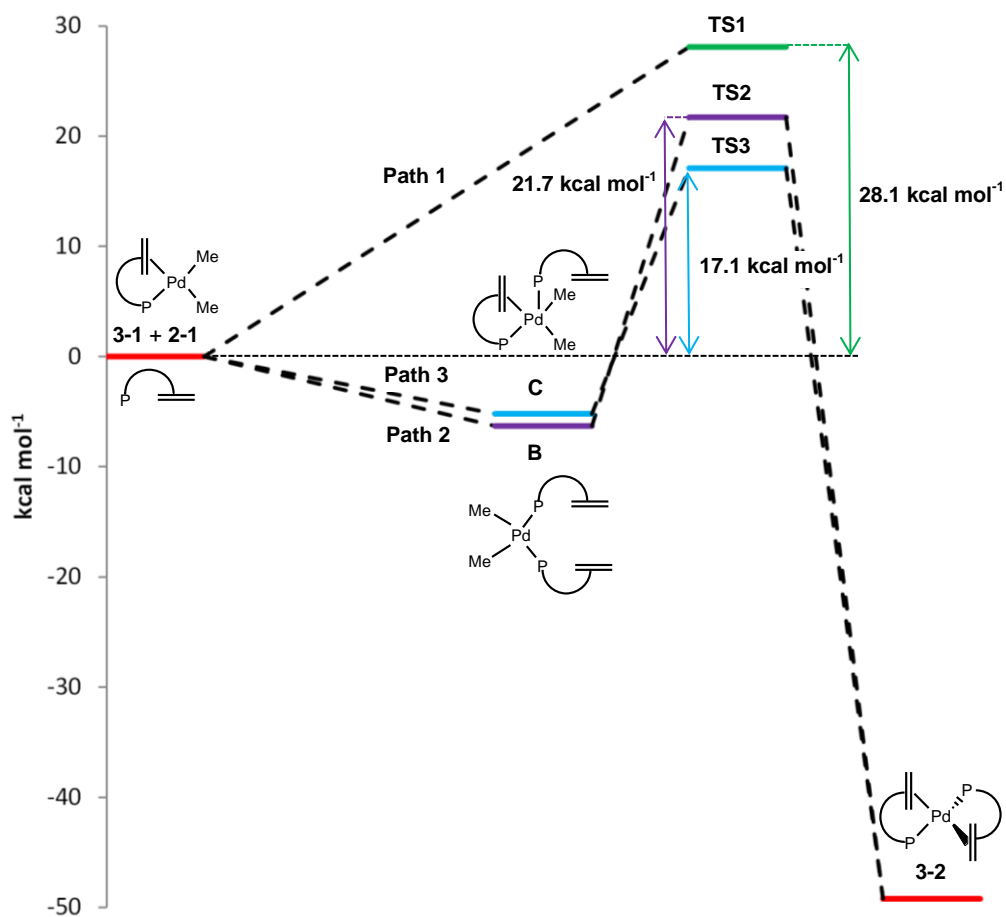


Figure 3.9: Reaction profile for the three possible pathways for the reductive elimination of ethane from 3-1 + 2-1. TSX = transition state for reductive elimination of ethane in path X.

Path 1: No interaction between **2-1** and **3-1**, ethane reductive elimination from 4-coordinate complex **3-1**.

The activation barrier to the reductive elimination of ethane directly from **3-1** to form **A** is moderately large ($\Delta G^\ddagger_{3-1 \rightarrow A} = 28.1 \text{ kcal mol}^{-1}$), this activation barrier will be compared with that for two further pathways in which **2-1** and **3-1** interact.

Path 2: Reductive elimination of ethane from *cis*-[PdMe₂(κ¹-P-**2-1**)₂] (**B**).

VT NMR spectroscopic studies on the interaction of **2-1** and **3-1** (Section 3.2.3.2) suggested the presence of **B** at low temperature, hence it was of interest to study a pathway containing **B**.⁹ The addition of a second equivalent of ligand **2-1** to complex **3-1**, to form complex **B**, *cis*-[PdMe₂(κ¹-P-**2-1**)₂], is a favourable process ($\Delta G_{r,3-1+2-1 \rightarrow B} = -6.3 \text{ kcal mol}^{-1}$). The barrier to ethane reductive elimination from **B** ($\Delta G^\ddagger_{B \rightarrow 3-2} = 28.0 \text{ kcal mol}^{-1}$) is almost identical to that from **3-1**. However, if one considers that **B** is stabilised compared to **3-1** ($\Delta G_{r,3-1+2-1 \rightarrow B} = -6.3 \text{ kcal mol}^{-1}$), the activation barrier starting from **3-1** becomes, $\Delta G^\ddagger = 21.7 \text{ kcal mol}^{-1}$ (Figure 3.9). Thus a pathway that proceeds *via* **B** has a lower activation barrier for the overall process than the path that proceeds directly from **3-1** and hence represents a plausible mechanism for the facile reductive elimination of ethane in the presence of two equivalents of ligand **2-1**.

Path 3: Reductive elimination of ethane from a 5-coordinate palladium intermediate (**C**).

It was calculated that the lowest energy 5-coordinate palladium intermediate, **C**, contained ligand **2-1** bound both in a mono- (through phosphorus) and a bi-dentate fashion in a distorted square-based pyramidal structure (Scheme 3.15 and Figure 3.10). Complex **C** is stabilised by a similar amount as **B** with respect to **3-1** ($\Delta G_{r,3-1+2-1 \rightarrow C} = -5.2 \text{ kcal mol}^{-1}$); it is assumed that the stabilisation occurs through donation of electron density from the phosphorus lone pair to the electron-poor palladium(II) centre relative to the presence of only a single P-donor-metal interaction in **3-1**. The activation barrier for ethane reductive elimination from **C** is lower ($\Delta G^\ddagger_{C \rightarrow 3-2} = 22.3 \text{ kcal mol}^{-1}$) than that from either **3-1** or **B**. Moreover, as **C** is stabilised compared to **3-1** ($\Delta G_{r,3-1+2-1 \rightarrow C} = -5.2 \text{ kcal mol}^{-1}$), the activation barrier starting from **3-1** becomes $\Delta G^\ddagger = 17.1 \text{ kcal mol}^{-1}$. Thus, a pathway that proceeds *via* the 5-coordinate species **C** has the lowest activation barrier for the overall process (**3-1** + **2-1** → **3-2**) for all three pathways investigated (Figure 3.9).

⁹ **B** not necessarily present under reaction conditions (RT), as cooling during the VT NMR spectroscopic study may have favoured the formation of **B**.

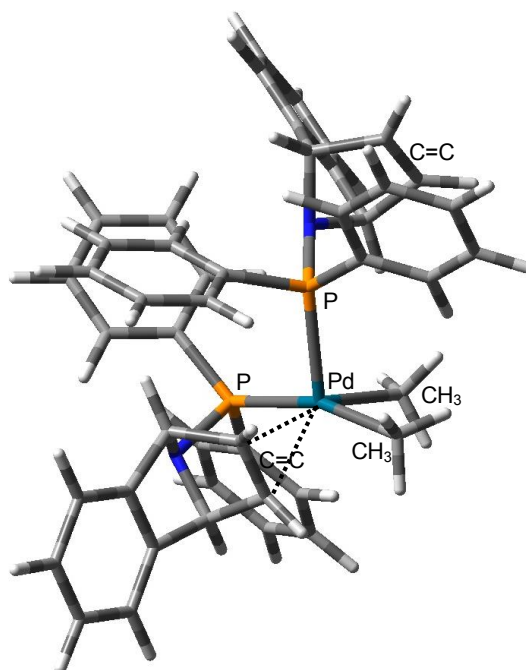
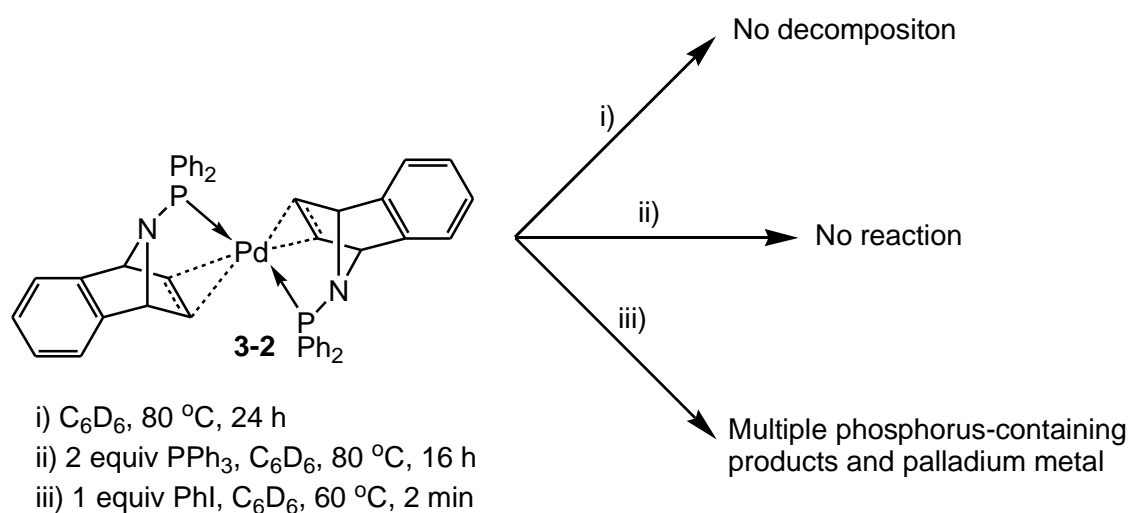


Figure 3.10: Calculated structure of complex **C**, $\text{cis-}[\text{PdMe}_2(\kappa^1\text{-P-2-1})(\kappa^2\text{-P,C-2-1})]$.

3.3 Stability and reactivity of complex $[\text{Pd}(\kappa^2\text{-P,C-2-1})_2]$ (**3-2**)



Scheme 3.16: Reactivity of $[\text{Pd}(\kappa^2\text{-P,C-2-1})_2]$ (**3-2**).

It is well established that palladium(0) has a lower affinity for alkenes than nickel(0), as it is a poorer π -donor, confirmed by the order of equilibrium constants $\text{M} = \text{Ni} \gg \text{Pt} > \text{Pd}$ in the reaction, $\text{M}(\text{PR}_3)_3 + \text{C}_2\text{H}_4 \leftrightarrow \text{M}(\text{C}_2\text{H}_4)(\text{PR}_3)_2 + \text{PR}_3$.¹⁹ Therefore, we expected $[\text{Pd}(\kappa^2\text{-P,C-2-1})_2]$, (**3-2**) to be generally more reactive than $[\text{Ni}(\kappa^2\text{-P,C-2-1})_2]$ (**2-6**), which

has been shown to be extremely stable (Section 2.2.4.2). Consequently, Section 3.3 describes experiments performed to help assess the stability and reactivity of **3-2**.

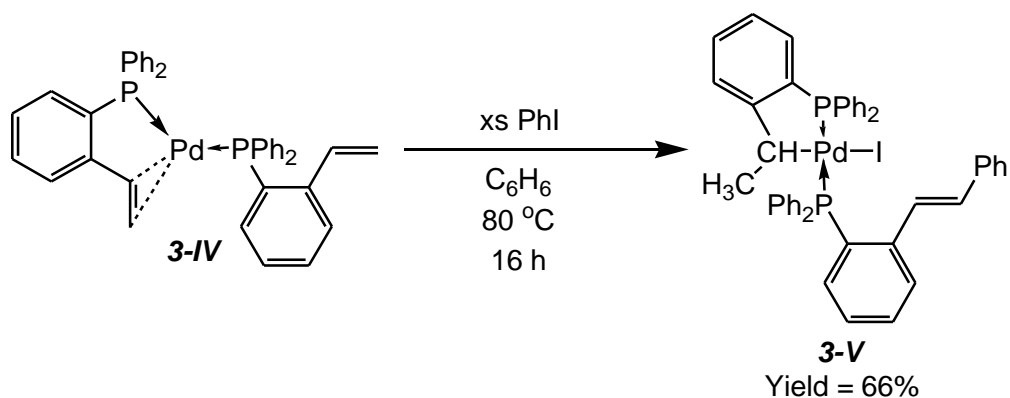
In contrast to the predicted reactivity, complex **3-2** exhibits a remarkable tolerance towards air/moisture, being stable in air and (non-dried) organic solutions for several days. Additionally, a C₆D₆ solution of **3-2** can be heated at 80 °C under an N₂ atmosphere for 24 h with no decomposition detected by ³¹P{¹H} NMR spectroscopy^h (Scheme 3.16).

As palladium has a lower affinity for alkenes than nickel one might expect that the alkene groups of **3-2** would be significantly easier to displace than in the nickel analogue **2-6**. However, heating (80 °C, 16 h) a solution of complex **3-2** with two equivalents of triphenylphosphine did not lead to the displacement of the alkene groups, signifying that the alkene groups are strongly bound to the palladium centre (Scheme 3.16).

The nickel analogue of **3-2** (**2-6**) was very stable and inert towards the oxidative addition of iodobenzene, showing no reaction with iodobenzene upon heating with excess iodobenzene at 80 °C for 16 h. Conversely, heating a solution of complex **3-2** with 10 equivalents of iodobenzene at 60 °C for 2 mins resulted in the precipitation of palladium metal. Analysis of the remaining solution by ³¹P{¹H} NMR spectroscopy revealed that all of complex **3-2** had been consumed and replaced by multiple phosphorus-containing species (Scheme 3.16). A control experiment showed that no reaction was observed between a solution of ligand **2-1** and iodobenzene upon heating at 60 °C for 15 minutes, suggesting that the iodobenzene was interacting with a palladium-containing species **3-2**. The precipitation of palladium metal suggests that the initial oxidative addition product of iodobenzene to **3-2** is not stable. In contrast to the previous observations (Section 2.2.4.2) the higher reactivity of **3-2** compared to **2-6** is thought to reflect the greater affinity of alkenes for nickel than for palladium.

The reaction of P-alkene palladium(0) complexes with iodobenzene is a known transformation. Bennett *et al.* have demonstrated the oxidative addition of iodobenzene to palladium P-alkene complex **3-IV** (Scheme 3.17), with the product subsequently undergoing rearrangement to **3-V**.

^h With reference to an internal phosphorus-containing standard (PPh₃) located within a sealed capillary



Scheme 3.17: Oxidative addition of iodobenzene to a (P-alkene)palladium(0) complex **3-IV** and subsequent rearrangement, as reported by Bennett and co-workers.²⁰

3.3.1 Utilising P-alkene ligand 2-1 in palladium-catalysed reactions

3.3.1.1 Suzuki-Miyaura cross-coupling

There is precedent for P-alkene ligands forming highly active and stable catalysts in the Suzuki-Miyaura cross-coupling of aryl bromides with phenylboronic acid. For example, Williams and co-workers observed that the P-alkene ligands **3-VI** and **3-VII** (Figure 3.11), formed significantly more active and stable catalysts with palladium than their saturated analogues.⁹ With the increased activity of **3-VI** and **3-VII** over their saturated analogues believed to be caused by a faster rate of transmetalation or the reductive elimination.⁹

Encouraged by the reactivity of the conveniently-prepared and air-/moisture-stable complex **3-2** with iodobenzene (Section 3.3), we tested **3-2** as a catalyst in palladium-mediated cross-coupling reactions. The Suzuki-Miyaura cross-coupling of unactivated aryl halides and phenyl boronic acid was chosen in the first instance (Scheme 3.18).ⁱ

ⁱ This is purely a feasibility study and no effort was made to optimise the reaction conditions.

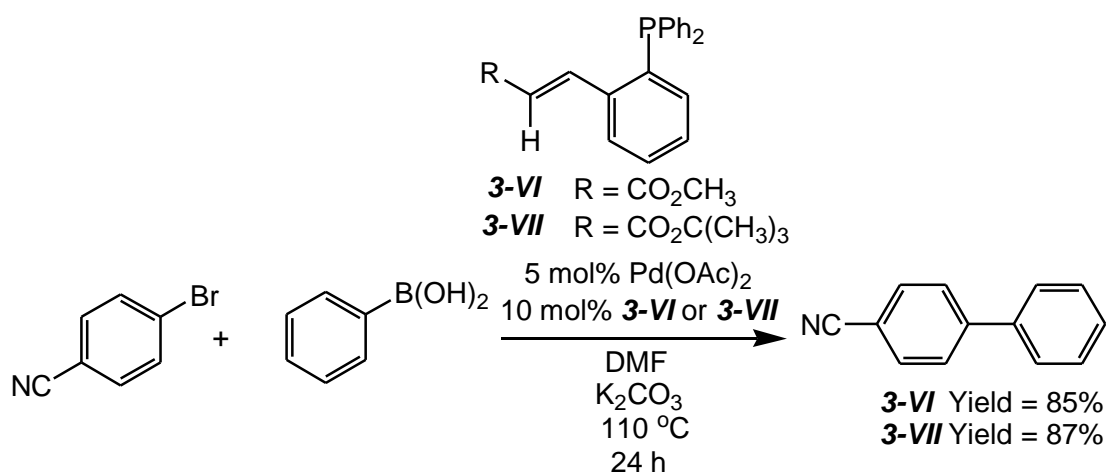
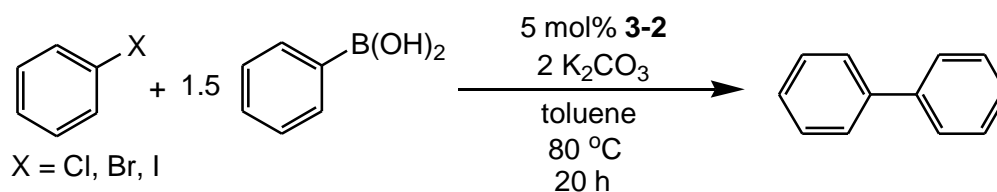


Figure 3.11: *P*-Alkene ligands developed by Williams *et al.* for use in Suzuki-Miyaura cross-coupling reactions.

Table 3.1 reports the yields of biphenyl produced^j after 20 h at 80 °C for the Suzuki-Miyaura cross-coupling of various aryl halides with phenyl boronic acid catalysed by 1 mol% **3-2**. The coupling of iodobenzene and phenyl boronic acid proceeded in good yield (entry 1), although slightly lower than with the more electron-rich Pd(0) source [Pd(PPh₃)₄] (entry 8). However, when a drop of mercury was added to the reaction mixture the yield of biphenyl dropped to <1% (entry 4). The addition of mercury is a qualitative test to verify if colloidal Pd(0) species are the active catalytic species.^k A positive mercury drop test implies that colloidal Pd(0), which is presumed to arise from decomposition of complex **3-2**, is the direct catalyst in the reaction. As the catalytically-active species is formed by the breakdown of **3-2**, then the electronic effects of **2-1** will have no impact on the reaction.



Scheme 3.18: Suzuki-Miyaura cross-coupling of phenylboronic acid and aryl halides utilising **3-2** as a pre-catalyst.

^j Determined by GC-FID, using nonane as an internal standard.

^k Colloidal Pd(0) reacts with Hg(0) forming an amalgam, thus quenching the palladium nanoparticles as they are released upon decomposition of the complex.

Entry	Aryl halide	Yield of biphenyl %
1	PhI	84
2	PhBr	33
3	PhCl	3
4	PhI ^a	<1
5	PhI ^b	0
6	PhI ^c	0
7	None	3
8	PhI ^d	98

Conditions: aryl halide (0.5 mmol), phenylboronic acid (0.75 mmol), K_2CO_3 (1.0 mmol), 1 mol% **3-2**, toluene (5.0 cm³), 80 °C, 20 h. Percentage yield determined by GC based on biphenyl (internal standard of nonane used), and averaged over two runs.

(a) 1 drop Hg added, (b) No **3-2** added, (c) No phenylboronic acid, (d) **3-2** replaced by $Pd(PPh_3)_4$

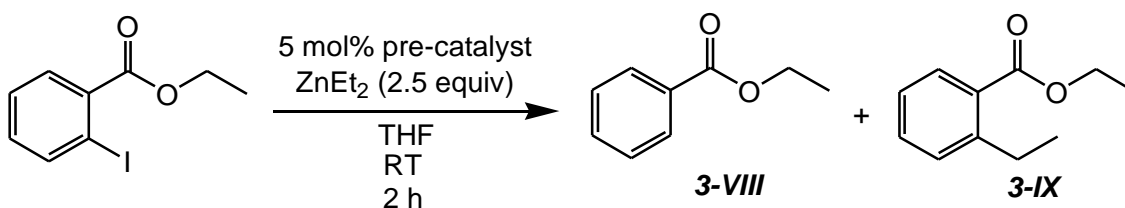
Table 3.1: Yields of biphenyl found for the Suzuki-Miyaura cross-coupling of phenylboronic acid and aryl halides utilising **3-2** as a pre-catalyst.

3.3.1.2 Negishi cross-coupling

The catalytic performance of ligand **2-1** was also tested in the Negishi cross-coupling of ethyl 2-iodobenzoate and diethylzinc, under conditions identical to those used by Lei and Espinet for the same transformation (Scheme 3.19).^{10, 21} The aforementioned cross-coupling has been established as a good test for the ability of a ligand to promote reductive elimination over competing β -hydride elimination (Section 3.1.2.2).¹⁰ The addition of various pre-catalysts containing the P-alkene ligand **2-1** to the Negishi cross-coupling of ethyl 2-iodobenzoate and diethylzinc afforded products formed by β -hydride elimination (**3-VIII**) and by cross-coupling (**3-IX**), with only traces (<1%) of other products detected (Table 2.2).¹ Best results utilising ligand **2-1** were obtained when $[PdCl_2(\kappa^1-P-2-1)]$ was used as the pre-catalyst (entry 3), giving greater selectivity and significantly higher activity than the use of a 1:1 mixture of $[PdCl_2(MeCN)_2]$ and **2-1** (entry 4). It is presumed that on using a 1:1 mixture of $[PdCl_2(MeCN)_2]$ and **2-1** not enough time was left before the zinc reagent was added in order to form $[PdCl_2(\kappa^2-P,C-2-1)]$ (2 minutes stirring). Pre-formed palladium(0) complex **3-2** proved a poor pre-catalyst for this reaction giving the lowest conversion to products **3-VIII** and **3-IX**, with 95% of the starting ethyl 2-iodobenzoate being left at the end of the reaction (entry 5); this is unsurprising due to **3-2** being highly stabilised by two electron deficient **2-1**

¹ Conversions were quantified by GC-FID analysis, and are the average of two runs.

ligands. In all reactions involving ligand **2-1**, the fraction of **3-IX** formed was poor, with **3-VIII** (β -hydride elimination product) dominating.



Scheme 3.19: Impact of different ligands on Csp^3 -involved Negishi cross-coupling.

Entry	Pre-catalyst	Conversion of ethyl 2-iodobenzoate / %	3-VIII : 3-IX
1	$[\text{Pd}(\text{PPh}_3)_4]$	100	43 : 57 ^m
2	$[\text{PdCl}_2(\text{PPh}_3)_2]$	100	94 : 6 ⁿ
3	2-1 + $[\text{PdCl}_2(\text{MeCN})_2]$	13	96 : 4
4	$[\text{PdCl}_2(\kappa^1\text{-P-2-1})]$	100	86 : 14
5	$[\text{Pd}(\kappa^1\text{-P-2-1})_2]$ (3-2)	5	98 : 2

Conditions: ethyl-2-iodobenzoate (1.0 mmol), Et_2Zn (2.5 mmol), 5 mol% pre-catalyst, THF (5.0 cm^3), RT, 2 h. Percentage conversion and selectivity determined by GC (internal standard of nonane used), and averaged over two runs.

Table 3.2: Catalytic results for the Negishi cross-coupling of diethylzinc and ethyl-2-iodobenzoate.

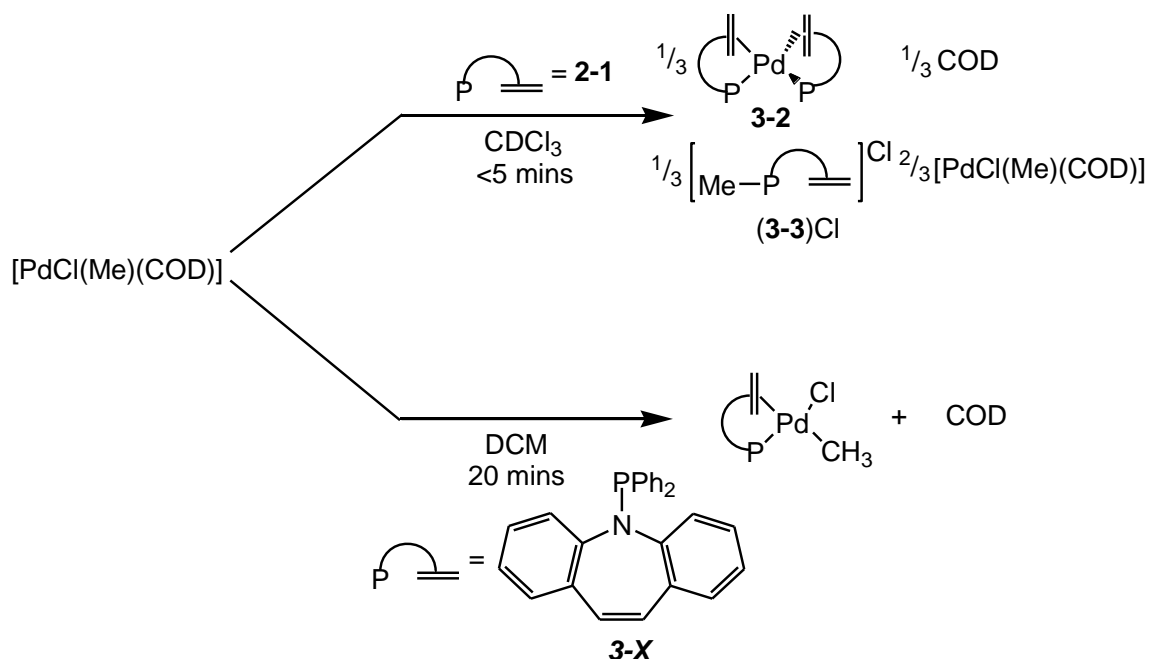
3.4 Coordination chemistry of P-alkene **2-1** with a $\text{PdCl}(\text{Me})$ fragment

Section 3.2 detailed that ligand **2-1** was able to promote the reductive elimination of ethane from palladium dimethyl complexes. Following this success, we next hoped to apply ligand **2-1** to some more difficult reductive elimination processes, e.g. alkyl halide reductive elimination. Due to significant M–Cl bond polarisation, the barrier to alkyl chloride reductive elimination is much greater than for alkyl-alkyl elimination. For example, the theoretical barriers to reductive elimination of ethane and chloromethane are reported by Suresh *et al.* to be approximately 20 kcal mol^{-1} higher in $[\text{PdCl}(\text{Me})(\text{PR}_3)_2]$ complexes than in equivalent $[\text{PdMe}_2(\text{PR}_3)_2]$ complexes.⁵ Whilst alkyl

^m **3-VIII** : **3-IX** ratio of 43.8 : 56.2 reported by Lei¹⁰

ⁿ **3-VIII** : **3-IX** ratio of 60.9 : 39.1 reported by Lei¹⁰

chloride reductive elimination is known for 5- and 6-coordinate transition metal complexes, to the best of our knowledge there are no examples of methyl chloride reductive elimination from 4-coordinate palladium(II) complexes.^{22, 23}

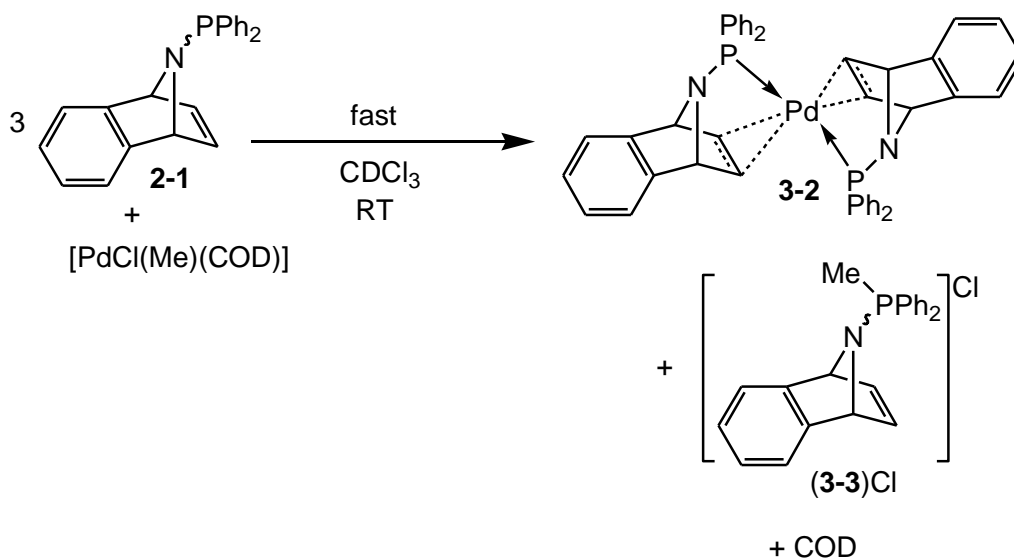


Scheme 3.20: The reaction of one equivalent of ligand **2-1** with [PdCl(Me)(COD)] (this work) and a contrasting reaction utilising P-alkene ligand **3-X** (by Oberhauser and co-workers²⁴).

The reaction between one equivalent of ligand **2-1** and [PdCl(Me)(COD)] resulted in the rapid formation of the palladium(0) complex **3-2**, consistent with MeCl reductive elimination at room temperature. However, on closer analysis of the reaction products an equimolar amount of the methyl phosphonium chloride salt of **2-1**, **(3-3)Cl**, is also obtained ($\delta^{31}\text{P}\{^1\text{H}\}$ 38.1 ppm) along with unreacted [PdCl(Me)(COD)] (Scheme 3.20). The presence of **(3-3)Cl** was confirmed by ESI mass spectrometry, showing a peak at $m/z = 342$ for the cationic **3-3⁺** fragment. The methyl phosphonium chloride salt **(3-3)Cl** also exhibited a distinctive and characteristic doublet resonance at 2.82 ppm, $^2J_{\text{PH}} = 13$ Hz by ^1H NMR spectroscopy, for the phosphorus-bonded methyl group. Notably, changing the stoichiometry of the reagents to three equivalents of **2-1** per [PdCl(Me)(COD)] afforded, rapidly and quantitatively, a 1:1:1 mixture of **3-2**, **(3-3)Cl** and COD as the only products (Scheme 3.21).

In contrast to the reactivity shown by P-alkene ligand **2-1** with [PdCl(Me)(COD)], P-alkene ligand (**3-X**) was shown by Oberhauser *et al.* to form the stable complex [PdCl(Me)(κ²-P,C-(**3-X**))] (Scheme 3.20), *i.e.* methyl and chloride ligands are not eliminated from the metal centre.²⁴ As both **2-1** and **3-X** contain an R₂N-PPh₂

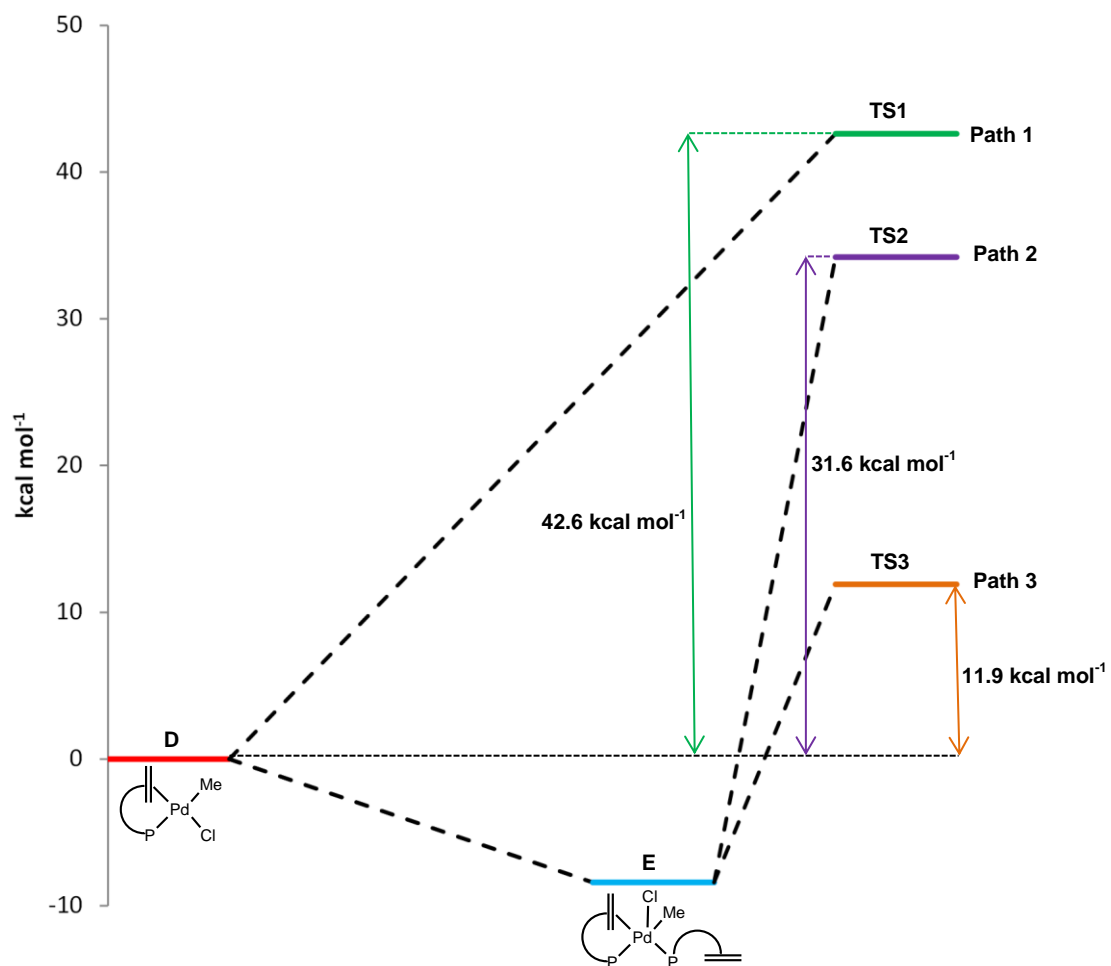
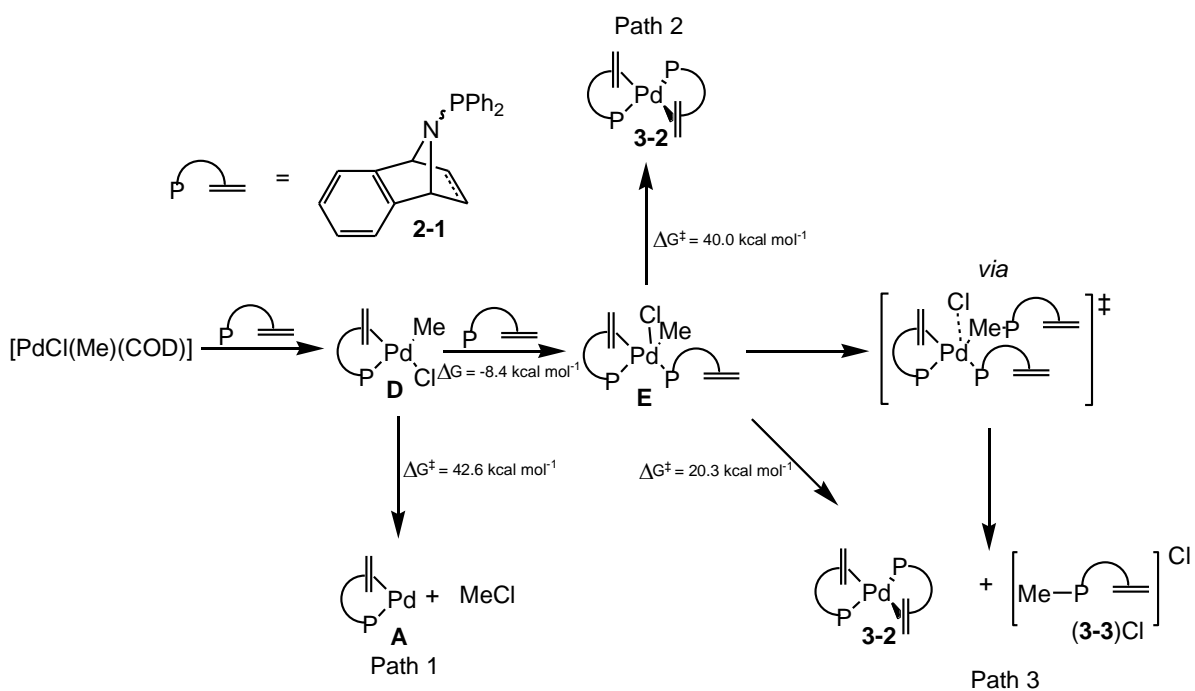
phosphine moiety (and hence a comparable Lewis basicity for the P-based donor) any difference in the reactivity between these two ligands with $[\text{PdCl}(\text{Me})(\text{COD})]$ must be attributed to the nature of the alkene moiety.



Scheme 3.21: Reaction between three equivalents of **2-1** and $[\text{PdCl}(\text{Me})(\text{COD})]$.

3.4.1 Investigating the mechanism of the reaction between P-alkene **2-1** and $[\text{PdCl}(\text{Me})(\text{COD})]$

The reaction of three equivalents of **2-1** with $[\text{PdCl}(\text{Me})(\text{COD})]$ led to the very rapid formation of complex **3-2** and phosphonium salt **(3-3)Cl**. Due to the high rate of reaction, no intermediates were detected by NMR spectroscopy on the way to the formation of **3-2** and **(3-3)Cl**. Therefore, in order to gain a greater understanding of the mechanism for the methyl and chloride ligand removal from the palladium centre a computational analysis of this system has been undertaken. The following calculations were performed by Karinne Miqueu, Jean-Marc Sotiropoulos, and Laura Estevez (Université de Pau), and were performed *in vacuo* at the B3LYP/SDD+f(Pd), 631G** (other atoms) level of theory. The following discussion relates to the complexes and reaction steps displayed in Scheme 3.22, it does not constitute a full analysis of all possible mechanisms, due to the large number of components involved and, hence, the number of reaction pathways achievable. We have suggested and then investigated plausible steps based on knowledge gained from studying the reaction of **2-1** with $[\text{PdMe}_2(\text{tmeda})]$ (Section 3.2.3) and on previous literature precedent.²²



Scheme 3.22: Proposed mechanisms and reaction profile for the elimination of methyl and chloride ligands from $[\text{PdCl}(\text{Me})(\text{COD})]$ investigated by computational analysis. TSX = transition state for the elimination of methyl and chloride ligands in path X.

Path 1: Reductive elimination of MeCl from a 4-coordinate complex

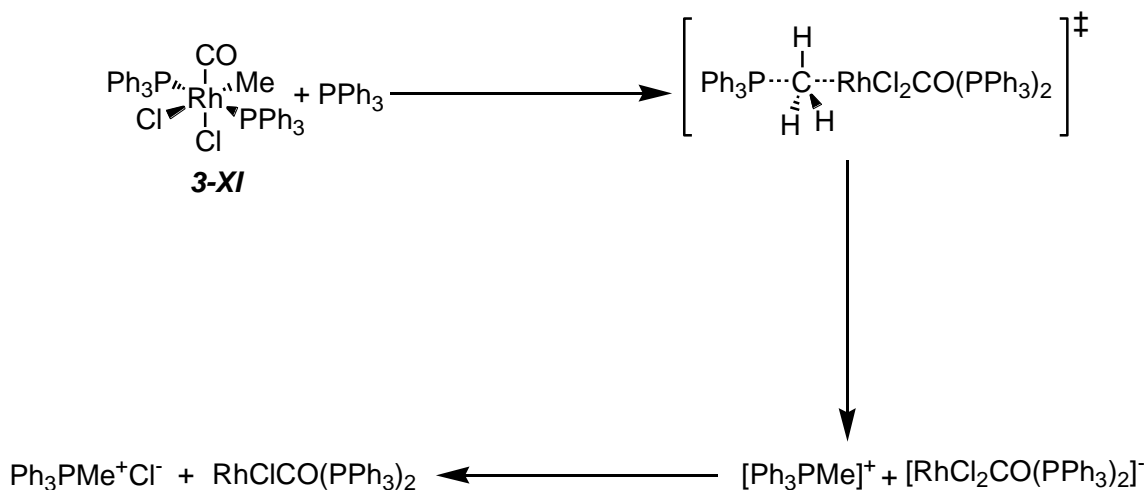
It is reasonable to suggest that $[\text{PdCl}(\text{Me})(\kappa^2\text{-P,C-2-1})]$ (**D**) could be formed in solution by the displacement of COD by **2-1**, but, the calculated barrier to reductive elimination of MeCl from **D** is very large, $\Delta G^\ddagger_{\text{D}\rightarrow\text{A}} = +42.6 \text{ kcal mol}^{-1}$, which is inconsistent with the high rate of reaction observed. Indeed, the barrier to MeCl reductive elimination from **D** is significantly larger than that calculated for the dimethyl analogue $[\text{PdMe}_2(\kappa^2\text{-P,C-2-1})]$ **3-1** ($\Delta G^\ddagger_{\text{3-1}\rightarrow\text{A}} = +28.1 \text{ kcal mol}^{-1}$), from which it is known that ethane reductive elimination takes significantly longer (5 days).

Path 2: Reductive elimination of MeCl from a 5-coordinate complex

It has been calculated that the formation of a 5-coordinate complex **E** by the addition of a second equivalent of **2-1** to **D** is favourable ($\Delta G_{\text{r,D}\rightarrow\text{E}} = -8.4 \text{ kcal mol}^{-1}$). However, the barrier to the reductive elimination of MeCl from **E** is comparable to that from **D**, $\Delta G^\ddagger_{\text{E}\rightarrow\text{3-2}} = +40.0 \text{ kcal mol}^{-1}$. Given the large barriers to reductive elimination of MeCl from **D** and **E**, we have discounted any proposed mechanism that involves direct reductive elimination of MeCl from a Pd(II)Cl(Me) complex.

Path 3: S_N2 attack of the phosphine group of P-alkene 2-1 on a palladium methyl group

As the direct reductive elimination of MeCl is highly unlikely due the high energy barriers calculated, we propose the existence of an alternative reaction pathway that does not involve direct MeCl reductive elimination, namely, the S_N2 attack of the phosphine moiety of **2-1** on a palladium methyl group. Whilst the formation of a methyl phosphonium chloride salt by S_N2 attack of a phosphine on a Pd(II)Cl(Me) complex is an unprecedented transformation, there is literature precedent for a similar transformation occurring with an octahedral rhodium complex. It was observed by Baird and co-workers that the reductive elimination of MeCl from $[\text{RhCl}_2(\text{Me})(\text{CO})(\text{PPh}_3)_2]$ (**3-XI**) was significantly enhanced in the presence of excess PPh₃ with the formation of the phosphonium salt, (MePPh₃)Cl (Scheme 3.23); the rates of reaction were of a convenient magnitude such that the reaction could be readily probed by NMR spectroscopy. Consequently, Baird proposes that as the formation of the phosphonium salt occurred at a rate faster than that observed for the reaction of free MeCl with PPh₃, then direct nucleophilic attack by the phosphine on the rhodium-bound methyl group was a plausible mechanism for Me-Cl elimination.²²



Scheme 3.23: Mechanism proposed by Baird et al. for the elimination of methyl and chloride ligands from $[\text{RhCl}_2(\text{Me})(\text{CO})(\text{PPh}_3)_2]$, adapted from Baird and co-workers.²²

With this alternative mechanism in mind we propose a mechanism that involves $\text{S}_{\text{N}}2$ attack of the phosphine moiety of a third equivalent of **2-1** on the methyl carbon of complex **E**, with the remaining palladium complex as the leaving group (Scheme 3.22). The energy barrier for this nucleophilic attack pathway is much lower ($\Delta G^\ddagger_{\text{E} \rightarrow \text{3-2} + (\text{3-3})\text{Cl}} = +20.3 \text{ kcal mol}^{-1}$) than direct reductive elimination of MeCl from **D** or **E** ($\sim 40 \text{ kcal mol}^{-1}$). If one considers the additional stability of **E** over **D**, the reaction barrier for the removal of the methyl and chloride ligands from **D** drops to $\Delta G^\ddagger = +11.9 \text{ kcal mol}^{-1}$. A reaction barrier of $\Delta G^\ddagger = +11.9 \text{ kcal mol}^{-1}$ is consistent with the high rate of reaction observed. The attack of phosphine on a palladium-bound methyl group *via* an $\text{S}_{\text{N}}2$ pathway is surprising given the electronegativities of the atoms involved (C = 2.55, P = 2.19), hence, the methyl group of **E** is presumably activated by the strongly electrophilic $\text{Pd}(\kappa^2\text{-P,C-2-1})$ fragment. The calculated structure of the transition state for the attack of **2-1** on methyl group of **E** *via* an $\text{S}_{\text{N}}2$ process is shown in Figure 3.12, the methyl group presents a trigonal planar structure about carbon, consistent with an $\text{S}_{\text{N}}2$ reaction.

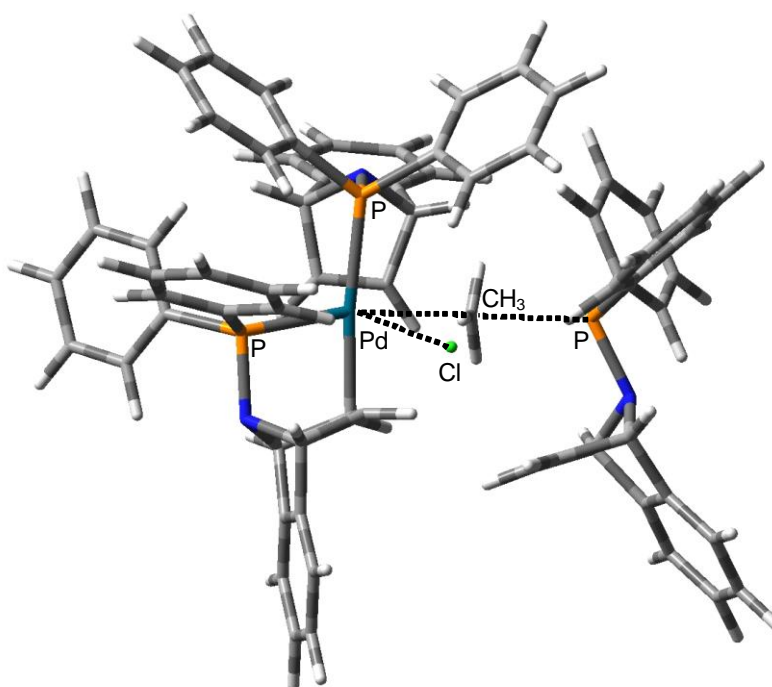


Figure 3.12: Calculated transition state structure for S_N2 attack of **2-1** on **E**.

In summary, the reaction of three equivalents of P-alkene **2-1** with $[\text{PdCl}(\text{Me})(\text{COD})]$ led to the very rapid formation to **3-2** and phosphonium salt (**3-3**)Cl, with no intermediates being detected by NMR spectroscopy. Computational calculations suggest that the methyl and chloride ligands were not removed from the metal centre by direct chloromethane reductive elimination (Scheme 3.22: path 1 + path 2) as the energy barriers are unfeasibly high. Instead, a pathway with a lower energy barrier involving the S_N2 nucleophilic attack of **2-1** on a palladium-methyl group is proposed (path 3), with the palladium-methyl group activated by the strongly electrophilic $\text{Pd}(\kappa^2\text{-P,C-2-1})$ fragment.

3.5 Synthesis and coordination chemistry of *N*-PPh₂-3-pyrroline – a less rigid and bulky analogue of P-alkene **2-1**

The alkene group of ligand **2-1** was designed to bind very strongly to a metal centre by virtue of being located in a rigid and strained framework. However, the alkene group of **2-1** was found to be very π -accepting and this was found to highly stabilise low oxidation state complexes of Pd(0) and Ni(0), limiting their reactivity. Hence there was a need for an analogue of **2-1** which is less π -accepting, that could form complexes with significantly different reactivity.

3.5.1 Synthesis of *N*-PPh₂-3-pyrroline (**3-4**)

This section details attempts to synthesise a less rigid and therefore less π -accepting analogue of **2-1**, namely, *N*-PPh₂-3-pyrroline (**3-4**). Compound **3-4** was chosen to mimic some of the features of the norbornene-based phosphine-alkene **2-1**, namely to include an alkene located within a 5-membered ring and a diphenylaminophosphine moiety, but have a less rigid and bulky skeleton, which could potentially lower the binding strength of the alkene group. The lower affinity of the alkene moiety of **3-4** to a metal compared to **2-1** is a manifestation of **3-4** being less strained and thus there is a smaller reduction in ring strain upon the alkene binding to a metal. It was envisaged that mono-cyclic P-alkene **3-4** would form complexes with significantly different reactivity to those formed with **2-1**. Consequently, this section of the thesis details the coordination chemistry of **3-4** to palladium and explores subsequently the reactivity of the ensuing complexes.

Ligand **3-4** bears resemblance to ligand **3-XII**, recently reported by Hayashi and co-workers, a chiral ligand based on the *N*-PPh₂-3-pyrroline backbone (Figure 3.13), which was synthesised in a relatively complex multi-step procedure. Bidentate coordination of **3-XII** to rhodium through the phosphine and alkene moieties was shown by X-ray diffraction studies,^{25, 26} something that suggests that **3-4** will also act as a bidentate ligand to late transition metals such as palladium.

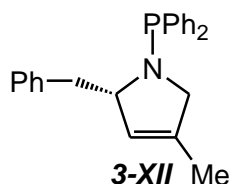
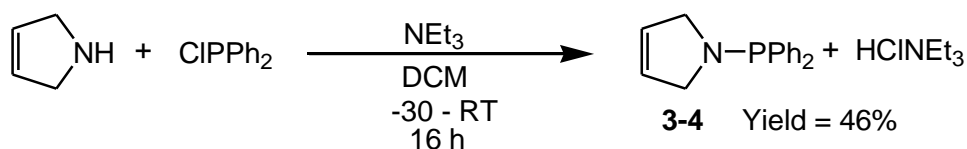


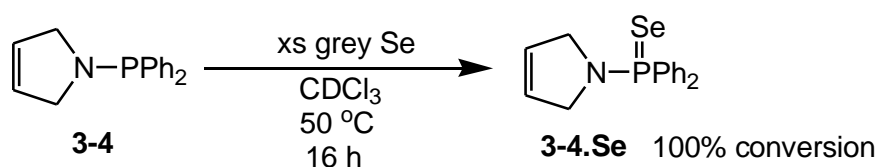
Figure 3.13: Ligand **3-XII**, a chiral P-alkene *N*-PPh₂-3-pyrroline-based ligand developed by Hayashi and co-workers.^{25, 26}



Scheme 3.24: Synthesis of *N*-PPh₂-3-pyrroline (**3-4**).

The ligand *N*-PPh₂-3-pyrroline (**3-4**) was prepared in moderate yield (46%) from 3-pyrroline *via* a straightforward nucleophilic substitution reaction with chlorodiphenylphosphine (Scheme 3.24) and was purified by vacuum distillation. The

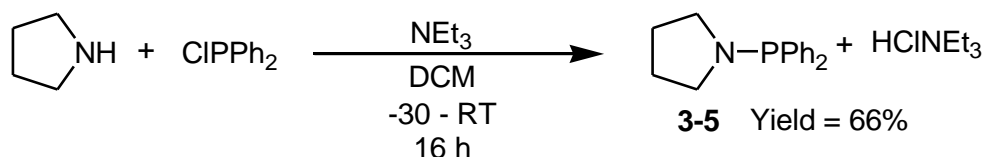
colourless, viscous oil produced solidified into a white solid upon cooling to $-20\text{ }^{\circ}\text{C}$, which did not melt upon warming to room temperature.⁹ Compound **3-4** was characterised by multinuclear NMR spectroscopy and elemental analysis. $^{31}\text{P}\{^1\text{H}\}$ NMR spectroscopy exhibits a singlet resonance at $+47.4\text{ ppm}$, typical of other aminodiphenylphosphines.²⁷ The alkene protons of the 3-pyrroline moiety appear as a broad singlet resonance at $+5.38\text{ ppm}$ by ^1H NMR spectroscopy, slightly shifted to lower frequency compared to 3-pyrroline (5.84 ppm).²⁸ The magnitude of the $^1J_{\text{Se-P}}$ coupling constant of 776 Hz for **3-4.Se** (synthesis in Scheme 3.25) confirms that the phosphorus donor moiety of **3-4** is weakly basic and is comparable to that of **2-1** ($^1J_{\text{Se-P}} = 792\text{ Hz}$).²⁹ Thus, it is reasonable to suggest that any differences in the coordination chemistry of **2-1** and **3-4** can be ascribed to the differences in the rigidity and steric bulk of the alkene-containing moiety.



Scheme 3.25: Synthesis of **3-4.Se**.

3.5.2 Synthesis of *N*-PPh₂-pyrrolidine (**3-5**)

The previously reported compound **3-5** was synthesised to probe the impact of the alkene moiety in **3-4** on its coordination chemistry compared to its saturated analogue, **3-5**. *N*-PPh₂-pyrrolidine (**3-5**), was synthesised using an analogous method to that for the preparation of **3-4** from the parent pyrrolidine (Scheme 3.26), giving a slight improvement in yield over a similar literature procedure used to synthesise **3-5**.³⁰



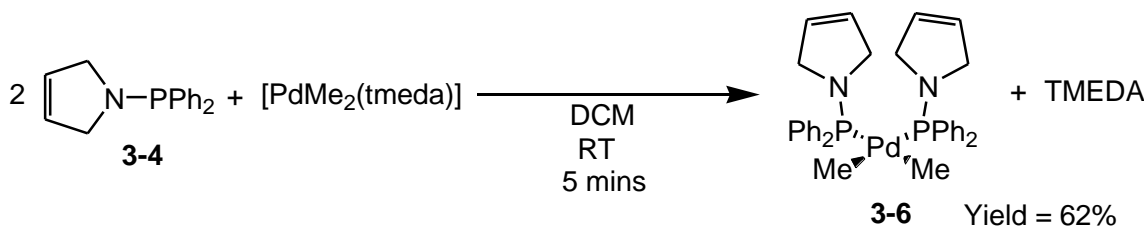
Scheme 3.26: Synthesis of *N*-PPh₂-pyrrolidine (**3-5**).

⁹ 3-Pyrroline is commercially available, but is easily synthesised by the reduction of pyrrole by Zn/HCl.

The spectroscopic data for **3-5** are consistent with those reported previously in the literature, showing a single resonance at 47.4 ppm by $^{31}\text{P}\{^1\text{H}\}$ NMR spectroscopy.³⁰ Notably, the value of $|^1J_{\text{Se-P}}|$ for **3-5.Se** is 748 Hz,³⁰ indicating in general terms that the inclusion of the alkene group in **3-4** makes the phosphorus moiety slightly less basic. It is proposed here that this difference in $|^1J_{\text{Se-P}}|$ between **3-4.Se** and **3-5.Se** is not due to direct electronic interaction between the alkene and the P-centre, but rather it can be attributed to small changes in the geometry around the phosphorus centre as enforced by the alkene group of **3-4.Se**.

3.5.3 Exploring the coordination chemistry of monocyclic P-alkene **3-4** with PdMe_2 fragments

In Section 3.2.2 it was reported that the addition of two equivalents of P-alkene **2-1** to $[\text{PdMe}_2(\text{tmEDA})]$ results in the reductive elimination of ethane and the formation of the homoleptic palladium(0) complex **3-2**, a process that is complete in 5 h at RT. To explore the importance of the bicyclic nature of ligand **2-1** an analogous reaction was attempted using monocyclic **3-4**.

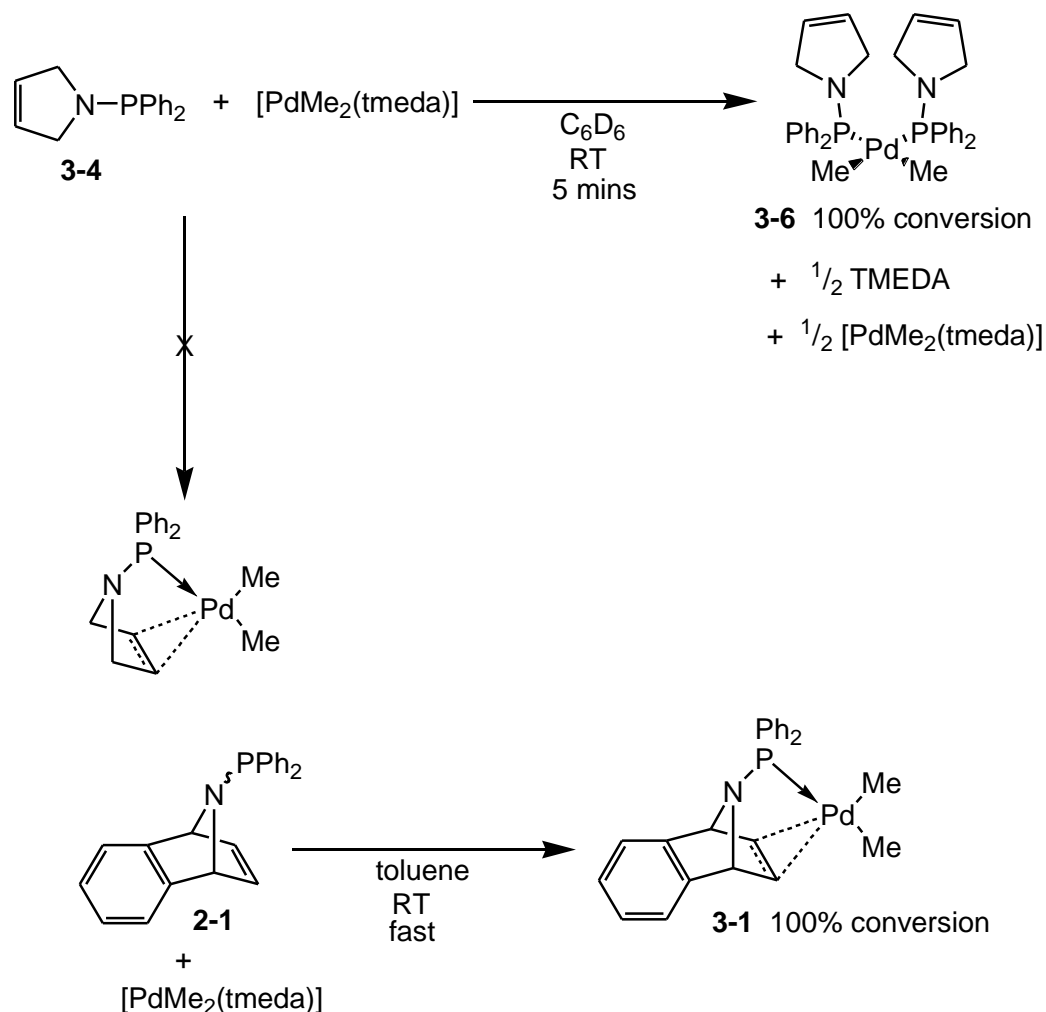


Scheme 3.27: Synthesis of $[\text{PdMe}_2(\kappa^1\text{-P-3-4})_2]$ (**3-6**).

The addition of 2 equivalents of **3-4** to $[\text{PdMe}_2(\text{tmEDA})]$ in C_6D_6 resulted in the rapid and quantitative conversion (via $^{31}\text{P}\{^1\text{H}\}$ NMR spectroscopy) to *cis*- $[\text{PdMe}_2(\kappa^1\text{-P-3-4})_2]$ (**3-6**). The *cis* orientation of the methyl groups is clear from the ^1H NMR spectrum of **3-6**, with the resonance of the methyl groups appearing as a doublet of doublets at 1.03 ppm, consistent with $^2J_{\text{PH}}$ coupling to two magnetically inequivalent phosphorus centres. The $^{31}\text{P}\{^1\text{H}\}$ NMR spectrum of **3-6** shows a singlet resonance at 70.8 ppm ($\Delta\delta$ +23.4 ppm), consistent with a palladium-bound phosphorus moiety.

To confirm the identity of **3-6** in the NMR-scale reaction above, compound **3-6** was also synthesised and isolated on a larger scale in 62% yield (Scheme 3.27) with characterisation accomplished by multinuclear NMR spectroscopy and elemental

analysis; spectroscopic data for **3-6** was consistent between the NMR-scale and the larger scale reaction.



Scheme 3.28: The addition of one equivalent of **3-4** to $[\text{PdMe}_2(\text{tmeda})]$.

Notably, the addition of just one equivalent of P-alkene **3-4** to $[\text{PdMe}_2(\text{tmeda})]$ resulted in the formation of **3-6**, leaving half an equivalent of unreacted $[\text{PdMe}_2(\text{tmeda})]$ (visible by ^1H NMR spectroscopy) (Scheme 3.28). The target complex, $[\text{PdMe}_2(\kappa^2\text{-P,C-3-4})]$, analogous to **3-1**, was not observed, emphasizing a lower tendency of **3-4** to bind in a bidentate fashion, something presumed to result from its greater flexibility. Alternatively, as **3-4** is significantly less bulky than **2-1**, then there is less steric conflict between the ligands in a *cis*- $(\kappa^1\text{-P})_2$ arrangement (Figure 3.14), making **3-6** a low energy conformation, unlike *cis*- $[\text{PdMe}_2(\kappa^1\text{-P-2-1})_2]$, which is likely to be destabilised by the bulky ligand **2-1**. In contrast to Hayashi's structurally similar P-alkene ligand (**3-XII**, Figure 3.13), no evidence of the coordination of the alkene group of **3-4** has been

obtained.^P It is proposed that in **3-XII** the bulky benzyl group at the 2-position forces the alkene group towards the metal centre.

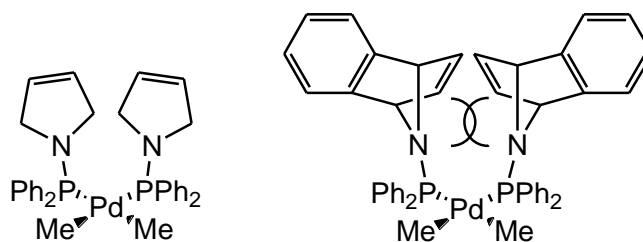
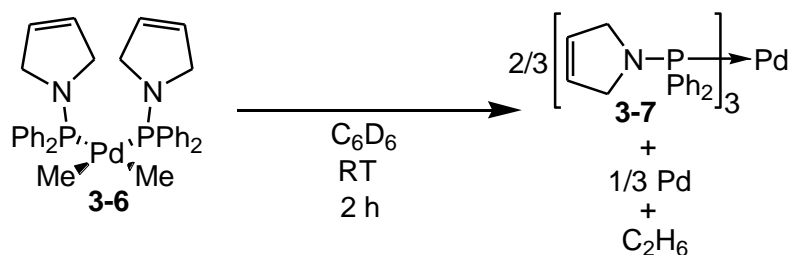


Figure 3.14: The steric repulsion between the cis-bound ligands is expected to be greater in the proposed complex $\text{cis-}[\text{PdMe}_2(\kappa^1\text{-P-2-1})_2]$ than in **3-6**.

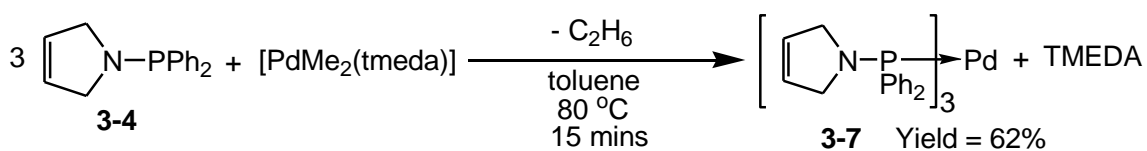
3.5.3.1 Ethane elimination from complex $[\text{PdMe}_2(\kappa^1\text{-P-3-4})_2]$ (**3-6**)

Complex **3-6** is not stable in solution at room temperature for prolonged periods of time. On leaving a C_6D_6 solution of **3-6** at room temperature for 2 h, signals attributed to complex **3-6** disappear completely, accompanied by the precipitation of palladium metal (Scheme 3.29). Analysis of the remaining solution by $^{31}\text{P}\{^1\text{H}\}$ NMR spectroscopy revealed a new broad singlet resonance at 66.9 ppm (FWHM = 16 Hz) (cf. **3-6** $\delta^{31}\text{P}$ 70.8 ppm). This new phosphorus-containing species has been identified as $[\text{Pd}(\kappa^1\text{-P-3-4})_3]$ (**3-7**) by comparison of the ^1H and ^{31}P NMR spectra with those of an independently synthesised authentic sample of **3-7** (Scheme 3.30). Additionally, analysis of the remaining solution by ^1H NMR spectroscopy showed that the resonance corresponding to the palladium-bound methyl groups of **3-6** (doublet of doublets at 1.03 ppm) had disappeared, something accompanied by the formation of ethane, which gives rise to a singlet at 0.80 ppm.³¹ Overall, very rapid ethane reductive elimination from complex **3-6** occurs, with the formation of two Pd(0) products.



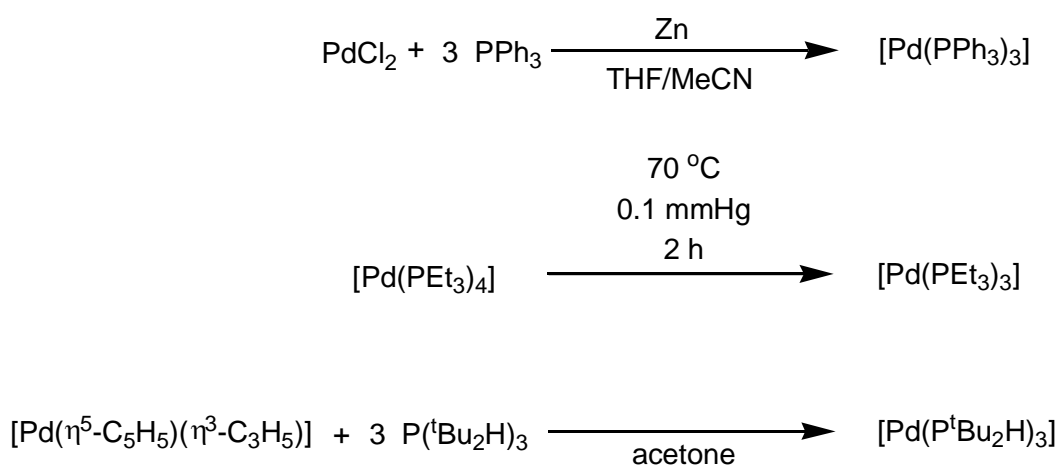
Scheme 3.29: Reductive elimination of ethane from $[\text{PdMe}_2(\kappa^1\text{-P-3-4})_2]$ (**3-6**).

^P It has been reported that **3-XII** can bind in a bidentate fashion in a rhodium(I) complex.²⁸



Scheme 3.30: Synthesis of $[\text{Pd}(\kappa^1\text{-P-3-4})_3]$ (3-7).

To the best of our knowledge, there are no reports of the formation of $[\text{Pd}(\text{PR}_3)_3]$ derivatives directly from *cis*- $[\text{PdMe}_2(\text{PR}_3)_2]$ complexes.^q However, there are numerous examples of $[\text{Pd}(\text{PR}_3)_3]$ complexes themselves, for example, $[\text{Pd}(\text{PPh}_3)_3]$, $[\text{Pd}(\text{PEt}_3)_3]$ and $[\text{Pd}(\text{P}^t\text{Bu}_2\text{H})_3]$, which can be synthesised by a variety of different methods (Scheme 3.31).³²⁻³⁴



Scheme 3.31: Different methods used to synthesise $[\text{Pd}(\text{PR}_3)_3]$ complexes.³²⁻³⁴

^q SciFinder search completed 11/12/13.

3.5.3.1.1 X-Ray crystallographic study of $[\text{Pd}(\kappa^1\text{-P-3-4})_3]$ (**3-7**)

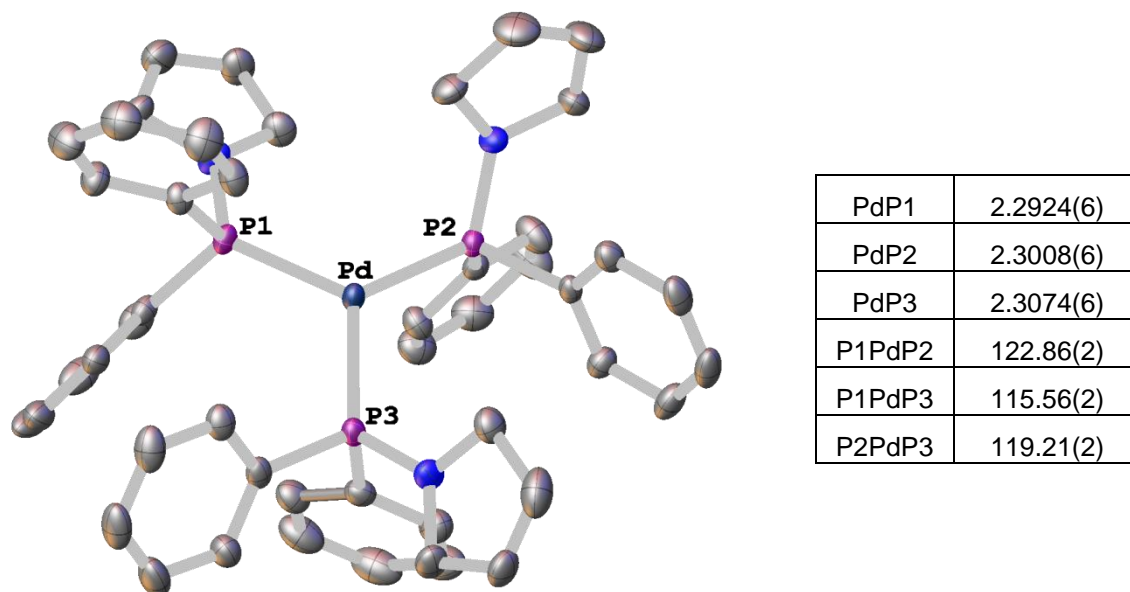


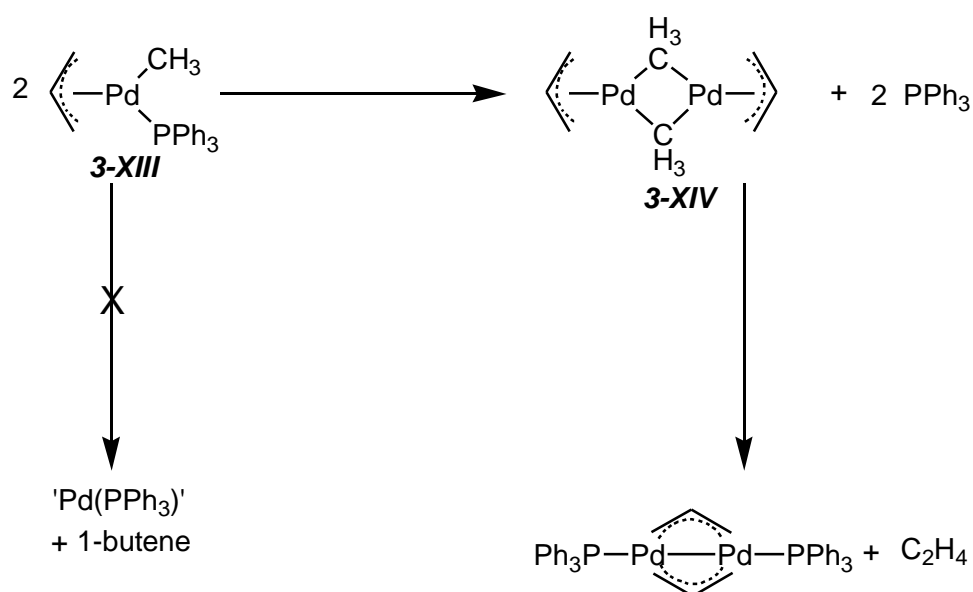
Figure 3.15: Molecular structure of $[\text{Pd}(\kappa^1\text{-P-3-4})_3]$ (**3-7**), with selected bond lengths (Å) and angles (°). Thermal ellipsoids set at 50% level.

Single crystals of **3-7** suitable for X-ray diffraction were grown by slow diffusion of hexane into a concentrated toluene solution; the ensuing molecular structure is shown in Figure 3.15. The palladium centre of complex **3-7** presents a tetragonally distorted trigonal planar structure, with the angle between the P1PdP2 plane and P3 being $164.04(3)^\circ$, which is similar to the distortion observed in $[\text{Pd}(\text{PPh}_3)_3]$ (angle between equivalent atoms = $165.88(3)^\circ$).³⁵ All the alkene groups of P-bound ligand **3-4** are pointing away from the palladium centre and thus show no interaction between the alkene group and the palladium centre.

3.5.3.1.2 Investigating the mechanism of ethane reductive elimination from $[\text{PdMe}_2(\kappa^1\text{-P-3-4})_2]$ (**3-6**)

To investigate the mechanism of reductive elimination from **3-6** giving rise to ethane, a deuterium labelling experiment was carried out. Equimolar amounts of complex **3-6** and its hexadeuterated dimethyl analogue, *cis*- $[\text{Pd}(\text{CD}_3)_2(\kappa^1\text{-P-3-4})_2]$, were dissolved in C_6D_6 . After 2h at RT, analysis of the resulting reaction mixture by ^1H NMR spectroscopy showed two resonances in the 0-1.5 ppm region with the same integration, a singlet resonance at 0.80 ppm (ethane)³¹ and a septet resonance at 0.77

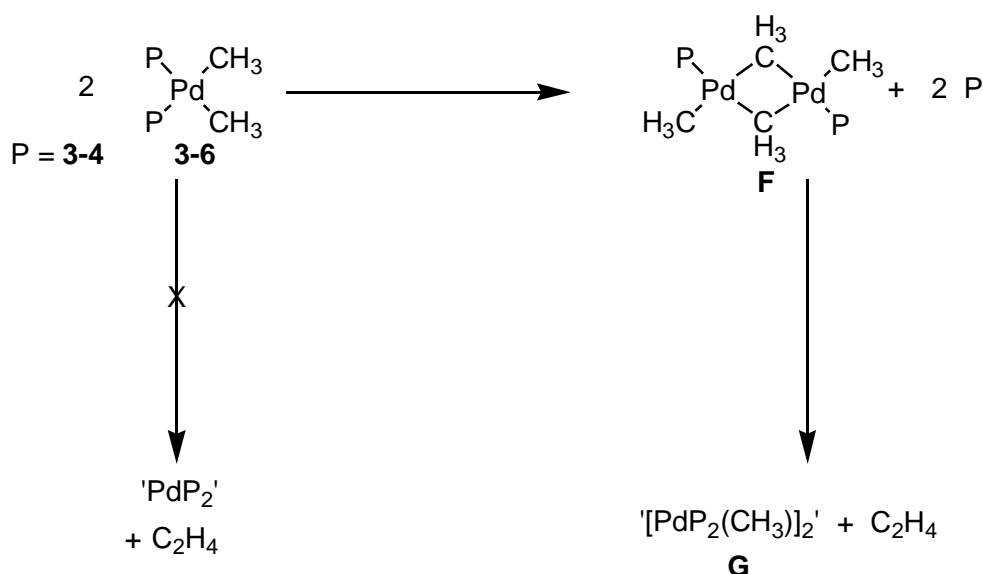
ppm ($^3J_{\text{HD}} = 1.3 \text{ Hz}$) (CH_3CD_3),³⁶ these data are indicative of an ethane : CH_3CD_3 ratio of 1:2. The formation of CH_3CD_3 is evidence that ethane results from reductive elimination and that the process is intermolecular and involves two or more palladium centres and not from direct reductive elimination of ethane from either **3-6** or *cis*- $[\text{Pd}(\text{CD}_3)_2(\kappa^1\text{-P-3-4})_2]$, since this latter pathway would not produce CH_3CD_3 .¹⁵ In contrast, the analogous deuterium crossover experiment performed by Stille and co-workers on *cis*- $[\text{PdMe}_2(\text{PPh}_3)_2]$ produced no CH_3CD_3 ,^r suggesting an intramolecular reductive elimination mechanism.¹⁵



Scheme 3.32: Ethane reductive elimination by an intermolecular mechanism from a methyl-bridged palladium dimer, adapted from Nakamura et al.³⁷

A definitive mechanism for ethane reductive elimination from **3-6** is hard to propose due to the intermolecular mechanism, which is a poorly studied transformation. However, there is some precedent for palladium methyl complexes to eliminate ethane *via* an intermolecular pathway.³⁷ Nakamura and co-workers observed that the major product formed upon thermolysis of **3-XIII** was ethane and not 1-butene, and that the ethane formed *via* a intermolecular mechanism (Scheme 3.32). They have postulated that ethane reductive elimination takes place from a palladium dimer with bridging methyl groups (**3-XIV**), formed by phosphine dissociation. This pathway was proposed based on the observation that thermolysis of an independently-synthesised authentic sample of **3-XIV** gave a very similar distribution of products.³⁷

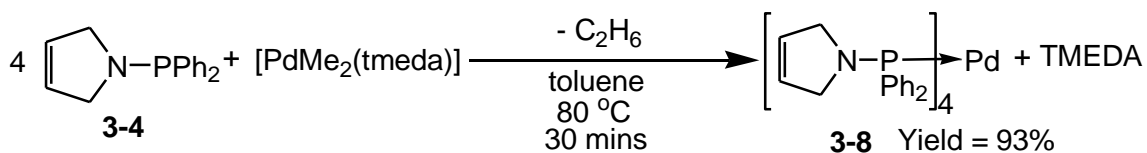
^r Required heating to 80 °C to facilitate reductive elimination.



Scheme 3.33: Proposed mechanism for the elimination of ethane from **3-6**.

Based upon the formation of CH_3CD_3 during the deuterium labelling experiment direct ethane reductive elimination from **3-6** can be discounted. We therefore propose an intermolecular mechanism for ethane reductive elimination from **3-6**. Specifically, ethane elimination from **F** formed from the dissociation of one equivalent of phosphine ligand **3-4** from $\text{cis-}[\text{PdMe}_2(\kappa^1\text{-P-3-4})_2]$ (**3-6**) with subsequent dimerization (Scheme 3.33). However, the reaction is complex and further ethane elimination steps must take place to form the required product distribution. We therefore suggest that the palladium-containing product of the reductive elimination step (**G**), can undergo further (undefined) rearrangements or dimerisation reactions to transform the remaining palladium-bound methyl groups into ethane. Significant further investigation is needed to elucidate the full mechanism due to the complex intermolecular transformation involving multiple metal centres.

3.5.4 Synthesis of $[\text{Pd}(\kappa^1\text{-P-3-4})_4]$ (**3-8**)

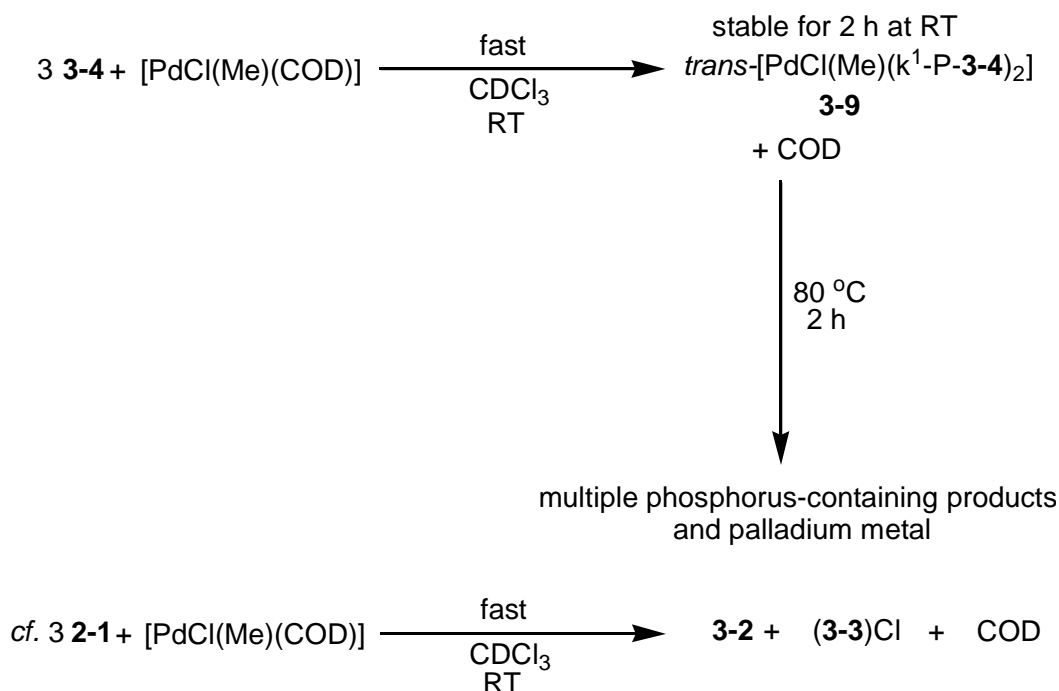


Scheme 3.34: Synthesis of $[\text{Pd}(\kappa^1\text{-P-3-4})_4]$ (**3-8**).

Complex **3-8**, $[\text{Pd}(\kappa^1\text{-P-3-4})_4]$, was synthesised to confirm that the phosphorus-containing product formed from the reductive elimination of ethane from **3-6** (reaction shown in Scheme 3.29) was the *tris*-substituted species **3-7** not its *tetrakis* analogue. Complex **3-8** was synthesised in 93% yield by heating a toluene solution of $[\text{PdMe}_2(\text{tmeda})]$ in the presence of four equivalents of **3-4** for 30 minutes (Scheme 3.34); the product was subsequently characterised by multinuclear NMR spectroscopic and CHN analyses. The *tetrakis*-phosphine complex **3-8** exhibits a very broad singlet resonance by ^{31}P NMR spectroscopy at +53.1 (FWHM = 385 Hz) ppm, with ^1H NMR spectroscopy confirming the equivalence of each of the four phosphine ligands **3-4**. Further evidence that **3-8** exists as a true *tetra*-coordinate species and not a mixture of **3-7** + **3-4** is given by solid-state $^{31}\text{P}\{^1\text{H}\}$ NMR spectroscopy of the material obtained from the reaction mixture upon removal of all volatile components, which shows a single resonance at 60.7 ppm and no trace of free phosphine.

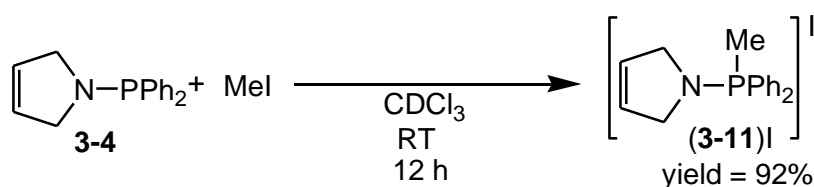
3.5.5 Coordination chemistry of P-alkene **3-4** and P-alkane **3-5** with $\text{PdCl}(\text{Me})$ fragment

Previously we have shown that the reaction of three equivalents of P-alkene **2-1** with $[\text{PdCl}(\text{Me})(\text{COD})]$ leads to the rapid formation of **3-2** and the methylphosphonium chloride salt of **2-1**, $(\text{3-3})\text{Cl}$, Section 3.4. Consequently, it was of interest to probe the potential for an analogous reaction with the significantly less rigid P-alkene **3-4**.

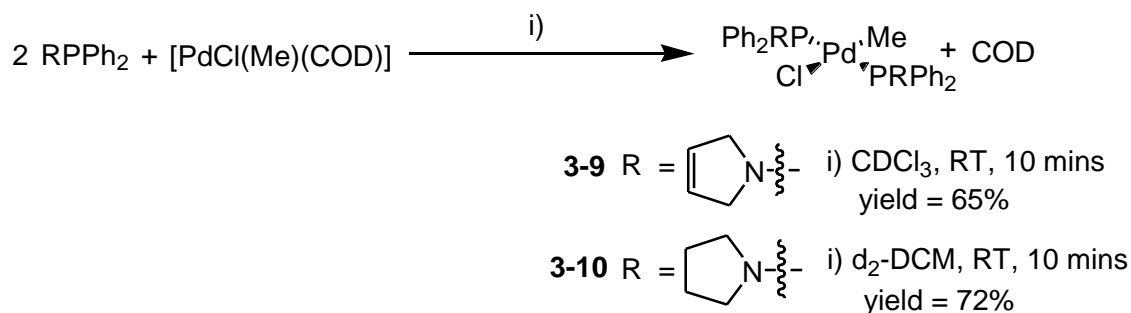


Scheme 3.35: The contrasting reactions between three equivalents of *P*-alkene ligands **2-1** and **3-4** with $[\text{PdCl}(\text{Me})(\text{COD})]$.

The addition of three equivalents of **3-4** to a CDCl_3 solution of $[\text{PdCl}(\text{Me})(\text{COD})]$ leads to the immediate formation of equimolar amounts of $\text{trans-}[\text{PdCl}(\text{Me})(\kappa^1\text{-P-}\mathbf{3-4})_2]$ (**3-9**) and free **3-4** (by $^{31}\text{P}\{^1\text{H}\}$ NMR spectroscopic analysis), Scheme 3.35. The resulting mixture is stable at room temperature for 2 h, which contrasts with the analogous reaction of $[\text{PdCl}(\text{Me})(\text{COD})]$ with **2-1**, which rapidly forms **3-2** and phosphonium salt (**3-3**)Cl. Subsequent thermolysis (80 °C, 2 h) of the reaction mixture obtained from treating $\text{trans-}[\text{PdCl}(\text{Me})(\kappa^1\text{-P-}\mathbf{3-4})_2]$ with **3-4** led to a colour change from yellow to red and the formation of palladium metal. Analysis of the reaction mixture by ^1H and $^{31}\text{P}\{^1\text{H}\}$ NMR spectroscopy showed multiple (>10) phosphorus-containing products, none of which could be assigned to the methylphosphonium chloride salt of **3-4**, which was predicted to give a characteristic doublet at approximately 3 ppm in the ^1H NMR spectra, by analogy with the independently-synthesised phosphonium salt (**3-11**)I, Scheme 3.36. As expected, compound (**3-11**)I shows a distinctive doublet ($^2J_{\text{PH}} = 13$ Hz) at 2.84 ppm for its phosphorus-bonded methyl group. It is clear that the rigid and bulky alkene moiety of **2-1** is key to its reactivity with the $\text{PdCl}(\text{Me})$ fragment by enforcing bidentate coordination. In Section 3.4.1 we proposed that the highly π -accepting alkene moiety of ligand **2-1** activates the palladium-bound methyl group of a $\text{PdCl}(\text{Me})$ fragment towards nucleophilic attack. In contrast, **3-4** binds to a $\text{PdCl}(\text{Me})$ fragment in a monodentate fashion and thus the alkene moiety is unable to activate the palladium bound methyl group towards nucleophilic attack.



Scheme 3.36: The synthesis of the methylphosphonium iodide salt of **3-4**, (**3-11**)I.



Scheme 3.37: Synthesis of *trans*-[PdCl(Me)(κ¹-P-**3-4**)₂] (**3-9**) and *trans*-[PdCl(Me)(κ¹-P-**3-5**)₂] (**3-10**).

As the addition of three equivalents of **3-4** to [PdCl(Me)(COD)] led to the formation of *trans*-[PdCl(Me)(κ¹-P-**3-4**)₂] (**3-9**) and free **3-4** it was of interest to synthesise an authentic sample of *trans*-[PdCl(Me)(κ¹-P-**3-4**)₂] (**3-9**) along with its saturated analogue *trans*-[PdCl(Me)(κ¹-P-**3-5**)₂] (**3-10**) for comparison. The addition of two equivalents of **3-4** or **3-5** to [PdCl(Me)(COD)] leads to the rapid formation of *trans*-[PdCl(Me)(κ¹-P-**3-4**)₂] (**3-9**) or *trans*-[PdCl(Me)(κ¹-P-**3-5**)₂] (**3-10**), respectively, in moderate yield (Scheme 3.37). The *trans* orientation of both phosphorus-containing groups in **3-9** and **3-10** is evident from ¹H NMR spectroscopy; the palladium-bound methyl group presents a triplet for both complexes (**3-9**: -0.19 (t, ³J_{PH} = 6.2 Hz) and **3-10**: -0.17 (t, ³J_{PH} = 6.1 Hz)).

3.5.5.1 X-Ray crystallographic study of *trans*-[PdCl(Me)(κ^1 -P-3-4)₂] (**3-9**) and *trans*-[PdCl(Me)(κ^1 -P-3-5)₂] (**3-10**)

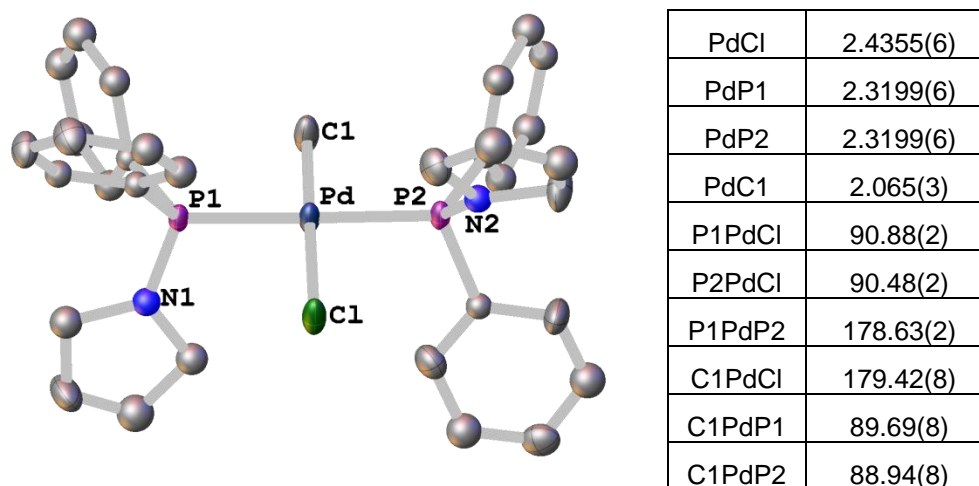


Figure 3.16: Molecular structure of *trans*-[PdCl(Me)(κ^1 -P-3-4)₂] (**3-9**), with selected bond lengths (Å) and angles (°). Thermal ellipsoids set at 50% level. The molecular structure contains a molecule of DCM which is omitted for clarity. One of the phenyl rings and the N-heterocycle on each phosphorus centre are in statistically mixed positions (not shown).

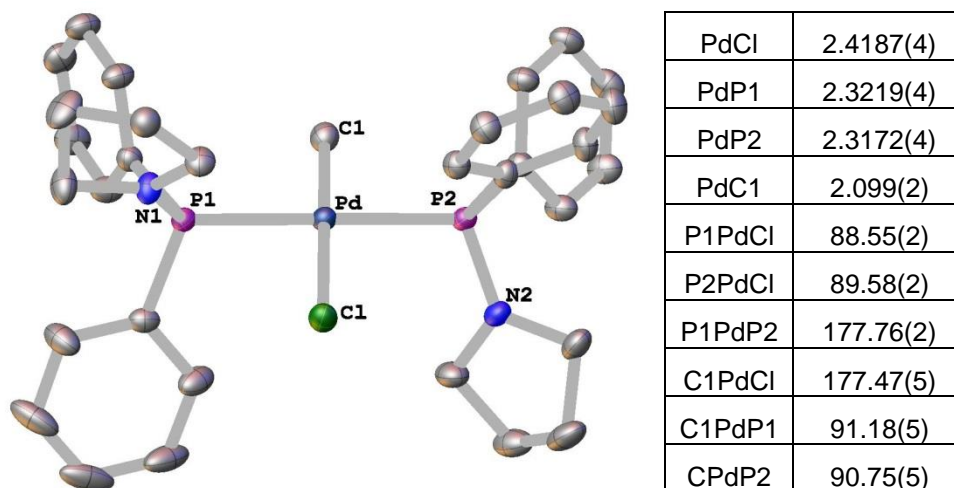


Figure 3.17: Molecular structure of *trans*-[PdCl(Me)(κ^1 -P-3-5)₂] (**3-10**), with selected bond lengths (Å) and angles (°), (thermal ellipsoids set at 50% level).

Single crystals of **3-9** suitable for X-ray diffraction were grown by layering a concentrated DCM solution with hexane; the ensuing molecular structure is shown in Figure 3.16. The palladium centre of complex **3-9** presents a slightly distorted square

planar structure, with a P1PdP2 angle of $178.63(2)^\circ$, with all the bond distances and angles about palladium being similar to those in previously-reported *trans*-[PdCl(Me)(PPh₃)₂].³⁸ As expected, the alkene groups of P-bound ligand **3-4** are pointing away from the palladium centre and thus show no interaction between the alkene group and either the palladium centre or any other ancillary ligands.

Single crystals of **3-10** suitable for X-ray diffraction were also grown, with the ensuing molecular structure shown in Figure 3.17. The molecular structure of **3-10** is very similar to **3-9**, showing that the inclusion of an unsaturated ligand in **3-9** has minimal impact on the structure of the ensuing complex, compared to the saturated analogue in **3-10**.

3.6 Chapter 3 summary and conclusions

Addition of one equivalent of the phosphine-alkene ligand **2-1** to $[\text{PdMe}_2(\text{tmeda})]$ resulted in the formation of *cis*- $[\text{PdMe}_2(\kappa^2\text{-P,C-2-1})]$ (**3-1**). Over a period of 5 days complex **3-1** evolves smoothly to afford half an equivalent of the palladium(0) complex $[\text{Pd}(\kappa^2\text{-P,C-2-1})_2]$ (**3-2**) and ethane as the only organic product, together with a quantity of elemental palladium. The reductive elimination of ethane from **3-1** is much faster than from the analogous dppe complex *cis*- $[\text{PdMe}_2(\text{dppe})]$ by virtue of the palladium centre being significantly less electron rich; elimination is believed to occur directly from the 4-coordinate species. The addition of small amounts of either PPh_3 or propene significantly speed up the reductive elimination of ethane from **3-1**, *via* formation of a 5-coordinate intermediate. In a similar fashion, when two equivalents of P-alkene ligand **2-1** per $[\text{PdMe}_2(\text{tmeda})]$ are used the reductive elimination of ethane is again fast, and is believed to proceed *via* a 5-coordinate intermediate $[\text{PdMe}_2(\kappa^2\text{-P,C-2-1})(\kappa^1\text{-P-2-1})]$ (**C**). A mechanism that proceeds *via* *cis*- $[\text{PdMe}_2(\kappa^1\text{-P-2-1})_2]$ (**B**) cannot be fully discounted as it was observed at low temperature by NMR spectroscopy. However, the activation barrier for ethane reductive elimination has been calculated to be higher from **B** than from **C**.

Phosphine-alkene ligand **2-1** gave poor performance in palladium-catalysed cross-coupling reactions, as electron withdrawing ligand **2-1** stabilises Pd(0) species. This stabilisation is so effective that the Pd(0) complexes do not readily undergo oxidative addition.

The reaction of three equivalents of P-alkene **2-1** with $[\text{PdCl}(\text{Me})(\text{COD})]$ led to the very rapid formation to **3-2** and phosphonium salt (**3-3**)Cl. Computational studies suggest that the methyl and chloride ligands were not removed from the metal centre by direct chloromethane reductive elimination as the energy barrier was unfeasibly high. Instead, a pathway with a lower energy barrier involving the $\text{S}_{\text{N}}2$ nucleophilic attack of **2-1** on a palladium-methyl group is proposed, with the palladium-methyl group activated by the strongly electrophilic $\text{Pd}(\kappa^2\text{-P,C-2-1})$ fragment.

Monocyclic P-alkene ligand **3-4** was designed to have a more flexible structure than that of the rigid phosphine-alkene ligand **2-1**, with a view to weakening the strength of the alkene-metal interaction and, hence, potentially accessing complexes that were more labile than those of **2-1**. However, notably, to date, no evidence was found to support the binding of the alkene moiety of **3-4** to a palladium centre. For example, while the complex *cis*- $[\text{PdMe}_2(\kappa^1\text{-P-3-4})_2]$ (**3-6**) undergoes facile reductive elimination of ethane at room temperature, there is subsequent preferential coordination of a third phosphine moiety to form $[\text{Pd}(\kappa^1\text{-P-3-4})_3]$ (**3-7**) and palladium metal. In contrast to ligand **2-1**, the reaction of **3-4** with $[\text{PdCl}(\text{Me})(\text{COD})]$ gave the formation of *trans*-

$[\text{PdCl}(\text{Me})(\kappa^1\text{-P-3-4})_2]$ (**3-9**) and did not remove the methyl and chloride ligands from the metal centre.

3.7 Future work

The alkene moiety of ligand **2-1** was designed to strongly bind to a metal centre and thus be highly π -accepting. However, the highly π -accepting nature of **2-1** led the formation of highly stabilised and thus unreactive metal complexes, e.g. $[\text{Ni}(\kappa^2\text{-P,C-2-1})_2]$ (**2-6**) and $[\text{Pd}(\kappa^2\text{-P,C-2-1})_2]$ (**3-2**). Initial attempts to synthesise a less π -accepting analogue of **2-1**, to potentially form complexes with greater reactivity by reducing the rigidity of the alkene moiety, led to the synthesis of ligand **3-4**. Ligand **3-4** was found to bind in a monodentate only fashion (through P) to Pd(II) and Pd(0) metal fragments. We propose that it would be possible to make a less π -accepting analogue of the bidentate ligand **2-1** by increasing the steric bulk of the alkene substituents (Figure 3.18). Increased steric bulk on the alkene moiety will hinder the bonding of the alkene moiety to a metal and thus be less π -accepting (Section 1.3).

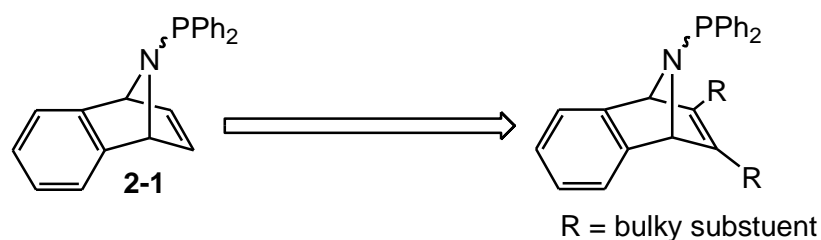


Figure 3.18: Proposed analogue of P-alkene ligand **2-1** with bulky alkene substituents to hinder alkene metal binding.

3.8 References

1. J. F. Hartwig, *Inorg. Chem.*, 2007, **46**, 1936-1947.
2. J. E. Marcone and K. G. Moloy, *J. Am. Chem. Soc.*, 1998, **120**, 8527-8528.
3. Z. Freixa and P. W. N. M. van Leeuwen, *Dalton Trans.*, 2003, 1890-1901.
4. V. P. Ananikov, D. G. Musaev and K. Morokuma, *Eur. J. Inorg. Chem.*, 2007, **2007**, 5390-5399.
5. P. K. Sajith and C. H. Suresh, *Inorg. Chem.*, 2011, **50**, 8085-8093.
6. M. Perez-Rodriguez, A. A. C. Braga, M. Garcia-Melchor, M. H. Perez-Temprano, J. A. Casares, G. Ujaque, A. R. de Lera, R. Alvarez, F. Maseras and P. Espinet, *J. Am. Chem. Soc.*, 2009, **131**, 3650-3657.
7. L. Abis, A. Sen and J. Halpern, *J. Am. Chem. Soc.*, 1978, **100**, 2915-2916.
8. J. B. Johnson and T. Rovis, *Angew. Chem. Int. Ed.*, 2008, **47**, 840-871.
9. D. B. G. Williams and M. L. Shaw, *Tetrahedron*, 2007, **63**, 1624-1629.
10. X. C. Luo, H. Zhang, H. Duan, O. Liu, W. Zhu, T. Zhang and A. Lei, *Org. Lett.*, 2007, **9**, 4571-4574.
11. W. Shi, Y. D. Luo, X. C. Luo, L. Chao, H. Zhang, J. Wang and A. W. Lei, *J. Am. Chem. Soc.*, 2008, **130**, 14713-14720.
12. T. Yamamoto, A. Yamamoto and S. Ikeda, *J. Am. Chem. Soc.*, 1971, **93**, 3350-3359.
13. K. Tatsumi, A. Nakamura, S. Komiya, A. Yamamoto and T. Yamamoto, *J. Am. Chem. Soc.*, 1984, **106**, 8181-8188.
14. E.-i. Negishi and L. Anastasia, *Chem. Rev.*, 2003, **103**, 1979-2018.
15. A. Gillie and J. K. Stille, *J. Am. Chem. Soc.*, 1980, **102**, 4933-4941.
16. W. De Graaf, J. Boersma, W. J. J. Smeets, A. L. Spek and G. Van Koten, *Organometallics*, 1989, **8**, 2907-2917.
17. H. Zhang, X. Luo, K. Wongkhan, H. Duan, Q. Li, L. Zhu, J. Wang, A. S. Batsanov, J. A. K. Howard, T. B. Marder and A. Lei, *Chem. Eur. J.*, 2009, **15**, 3823-3829.
18. B. Cordero, V. Gomez, A. E. Platero-Prats, M. Reves, J. Echeverria, E. Cremades, F. Barragan and S. Alvarez, *Dalton Trans.*, 2008, 2832-2838.
19. C. A. Tolman, W. C. Seidel and D. H. Gerlach, *J. Am. Chem. Soc.*, 1972, **94**, 2669-2676.
20. M. A. Bennett and P. N. Kapoor, *J. Organomet. Chem.*, 1987, **336**, 257-269.
21. E. Gioria, J. M. Martínez-Ilarduya, D. García-Cuadrado, J. A. Miguel, M. Genov and P. Espinet, *Organometallics*, 2013, **32**, 4255-4261.

22. E. L. Weinberg and M. C. Baird, *J. Organomet. Chem.*, 1979, **179**, C61-C64.
23. P. W. Vickers, J. M. Pearson, T. Ghaffar, H. Adams and A. Haynes, *J. Phys. Org. Chem.*, 2004, **17**, 1007-1016.
24. L. Bettucci, C. Bianchini, W. Oberhauser, M. Vogt and H. Grutzmacher, *Dalton Trans.*, 2010, **39**, 6509-6517.
25. R. Shintani, R. Narui, Y. Tsutsumi, S. Hayashi and T. Hayashi, *Chem. Commun.*, 2011, **47**, 6123-6125.
26. R. Narui, S. Hayashi, H. Otomo, R. Shintani and T. Hayashi, *Tetrahedron: Asymmetry*, 2012, **23**, 284-293.
27. P. W. Dyer, J. Fawcett, M. J. Hanton, R. D. W. Kemmitt, R. Padda and N. Singh, *Dalton Trans.*, 2003, 104-113.
28. J. S. Warmus, G. J. Dilley and A. I. Meyers, *J. Org. Chem.*, 1993, **58**, 270-271.
29. McFarlan.W and D. S. Rycroft, *J. Chem. Soc., Dalton Trans.*, 1973, 2162-2166.
30. M. N. Chevykalova, L. F. Manzhukova, N. V. Artemova, Y. N. Luzikov, I. E. Nifant'ev and E. E. Nifant'ev, *Russ. Chem. Bull.*, 2003, **52**, 78-84.
31. G. R. Fulmer, A. J. M. Miller, N. H. Sherden, H. E. Gottlieb, A. Nudelman, B. M. Stoltz, J. E. Bercaw and K. I. Goldberg, *Organometallics*, 2010, **29**, 2176-2179.
32. P. Giannoccaro, A. Sacco and G. Vasapollo, *Inorg. Chim. Acta*, 1979, **37**, L455-L456.
33. R. A. Schunn, *Inorg. Chem.*, 1976, **15**, 208-212.
34. P. Leoni, *Organometallics*, 1993, **12**, 2432-2434.
35. C. Tejel, L. Asensio, M. P. del Río, B. de Bruin, J. A. López and M. A. Ciriano, *Angew. Chem. Int. Ed.*, 2011, **50**, 8839-8843.
36. L. M. Slaughter, P. T. Wolczanski, T. R. Klinckman and T. R. Cundari, *J. Am. Chem. Soc.*, 2000, **122**, 7953-7975.
37. Y. Hayashi, Y. Nakamura and K. Isobe, *J. Chem. Soc., Chem. Commun.*, 1988, 403-404.
38. A. Bacchi, M. Carcelli, C. Pelizzi, G. Pelizzi, P. Pelagatti and S. Ugolotti, *Eur. J. Inorg. Chem.*, 2002, **2002**, 2179-2187.

4 Chapter 4: Synthesis and coordination chemistry of novel POCOP pincer ligands

4.1 Introduction

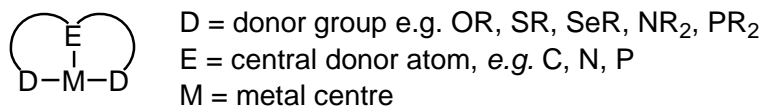


Figure 4.1: General representation of pincer complexes, adapted from Morales-Morales.¹

A pincer-type ligand comprises of one central donor atom E and two *trans*-positioned donor groups D, which bind to a metal centre using three adjacent co-planar sites (Figure 4.1). Pincer ligands can take many forms and can contain a variety of chemical motifs at the donor positions, which include phosphorus, nitrogen, and carbon among others (Figure 4.1).

Complexes containing pincer ligands have found application in a diverse array of different areas. For example, pincer-based complexes have been used as chemical sensors,² synthons for the construction of dendrimeric materials,³ and pharmaceutically-active complexes.⁴ However, the major application of pincer ligand-containing complexes is as catalysts for a range of reactions (Section 4.1.3).

In this regard metal complexes bearing pincer ligands have received unparalleled interest as homogeneous catalysts due to their high thermal stability, which allows reactions to be carried out at high temperatures, and is a manifestation of the tridentate, chelating coordination and often rigid structure.^{1, 5-7} Furthermore, pincer ligands are able to tightly control the coordination geometry of metals, thus providing a degree of selectivity to reactions that take place on the metal centre. In addition, the ease and scope with which pincer ligands may be modified, provides excellent means of modulating/tuning the control imposed by pincer ligands at the metal. Some of the ways in which the structure of a pincer ligand can be modified to affect the reactions taking place at the coordinated metal centre are summarised in Figure 4.2.

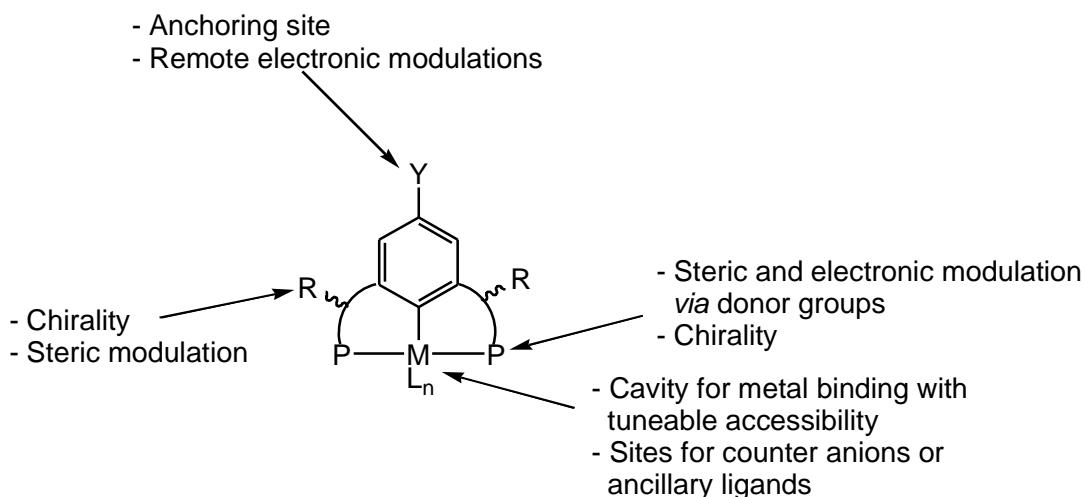


Figure 4.2: A description of the potential features of pincer-type ligands bearing an aromatic backbone, adapted from Morales-Morales.⁵

4.1.1 Pincer ligand nomenclature

A commonly-used notation for the naming of pincer ligands and their complexes is to describe the ligand only by the potentially metal-binding atoms, in the form ABC, e.g. PCP (phosphorus-carbon-phosphorus). This terminology can be extended to include spacer atoms in the form ASBSC, e.g. POCOP, although if the spacer atom (S) is carbon it is usually excluded from the abbreviation (Figure 4.3). The abbreviation system described above (ASBSC) will be used throughout this report.

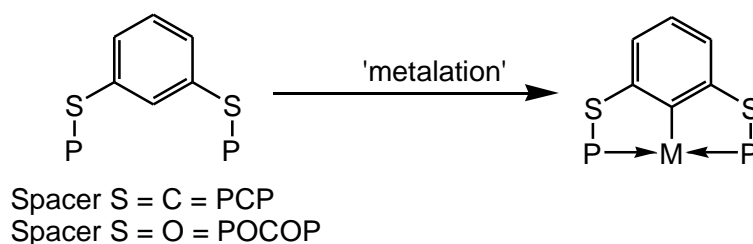
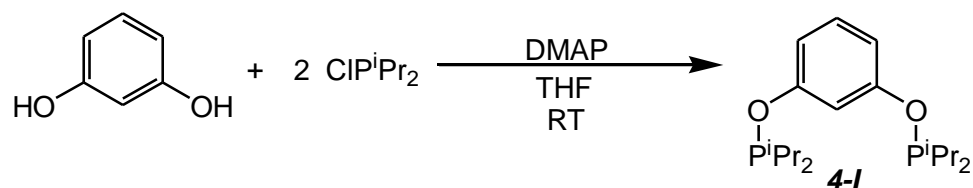


Figure 4.3: Generic structure of and notation describing pincer ligands contained in this report.

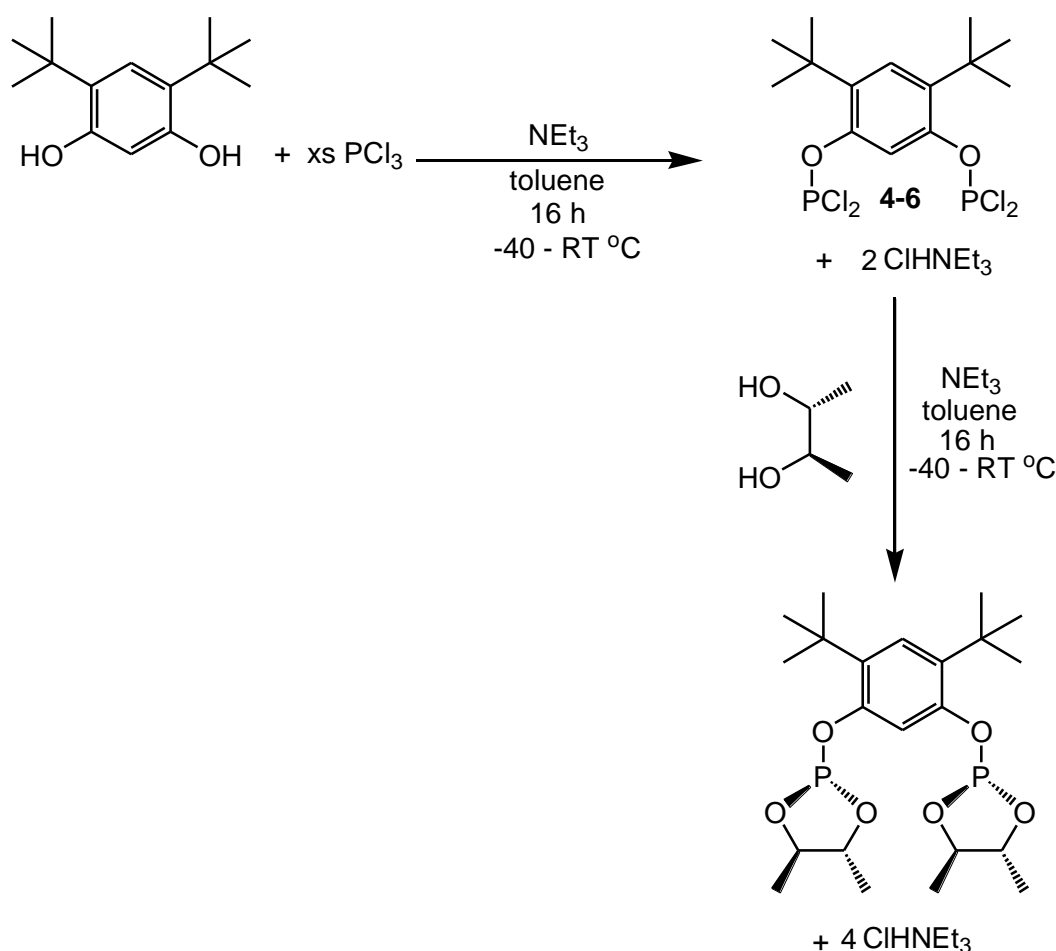
The highly tuneable structure of pincer ligands gives them broad utility as ligands in metal-catalysed reactions, due to their ability to fine-tune the environment of the metal centre to which they are attached. Due to the highly versatile structure many different syntheses have been developed. The next section details the methods that have been utilised to synthesise POCOP-type pincer ligands, which are the focus of this thesis.

4.1.2 Synthesis of POCOP ligands



Scheme 4.1: Synthesis of the first POCOP ligand reported by Jensen *et al.*⁸

The first POCOP ligand (**4-I**) to be reported was synthesised by Jensen *et al.* in 2000, 25 years after the first PCP ligand, despite their synthesis being considerably more simple due to the relative synthetic ease of making a P-O compared to a P-C bond.⁸ To date, most POCOP ligands have been synthesised from 1,3-benzenediol (resorcinol) or derivatives thereof, *via* simple salt elimination with R_2PCl precursors. For example, ligand **4-I** was synthesised through the addition of two equivalents of ClP^iPr_2 to resorcinol in the presence of 4-dimethylaminopyridine (DMAP) to act as a base at RT (Scheme 4.1).⁸ A disadvantage of this technique is that if the R_2PCl precursor is not commercially available, then additional steps are required for its prior preparation. Whilst the reaction between resorcinol and R_2PCl precursors is by far the most common method of synthesising POCOP ligands there are a few other methods available, which are detailed below.



Scheme 4.2: Synthesis of a *P*-chiral POCOP pincer ligand via dichlorophosphinite 1,3- $\{(Cl_2PO)_2C_{14}H_{20}\}$ (**4-6**), reported by Bedford and Pringle.⁹

A second general approach for the synthesis of POCOP ligands proceeds *via* a dichlorophosphinite precursor, 1,3- $\{(Cl_2PO)_2C_{14}H_{20}\}$ (**4-6**), developed by Bedford and Pringle (Scheme 4.2).⁹ Although the use of precursor **4-6** is advantageous, since reaction with a vast range of alcohols and secondary amines is potentially possible, hence giving access to a host of diphosphite and diamino phosphinite POCOP ligands, it has yet to be fully exploited with only chiral diphosphite ligands having been developed to date. Importantly, compound **4-6** has *tert*-butyl groups at the 4- and 6-positions of the aromatic ring, which have been shown to speed up the metallation (*i.e.* C–H activation) of electron deficient *bis*(phosphite) POCOP ligands to palladium, by preventing the ligand adopting a bridging coordination mode (Figure 4.4).⁹ Nevertheless, the inclusion of these *tert*-butyl does have some disadvantages, as the resulting ligands are less atom-efficient and more expensive than the equivalent resorcinol-derived ligands.

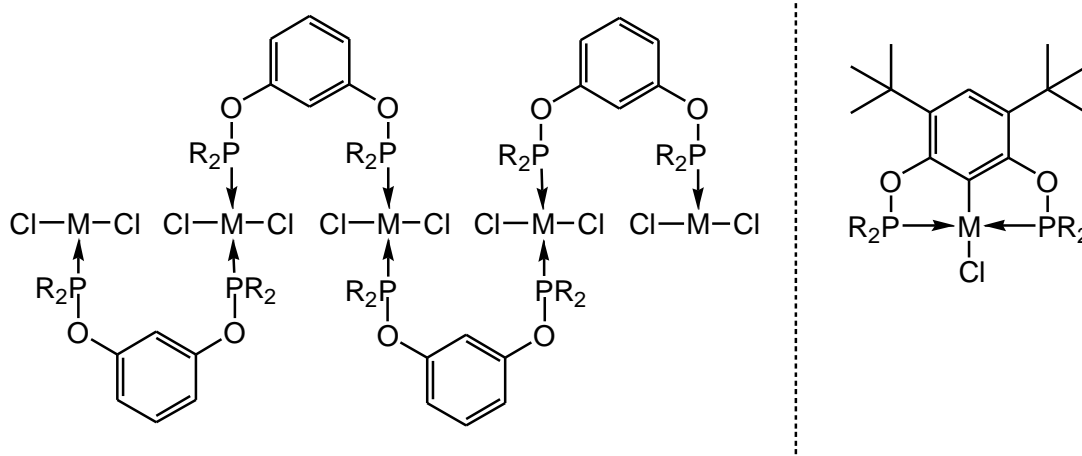
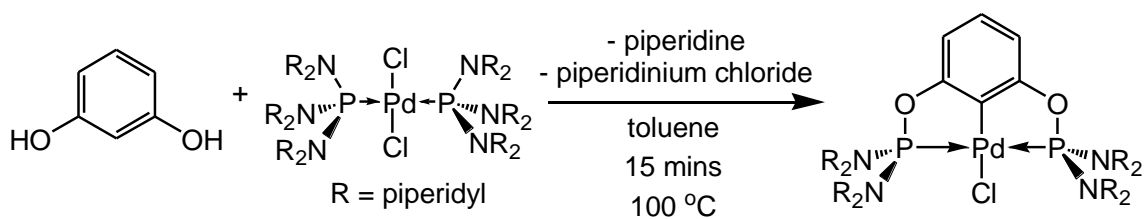


Figure 4.4: The steric bulk of the *tert*-butyl substituent on the aromatic ring limits rotation around the C–O and O–P bonds which disfavors the formation of insoluble polymeric species, caused by the ligand adopting a bridging mode (left). The formation of the required monomeric species is consequently favoured (right).

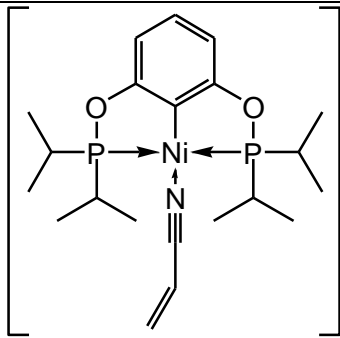
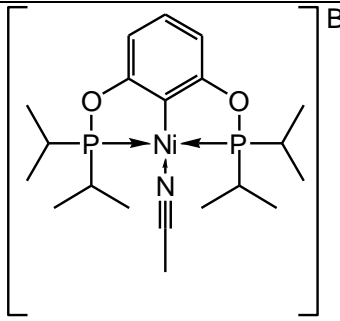
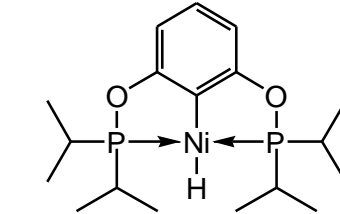
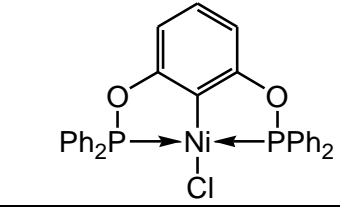
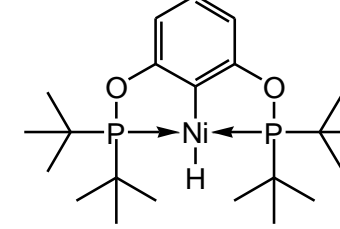
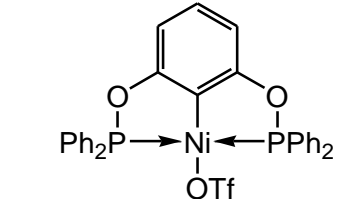


Scheme 4.3: Metal-templated synthesis of a POCOP ligand, developed by Frech and co-workers.¹⁰

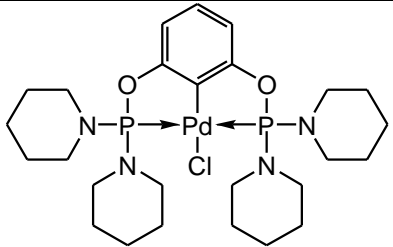
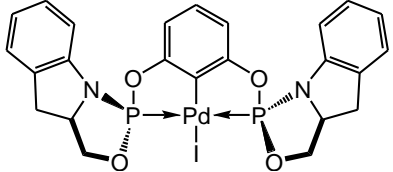
A third and final method for the synthesis of POCOP scaffolds, which has found very limited application as it is not general and not applicable to other metals and ligands, is a metal-templated route developed by Frech and co-workers. Specifically, a piperidiny-substituted ligand was prepared ‘on-metal’ by the addition of resorcinol to *cis*-[PdCl₂(P(pip)₃)₂], (Scheme 4.3) (pip = piperidine).¹⁰ Although limited in scope, the advantage of this metal-templated method is that the independent synthesis of air- and moisture-sensitive ligands is unnecessary.

4.1.3 Application of POCOP pincer ligands in catalysis

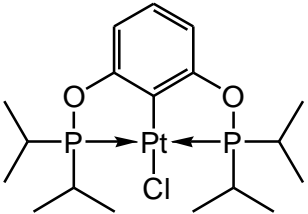
Since they were first reported in 2000, POCOP-type ligands have been used in transition metal-based catalysts for a diverse range of reactions, employing a variety of different metals.^{8, 11} A broad summary of catalytic transformations mediated by POCOP ligand-containing complexes is given in Table 4.1.

Entry	Pre-catalyst	Reaction catalysed	Author
<i>Nickel-catalysed</i>			
1		Michael addition	Zargarian <i>et al.</i> ¹²
2		Hydroamination	Zargarian <i>et al.</i> ¹³
3		Hydrosilylation	Guan <i>et al.</i> ¹⁴
4		Cross-coupling of aryl iodides and aryl thiols	Guan <i>et al.</i> ¹⁵
5		Reduction of carbon dioxide with a borane	Guan <i>et al.</i> ¹⁶⁻¹⁸
6		Hydroamination Alcoholysis	Zargarian <i>et al.</i> ¹⁹

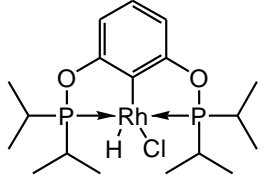
7		Suzuki-Miyaura cross-coupling	Morales-Morales <i>et al.</i> ²⁰
8		Aldehyde cyanomethylation	Guan <i>et al.</i> ^{1, 21}
<i>Palladium-catalysed</i>			
9		Heck cross-coupling	Jensen <i>et al.</i> ⁸
10		Suzuki-Miyaura cross-coupling Allyl stannane carboxylation	Bedford <i>et al.</i> ¹¹ Wendt <i>et al.</i> ²²
11		Sulfonimine asymmetric allylation	Szabó <i>et al.</i> ²³
12		Suzuki-Miyaura cross-coupling	Uozumi <i>et al.</i> ²⁴
13		Heck and Stille cross-coupling	Fukuzumi <i>et al.</i> ²⁵

14		Suzuki-Miyaura cross-coupling	Frech <i>et al.</i> ¹⁰
15		Sulfonimine asymmetric allylation	Klein Gebbink <i>et al.</i> ²⁶

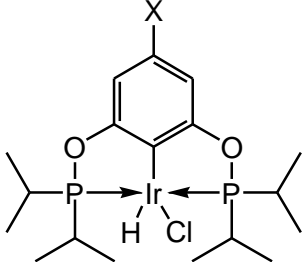
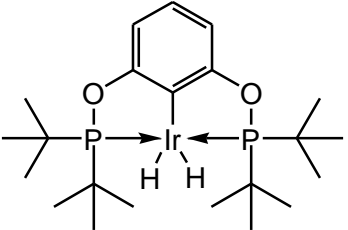
Platinum-catalysed

16		Hydroxylation	Jensen <i>et al.</i> ²⁷
----	-----------------------------------------------------------------------------------	---------------	------------------------------------

Rhodium-catalysed

17		Kumada-Tamao-Corriu cross-coupling	Ozerov <i>et al.</i> ²⁸
----	------------------------------------------------------------------------------------	------------------------------------	------------------------------------

Iridium-catalysed

18	 X = H, Me, OMe, F	Alkene transfer dehydrogenation	Brookhart <i>et al.</i> ²⁹
19		Ammonia borane dehydrogenation	Goldberg <i>et al.</i> ³⁰

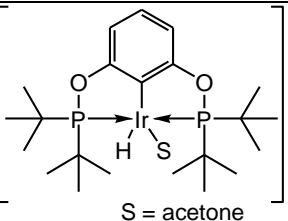
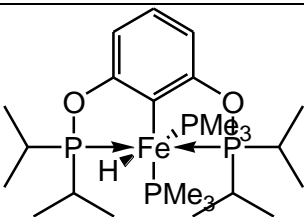
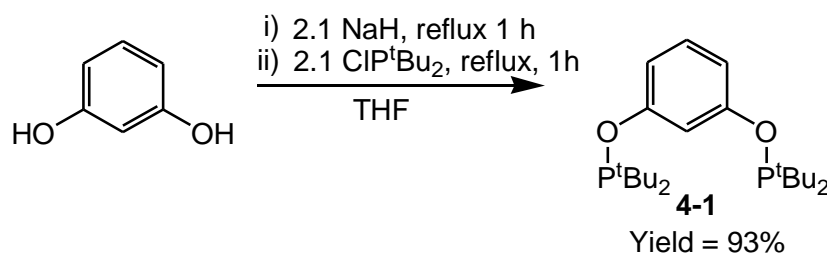
20	 <p style="text-align: center;">S = acetone</p>	Reduction of alkyl halides Hydrosilylation Carbon dioxide reduction Amide reduction	Brookhart <i>et al.</i> ³¹⁻³⁴
<i>Iron-catalysed</i>			
21		Hydrosilylation	Guan <i>et al.</i> ³⁵

Table 4.1: A summary of the application of POCOP ligands in transition metal-mediated catalysis since 2000.

The reactivity of POCOP-type ligands can be fine-tuned by modifying the steric and electronic properties of the donor groups, which is of fundamental interest in catalyst design, in the quest to form catalysts that are more active and/or selective. However, the work summarised in Table 4.1 shows that, to date, there has been comparatively little modification of the phosphorus donor groups in known POCOP-containing catalysts, with aryl and alkyl phosphorus substituents being prevalent. Therefore, we set out to synthesise a range of new POCOP ligands containing phosphorus donors with varying steric and electronic demands, and to systematically study the impacts of changing the phosphorus substituent on a metal centre, which will be advantageous in helping to predict future structure reactivity relationships.

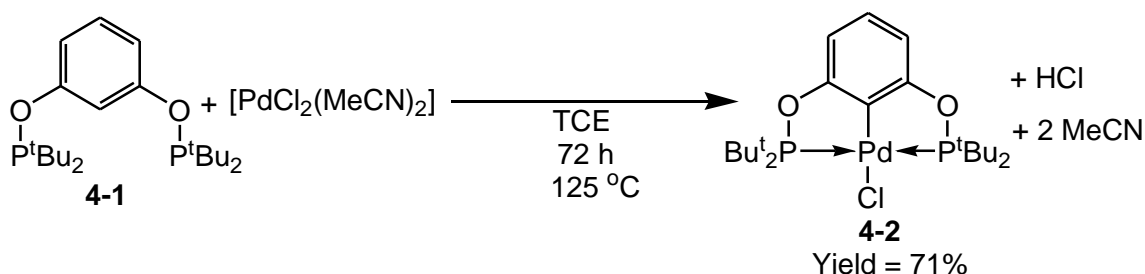
4.2 Synthesis of [PdCl(κ^3 -P,C,P-4-1)] (4-2)

The synthesis of a range of new POCOP ligands containing phosphorus donors with varying steric and electronic demands is reported later in this chapter. Firstly, the previously reported ligand 1,3- $\{(\text{tBu}_2\text{PO})_2\text{C}_6\text{H}_4\}$ (**4-1**) was synthesised to give a good model system against which the newly synthesised ligands could be compared. This particular 1,3- $\{(\text{tBu}_2\text{PO})_2\text{C}_6\text{H}_4\}$ (**4-1**) system was chosen as it is one of the most commonly used POCOP-type pincer ligands, having been complexed to a range of metals including Mo,³⁶ Ru,³⁷ Co,³⁸ Rh,³⁹ Ir,²⁹ Ni,¹⁴ and Pd.^{22, 40}



Scheme 4.4: Synthesis of compound **4-1** as described by Brookhart and co-workers.²⁹

Compound **4-1** was synthesised in an identical method to that described by Brookhart and co-workers, namely the diphosphorylation of resorcinol (1,3-benzenediol) with di-*tert*-butylchlorophosphine using sodium hydride as a base and was isolated in 93% yield (Scheme 4.4).²⁹



Scheme 4.5: Synthesis of $[PdCl(\kappa^3\text{-P,C,P-4-1})]$ (**4-2**).

Subsequently, we prepared the novel pincer complex **4-2** by cyclopalladation of ligand **4-1** at moderately high temperature (125 °C), using $[PdCl_2(MeCN)_2]$ as the source of palladium (Scheme 4.5). The elevated temperature was necessary in order to facilitate C-H activation of the 2-position of **4-1**, a process that was found to proceed with or without the presence of NEt_3 as a base. The resulting complex **4-2** was obtained following recrystallisation (71% yield).⁵

Complex **4-2** presents a singlet resonance at 192.2 ppm ($\Delta\delta = +39.1$ ppm) by $^{31}P\{^1H\}$ NMR spectroscopy. The *tert*-butyl group appears as a virtual triplet resonance in the 1H NMR spectrum of **4-2**, as the two phosphorus nuclei are equivalent and the coupling pattern can be ascribed to an AA'XX' spin system; this type of non-first order coupling is also reported for the related iridium complex $[IrCl(H)(\kappa^3\text{-P,C,P-4-1})]$.⁴¹ The palladium-bound carbon of complex **4-2** displays a triplet resonance ($^2J_{PC} = 2$ Hz) at 129.9 ($\Delta\delta$ of +24 ppm), clearly demonstrating that **4-1** is bound to the palladium centre in a tridentate fashion.

⁵ At the time of initial synthesis complex **4-2** was a novel complex although an alternative, lower yielding synthesis (31%), has since been published by Koridze *et al.*⁴⁰

4.2.1 X-Ray crystallographic study of $[\text{PdCl}(\kappa^3\text{-P,C,P-4-1})]$ (**4-2**)

The molecular structure of complex $[\text{PdCl}(\kappa^3\text{-P,C,P-4-1})]$ (**4-2**) was determined by single-crystal X-ray diffraction (Figure 4.5), with suitable crystals grown by slow diffusion of hexane into a concentrated DCM solution of **4-2**. The palladium atom is in a distorted square-planar geometry with a P(1)-Pd-P(2) bite angle of $160.14(2)^\circ$, which is smaller than that in the analogous nickel complex, $[\text{NiCl}(\kappa^3\text{-P,C,P-4-1})]$, ($164.18(3)^\circ$).¹⁴ The Pd-Cl bond ($2.3801(5) \text{ \AA}$) is longer than that determined for *trans*- $[\text{PdCl}_2(\text{P}(\text{OH})^t\text{Bu}_2)_2]$ ($2.3132(3) \text{ \AA}$) due to the presence of the strongly *trans*-influencing C1 atom.⁴² Comparison of the molecular structure of **4-2** with that of *trans*- $[\text{PdCl}_2(\text{P}(\text{OH})^t\text{Bu}_2)_2]$ shows that the tether linking the two phosphines moieties distorts the square planar geometry, as **4-2** is not perfectly *trans*-spanning (Figure 4.6).

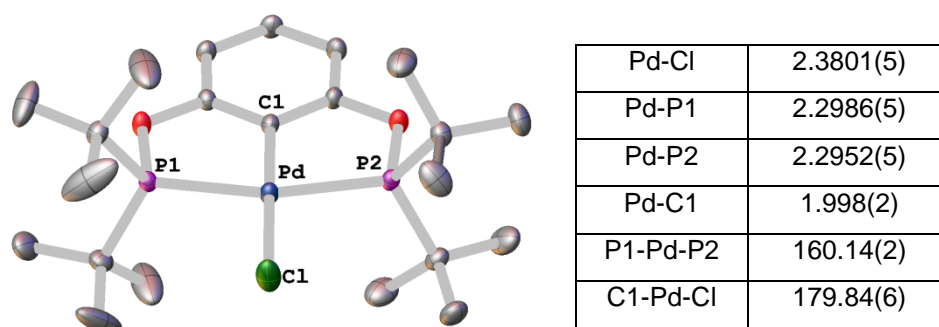


Figure 4.5: Molecular structure of $[\text{PdCl}(\kappa^3\text{-P,C,P-4-1})]$ (**4-2**) with selected bond lengths (\AA) and angles ($^\circ$), (thermal ellipsoids set at 50% level).

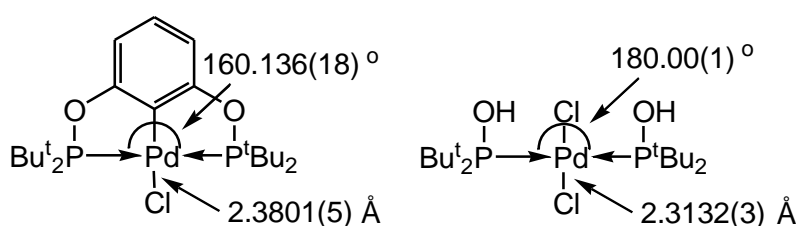


Figure 4.6: Comparison of the bond lengths and angles about palladium in **4-2** with those of *trans*- $[\text{PdCl}_2(\text{P}(\text{OH})^t\text{Bu}_2)_2]$.

The molecular structure of **4-2** can be used to help quantify the steric bulk of the coordinated ligand **4-1**. The steric and electronic properties of ligand **4-1**, often qualitatively considered to be very bulky and electron rich, will later be quantified using a variety of methods (Sections 4.3.3.2 and 4.3.3.3), something that has not been done to this date. After quantification of the steric and electronic properties of **4-1** it will be used

as a baseline comparison to the novel POCOP ligands described in the following sections.

4.3 Synthesis of POCOP pincer compounds and the assessment of their electronic and steric properties

Amongst the most commonly used POCOP pincer ligands used in coordination chemistry studies and catalysis are 1,3- $\{(R_2PO)_2C_6H_4\}$, where R is ^tBu, ⁱPr and Ph.[†] The prevalence of systems bearing these particular substituents at phosphorus can be attributed to their facile and well-established synthesis from commercially available reagents.^{8, 11, 29} However, excluding chiral POCOP pincer ligands, there has been surprisingly little variation of the substituents at phosphorus, and certainly no systematic study of the preparation of pincer ligands with different steric and electronic properties. The study and quantification of how changes to the phosphorus substituents of POCOP ligands impacts on the steric and electronic properties of a metal centre is a vital consideration in the rational design of new ligands for catalytic applications. Although this thesis will not investigate any specific catalytic application of the newly synthesised POCOP ligands, it will explore in detail the synthetic strategies required to design new POCOP ligands and the subsequent quantification of their steric and electronic properties.

The lack of research into phosphite-containing pincer ligands is exemplified by there being only one example of a non-chiral phosphite-containing pincer ligand known (**4-II**) (Figure 4.7).^{9, 23, 43-45} Phosphite-containing pincer ligands are generally regarded as less electron-rich donor ligands than the commonly used alkyl and aryl counterparts; the electronic character of a ligand plays an important role in the reactivity of the subsequent complex. Furthermore, phosphite-containing ligands differ from the commonly used alkyl and aryl phosphinite-containing ligands, as the steric bulk is located comparatively further away from the phosphorus centre, creating a 'pocket' close to the metal centre.

[†] CSD search 21/11/13 showed that of the 122 known $[M(1,3-(R_2PO)_2C_6H_3)]$ molecular structures reported, R = ^tBu (32 structures), ⁱPr (34 structures), Ph (35 structures).

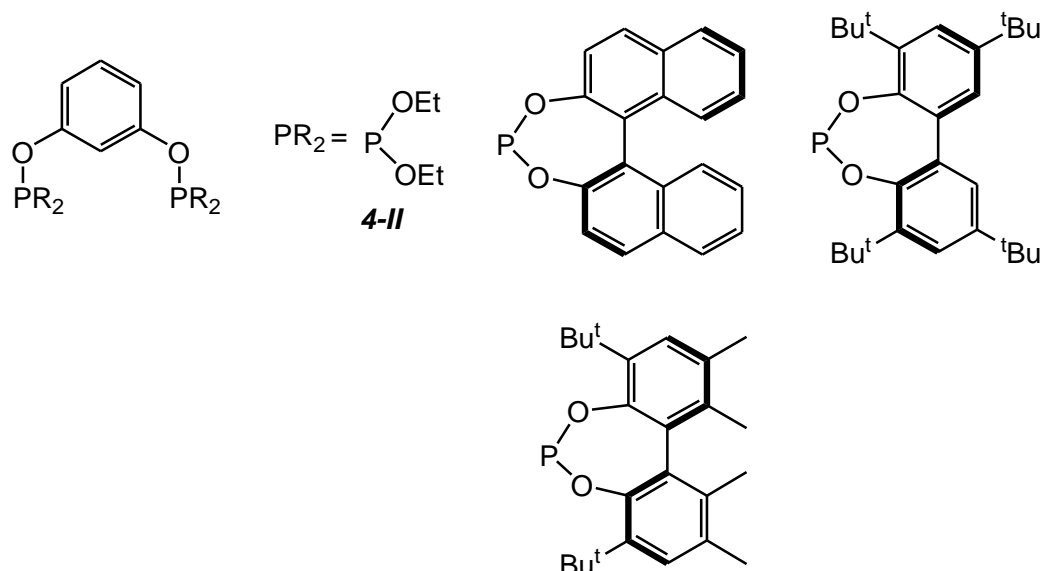


Figure 4.7: Known phosphite-containing pincer ligands.^{9, 23, 43-45}

Similarly, diaminophosphinite-containing pincer ligands have been very poorly studied, with only two known examples of diaminophosphinite-containing pincer complexes known (Figure 4.8).^{10, 24} Such diaminophosphinite pincer ligands would be expected to be comparatively electron rich due to donation from the nitrogen lone pair to phosphorus (Section 1.2), but have the possibility to be very bulky as two substituents are located at each heteroatom on phosphorus, a characteristic that has not been exploited to date.

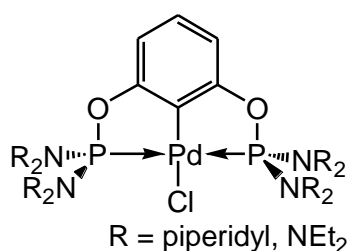
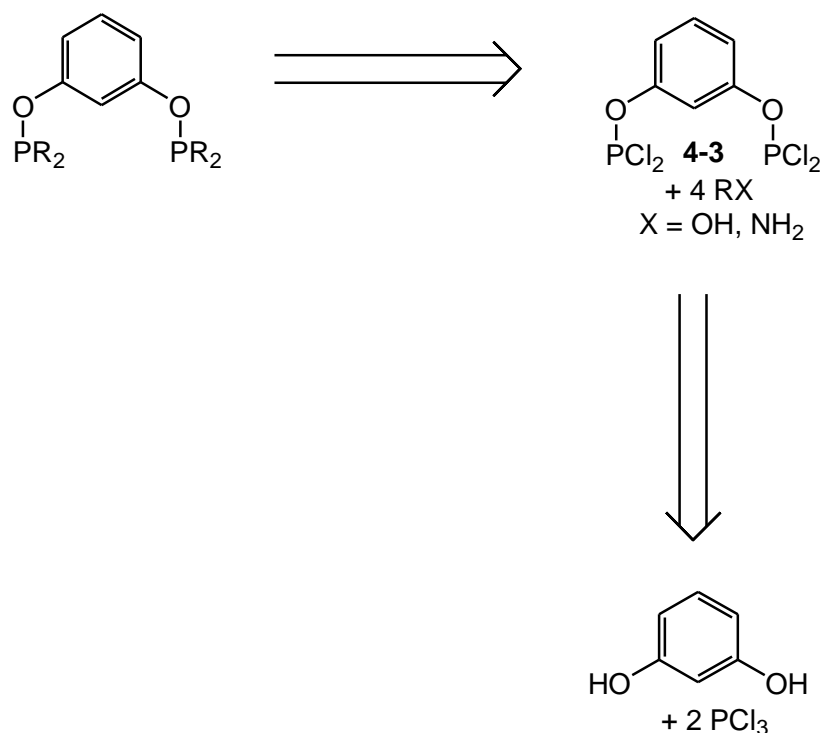


Figure 4.8: Known diaminophosphinite-containing pincer complexes.^{39, 40}

4.3.1 Development of a new synthetic route to POCOP pincer ligands

The known synthetic methods of producing POCOP ligands described in Section 4.1.2 gives access to a wide range of POCOP ligands. However, we postulated that we could extend the methodology developed by Bedford and Pringle (*via* a dichlorophosphinite intermediate) to the synthesis of POCOP ligands that do not contain a *tert*-butyl-substituted aromatic ring, for when the inclusion of *tert*-butyl groups

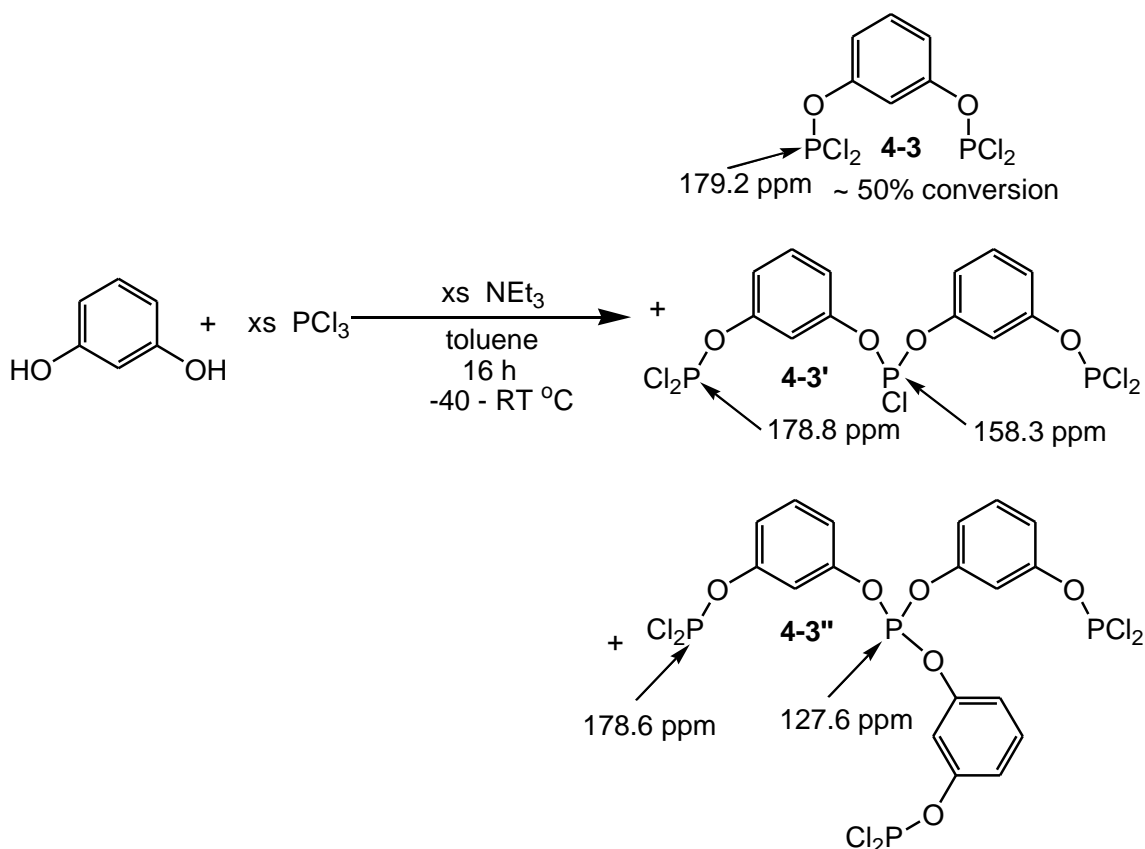
on the backbone are unwanted/unnecessary. A retrosynthetic pathway for the synthesis of POCOP pincer ligands *via* 1,3- $\{(Cl_2PO)_2C_6H_4\}$ **4-3** is shown in Scheme 4.6, an approach that should allow the facile and rapid synthesis of a range of phosphite and diaminophosphinite POCOP ligands using readily available alcohols and amines.



Scheme 4.6: Retrosynthetic analysis of a generic POCOP pincer compound synthesised *via* 1,3- $\{(Cl_2PO)_2C_6H_4\}$, (**4-3**).

4.3.1.1 Synthesis of 1,3- $\{(Cl_2PO)_2C_6H_4\}$ (**4-3**)

There is one previous report of the synthesis of compound 1,3- $\{(Cl_2PO)_2C_6H_4\}$ (**4-3**) from 1894, which involved heating resorcinol in excess trichlorophosphine at reflux for 10 h, with **4-3** characterised by elemental analysis (but incorrect to modern standards).⁴⁶ Thus, as a starting point for this investigation of an alternative building block for the synthesis of pincer ligands, variants on this previously-reported synthesis of **4-3** were explored.



Scheme 4.7: Attempted synthesis of 1,3-((Cl₂PO)₂C₆H₄) (**4-3**), with proposed assignment of ³¹P{¹H} NMR spectroscopic resonances obtained from the crude reaction mixture.

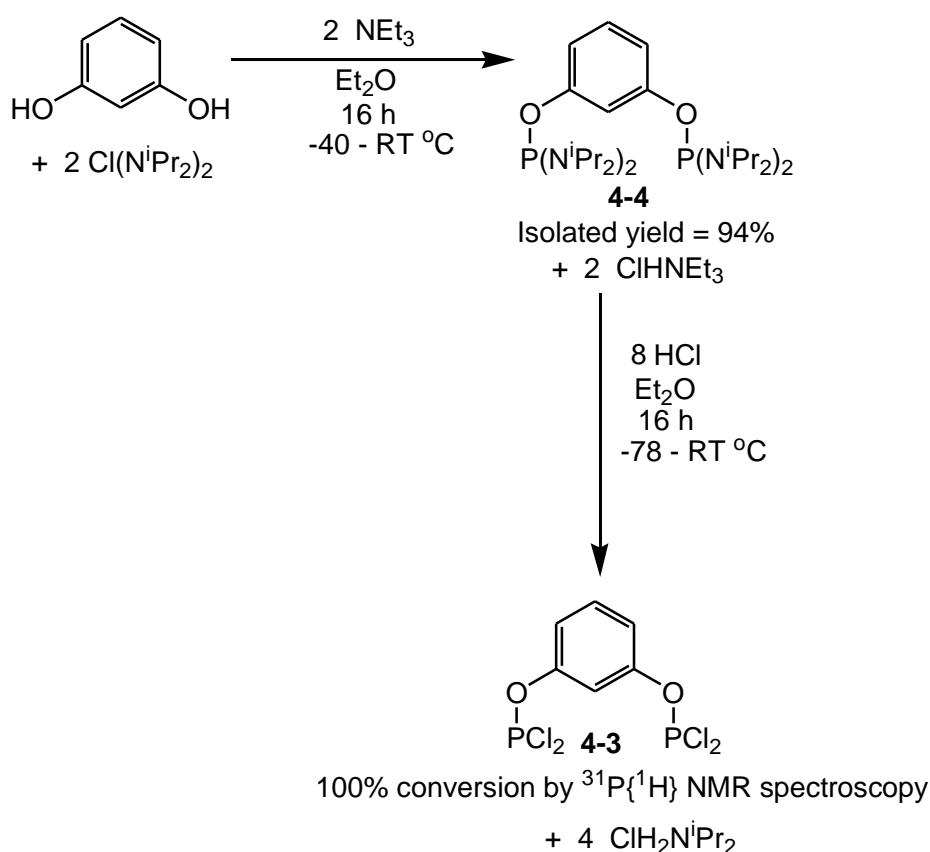
Attempts to synthesise compound **4-3** by the slow addition of triethylamine to a cooled mixture of resorcinol and excess PCl₃ in toluene,^u resulted in the formation of multiple phosphorus-containing products in solution (Scheme 4.7). Analysis of the reaction mixture by ³¹P{¹H} NMR spectroscopy showed a major product (approx. 50% conversion by integration) giving rise to a resonance at 179.2 ppm, which is consistent with the formation of compound **4-3** by comparison of the ³¹P{¹H} NMR spectroscopic data of the known and related compound (PhO)PCl₂ (177.8 ppm).⁴⁷ However, there were additional resonances in the ³¹P{¹H} NMR spectrum at 178.8, 178.6, 158.3, and 127.6 ppm, which are proposed to belong to two additional by-products **4-3'** and **4-3''** each containing two different phosphorus environments (Scheme 4.7). Whilst the individual by-products were not separated and characterised, their identity can be surmised by comparison with data from the known compounds (PhO)₂PCl (³¹P{¹H} δ = 156.8 ppm)⁴⁷ and (PhO)₃P (³¹P{¹H} δ = 128.6 ppm).⁴⁸ This analysis suggests the formation of products containing (ArO)₂PCl (**4-3'**) and (ArO)₃P (**4-3''**) linkages formed by multiple additions of resorcinol to each PCl₃ centre.

^u An analogous method to that described by Bedford and Pringle for the synthesis of **4-6** (Scheme 4.2).⁹

Whereas the reaction of resorcinol with PCl_3 led to the formation of multiple products, the analogous reaction of 4,6-di-*tert*-butylresorcinol with PCl_3 , as described by Bedford and Pringle (Scheme 4.2),⁹ led to the formation of only a single product, **4-6**. It is therefore clear that the bulky *tert*-butyl groups on the aromatic ring prevent multiple substitutions of resorcinol on PCl_3 due to steric reasons. Hence, an alternative synthesis of **4-3** that prevents multiple substitutions at the phosphorus centre was needed, detailed below.

4.3.1.1.1 *In situ* synthesis of 1,3- $\{(\text{Cl}_2\text{PO})_2\text{C}_6\text{H}_4\}$ (**4-3**) via 1,3- $\{(\text{iPr}_2\text{N})_2\text{PO}\}_2\text{C}_6\text{H}_4$ (**4-4**)

Since the reaction of resorcinol with PCl_3 led to the formation of multiple P-O linkages (Scheme 4.7), an alternative synthesis of **4-3** was needed. To this end a diamino-protected analogue was synthesised (**4-4**). The two amino protecting groups can be removed by the addition of HCl to yield the desired compound 1,3- $\{(\text{Cl}_2\text{PO})_2\text{C}_6\text{H}_4\}$ **4-3**.

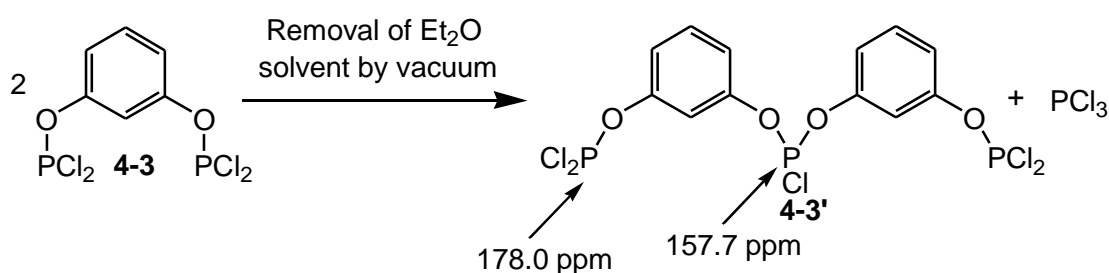


Scheme 4.8: Synthesis of 1,3- $\{(\text{iPr}_2\text{N})_2\text{PO}\}_2\text{C}_6\text{H}_4$ (**4-4**) and subsequent conversion to 1,3- $\{(\text{Cl}_2\text{PO})_2\text{C}_6\text{H}_4\}$ (**4-3**).

Thus, the diamino-protected species $1,3-\{(\text{}^i\text{Pr}_2\text{N})_2\text{PO}\}_2\text{C}_6\text{H}_4$ (**4-4**) was isolated in good yield (94%) by the diphosphorylation of resorcinol with *bis*(diisopropylamino)chlorophosphine in the presence of triethylamine (Scheme 4.8). Characterisation of compound **4-4** was achieved by multinuclear NMR spectroscopy and CHN analysis. A single resonance at 119.4 ppm was observed by $^{31}\text{P}\{^1\text{H}\}$ NMR spectroscopy. By ^1H NMR spectroscopy two resonances for each CH and CH_3 group of the N^iPr_2 moiety (relative intensity 1:1) are observed, which arises due to steric crowding around the phosphorus centre preventing free rotation. Together these data are consistent with the formation of the target compound **4-4**.

4.3.1.1.2 Synthesis of $1,3-\{(\text{Cl}_2\text{PO})_2\text{C}_6\text{H}_4\}$ (**4-3**) from $1,3-\{(\text{}^i\text{Pr}_2\text{N})_2\text{PO}\}_2\text{C}_6\text{H}_4$ (**4-4**)

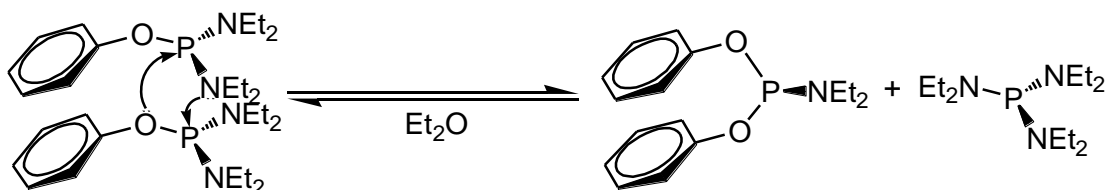
It was proposed that the addition of HCl to **4-4** would result in the formation of the target compound **4-3**. Indeed, the addition of eight equivalents of HCl (2M in Et_2O) to an Et_2O solution of **4-4** resulted in its quantitative conversion to **4-3** according to $^{31}\text{P}\{^1\text{H}\}$ NMR spectroscopy, with no evidence for the formation of any oligomeric species (Scheme 4.8). Eight equivalents of HCl are required as the HN^iPr_2 leaving group displaced will also react with HCl to form a quaternary ammonium salt. The quaternary ammonium salt formed can subsequently be removed by simple filtration of the Et_2O solution leaving a solution of compound **4-3**. Notably, it was found that even using an excess of HCl (16 equivalents) did not lead to cleavage of the P-O bond.



Scheme 4.9: Bimolecular rearrangement of **4-3** upon removal of solvent.

It is noteworthy that it was not possible to isolate **4-3** in its pure form. All attempts to remove the solvent resulted in the formation of a significant amount (approx. 60% of all phosphorus-containing products by ^{31}P NMR spectroscopy) of another phosphorus-containing species. This product resulting from the evolution of **4-3** is believed to be the coupled species **4-3'** by analysis of the $^{31}\text{P}\{^1\text{H}\}$ NMR spectrum, which exhibited two

singlets at 157.7 and 178.0 ppm integral 1:2, consistent with the expected spectrum of **4-3'** (Scheme 4.9).



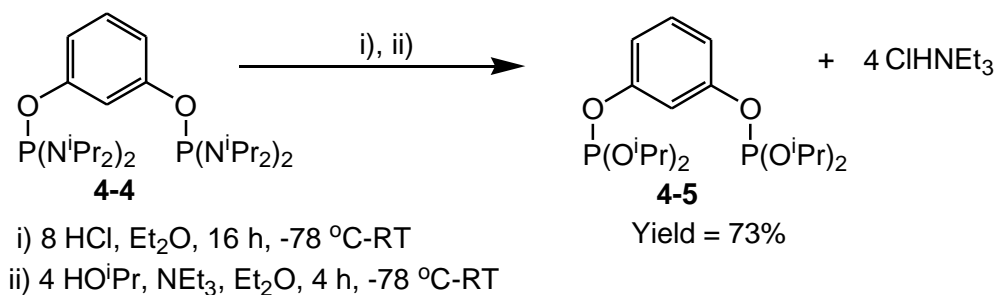
Scheme 4.10: The mechanism proposed by Nifantev and co-workers for the bimolecular rearrangement of $\text{PhOP}(\text{NEt}_2)_2$.⁴⁹

It has been reported by Nifantev *et al.* that the compound $\text{PhOP}(\text{NEt}_2)_2$ undergoes a bimolecular rearrangement upon prolonged standing in Et_2O solution, to form an equilibrium mixture (Scheme 4.10). A mechanism has been proposed by Nifantev in which π -stacking interactions bring two molecules close together, which then allows an intermolecular rearrangement to take place.⁴⁹

With this in mind it is reasonable to suggest that compound **4-3** is rearranging by a similar mechanism to that proposed by Nifantev, but the reaction is not reversible since the PCl_3 (Bp 75 °C)⁵⁰ produced is removed along with the solvent under vacuum. In contrast, it is possible to remove the solvent from a solution of **4-6** without a bimolecular rearrangement occurring, as the bulky *tert*-butyl groups on the aromatic backbone of **4-6** disrupt the π -stacking interactions and prevent the close approach of two molecules. Consequently, all further reactions involving **4-3** must proceed *via* the generation and use of **4-3** *in situ*, without its prior isolation.

4.3.1.2 Synthesis of 1,3-(((ⁱPrO)₂PO)₂C₆H₄) (4-5)

As a proof of concept for the utility of **4-3** as a reagent for the synthesis of POCOP ligands, the diisopropoxide derivative 1,3-(((ⁱPrO)₂PO)₂C₆H₄) (**4-5**) was synthesised. Sequential addition of HCl followed by HOⁱPr/ NEt_3 to a diethyl ether solution of **4-4** afforded the desired compound **4-5** in good yield (Scheme 4.11).

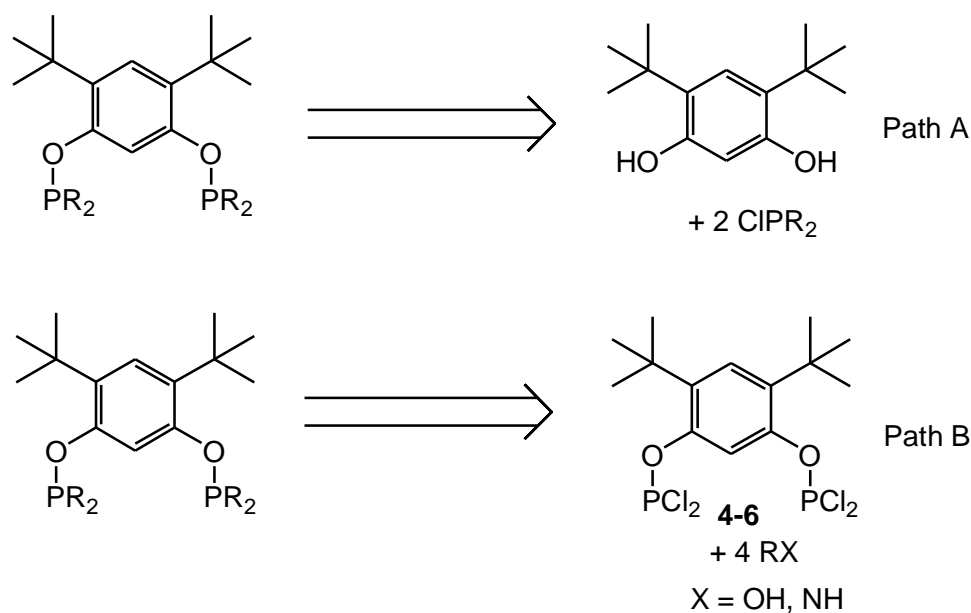


Scheme 4.11: Synthesis of 1,3-{{(ⁱPrO)₂PO}₂C₆H₄} (**4-5**).

Whilst the formation of 1,3-{{Cl₂PO}₂C₆H₄} (**4-3**) *in situ* by the addition of HCl to 1,3-{{(ⁱPr₂N)₂PO}₂C₆H₄} (**4-4**) opens an important new synthetic route for the synthesis of POCOP ligands it does not offer any significant advantages over the methodology described by Bedford and Pringle (*via* **4-6**).⁹ Consequently, we decided to develop a range of POCOP pincer ligands (described in the following sections) based around an aromatic core containing *tert*-butyl groups at the 4 and 6 positions using the methodology described by Bedford and Pringle (*via* **4-6**).⁹ Furthermore, we believed that the benefits of enhanced rates of C-H activation caused by the inclusion of *tert*-butyl groups on the aromatic core of POCOP ligands (Section 4.1.2) will be advantageous during the synthesis of electron deficient POCOP ligands.

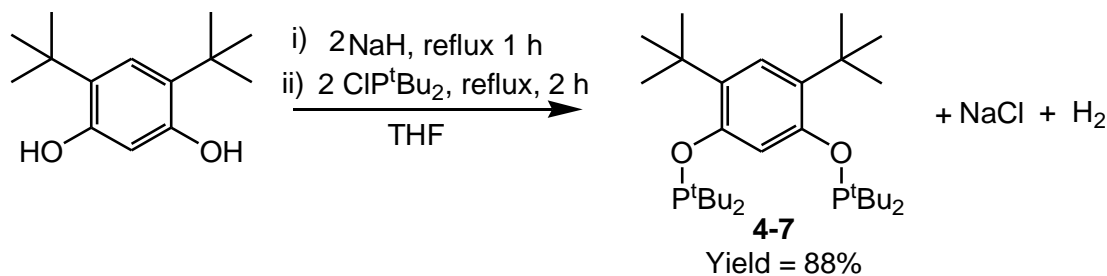
4.3.2 Synthesis of a range of novel POCOP pincer compounds

Two synthetic approaches were identified that would give access to the desired ligand architecture, with a retrosynthetic analysis of the two pathways being shown in Scheme 4.12. Path A will be used to synthesise phosphinite-containing ligands, while path B (*via* the dichlorophosphinite species **4-6**) will be used to synthesise phosphite- and diaminephosphinite-containing POCOP ligands. This dual approach would allow us to synthesise a range of novel POCOP ligands in the most efficient manner.



Scheme 4.12: Retrosynthetic analysis of the synthesis of a POCOP pincer compound containing *tert*-butyl group on the aromatic ring.

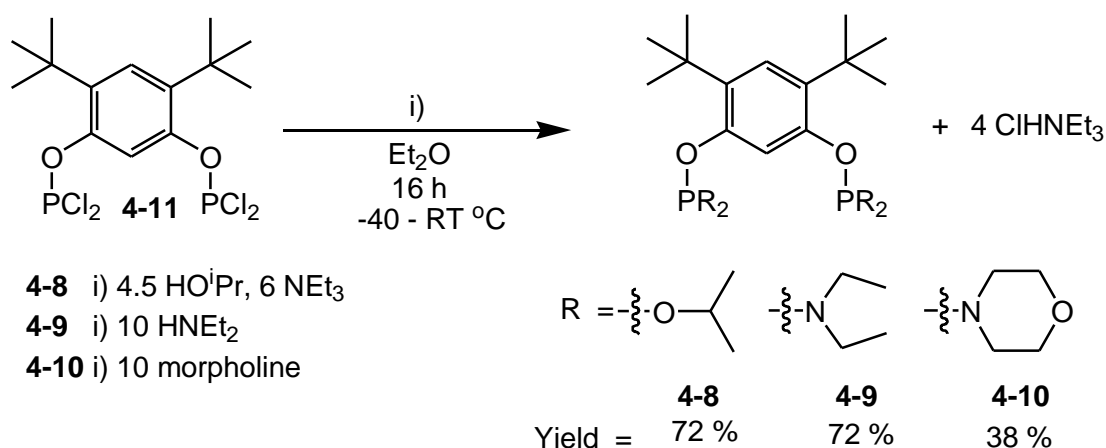
4.3.2.1 Synthesis of 1,3- $\{({}^t\text{Bu}_2\text{PO})_2\text{C}_{14}\text{H}_{20}\}$ (**4-7**)



Scheme 4.13: Synthesis of compound **4-7** as described by Driess and Hartwig.⁵¹

Initially, the known compound 1,3- $\{({}^t\text{Bu}_2\text{PO})_2\text{C}_{14}\text{H}_{20}\}$ (**4-7**) was targeted in order to probe the effects of the *tert*-butyl-substituted aromatic backbone on the structure of subsequent metal complexes of this scaffold, compared to those of the previously synthesised ligand **4-1**, which contains hydrogen atoms in the same positions. To this end, compound **4-7** was synthesised in good yield (88%) by the method described by Driess and Hartwig, namely the diphosphorylation of 4,6-di-*tert*-butylresorcinol with di-*tert*-butylchlorophosphine using sodium hydride as a base (Scheme 4.13). The spectroscopic data obtained for the product were identical to those reported by Driess and Hartwig, with a singlet resonance at 145.6 ppm by ${}^{31}\text{P}\{^1\text{H}\}$ NMR spectroscopy.⁵¹

4.3.2.2 Synthesis of 1,3- $\{(R_2PO)_2C_{14}H_{20}\}$, R = OⁱPr (4-8), NEt₂ (4-9), and morpholine (4-10)



Scheme 4.14: Synthesis of compounds **4-8**, **4-9** and **4-10**.

Ligand	δ ³¹ P{ ¹ H} (CDCl ₃)
4-7	145.6 ^a
4-8	134.9 ^a
4-9	126.2 ^b
4-10	121.4 ^b
4-12	104.6 ^b

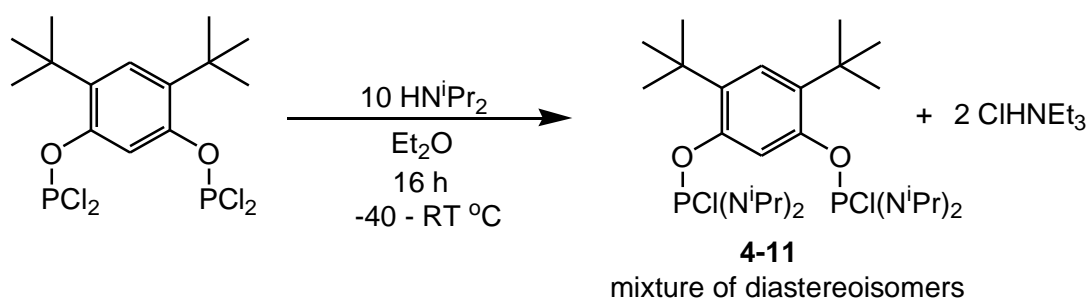
Table 4.2: ³¹P{¹H} NMR spectroscopic data for compounds **4-7** to **4-10** and **4-12**. (a) 283 MHz, (b) 243 MHz

Next, three novel ligands of the form 1,3- $\{(R_2PO)_2C_{14}H_{20}\}$ were synthesised by the addition of excess 2-propanol (**4-8**), diethylamine (**4-9**) and morpholine (**4-10**) to **4-6** (Scheme 4.14). During the synthesis of compound **4-8** triethylamine was used as an external base to remove HCl, whereas during the synthesis of **4-9** and **4-10** excess of the amine was used as the base. A comparison of the ³¹P{¹H} NMR spectroscopic data for the novel POCOP ligands is given in Table 4.2.

Despite its simplicity it was found that this method (addition of excess amine to **4-6**) of synthesising diamminophosphinite-containing pincer ligands from **4-6** was not applicable for all amines tested (including diisopropylamine and pyrrole), detailed below.

4.3.2.3 Attempted synthesis of 1,3- $\{(R_2PO)_2C_{14}H_{20}\}$, $R = N^iPr_2$

While attempting to synthesise the extremely bulky POCOP ligand bearing diisopropylamino substituents at phosphorus, only one of the chloride groups on each phosphorus centre of **4-6** was substituted, which resulted in the formation of two diastereoisomers of **4-11** (Scheme 4.15). The replacement of only one chlorine per phosphorus centre to form **4-11** was confirmed by CHN analysis and integration of its 1H NMR spectrum. The two diastereoisomers of **4-11** exhibit ^{31}P NMR spectroscopic resonances at 164.8 and 165.0 ppm in a ratio of 1:0.8.^v



Scheme 4.15: Synthesis of compound **4-11**.^w

As stated, compound **4-11** was formed as two diastereoisomers, one of which has two enantiomers (Figure 4.9). We were not able to ascertain experimentally which diastereoisomer is the slightly more favoured (*cf.* the NMR spectroscopic data). However, we propose that the *R,R* and *S,S* enantiomers will have a lower steric repulsion between the two bulky diisopropylamine groups located on the two phosphorus moieties than that of the *R,S* diastereoisomer and, thus, will be slightly favoured.

^v By integration of the ^{31}P NMR spectrum.

^w All efforts to separate the two diastereoisomers failed.

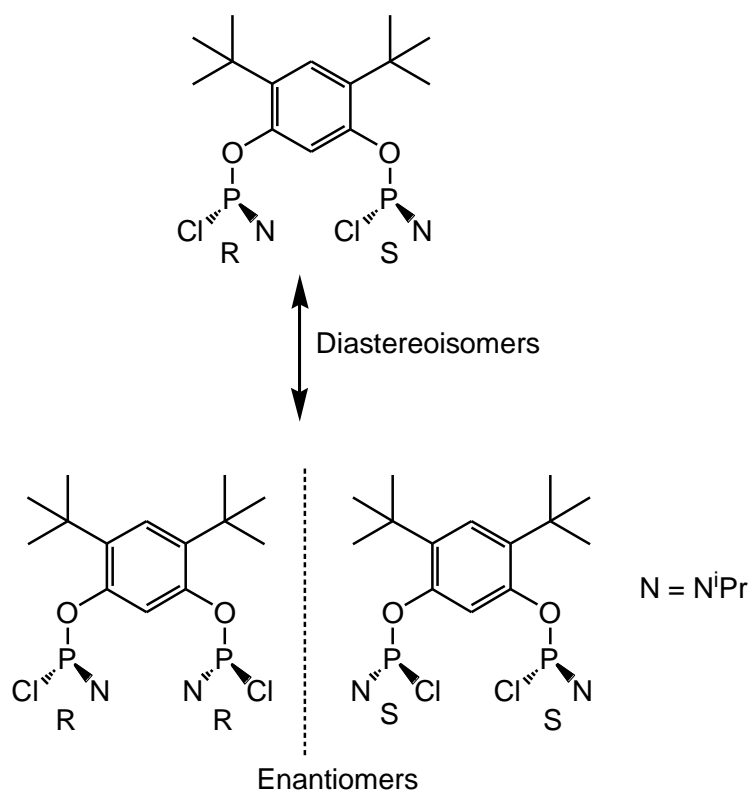
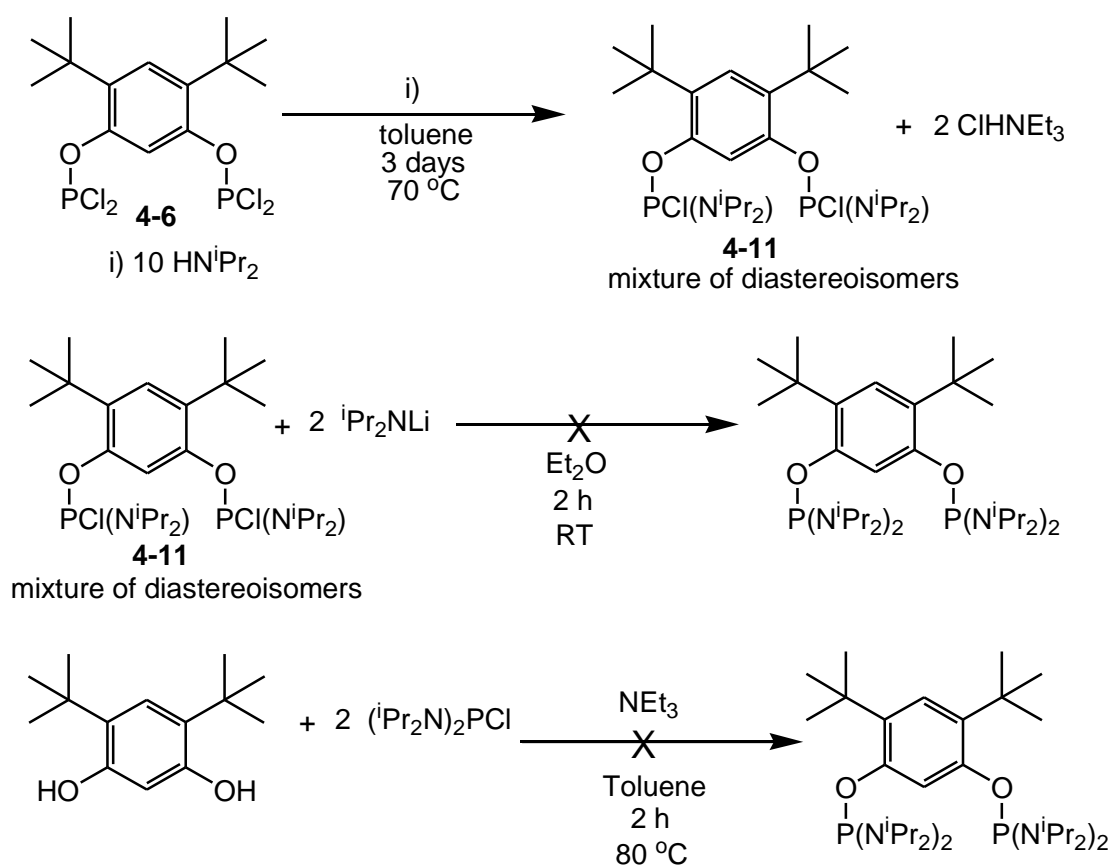


Figure 4.9: Diastereoisomers and enantiomers of **4-11**.

4.3.2.3.1 Further attempts to synthesise $1,3-\{(R_2PO)_2C_{14}H_{20}\}$, R = NⁱPr₂

As the addition of excess diisopropylamine to **4-6** led to the substitution of only one chloride group per phosphorus centre, alternative syntheses of the *tetra*-substituted compound $1,3-\{(R_2PO)_2C_{14}H_{20}\}$, where R = NⁱPr₂, were attempted. However, all efforts to synthesise the *tetra*-substituted compound failed; these tests are detailed below and are summarised in Scheme 4.16.

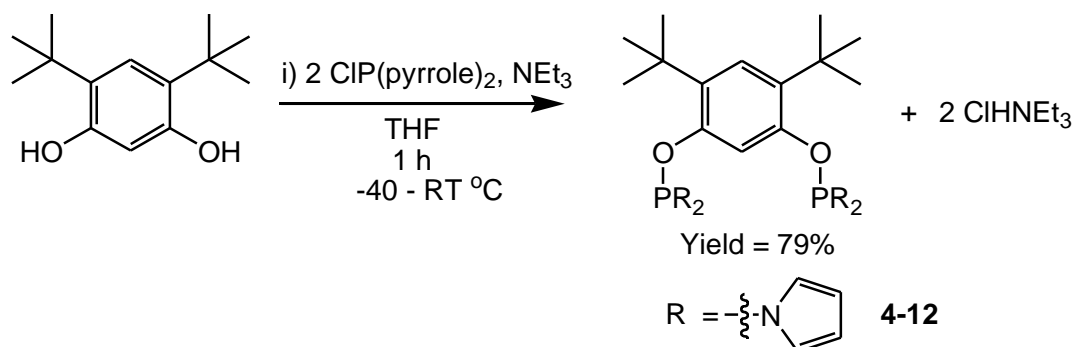
- Increasing the reaction temperature to 70 °C (changing solvent to toluene) for 3 days again led to the formation of **4-11**.
- No reaction of **4-11** was seen with lithium diisopropylamide.
- No reaction observed between *bis*(diisopropylamino)chlorophosphine and 4,6-*di-tert*-butylresorcinol, with starting materials being recovered.



Scheme 4.16: Attempts to synthesise 1,3- $\{(R_2PO)_2C_{14}H_{20}\}$, $R = N^iPr_2$.

The lack of reaction between *bis*(diisopropylamino)chlorophosphine and 4,6-*di-tert*-butylresorcinol contrasts with the facile reaction of resorcinol with *bis*(diisopropylamino)chlorophosphine (Scheme 4.8). The failure to form the *tetra*-coordinated species is attributed to the steric repulsion between the *tert*-butyl groups located on the aromatic backbone and the bulky diisopropylamine groups. Consequently, incorporation of the *tert*-butyl groups on the aromatic backbone has reduced the amount of steric bulk that can be loaded onto each phosphorus centre, which precludes the synthesis of extremely bulky POCOP ligands. It is not just highly bulky amines that do not react completely with **4-6** to displace all four chloride groups, detailed below.

4.3.2.4 Synthesis of 1,3- $\{(R_2PO)_2C_{14}H_{20}\}$, R = pyrrole, (**4-12**)



Scheme 4.17: Synthesis of compound **4-12**.

Compound 1,3- $\{(R_2PO)_2C_{14}H_{20}\}$, R = pyrrole (**4-12**) was targeted as N-pyrrolyl phosphines are known to be highly π -accepting, which could have significant impact on the chemistry of a coordinated metal centre.⁵² However, it was also not possible to synthesise **4-12** by the addition of excess pyrrole to **4-6**, with again only one chloride group being substituted on each phosphorus centre. This is seemingly due to pyrrole being too poor a nucleophile and not due to steric reasons (as was the case for diisopropylamine) as compound **4-12** was synthesised in good yield using an alternative strategy, namely by the addition of $CIP(pyrrole)_2$ to 4,6-di-*tert*-butylresorcinol, with the reaction being complete after stirring at RT for 1h (Scheme 4.17).

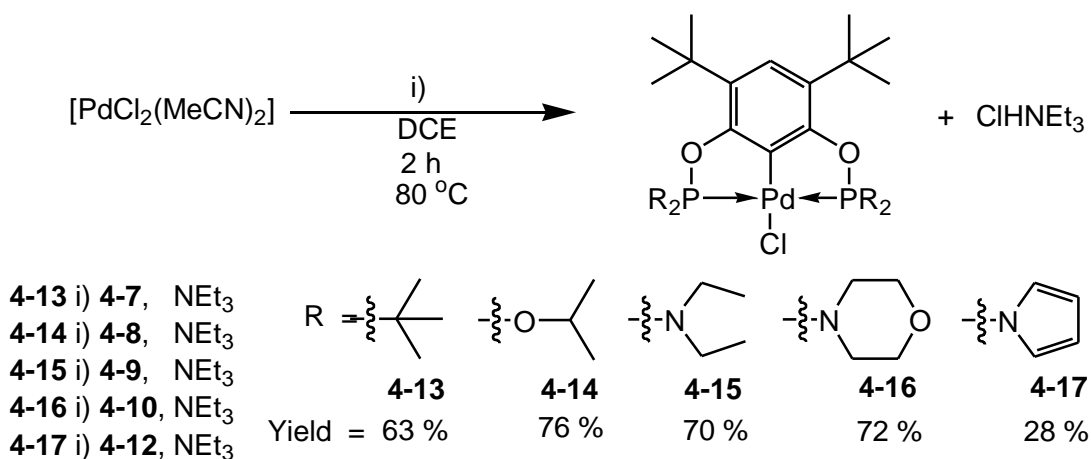
Now that a range of POCOP ligands have been synthesised, the quantification of their steric and electronic properties is needed, detailed in the next section.

4.3.3 Quantification of the electronic and steric properties of POCOP ligands **4-1**, **4-7** to **4-10**, and **4-12**

The palladium complexes of the ligands described in Section 4.3.2. were prepared to probe the impact of changing the phosphine substituents on both the steric and electronic environment of a metal centre. Firstly, the quantification of the steric demands of the various ligands (L) was done by measuring the percentage buried volume ($\%V_{Bur}$) of the ligand on a palladium chloride fragment $[PdCl(\kappa^3\text{-P,C,P-L})]$.^{53, 54} Secondly, abstraction of the chloride ligand of $[PdCl(\kappa^3\text{-P,C,P-L})]$ under an atmosphere of CO was used to afford palladium carbonyl complexes, which will subsequently be

analysed by IR spectroscopy such that the differences in CO stretching frequencies can be used to quantify the electron density of the palladium centre.

4.3.3.1 Synthesis of palladium chloride complexes $[\text{PdCl}(\kappa^3\text{-P,C,P-L})]$, L = 4-7 to 4-10, and 4-12



Scheme 4.18: Synthesis of palladium complexes 4-13 to 4-17.

Five new palladium chloride complexes of ligands 4-7 to 4-10 and 4-12 were synthesised by cyclopalladation at elevated temperature, using $[\text{PdCl}_2(\text{MeCN})_2]$ as the source of palladium (Scheme 4.18). In each case, triethylamine was used to scavenge the HCl produced during the reaction, in order to prevent cleavage of the P-N bond in the free ligand (reactions containing aminophosphine ligands 4-9, 4-10, and 4-12). The yields of the resulting palladium complexes were good (63-76%), except for cases involving the pyrrole-containing ligand (4-12), from which an unidentified oily brown by-product formed in addition to 4-17, which reduced the yield of 4-17 dramatically to 28%. All five complexes (4-13 to 4-17) were characterised by CHN analysis and multinuclear NMR spectroscopy; the $^{31}\text{P}\{^1\text{H}\}$ NMR spectroscopic data are presented in Table 4.3.

Complex	$\delta^{31}\text{P}\{\text{H}\}$ (CDCl_3)	$\Delta\delta^{31}\text{P}\{\text{H}\}$
4-13	191.3 ^a	+45.7
4-14	140.6 ^a	+5.7
4-15	147.4 ^b	+21.2
4-16	142.9 ^b	+21.5
4-17	126.3 ^a	+21.7

Table 4.3: $^{31}\text{P}\{\text{H}\}$ NMR spectroscopic data for complexes **4-13** to **4-17**. (a) 283 MHz, (b) 243 MHz

4.3.3.1.1 X-Ray crystallographic study of complexes $[\text{PdCl}(\kappa^3\text{-P,C,P-L})]$, L = **4-7** to **4-10**, and **4-12**

The structures of the pincer complexes **4-13** to **4-17** were unambiguously determined by X-ray diffraction analyses (Figure 4.10 and Table 4.4). In each case the complexes adopt a distorted square-planar geometry about the palladium centre. The P1-Pd-P2 angles of the pincer complexes **4-13** to **4-17** are bent ($157.92(2)^\circ$ – $162.36(5)^\circ$), with all falling within the range of angles measured for other previously-reported POCOP complexes.^x The Pd-Cl bond distances vary in length from 2.3547(6) to 2.3830(6) Å, with longer bonds observed for the more electron-rich metal centres **4-13** and **4-15** compared to those for electron-poor metal centres **4-14** and **4-17**.

	4-13	4-14	4-15	4-16	4-17
Pd-Cl	2.3808(5)	2.3610(9)	2.3830(6)	2.367(1)	2.3547(6)
Pd-P	2.2808(4)	2.2703(9)	2.2644(5)	2.257(1)	2.2460(6)
Pd-P	2.2808(4)	2.2529(9)	2.2681(6)	2.280(1)	2.2403(6)
Pd-C1	2.008(2)	1.997(4)	1.996(2)	1.987(5)	2.011(2)
P-Pd-P	160.89(2)	162.17(3)	161.14(2)	162.36(5)	157.92(2)
C1-Pd-Cl	180	177.3(1)	178.19(6)	176.3(1)	179.55(6)

Table 4.4: Selected bond lengths (Å) and angles ($^\circ$) of palladium complexes **4-13** to **4-17**.

^x CSD search 6/12/13.

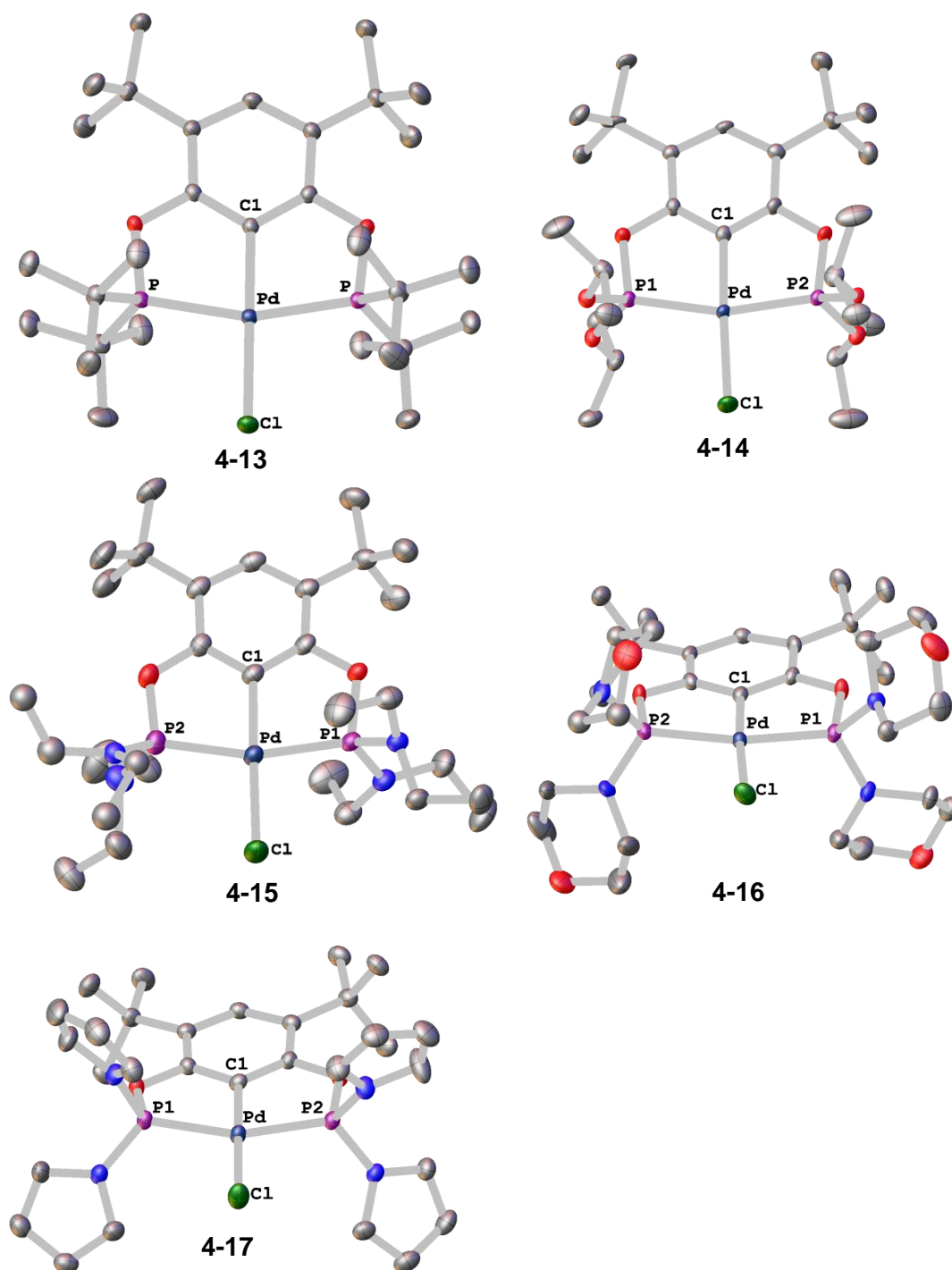


Figure 4.10: Molecular structures of complexes 4-13 to 4-17, (thermal ellipsoids set at 50% level).

4.3.3.2 Assessment of the steric properties of POCOP ligands

We have used the percentage buried volume ($\%V_{\text{Bur}}$) method (Section 1.1.2) to quantify the steric bulk of the pincer ligands **4-1**, **4-7** to **4-10** and **4-12**.^{53, 54} Here the experimentally-determined molecular structures of the palladium chloride complexes **4-2** and **4-13** to **4-17** were used to generate the required Cartesian-coordinate file and the file was processed using SambVca© software.⁵³ A representative example of the calculation is shown in Appendix 3.

Complex	Ligand (phosphorus substituent)	$\%V_{\text{bur}}$ of POCOP ligand / %
4-2	4-1 (^t Bu)	71
4-13	4-7 (^t Bu)	72
4-14	4-8 (O ⁱ Pr)	64
4-15	4-9 (NEt ₂)	70
4-16	4-10 (morpholine)	67
4-17	4-12 (pyrrole)	63

Table 4.5: Percentage buried volume ($\%V_{\text{Bur}}$) of the variously-substituted POCOP ligands in complexes **4-2** and **4-13** to **4-17**.

The ligands with the largest values of $\%V_{\text{Bur}}$ are the *tert*-butyl-phosphine-substituted systems **4-1** and **4-7**, at 71 and 72%, respectively, and the diethylamino-substituted ligand **4-9** (70%) (Table 4.5). A relative ordering of the various pincer ligands in terms of their steric demands is presented in Figure 4.11. Comparing **4-1** with its PCP analogue (Table 4.6, entry 1) it is observed that changing the oxygen atom in the linker arm to carbon has no effect on the steric bulk of the ligand as might be expected. However, it is noticeable that the morpholine-substituted ligand **4-10** has a slightly smaller $\%V_{\text{Bur}}$ (67%) than the diethylamino-substituted ligand **4-9** (70%), illustrating that non-cyclic phosphine-substituents give the pincer ligand more steric bulk.

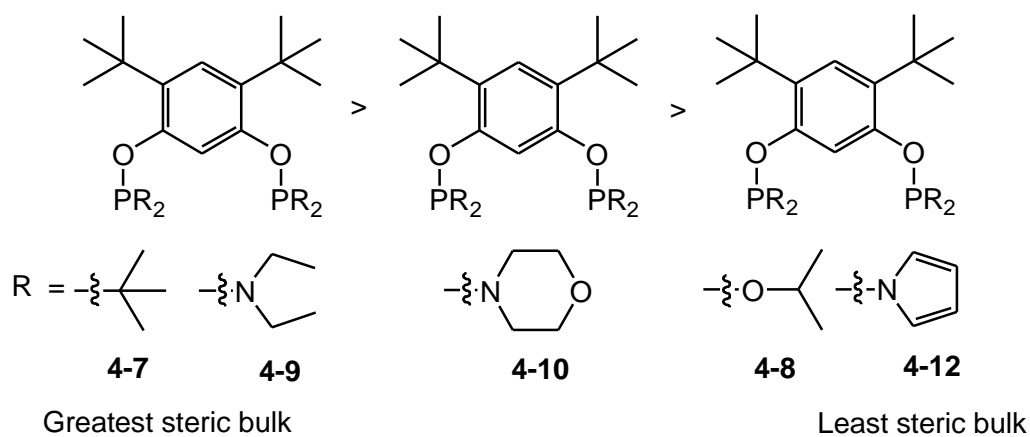


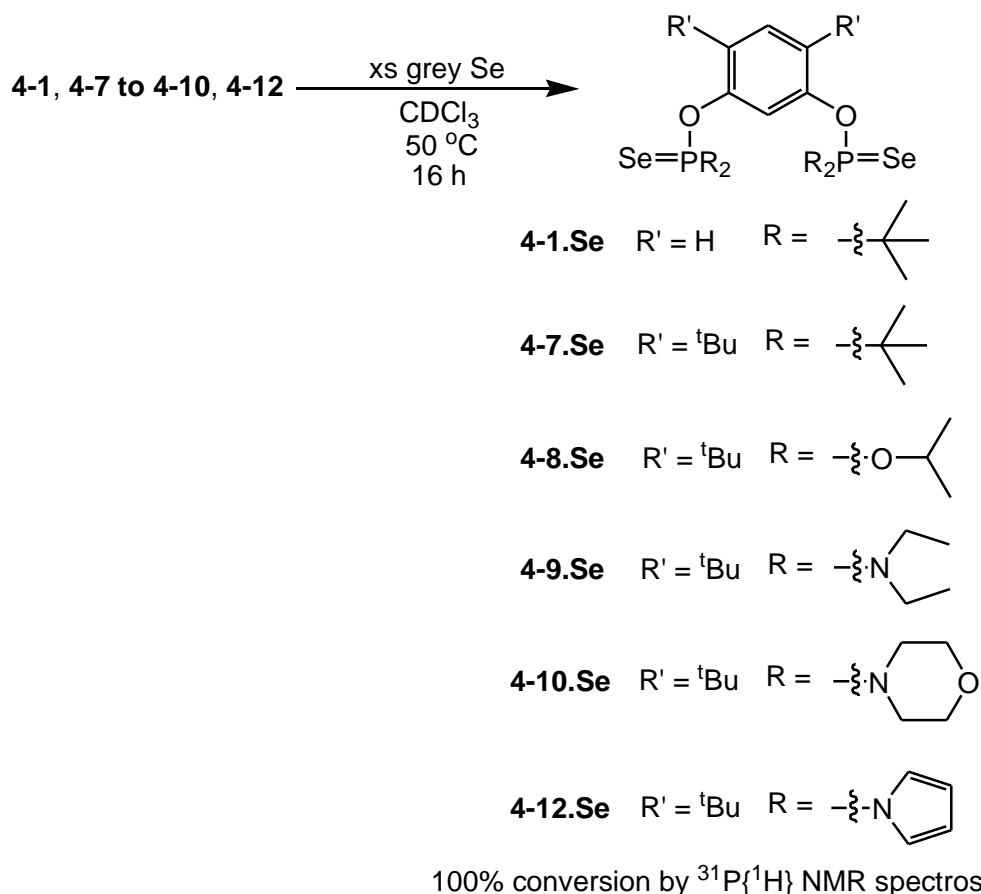
Figure 4.11: The relative ordering of the pincer ligands **4-7** to **4-10** and **4-12** according to their steric demands.

Entry	Complex	% V_{bur} of pincer ligand / %
1		71
2		62
3		65
4		54

Table 4.6: % V_{Bur} of various known pincer ligands, calculated by Roddick.⁵⁵

4.3.3.3 Assessment of the electronic properties of POCOP ligands

Two methods for assessing the electronic character of the POCOP pincer ligands **4-1**, **4-7** to **4-10**, **4-12**, were used. Firstly, the corresponding phosphine selenides were synthesised (Scheme 4.19) and the $|^1J_{\text{SeP}}|$ coupling constants then measured (Table 4.7). The pyrrole-substituted and phosphite-containing ligands **4-12** and **4-8** have the least basic phosphorous lone-pairs, with large magnitudes of the $^1J_{\text{SeP}}$ coupling constants for **4-12.Se** and **4-8.Se** of 993 and 965 Hz, respectively. The most basic phosphorus lone pairs are found for the *tert*-butyl-phosphine-substituted ligands **4-1** and **4-7**, as expected for phosphorus ligands containing two highly electron releasing substituents. However, the value of the $|^1J_{\text{SeP}}|$ coupling constants is only a measure of the σ -donor ability of the phosphorus lone-pair, and a complementary technique is needed to assess the overall electronic character of the entire ligand.



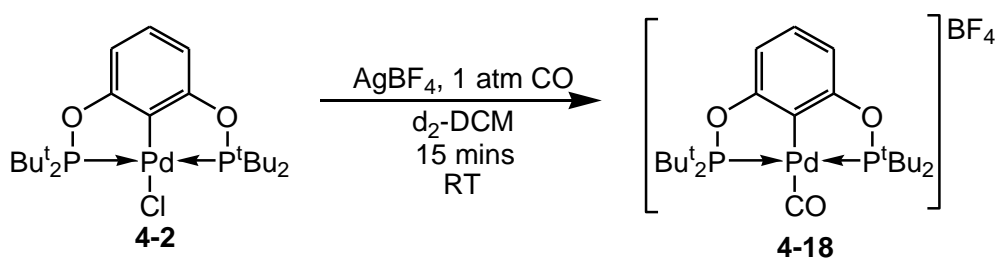
Scheme 4.19: Synthesis of phosphorus selenides **4-1.Se**, **4-7.Se** to **4-10.Se** and **4-12.Se**.

Ligand	$ ^1J_{\text{SeP}} $ coupling constant / Hz (phosphine-selenide)	ν_{CO} (Pd–CO) / cm^{-1} (palladium-carbonyl complex)
4-1	797 (4-1.Se)	2119 (4-18)
4-7	806 (4-7.Se)	2116 (4-19)
4-8	965 (4-8.Se)	2145 (4-20)
4-9	855 (4-9.Se)	2116 (4-21)
4-10	881 (4-10.Se)	2136 (4-22)
4-12	993 (4-12.Se)	-

Table 4.7: $|^1J_{\text{SeP}}|$ coupling constants for phosphine selenides **4-1.Se**, **4-7.Se** to **4-10.Se**, **4-12.Se** and the carbonyl stretching frequency for palladium complexes **4-18** to **4-22**.

To assess and compare the electronic properties of the various synthesised POCOP pincer ligands, we turned to the cationic palladium carbonyl derivatives (Schemes 4.20 and 4.21). Infrared analysis of carbonyl complexes is a common technique used to probe the electronic character of ligands, as it gives a good estimation of both σ -donation and π -back-donation (Section 1.1.3). Whilst nickel and rhodium carbonyl complexes are most commonly used as they readily form stable carbonyl complexes, a number of examples of using palladium carbonyl complexes to assess the electronic character of pincer ligands have been reported. Representative palladium-bound carbonyl stretching frequencies are given in Table 4.8.^{10, 56} The carbonyl ligand of palladium carbonyl complexes tend to be labile due to weak palladium to CO-back-donation, which tends to preclude their isolation.⁵⁷ The lability of palladium carbonyl ligands sometimes requires the infrared spectra to be collected under an atmosphere of CO to prevent dissociation of CO, although it was not the case with the complexes in this thesis.⁵⁸

The palladium carbonyl complexes **4-18** to **4-22** were prepared from the corresponding palladium chlorides by abstraction of the chloride ligand with AgBF_4 , followed by the addition of 1 atm of CO. In each case, this gave quantitative conversion, by $^{31}\text{P}\{^1\text{H}\}$ NMR spectroscopy, to the desired carbonyl complexes (Schemes 4.20 and 4.21). The palladium carbonyl complexes were characterised by multinuclear NMR and infrared spectroscopies. It is notable that the corresponding palladium carbonyl complex of the pyrrole-substituted ligand **4-12**, **4-23** could not be prepared by this method, with rapid decomposition occurring instead, leading to precipitation of palladium metal upon addition of CO. This is possibly caused by the CO displacing the especially poorly donating N-pyrrolyl phosphine arm, and hence leading to decomposition.



Quantitative conversion by ^{31}P NMR spectroscopy

Scheme 4.20: Synthesis of palladium carbonyl complex **4-17**.

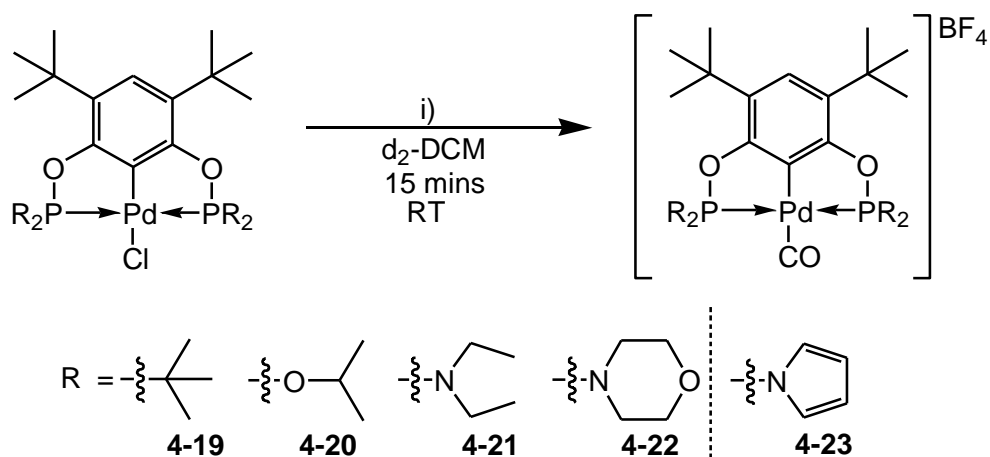
4-19 i) **4-13**, AgBF_4 , 1 atm CO

4-20 i) **4-14**, AgBF_4 , 1 atm CO

4-21 i) **4-15**, AgBF_4 , 1 atm CO

4-22 i) **4-16**, AgBF_4 , 1 atm CO

4-23 i) **4-17**, AgBF_4 , 1 atm CO



Quantitative conversion by ^{31}P NMR spectroscopy

| rapid decomposition upon addition of CO

Scheme 4.21: Synthesis of palladium carbonyl complexes **4-19** to **4-22**.

The carbonyl stretching frequencies determined for palladium complexes **4-18** to **4-22** varied across a range of 29 cm^{-1} , with **4-19/4-21** being the lowest (2116 cm^{-1}) and **4-20** the highest (2145 cm^{-1}), Table 4.7. By examination of the palladium carbonyl stretching frequencies of complexes **4-18** and **4-19** (2119 and 2116 cm^{-1}) it may be seen that, as expected, the inclusion of *tert*-butyl groups on the aromatic backbone of the pincer ligand has no effect on the electronic character of the overall ligand, presumably due to its large distance from the metal centre. However, a much greater effect on the electronic properties is seen upon changing the linker arm atom from carbon to oxygen (Table 4.8, Entry 1, 2078 cm^{-1} , cf. **4-18**, 2119 cm^{-1}), the electronegative oxygen next to the phosphorus centre making the POCOP ligand **4-1** less electron-rich than its PCP analogue.

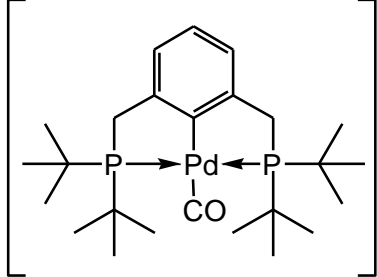
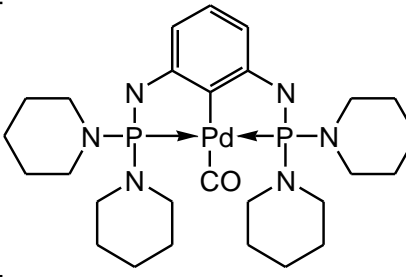
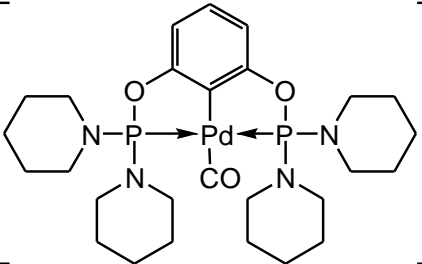
Entry	Complex	$\nu(\text{CO}) / \text{cm}^{-1}$
1		2078 ⁵⁶
2		2106 ¹⁰
3		2133 ¹⁰

Table 4.8: Known carbonyl stretching frequencies for cationic palladium pincer-type complexes.

There is a rough positive correlation between the magnitudes of the $^1J_{\text{SeP}}$ coupling constants and the CO stretching frequencies of the species containing the same ligand, suggesting that the σ -donation ability of the phosphine-moiety is the dominating factor in determining the electronic properties of the entire ligand and hence that of the coordinated metal centre. Therefore, based on the very large $^1J_{\text{SeP}}$ coupling constant for the pyrrole-substituted species **4-12.Se** (993 Hz), we propose that **4-12** is even more electron deficient than **4-8** and is the most electron deficient of the ligands in the range synthesised.

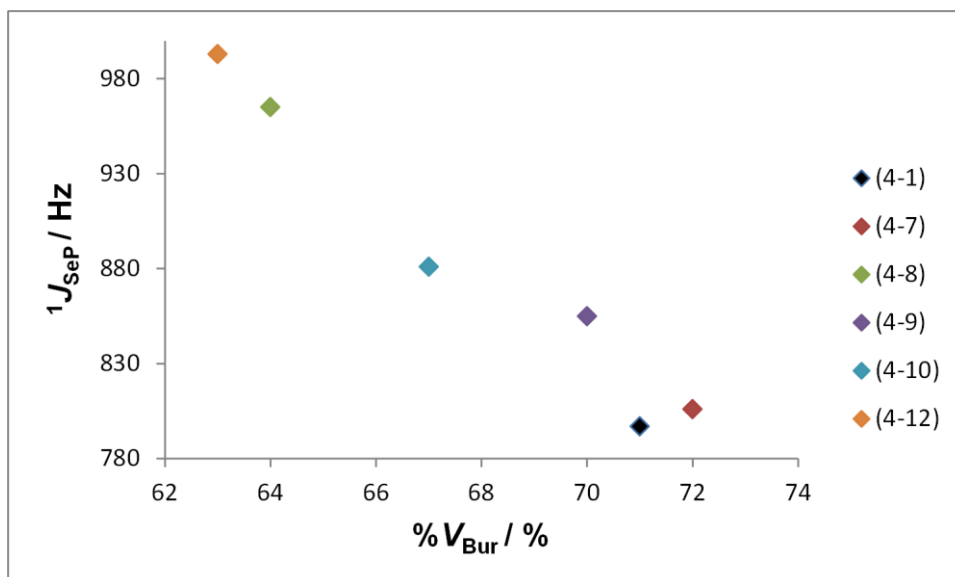


Figure 4.12: A plot of the $|^1J_{SeP}|$ coupling constants for the relevant phosphine-selenides of the POCOP ligands described in this thesis against the $\%V_{bur}$ calculated from the palladium complexes of the same ligands.

The steric and electron demands of the POCOP ligands synthesised in this chapter have now been assessed. Figure 4.12 clearly shows that the six POCOP ligand synthesised in this chapter exhibit a trend between their steric and electronic demands. The most electron rich ligands display the largest steric demand whereas the least electron rich ligands display the lowest steric demand.

4.4 Chapter 4 summary and conclusions

The formation of 1,3- $\{(\text{Cl}_2\text{PO})_2\text{C}_6\text{H}_4\}$ (**4-3**) *in situ* by the addition of HCl to 1,3- $\{((\text{Pr}_2\text{N})_2\text{PO})_2\text{C}_6\text{H}_4\}$ (**4-4**) opens an important new synthetic route for the synthesis of POCOP ligands containing phosphite and diaminophosphinite moieties.

Four novel POCOP ligands have been synthesised giving significant variation in the steric and electronic properties over the commonly used ligand **4-1** by using heteroatom atom-substituted phosphorus atoms. The steric and electronic properties of the POCOP ligands (L) were quantified, with palladium chloride complexes ($[\text{PdCl}(\kappa^3\text{-P,C,P-L})]$) synthesised in order to assess steric bulk of the ligands using the percentage buried volume ($\%V_{bur}$) method. The electronic properties of the newly synthesised POCOP ligands were assessed by comparison of the $|^1J_{\text{SeP}}|$ values for the corresponding phosphine selenides and by the carbonyl stretching frequencies of palladium carbonyl complexes $[\text{Pd}(\text{CO})(\kappa^3\text{-P,C,P-L})]\text{BF}_4$.

Placing *tert*-butyl groups on the aromatic backbone of the POCOP ligand has little effect on the electronic and steric properties at the metal centre, as evident by the palladium carbonyl stretching frequencies of **4-18** and **4-19**, plus the calculated $\%V_{bur}$ of ligands **4-1** and **4-7** for their palladium chloride complexes (**4-2** and **4-13**). However, the presence of *tert*-butyl groups on the aromatic backbone does preclude the synthesis of ligands with extremely bulky substituents at phosphorus.

4.5 Future work

Figure 4.12 showed that the POCOP ligands synthesised in this chapter exhibited a trend between their steric and electronic demands with the most bulky ligands being the most electron rich. Consequently it would be advantageous to synthesise POCOP ligands with alternate steric and electronic demands, proposed synthetic targets are displayed in Figure 4.13.

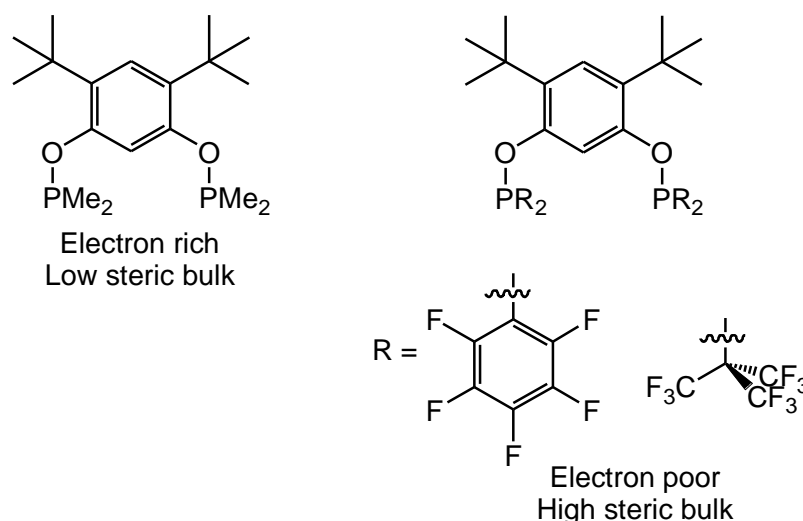


Figure 4.13: Proposed POCOP ligands have different steric and electronic demands to those described in this thesis.

It will be possible to test the palladium chloride complexes described in this thesis (**4-2**, **4-7** to **4-12**) as catalysts for a range of palladium-catalysed cross-coupling reactions, to investigate the impact of changing the steric and electronic impact of the ligand. Whilst the limitations of pincer complexes in Pd(0)/Pd(II) redox cross-coupling reactions are well known,⁷ where catalytically active Pd(0) nanoparticles are believed to be the active catalyst,^y there are examples of electron rich pincer palladium complexes that are believed to catalyse cross-coupling reactions through a Pd(II)/Pd(IV) redox process.¹⁰ This type of application would benefit significantly from the fine-tuning of the steric and electronic properties of the ligand.

Finally, Table 4.1 demonstrated the wide catalytic utility of POCOP-type ligands, consequently the ligands **4-7** to **4-10** and **4-12** could be coordinated to an expanded array of metal fragments (e.g. NiX, where X = Cl, H, or OTf and IrX₂ where X = Cl(H), H₂ or (H)acetone), and tested in a range of metal-catalysed processes.

^yIf Pd(0) nanoparticles are the active catalyst then changing the steric and electronic properties of the pincer ligands to alter reactivity/selectivity is irrelevant.

4.6 References

1. J. M. Serrano-Becerra and D. Morales-Morales, *Current Organic Synthesis*, 2009, **6**, 169-192.
2. M. Albrecht, M. Lutz, A. L. Spek and G. van Koten, *Nature*, 2000, **406**, 970-974.
3. P. A. Chase, R. J. M. K. Gebbink and G. van Koten, *J. Organomet. Chem.*, 2004, **689**, 4016-4054.
4. D. Beccati, K. M. Halkes, G. D. Batema, G. Guillena, A. Carvalho de Souza, G. van Koten and J. P. Kamerling, *ChemBioChem*, 2005, **6**, 1196-1203.
5. D. Morales-Morales, *Mini-Reviews in Organic Chemistry*, 2008, **5**, 141-152.
6. J. Choi, A. H. R. MacArthur, M. Brookhart and A. S. Goldman, *Chem. Rev.*, 2011, **111**, 1761-1779.
7. N. Selander and K. J. Szabó, *Chem. Rev.*, 2010, **111**, 2048-2076.
8. D. Morales-Morales, C. Grause, K. Kasaoka, R. Redon, R. E. Cramer and C. M. Jensen, *Inorg. Chim. Acta*, 2000, **300**, 958-963.
9. R. A. Baber, R. B. Bedford, M. Betham, M. E. Blake, S. J. Coles, M. F. Haddow, M. B. Hursthouse, A. G. Orpen, L. T. Pilarski, P. G. Pringle and R. L. Wingad, *Chem. Commun.*, 2006, 3880-3882.
10. J. L. Bolliger, O. Blacque and C. M. Frech, *Angew. Chem. Int. Ed.*, 2007, **46**, 6514-6517.
11. R. B. Bedford, S. M. Draper, P. N. Scully and S. L. Welch, *New J. Chem.*, 2000, **24**, 745-747.
12. V. Pandarus and D. Zargarian, *Organometallics*, 2007, **26**, 4321-4334.
13. A. Castonguay, D. M. Spasyuk, N. Madern, A. L. Beauchamp and D. Zargarian, *Organometallics*, 2009, **28**, 2134-2141.
14. S. Chakraborty, J. A. Krause and H. Guan, *Organometallics*, 2009, **28**, 582-586.
15. J. Zhang, C. M. Medley, J. A. Krause and H. Guan, *Organometallics*, 2010, **29**, 6393-6401.
16. S. Chakraborty, J. Zhang, J. A. Krause and H. Guan, *J. Am. Chem. Soc.*, 2010, **132**, 8872-8873.
17. S. Chakraborty, Y. J. Patel, J. A. Krause and H. Guan, *Polyhedron*, 2012, **32**, 30-34.
18. S. Chakraborty, J. Zhang, Y. J. Patel, J. A. Krause and H. Guan, *Inorg. Chem.*, 2012, **52**, 37-47.
19. A. B. Salah, C. Offenstein and D. Zargarian, *Organometallics*, 2011, **30**, 5352-5364.
20. F. Estudiante-Negrete, S. Hernández-Ortega and D. Morales-Morales, *Inorg. Chim. Acta*, 2012, **387**, 58-63.

21. S. Chakraborty, Y. J. Patel, J. A. Krause and H. Guan, *Angew. Chem. Int. Ed.*, 2013, **52**, 7523-7526.
22. R. Johansson and O. F. Wendt, *Dalton Trans.*, 2007, 488-492.
23. O. A. Wallner, V. J. Olsson, L. Eriksson and K. J. Szabo, *Inorg. Chim. Acta*, 2006, **359**, 1767-1772.
24. T. Kimura and Y. Uozumi, *Organometallics*, 2006, **25**, 4883-4887.
25. S. Ogo, Y. Takebe, K. Uehara, T. Yamazaki, H. Nakai, Y. Watanabe and S. Fukuzumi, *Organometallics*, 2006, **25**, 331-338.
26. J. Li, M. Lutz, A. L. Spek, G. P. M. van Klink, G. van Koten and R. J. M. K. Gebbink, *Organometallics*, 2010, **29**, 1379-1387.
27. Z. Wang, S. Sugiarti, C. M. Morales, C. M. Jensen and D. Morales-Morales, *Inorg. Chim. Acta*, 2006, **359**, 1923-1928.
28. S. D. Timpa, C. M. Fafard, D. E. Herbert and O. V. Ozerov, *Dalton Trans.*, 2011, **40**, 5426-5429.
29. I. Gottker-Schnetmann, P. White and M. Brookhart, *J. Am. Chem. Soc.*, 2004, **126**, 1804-1811.
30. M. C. Denney, V. Pons, T. J. Hebden, D. M. Heinekey and K. I. Goldberg, *J. Am. Chem. Soc.*, 2006, **128**, 12048-12049.
31. J. Yang and M. Brookhart, *J. Am. Chem. Soc.*, 2007, **129**, 12656-12657.
32. S. Park and M. Brookhart, *Organometallics*, 2010, **29**, 6057-6064.
33. S. Park, D. Bézier and M. Brookhart, *J. Am. Chem. Soc.*, 2012, **134**, 11404-11407.
34. S. Park and M. Brookhart, *J. Am. Chem. Soc.*, 2011, **134**, 640-653.
35. P. Bhattacharya, J. A. Krause and H. Guan, *Organometallics*, 2011, **30**, 4720-4729.
36. T. J. Hebden, R. R. Schrock, M. K. Takase and P. Muller, *Chem. Commun.*, 2012, **48**, 1851-1853.
37. D. M. Ivanov, S. A. Kuklin, A. V. Polezhaev, P. V. Petrovskii, A. F. Smol'yakov, F. M. Dolgushin, M. G. Ezernitskaya, A. S. Peregudov and A. A. Koridze, *Russ. Chem. Bull.*, 2009, **58**, 1701-1706.
38. T. J. Hebden, A. J. St. John, D. G. Gusev, W. Kaminsky, K. I. Goldberg and D. M. Heinekey, *Angew. Chem. Int. Ed.*, 2011, **50**, 1873-1876.
39. M. Montag, I. Efremenko, R. Cohen, L. J. Shimon, G. Leitus, Y. Diskin-Posner, Y. Ben-David, H. Salem, J. M. Martin and D. Milstein, *Chem. Eur. J.*, 2010, **16**, 328-353.
40. A. V. Polukeev, S. A. Kuklin, P. V. Petrovskii, S. M. Peregudova, A. F. Smol'yakov, F. M. Dolgushin and A. A. Koridze, *Dalton Trans.*, 2011, **40**, 7201-7209.

41. I. Gottker-Schnetmann and M. Brookhart, *J. Am. Chem. Soc.*, 2004, **126**, 9330-9338.
42. I. J. S. Fairlamb, S. Grant, A. C. Whitwood, J. Whitthall, A. S. Batsanov and J. C. Collings, *J. Organomet. Chem.*, 2005, **690**, 4462-4477.
43. M. Rubio, A. Suarez, D. del Rio, A. Galindo, E. Alvarez and A. Pizzano, *Organometallics*, 2009, **28**, 547-560.
44. M. Rubio, A. Suarez, D. del Rio, A. Galindo, E. Alvarez and A. Pizzano, *Dalton Trans.*, 2007, 407-409.
45. V. I. Sokolov and L. A. Bulygina, *Russ. Chem. Bull.*, 2004, **53**, 2355-2356.
46. W. Knauer, *Ber. Bunsen-Ges. Phys. Chem*, 1894, **27**, 2565-2572.
47. H. R. Hudson, A. Kow and J. C. Roberts, *J. Chem. Soc. Perk. Trans. 2*, 1983, 1363-1368.
48. M. Stratakis, C. Rabalakos and N. Sofikiti, *Tetrahedron Lett.*, 2003, **44**, 349-351.
49. E. N. Rasadkina, P. V. Slitikov and E. E. Nifant'ev, *Russ. J. Gen. Chem.*, 2006, **76**, 183-197.
50. H. H. Anderson, *J. Am. Chem. Soc.*, 1953, **75**, 1576-1578.
51. A. Brück, D. Gallego, W. Wang, E. Irran, M. Driess and J. F. Hartwig, *Angew. Chem. Int. Ed.*, 2012, **51**, 11478-11482.
52. K. G. Moloy and J. L. Petersen, *J. Am. Chem. Soc.*, 1995, **117**, 7696-7710.
53. A. Poater, B. Cosenza, A. Correa, S. Giudice, F. Ragone, V. Scarano and L. Cavallo, *Eur. J. Inorg. Chem.*, 2009, 1759-1766.
54. H. Clavier and S. P. Nolan, *Chem. Commun.*, 2010, **46**, 841-861.
55. D. M. Roddick, in *Organometallic Pincer Chemistry*, eds. G. van Koten and D. Milstein, Springer-Verlag Berlin, Berlin, Editon edn., 2013, vol. 40, pp. 49-88.
56. R. Gerber, T. Fox and C. M. Frech, *Chem. Eur. J.*, 2010, **16**, 6771-6775.
57. E. P. Kuendig, D. McIntosh, M. Moskovits and G. A. Ozin, *J. Am. Chem. Soc.*, 1973, **95**, 7234-7241.
58. J. Lisena, J. Monot, S. Mallet-Ladeira, B. Martin-Vaca and D. Bourissou, *Organometallics*, 2013, **32**, 4301-4305.

5 Chapter 5: Exploratory reactions into a novel palladium hydride complex

Chapter 5 reports some exploratory reactions into a novel palladium hydride complex bearing a pincer-type POCOP ligand to help gauge the reactivity of the palladium hydride bond and assess its application as a catalyst in a variety of reactions.

5.1 Introduction

Palladium hydride complexes are generally regarded as being highly reactive,¹ but have been proposed as intermediates in a wide range of palladium-catalysed reactions. For example palladium-catalysed oxidations,² carbonylation of ethylene,³ and in hydrodefluorination.⁴

Despite their numerous applications, many soluble molecular palladium hydride complexes are unstable and cannot be isolated, only generated and characterised *in situ*.¹ In contrast, palladium hydride complexes bearing ancillary pincer ligands are significantly more stable; something proposed to result by virtue of the rigid structure of the pincer ligand (Figure 5.1).⁵⁻⁷ Consequently, these isolable palladium hydride pincer complexes can be used as models for the study of fundamental reactions involving a Pd–H bond. Indeed, the insertion of unsaturated molecules into metal-hydride bonds is among the most important stoichiometric and catalytic reactions occurring at a metal centre.⁸ For instance, hydride migration to a coordinated alkene, also known as alkene insertion into an M–H bond, has been considered to be the key elementary step in the hydrogenation, hydroformylation and isomerisation of alkenes.

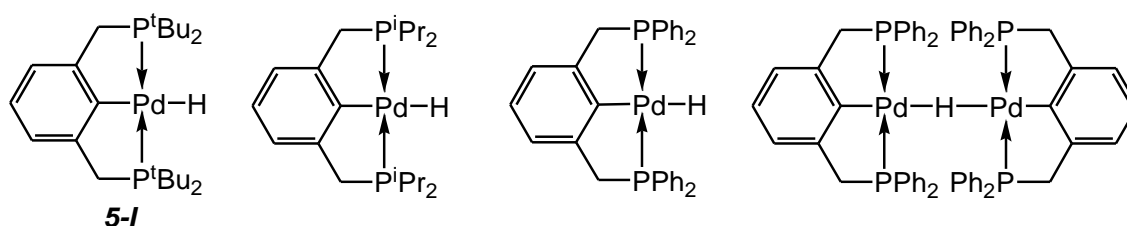
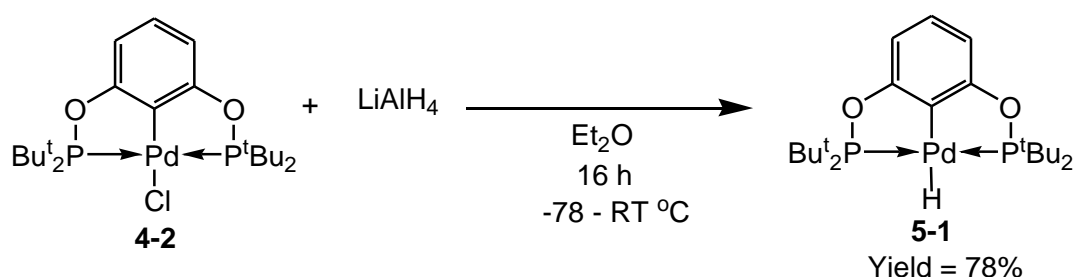


Figure 5.1: Known pincer ligand-substituted palladium hydride complexes.⁵⁻⁷

Consequently, the work described in this chapter sought to synthesise a palladium hydride complex bearing a POCOP-type ligand as, noticeably, there are no known palladium hydride complexes bearing this type of scaffold, despite the more facile synthesis of the phosphinite derivatives over their PCP analogues. Therefore, the novel palladium hydride complex [PdH(κ^3 -P,C,P-4-1)] (**5-1**) was synthesised and its reactivity

with small molecules of potential importance in catalysis (e.g. ethylene, acetone, carbon dioxide) probed, together with its use in certain catalytic applications (e.g. alkene isomerisation and hydrosilylation). It was reasoned that the more electron deficient palladium centre of **5-1** compared to **5-1**^z could lead to significantly different reactivity of the Pd–H bond.

5.2 Synthesis of [PdH(κ^3 -P,C,P-4-1)] (**5-1**)



Scheme 5.1: Synthesis of [PdH(κ^3 -P,C,P-4-1)] (**5-1**).

With the target Pd hydride complex [PdH(κ^3 -P,C,P-4-1)] (**5-1**) in mind, it was envisaged that treatment of the palladium chloride complex [PdCl(κ^3 -P,C,P-4-1)] (**4-2**) with a source of hydride should permit access to the desired complex.^{2, 5} Indeed, this proved to be the case, with the addition of LiAlH₄ to the palladium chloride complex **4-2** affording **5-1** in 78% yield (Scheme 5.1); **5-1** was subsequently characterised by multi-nuclear NMR spectroscopy and CHN analyses. Notably, the ¹H NMR spectrum of **5-1** in C₆D₆ revealed a characteristic triplet resonance at –2.49 ppm (²J_{PH} = 18.5 Hz) for the palladium hydride. This chemical shift for the hydride ligand is typical for a late transition metal hydride such as those of palladium.⁹ Disappointingly, a related synthesis and characterisation of **5-1** has very recently been reported during the preparation of this thesis (Jan. 2014).¹⁰

5.2.1 Reactivity of the palladium hydride complex [PdH(κ^3 -P,C,P-4-1)] (**5-1**)

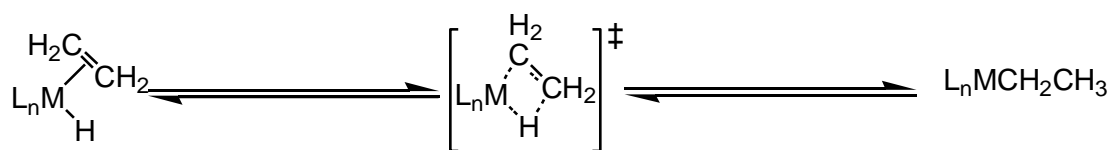
To help gauge the reactivity of the palladium hydride bond of complex **5-1** the insertion of C=C (ethylene) and C=O (acetone and CO₂) bonds were attempted. The insertion of C=C and C=O bonds into a palladium hydride bond both represent key steps in many

²Electronic impact of 1,3-((^tBu₂PO)₂C₆H₄) (**4-1**) and 1,3-((^tBu₂PCH₂)₂C₆H₄) is assessed in Section 4.3.3.3.

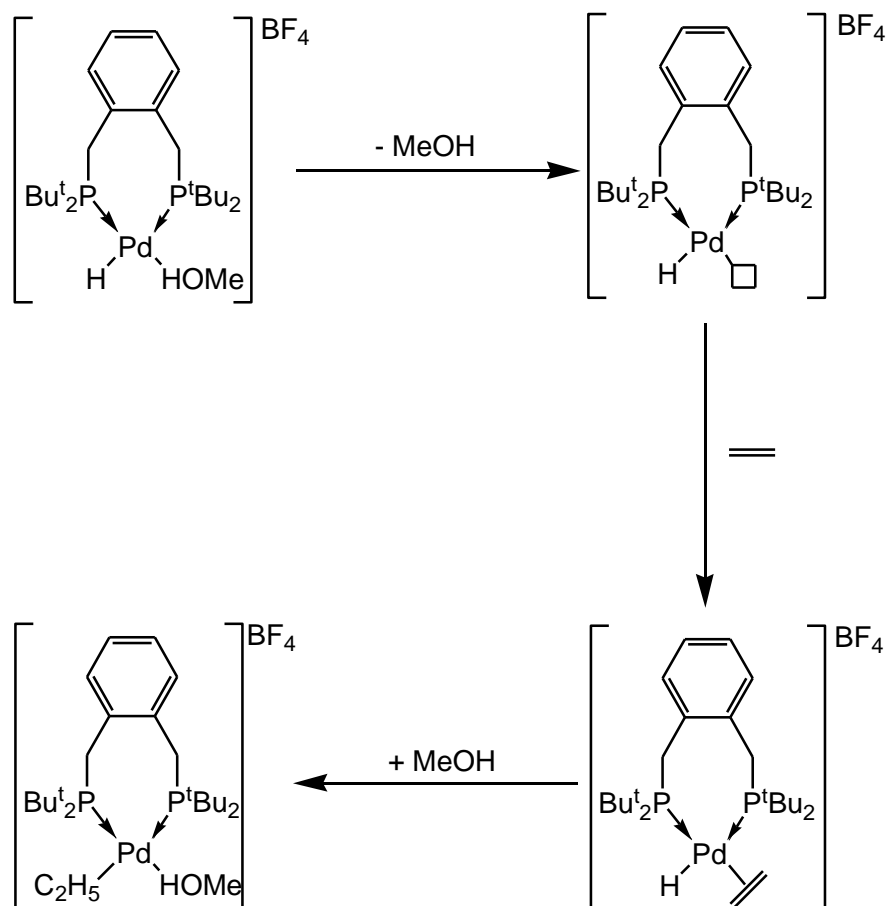
catalytic cycles.^{1, 11, 12} The ability of complex **5-1** to catalyse alkene isomerisation and the hydrosilylation of an aldehyde will be assessed later.

5.2.1.1 Attempted reaction of ethylene with [PdH(κ^3 -P,C,P-4-1)] (**5-1**)

There are examples of discrete palladium hydride complexes that react rapidly with ethylene at room temperature to form ethane complexes. For example, the addition of one equivalent of ethylene to [PdH(L^ΛL)(MeOH)]BF₄ (L^ΛL = 1,2-(CH₂P^tBu₂)₂C₆H₄) resulted in the immediate formation of [PdEt(L^ΛL)(MeOH)]BF₄.¹² The generally accepted mechanism of alkene insertion into a metal hydride bond is that initial coordination of the alkene to the metal centre occurs with a *cis/pseudo-cis* orientation. Subsequently, migratory insertion of the alkene into the metal hydride bond takes place in a concerted fashion *via* a cyclic transition state (Scheme 5.2).¹³ It is assumed that in the case of [PdH(L^ΛL)(MeOH)]BF₄ the labile methanol ligand dissociates from the metal centre to form a free coordination site for ethylene binding (Scheme 5.3).

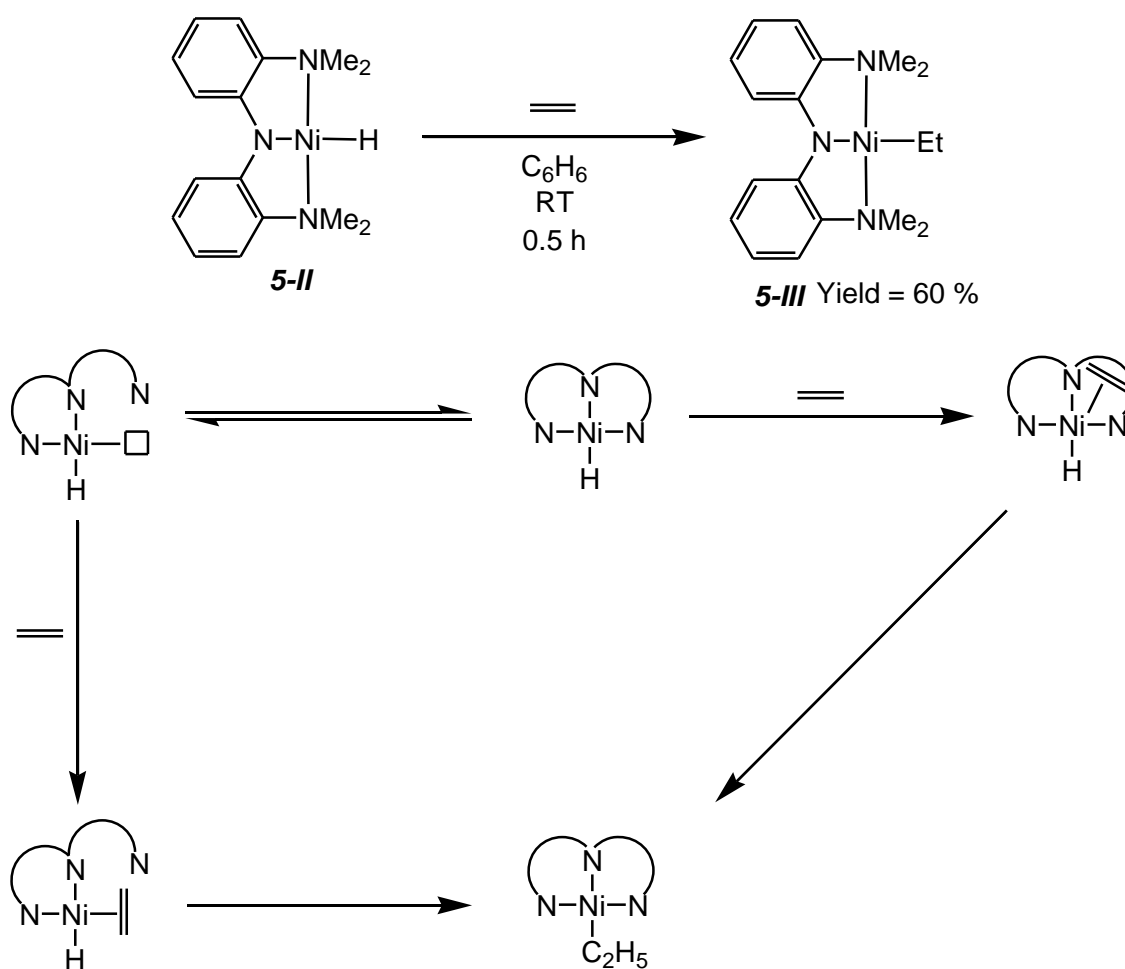


Scheme 5.2: The mechanism of alkene insertion into a metal hydride bond, adapted from Bercaw *et al.*¹³

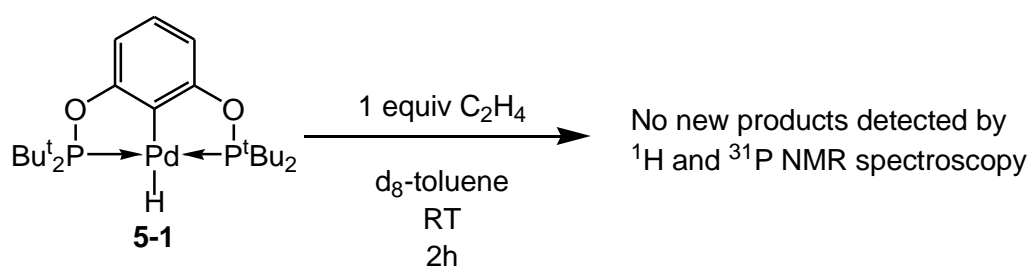


Scheme 5.3: Proposed mechanism of alkene insertion into a palladium hydride bond of $[PdH(L^L)(MeOH)]BF_4$ ($L^L = 1,2-(CH_2P^tBu_2)_2C_6H_4$).¹²

It might be anticipated that the ability to generate a free coordination site on the metal centre could render group 10 metal pincer ligand hydride complexes inert towards ethylene insertion, due to their strong multidentate coordination. However, it has recently been reported by Hu and co-workers that ethylene inserts rapidly into the nickel hydride bond of the d^8 square planar complex **5-II** to form the nickel alkyl complex **5-III** (Scheme 5.4).¹⁴ Whilst a mechanism was not proposed by the authors, it would appear likely that the insertion takes place by one of two mechanisms: Either one of the amine arms dissociates from the metal centre to generate the required free coordination site (Scheme 5.4), or alternatively, the alkene could bind to the metal centre to form a 5-coordinate complex before migratory insertion into the Ni–H bond (Scheme 5.4) occurs. Consequently, it was of interest to assess the reactivity of ethylene with **5-1**.



Scheme 5.4: The insertion of ethylene into the Ni-H bond of **5-II**, developed from Hu et al. and the proposed mechanisms for this insertion process.¹⁴



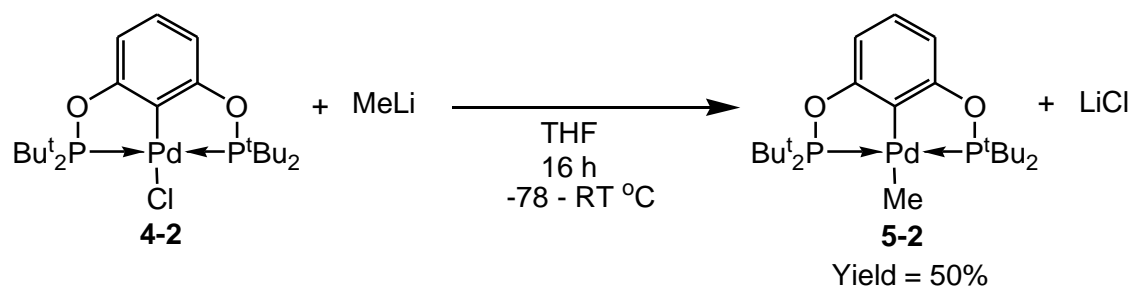
Scheme 5.5: The addition of ethylene to **5-1**.

With the reactivity of this nickel hydride pincer complex in mind, it was of interest to probe the reaction of the related Pd-H complex **5-1**. However, the addition of ethylene to a solution of **5-1** led to no new products being detected by ^1H and $^{31}\text{P}\{^1\text{H}\}$ NMR spectroscopies (Scheme 5.5), with just resonances for **5-1** and ethylene being observed. We propose that the phosphine moieties of **4-1** are too strongly bound to the palladium centre in **5-1** and thus are not able to dissociate from the metal to reveal a free coordination site for the ethylene to bind to. Similarly, a combination of geometric

constraints imposed by the comparatively rigid POCOP metal scaffold together with the electronic preference of the d^8 palladium centre to retain a square planar geometry prevents complex **5-1** from expanding its coordination sphere to accommodate a bound ethylene in a five-coordinate structure.

5.2.1.1.1 Synthesis of $[PdMe(\kappa^3\text{-P,C,P-4-1})]$ (**5-2**)

In Section 5.2.1.1 we observed that ethylene did not insert into the Pd–H bond of **5-1** to form the required palladium alkyl complex. We postulated that the phosphine moieties of **4-1** were too strongly bound to the palladium centre to generate the required free coordination site, coupled with an electronic preference for four-coordinate square planar coordination. However, there exists another possibility for the perceived lack of reaction observed between **5-1** and ethylene. If olefin insertion were to occur this would generate a highly *trans*-influencing ethyl ligand, which would be located *trans* to the strongly *trans*-influencing aryl group of the POCOP ligand, a highly disfavoured configuration. As a result of this unfavourable electronic competition in this *trans* orientation the insertion of ethylene into the Pd–H of **5-1** could be precluded. In order to probe this effect, attempts were made to directly prepare the model palladium methyl complex $[PdMe(\kappa^3\text{-P,C,P-4-1})]$ (**5-2**).



Scheme 5.6: Synthesis of $[PdMe(\kappa^3\text{-P,C,P-4-1})]$ (**5-2**).

Notably, treating the palladium chloride complex **4-2** with one equivalent of MeLi gave rise to the corresponding Pd–Me derivative $[PdMe(\kappa^3\text{-P,C,P-4-1})]$ (**5-2**), which was isolated in moderate yield as a white solid after recrystallisation from Et_2O (Scheme 5.6). The $^{31}\text{P}\{^1\text{H}\}$ NMR spectra of complex **5-2** displays a singlet resonance at 193.1 ppm and the palladium-bound methyl group is clearly evident in the ^1H and $^{13}\text{C}\{^1\text{H}\}$ NMR spectra of **5-2**, exhibiting triplet resonances at -0.02 ppm, $^3J_{\text{PH}} = 5.0$ Hz and -17.8 ppm, $^2J_{\text{PC}} = 10$ Hz, respectively. Furthermore, the methyl complex **5-2** was found

to be thermally stable and resistant to air and moisture in the solid state and in solution for prolonged periods of time (weeks).

5.2.1.1.2 X-Ray crystallographic study of $[\text{PdMe}(\kappa^3\text{-P,C,P-4-1})]$ (**5-2**)

To further confirm the identity of the methyl complex and to probe the comparative *trans* influences of the ligated alkyl and aryl moieties, single crystals of complex **5-2** suitable for X-ray diffraction were grown by slow evaporation of Et_2O . The ensuing molecular structure of **5-2** confirms the expected distorted square-planar geometry about the palladium centre ($\text{P1-Pd-P2} = 158.98(2)^\circ$) (Figure 5.2). As expected, the Pd- CH_3 bond is lengthened due to the high *trans*-influence of C_{sp^2} atom ($2.147(2) \text{ \AA}$), when compared to the Pd- CH_3 distance in *trans*- $[\text{PdCl}(\text{Me})(\text{PPh}_3)_2]$ (Pd- $\text{CH}_3 = 2.058(7) \text{ \AA}$).¹⁵ The presence of the highly *trans*-influencing methyl group leads to significant changes to the molecular structure of the Pd(II) POCOP fragment compared with $[\text{PdCl}(\kappa^3\text{-P,C,P-4-1})]$ (**4-2**), most notably, a significantly lengthened Pd-aryl bond ($2.031(2) \text{ \AA}$) compared to $1.998(2) \text{ \AA}$ in **4-2**. Thus, the positioning of two highly *trans*-influencing groups (methyl and C_{sp^2}) in a *trans* orientation leads to substantial lengthening of the palladium carbon bonds, but it is a stable arrangement. Consequently, from these observations, the preference of the Pd-H complex of **5-1** to not offer a vacant coordination site for ethylene binding is believed to prevent ethylene insertion into the Pd-H bond of **5-1**.

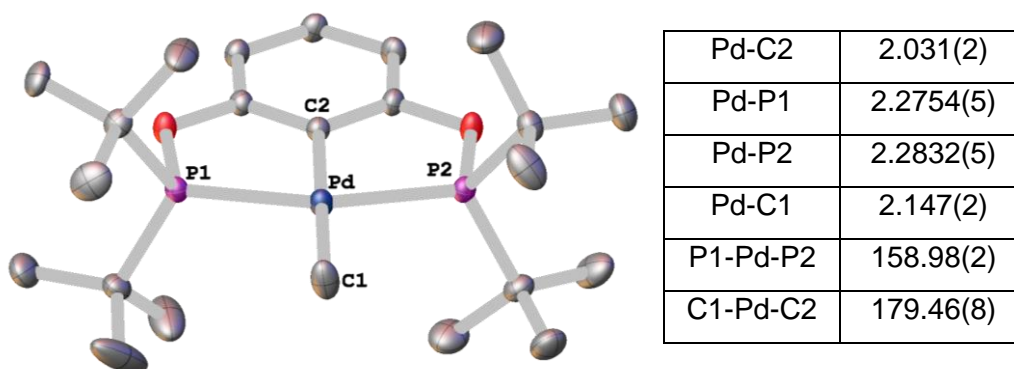
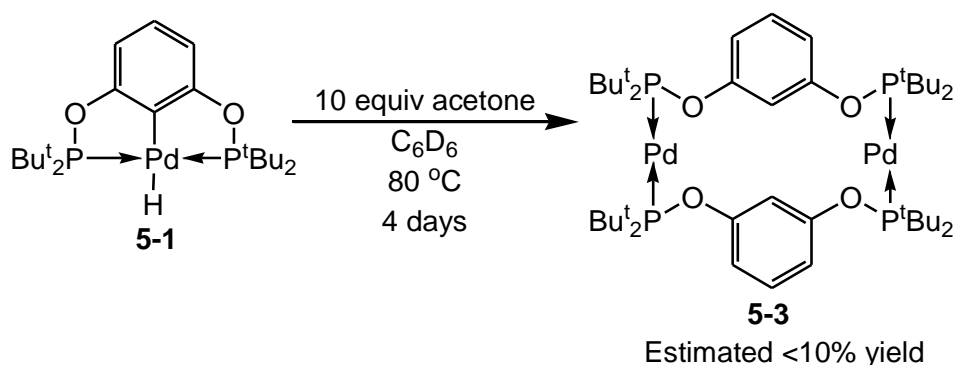


Figure 5.2: Molecular structure of $[\text{PdMe}(\kappa^3\text{-P,C,P-4-1})]$ (**5-2**), with selected bond lengths (\AA) and angles ($^\circ$), (thermal ellipsoids set at 50% level).

5.2.1.2 Attempted reaction of acetone with $[\text{PdH}(\kappa^3\text{-P,C,P-4-1})]$ (**5-1**)

In line with the Dyer group's general interest in the activation of small molecules, it was of interest to test the reactivity of **5-1** with acetone, in order to explore the potential of these systems to mediate synthetically and commercially relevant ketone reduction. To this end, a solution of complex **5-1** was heated with ten equivalents of previously dried acetone at 60 °C for 1 h. This resulted in the formation of no new products (by ^1H and ^{31}P NMR spectroscopy). However, subsequent heating of the reaction mixture at 80 °C for 4 days resulted in the formation of multiple unidentified products in solution as evidenced by $^{31}\text{P}\{^1\text{H}\}$ NMR spectroscopy, accompanied by the formation of a few pale yellow crystals (estimated <10% yield) (Scheme 5.7). A subsequent X-ray diffraction study of the pale yellow crystals was undertaken and showed that this material is an unusual dimeric Pd(0) complex $[\mu\text{-(4-1)Pd}]_2$ (**5-3**).



Scheme 5.7: The reaction of acetone with hydride complex **5-1**.

5.2.1.2.1 X-Ray crystallographic study of $[\mu\text{-(4-1)Pd}]_2$ (**5-3**)

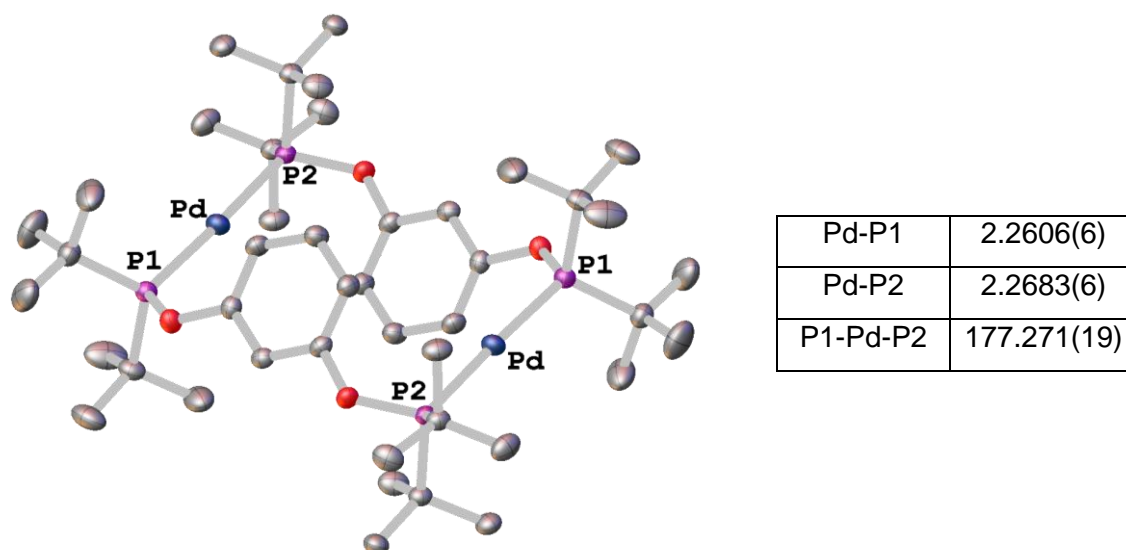


Figure 5.3: Molecular structure of $[\mu\text{-(4-1)Pd}]_2$ (**5-3**), with selected bond lengths (Å) and angles (°). C_6D_6 molecule omitted for clarity, (thermal ellipsoids set at 50% level).

The molecular structure of **5-3** is presented in Figure 5.3, which includes a C_6D_6 molecule (omitted for clarity). The two PdP_2 fragments are nearly linear ($\text{P1-Pd-P2} = 177.27(2)^\circ$) and adopt a near-parallel orientation with a distance of $4.020(3)$ Å between the aromatic rings. The mean Pd-P distance of $2.2645(8)$ Å is shorter than that in **4-2** ($2.2969(7)$ Å), the monomeric palladium(II) chloride complex of the same ligand.

5.2.1.2.2 Proposed mechanism for the formation of $[\mu\text{-(4-1)Pd}]_2$ (**5-3**)

The formation of pincer ligand-bridged palladium dimers comparable to **5-3** is known for other types of pincer ligands, specifically $1,3\text{-}\{(\text{iBu}_2\text{PCH}_2)_2\text{C}_6\text{H}_4\}$ and $1,3\text{-}\{(\text{iPr}_2\text{PCH}_2)_2\text{C}_6\text{H}_4\}$. However, with these two ligands the two resulting PdP_2 fragments are orientated orthogonally (Figure 5.4), as opposed to a parallel arrangement as in complex **5-3**.^{16, 17} Cámpora and co-workers have observed the formation of a dimeric palladium(0) complex **5-V** from a palladium(II) hydride (**5-IV**) in methanol solution, which is similar in structure to complex **5-3** (Scheme 5.8).¹⁶ They propose a mechanism involving proton transfer from the alcohol solvent to the metal to generate a Pd(IV) intermediate, which subsequently undergoes reductive C-H coupling.

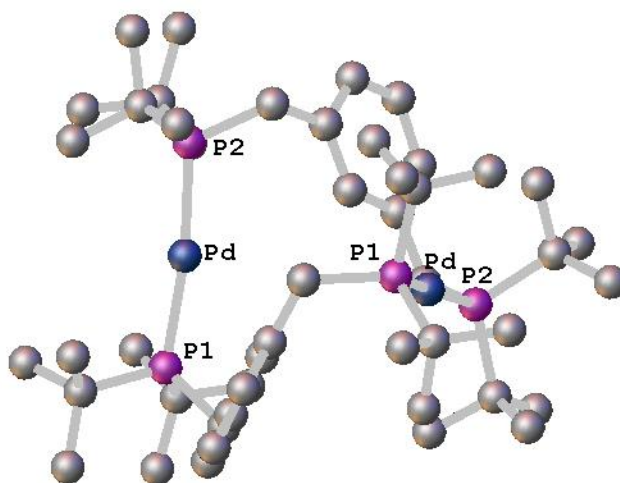
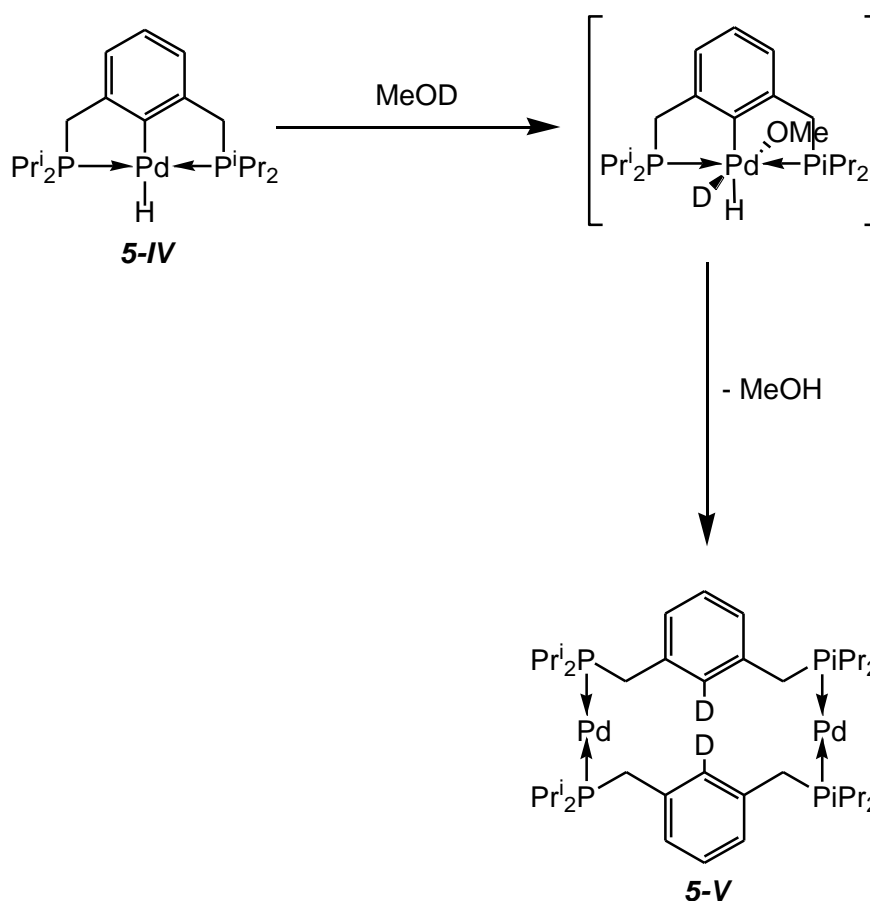


Figure 5.4: Molecular structure of **5-V**, determined by Cámpora et al.¹⁶



Scheme 5.8: Mechanism for formation of dimeric palladium(0) complex **5-V** from a palladium(II) hydride **5-IV** in methanol proposed by Cámpora et al.¹⁶

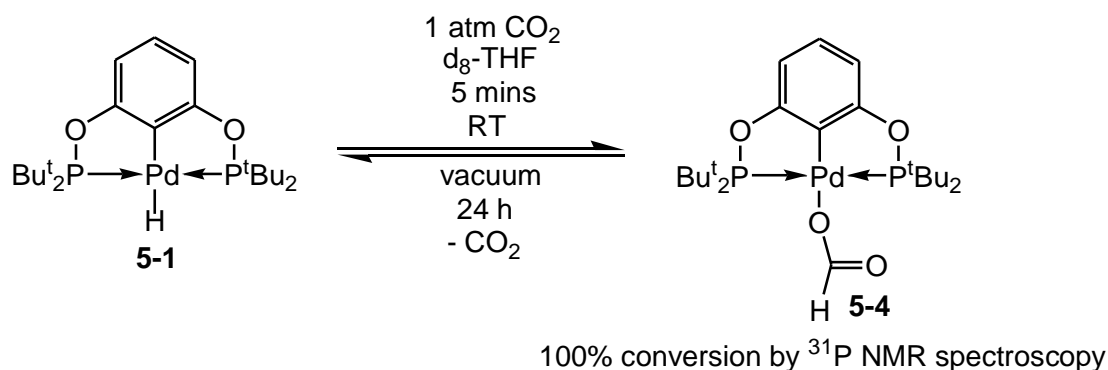
The formation of the dimeric complex **5-3** from **5-1** could involve a mechanism similar to that proposed by Cámpora (protonation to a Pd(IV) intermediate), but the source of protons is less obvious as the solvent used was rigorously-dried C_6D_6 , and hence could

originate from proton abstraction from acetone, thermal breakdown of **5-1** or, despite rigorous drying of both the C₆D₆ and the acetone, adventitious water. In summary complex **5-3** was serendipitously formed in low yield by a suspected acid-catalysed rearrangement of **5-1**.

It would be of interest to develop a larger scale synthesis of **5-3** and explore its reactivity. However, due to time constraints, exploring the reactivity of **5-3** was deemed to be outside the scope of this current project.

5.2.1.3 Reversible insertion of carbon dioxide into palladium hydride bond of [PdH(κ^3 -P,C,P-4-1)] (**5-1**)

The insertion of CO₂ into a metal hydride bond has been proposed as an important step in the transition metal-catalysed reduction of CO₂ to potentially useful products such as formic acid and methanol derivatives.¹⁸⁻²¹ Furthermore, Guan and co-workers have recently disclosed the reduction of CO₂ using a nickel hydride pincer complex in the presence of a borane.²¹ Hence, it was of interest to explore the reactivity of **5-1** with CO₂.



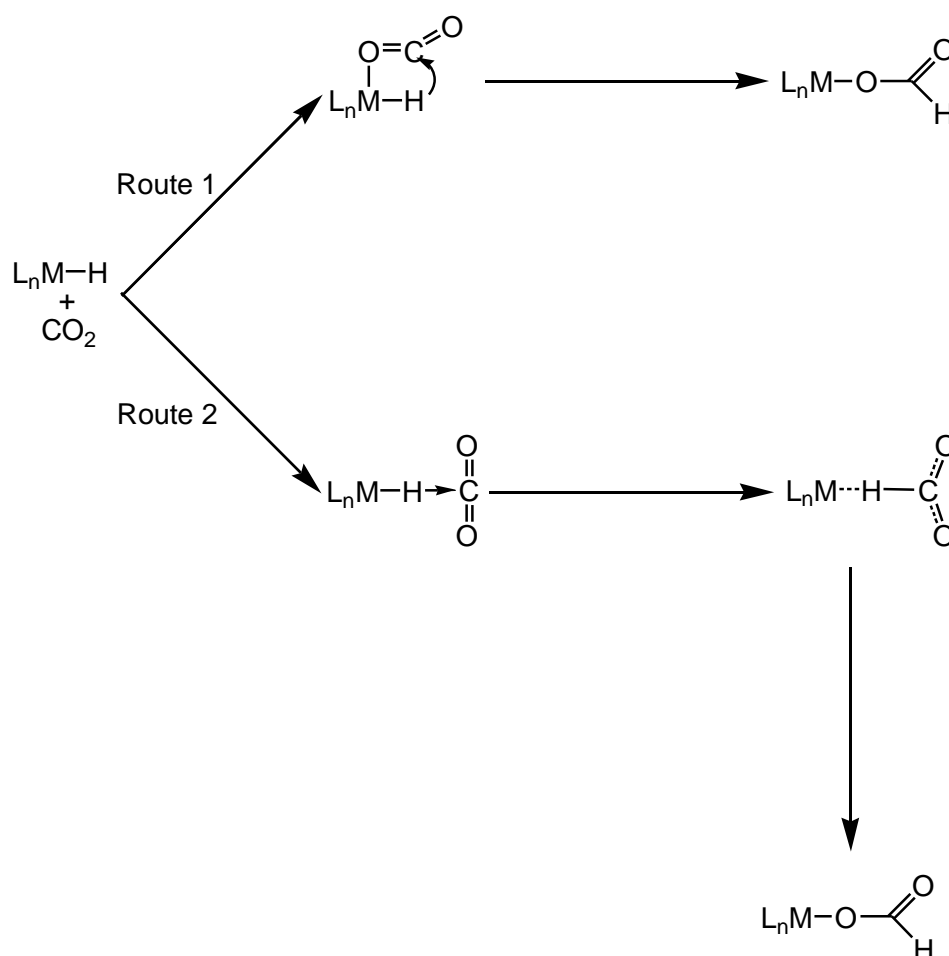
Scheme 5.9: Reversible insertion of CO₂ observed into the palladium hydride bond of [PdH(κ^3 -P,C,P-4-1)] (**5-1**).

Despite the pincer hydride complex **5-1** showing limited reactivity^{aa} towards the C=O bond of acetone and the high thermodynamic stability of CO₂, exposure of a solution of the palladium hydride complex **5-1** to 1 atm CO₂ led to the rapid (<5 mins) and complete consumption of **5-1** (evidenced by ¹H and ³¹P{¹H} NMR spectroscopy) and the generation of the corresponding metal formate complex [Pd(OC(H)O)(κ^3 -P,C,P-4-1)] (**5-4**) (Scheme 5.9). *In situ* analysis of complex **5-4** by ¹H NMR spectroscopy

^{aa} Heating at 80 °C for a prolonged period (4 days) required.

revealed a triplet resonance at 8.22 ppm, which was attributed to the proton of the metal formate group. The insertion of CO₂ into the palladium hydride bond of **5-1** was found to be reversible, with exposure of **5-4** to vacuum (1 x 10⁻² mbar) for 24 h resulting in complete reversion to **5-1**.

There are two proposed mechanisms for the direct insertion of CO₂ into a metal hydride bond. Firstly, by pre-coordination of CO₂ to the metal centre followed by hydride migration to CO₂ (Route 1, Scheme 5.10).²² Secondly, *via* the direct addition of hydride to CO₂ and the subsequent rotation of the formate ligand (Route 2, Scheme 5.10).²²

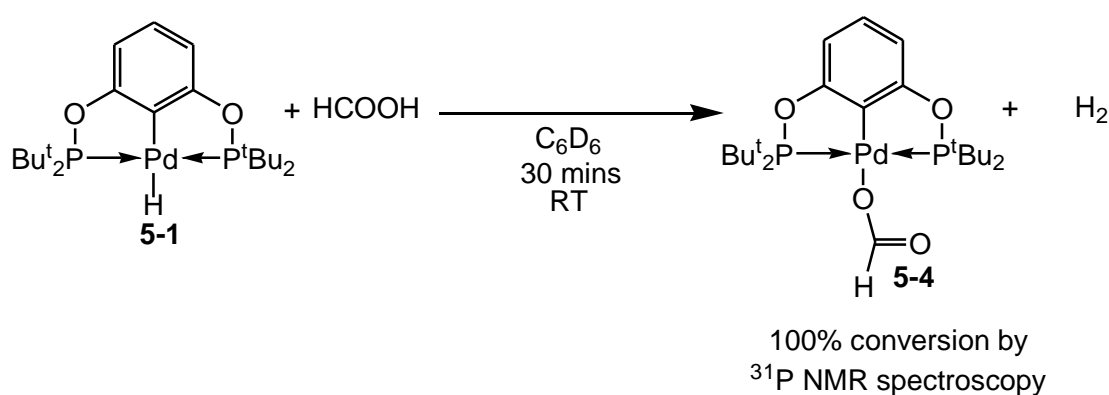


Scheme 5.10: Two proposed mechanisms of CO₂ insertion into a metal hydride bond, adapted from Yoshizawa *et al.*²²

As there is no free coordination site on the palladium hydride complex **5-1**, a mechanism for CO₂ insertion that involves the pre-coordination of CO₂ to the metal is unlikely (Route 1 Scheme 5.10; *cf.* attempted reaction of **5-1** with C₂H₄, Section 5.2.1.1). Therefore, we propose that CO₂ inserts into the Pd-H bond of **5-1** by the direct addition of hydride to CO₂ and the subsequent rotation of the formate ligand, namely via a Route 2 type mechanism (see Scheme 5.10). Here, the two

electronegative oxygen groups of CO₂ make the carbon atom sufficiently electrophilic that it is able to interact with the hydride ligand. In contrast, the carbonyl carbon centre of acetone is both less electrophilic and less sterically accessible, hence acetone is not able to insert by the same mechanism as CO₂ into the Pd–H bond of **5-1** (Route 2, Scheme 5.10). This significant hydridic character of the Pd–H moiety of **5-1** is consistent with the location of the hydride trans to the strongly *trans*-influencing aryl component of the POCOP ligand.

An alternative synthesis of **5-4** from **5-1** was achieved by the addition of formic acid, with complete conversion to **5-4** and H₂ (detected by ¹H NMR spectroscopy) being complete within 30 minutes (Scheme 5.11).



Scheme 5.11: Synthesis of complex **5-4** via reaction of formic acid and **5-1**.

5.2.1.3.1 X-Ray crystallographic study of [Pd(OC(H)O)(κ³-P,C,P-4-1)] (**5-4**)

Crystals of complex **5-4** suitable for X-ray diffraction were grown by slow cooling of a hot toluene solution. The ensuing molecular structure of **5-4** revealed a distorted square-planar geometry about the palladium centre with the O3 group of the palladium bound formate group being significantly distorted away from the plane defined by the atoms P1, P2, Pd and C2, something reflected in the C2–Pd–O3 angle of 169.57(6)°, compared to the equivalent C1–Pd–Cl angle of 179.84(6)° in complex **4-2** (Figure 5.5). The η¹ coordination of the formate moiety is suggested by the long through-space Pd-to-O4 distance of 3.293(2) Å and by the O3–C1–O4 angle, 128.6(2)°; the largest known O–C–O bite angle for an η²-bound transition metal formate group is 126.2(2)°. ²³

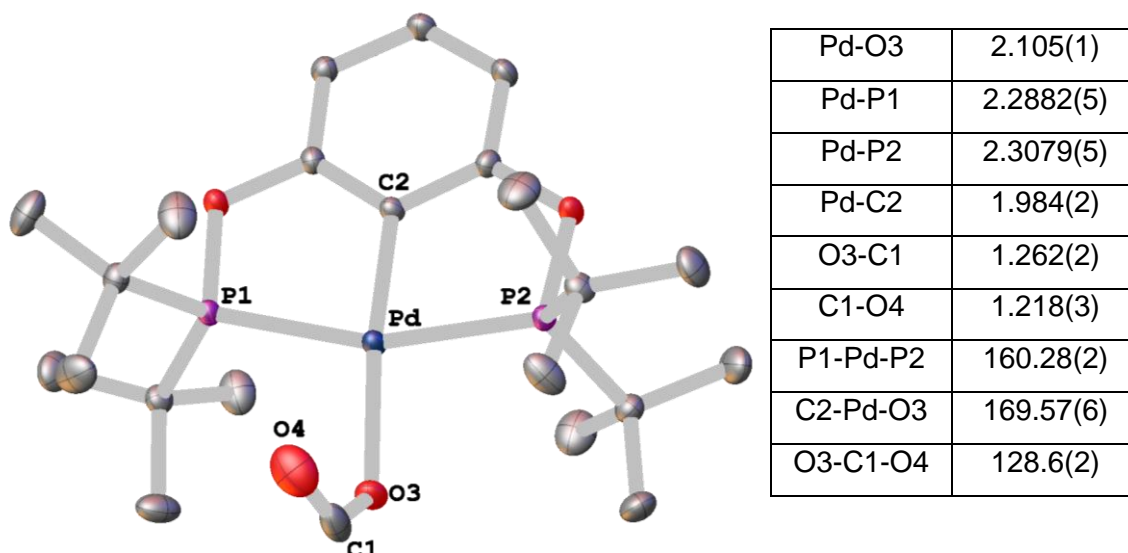
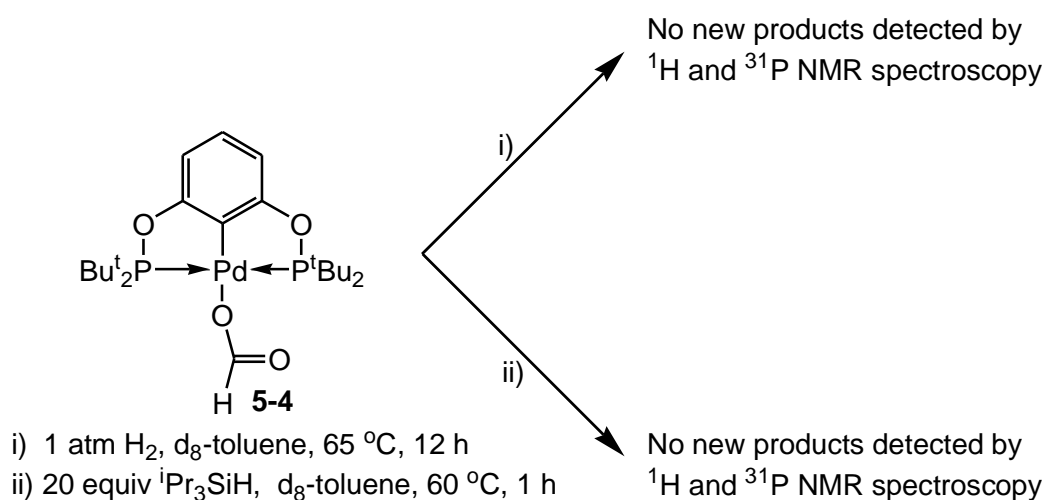


Figure 5.5: Molecular structure of $[Pd(OC(H)O)(\kappa^3\text{-P,C,P-4-1})]$ (**5-4**) with selected bond lengths (Å) and angles ($^\circ$), (thermal ellipsoids set at 50% level).

5.2.1.3.2 Attempted further reactivity of complex 5-4



Scheme 5.12: Attempted further reactivity of the complex $[Pd(OC(H)O)(\kappa^3\text{-P,C,P-4-1})]$ (**5-4**).

The insertion of CO₂ into the Pd-H of **5-1** represents an important first step in the reduction of CO₂. However, the creation of a catalytic cycle for the reduction of CO₂ catalysed by **5-1** requires the ability to regenerate complex **5-1** from **5-4**. Consequently, the reaction of **5-4** with various mild reducing agents was attempted. Hydrogen is the ideal reducing agent for this application due to its relatively low cost and would give a highly atom efficient reaction. However, the exposure of **5-4** to 1 atm H₂ did not result in any reaction (monitoring by ¹H and ³¹P{¹H} NMR spectroscopy), Scheme 5.12.

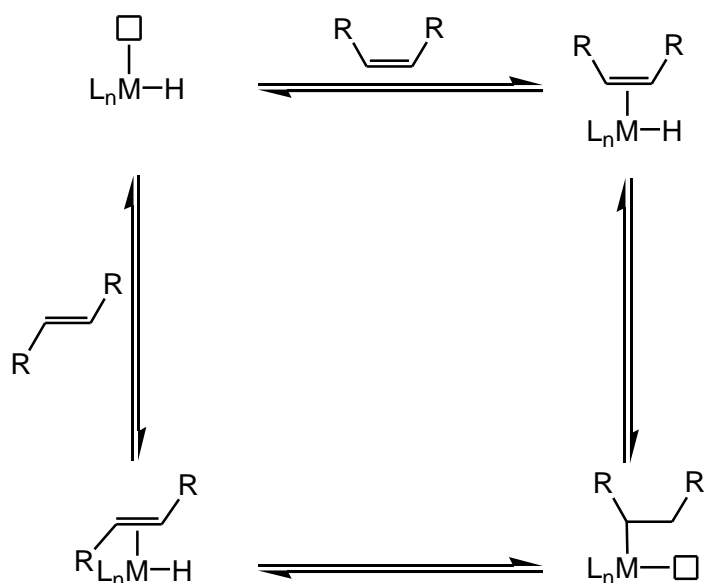
In an alternative strategy, it was reasoned that since silicon has a high affinity for oxygen, then the reaction of **5-4** with a silane reagent could break the Pd-O bond to form a strong Si-O bond and regenerate complex **5-1**. However, despite the high affinity of oxygen for silicon, reactions of complex **5-4** with even an excess of triisopropylsilane also showed no reaction (monitoring by ^1H and $^{31}\text{P}\{^1\text{H}\}$ NMR spectroscopy), Scheme 5.12.

Together, these attempts to regenerate the hydride complex **5-1** from the CO_2 inserted formate derivative **5-4** by comparatively mild chemical means were unsuccessful (addition of H_2 or triisopropylsilane). This suggests that a stronger reducing agent and/or harsher conditions are needed to create a catalytic process for reducing CO_2 with **5-1**. Due to time constraints, subjecting complex **5-4** to stronger reducing agents and/or harsher conditions is outside the scope of this chapter/thesis, where we are looking to probe the reactivity of **5-1**.

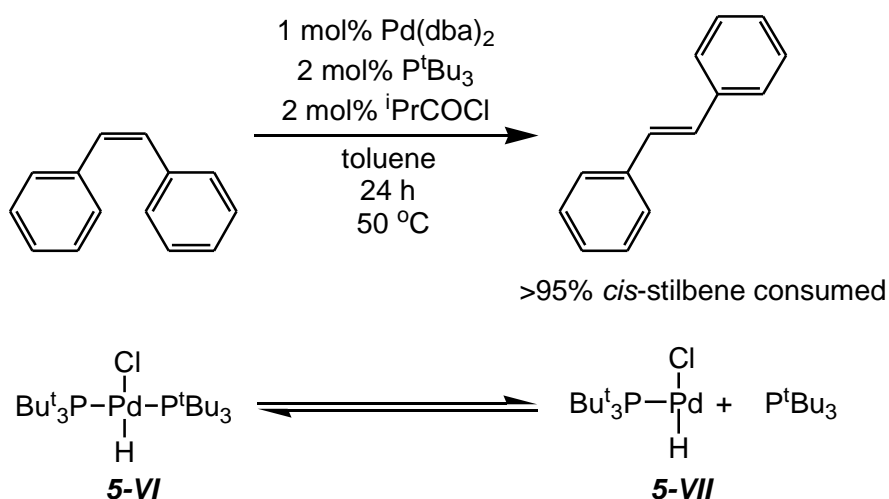
Next to further probe the reactivity of **5-1** the ability of **5-1** to catalyse alkene isomerisation and hydrosilylation has been assessed.

5.2.1.4 Isomerisation of *cis*-stilbene catalysed by **5-1**

Despite the lack of reaction observed between palladium hydride **5-1** and ethylene the ability of **5-1** to catalyse the *cis*-to-*trans* isomerisation of *cis*-stilbene was assessed, since much higher concentrations of this liquid alkene would be achievable in solution (compared with gaseous ethylene, which has only moderate solubility), which could help to facilitate coordination of the alkene and hence, subsequent insertion into the Pd-H bond. This is important since alkene insertion into a Pd-H bond is a key step in alkene *cis*-to-*trans* isomerisation, which is believed to proceed *via* the mechanism shown in Scheme 5.13.

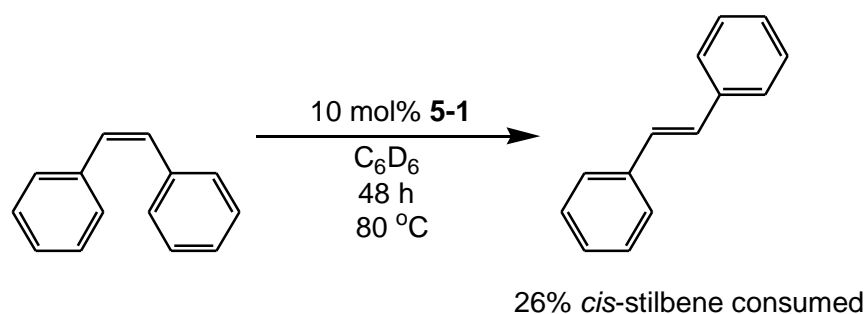


Scheme 5.13: Mechanism of alkene *cis-to-trans* isomerisation catalysed by a metal hydride complex, adapted from Crabtree.²⁴



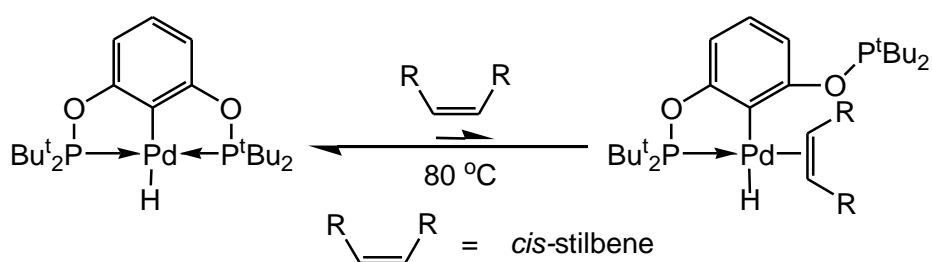
Scheme 5.14: *cis-to-trans* Isomerisation of *cis*-stilbene catalysed by **5-VI** formed *in situ* using the methodology developed by Lindhardt and Skrydstrup and co-workers.¹¹

Bulky palladium hydride complexes have been shown to be efficient catalysts for the isomerisation of alkenes. For example, a generated palladium hydride complex **5-VI** formed *in situ* from a 1:2:2 mixture of Pd(dba)₂, P^tBu₃ and isobutyryl chloride has been shown to catalyse the *cis-to-trans* isomerisation of *cis*-stilbene within 24 h at 50 °C (Scheme 5.14).¹¹ It is reported that the long catalytic lifetime and increased stability of **5-VI** compared to that of other palladium hydride complexes may be explained by the large steric bulk of the two coordinating P^tBu₃ ligands, forcing them to be placed *trans* to each other in the square-planar structure of the Pd(II) complex, thus retarding decomposition *via* reductive elimination of HCl.²⁵



Scheme 5.15: *cis*-to-*trans* Isomerisation of *cis*-stilbene catalysed by **5-1**.

It was proposed that complex **5-1** would be even more stable than **5-VI** as the ligand **4-1** fixes two bulky phosphine moieties in a *trans* geometry, which could lead to longer catalytic lifetimes and may afford enhanced olefin isomerization performance (if the olefin can be forced into the palladium's coordination sphere). Indeed, somewhat surprisingly perhaps, the discrete hydride complex **5-1** does catalyse the *cis*-to-*trans* isomerisation of *cis*-stilbene, albeit at a significantly slower rate than achieved by **5-VI**. For example, heating a deuterated benzene solution of *cis*-stilbene at 80 °C with 10 mol% **5-1** for 48 h resulted in the conversion of just 26% of the *cis*-stilbene to new products (Scheme 5.15), after 7 days the conversion had increased to 68% with 60% of **5-1** remaining intact (according to ^1H NMR spectroscopic analysis^{bb}). For note, a control experiment in the absence of palladium hydride **5-1**, showed no conversion of *cis*-stilbene under the same reaction conditions.



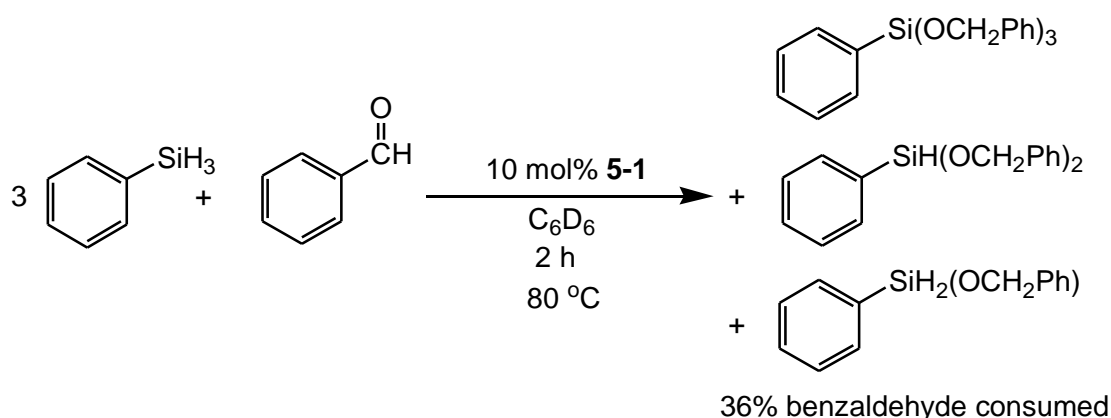
Scheme 5.16: Formation of the proposed active catalyst for *cis*-to-*trans*-isomerisation of *cis*-stilbene

It is believed that the activity of **5-1** is low because there is no easily assessable free site on the metal centre for the coordination of the alkene moiety prior to insertion into the palladium hydride bond, as the donor moieties of **5-1** are not labile. However, as there is a high concentration of *cis*-stilbene with respect to **5-1** and the relatively high temperatures at which the reaction was carried out we propose that there is limited

^{bb} Internal standard (toluene) used.

displacement of a phosphine donor moiety in **5-1** by *cis*-stilbene (Scheme 5.16), resulting in the catalysis observed. Alternatively, as 40% of **5-1** was destroyed after 7 days it is possible that the catalytic activity observed is due to catalysis by decomposition products (e.g. palladium nanoparticles).^{cc} By contrast P^tBu_3 ligands are significantly more labile and the active catalyst which promotes the *cis*-to-*trans*-isomerisations when using **5-VI** has been proposed to be **5-VII**, carrying one phosphine ligand and a free site for the coordination of the alkene moiety prior to isomerization.¹¹

5.2.1.5 Hydrosilylation of benzaldehyde with phenylsilane catalysed by **5-1**



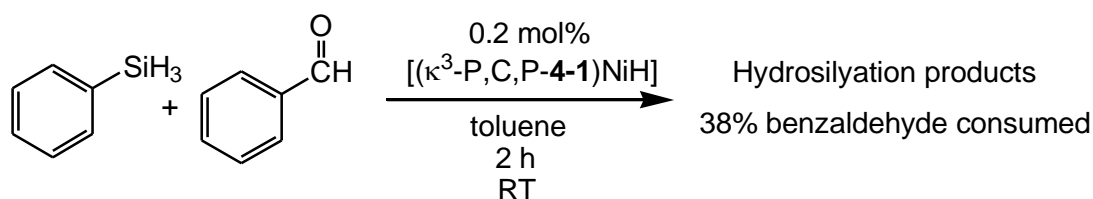
Scheme 5.17: Hydrosilylation of benzaldehyde with phenyl silane catalysed by **5-1**.

The analogous nickel complex of **5-1**, $[NiH(\kappa^3-P,C,P-4-1)]$, has been shown to be an active catalyst for hydrosilylation of aldehydes.²⁶ With this in mind, it was decided to examine complex **5-1** as a hydrosilylation catalyst to investigate the effect of changing the metal centre to palladium.

Complex **5-1** does indeed catalyse the hydrosilylation of benzaldehyde in the presence of phenylsilane, with 36% conversion to the hydrosilation products being achieved after 2 h at 80 °C (10 mol% **5-1** loading), as confirmed by 1H NMR spectroscopy (Scheme 5.17). After 2 h at 80 °C 80% of **5-1** had remained intact (by 1H NMR spectroscopy^{dd}), showing that **5-1** was quite robust.^{cc} In the absence of the palladium hydride pre-catalyst there was no consumption of benzaldehyde observed under the same conditions.

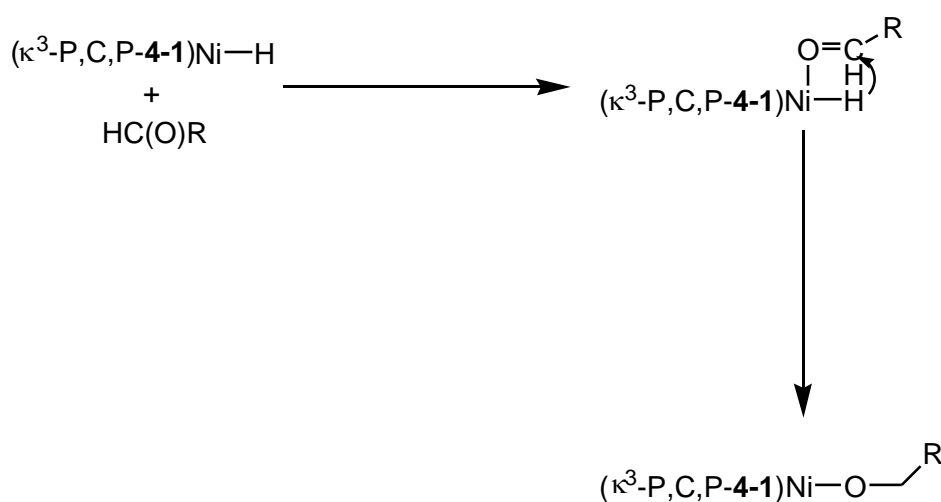
^{cc} Unfortunately no Hg drop test was carried out on this reaction to discount the possibility of catalysis by Pd nanoparticles.

^{dd} Internal standard (toluene) used.



Scheme 5.18: Hydrosilylation of benzaldehyde with phenyl silane catalysed by $[\text{NiH}(\kappa^3\text{-P,C,P-4-1})]$, reported by Guan and co-workers.²⁶

In contrast, the analogous nickel system, $[\text{NiH}(\kappa^3\text{-P,C,P-4-1})]$, is considerably more active, resulting in 38% conversion of benzaldehyde being achieved after just 2 h at room temperature with only 0.2 mol% Ni loading (Scheme 5.18). We propose that the nickel analogue $[\text{NiH}(\kappa^3\text{-P,C,P-4-1})]$ is more active than the palladium system $[\text{PdH}(\kappa^3\text{-P,C,P-4-1})]$ (**5-1**) presented in this work, as the soft phosphine donors of **4-1** are less strongly bound to the comparatively hard nickel centre. A more weakly bound and hence more labile phosphine moiety on nickel will give easier access to a free coordination site on the metal centre aiding carbonyl insertion into the metal hydride bond. Alternatively, the carbonyl insertion into the Ni-H bond of $[\text{NiH}(\kappa^3\text{-P,C,P-4-1})]$ may be aided by the greater ability of Ni(II) to form complexes with a coordination number greater than four compared to palladium(II), allowing the insertion of an aldehyde into a M-H bond by pre-coordination of the carbonyl group (Scheme 5.19).



Scheme 5.19: Proposed mechanism for insertion of an aldehyde into the Ni-H bond of $[\text{NiH}(\kappa^3\text{-P,C,P-4-1})]$ via pre-coordination of the aldehyde.

5.3 Chapter 5 summary and conclusions

The synthesis of a novel stable palladium hydride complex $[\text{PdH}(\kappa^3\text{-P,C,P-4-1})]$ (**5-1**) has been achieved by the treatment of $[\text{PdCl}(\kappa^3\text{-P,C,P-4-1})]$ (**4-2**) with LiAlH_4 .^{ee} The palladium hydride complex **5-1** was found to be inert towards the insertion of ethylene. However, complex **5-1** was shown to be a (poor) catalyst for alkene isomerisation, with high catalyst loading and reaction temperatures giving low activity. Despite showing modest reactivity with C=C bonds complex **5-1** was shown to reversibly insert CO_2 into the palladium hydride bond in a facile manner. Attempts to regenerate **5-1** from the CO_2 inserted product (**5-4**) by the addition of mild reducing agents (to make this process catalytic) were unsuccessful, suggesting that a stronger reducing agent and/or harsher conditions are needed to create a catalytic process for the reduction of CO_2 .

^{ee}As mentioned above, disappointingly, a related synthesis and characterisation of **5-1** has very recently been reported just prior to submission of this thesis (Jan. 2014) by Guan and co-workers, *Inorg. Chem. Front.*, 2014, **1**, 71-82.

5.4 References

1. V. V. Grushin, *Chem. Rev.*, 1996, **96**, 2011-2034.
2. M. C. Denney, N. A. Smythe, K. L. Cetto, R. A. Kemp and K. I. Goldberg, *J. Am. Chem. Soc.*, 2006, **128**, 2508-2509.
3. G. R. Eastham, R. P. Tooze, M. Kilner, D. F. Foster and D. J. Cole-Hamilton, *J. Chem. Soc., Dalton Trans.*, 2002, 1613-1617.
4. D. Breyer, T. Braun and A. Penner, *Dalton Trans.*, 2010, **39**, 7513-7520.
5. C. J. Moulton and B. L. Shaw, *J. Chem. Soc., Dalton Trans.*, 1976, 1020-1024.
6. L. M. Martínez-Prieto, C. Melero, D. del Río, P. Palma, J. Cámpora and E. Álvarez, *Organometallics*, 2012, **31**, 1425-1438.
7. H. Rimml and L. M. Venanzi, *J. Organomet. Chem.*, 1984, **260**, C52-C54.
8. J. P. Collman, L. S. Hegedus, J. R. Norton and R. G. Finke, *Principles and Applications of Organotransition metal Chemistry*, University Science Books, Mill Valley, CA, 1987.
9. B. T. Heaton, S. P. A. Hebert, J. A. Iggo, F. Metz and R. Whyman, *J. Chem. Soc., Dalton Trans.*, 1993, 3081-3084.
10. A. Adhikary, J. R. Schwartz, L. M. Meadows, J. A. Krause and H. Guan, *Inorganic Chemistry Frontiers*, 2014, **1**, 71-82.
11. D. Gauthier, A. T. Lindhardt, E. P. K. Olsen, J. Overgaard and T. Skrydstrup, *J. Am. Chem. Soc.*, 2010, **132**, 7998-8009.
12. G. R. Eastham, B. T. Heaton, J. A. Iggo, R. P. Tooze, R. Whyman and S. Zacchini, *Chem. Commun.*, 2000, 609-610.
13. N. M. Doherty and J. E. Bercaw, *J. Am. Chem. Soc.*, 1985, **107**, 2670-2682.
14. J. Breitenfeld, R. Scopelliti and X. Hu, *Organometallics*, 2012, **31**, 2128-2136.
15. A. Bacchi, M. Carcelli, C. Pelizzi, G. Pelizzi, P. Pelagatti and S. Ugolotti, *Eur. J. Inorg. Chem.*, 2002, **2002**, 2179-2187.
16. C. Melero, L. M. Martinez-Prieto, P. Palma, D. del Rio, E. Alvarez and J. Campora, *Chem. Commun.*, 2010, **46**, 8851-8853.
17. G. R. Fulmer, A. N. Herndon, W. Kaminsky, R. A. Kemp and K. I. Goldberg, *J. Am. Chem. Soc.*, 2011, **133**, 17713-17726.
18. P. G. Jessop, F. Joo and C. C. Tai, *Coord. Chem. Rev.*, 2004, **248**, 2425-2442.
19. Y.-N. Li, R. Ma, L.-N. He and Z.-F. Diao, *Catal. Sci. Technol.*, 2014, Advance Article, DOI: 10.1039/C1033CY00564J
20. M. S. Jeletic, M. T. Mock, A. M. Appel and J. C. Linehan, *J. Am. Chem. Soc.*, 2013, **135**, 11533-11536.
21. S. Chakraborty, J. Zhang, J. A. Krause and H. Guan, *J. Am. Chem. Soc.*, 2010, **132**, 8872-8873.

22. J. Li and K. Yoshizawa, *Bull. Chem. Soc. Jpn.*, 2011, **84**, 1039-1048.
23. B. Chen, *Acta Crystallogr. Sect. E: Struct. Rep. Online*, 2011, **67**, m996.
24. R. Crabtree, *The Organometallic Chemistry of the transition metals*, John Wiley, New York, 1988.
25. I. D. Hills and G. C. Fu, *J. Am. Chem. Soc.*, 2004, **126**, 13178-13179.
26. S. Chakraborty, J. A. Krause and H. Guan, *Organometallics*, 2009, **28**, 582-586.

6 Chapter 6: Summary and outlook

Chapter 2 introduced a new structural motif in the comparatively rare phosphine-alkene-type heteroditopic ligand class, compound **2-1**, based around a 7-aza-benzobicyclo[2.2.1]hept-2-ene moiety. The structure of the alkene-containing moiety is key to its coordination chemistry as the alkene group is located in a constrained, rigid 5-membered ring, which was introduced in order to encourage strong alkene-metal binding in order to relieve ring strain.

Based upon interpretation of infrared stretching frequencies of rhodium $[\text{Rh}(\text{CO})(\kappa^2\text{-P,C-2-1})_2]\text{Cl}$ (**2-3**) and chromium carbonyl $[\text{Cr}(\text{CO})_4(\kappa^2\text{-P,C-2-1})]$ (**2-4**) complexes of ligand **2-1**, this particular *aza*-phosphine-alkene can be considered significantly more electron-withdrawing than commonly used bidentate diphosphines such as dppe. The electron deficient nature of **2-1** is believed to stem from the presence of both the π -accepting alkene moiety and the poorly basic phosphine donor.

It was hoped that the electron-deficient ligand **2-1** would give significant benefits to palladium-catalysed cross-coupling reactions where slow reductive elimination was a problem. Such an effect had been shown previously for P-alkene ligands containing electron-deficient alkene groups, in the work of Lei *et al* (Section 3.1.2).

Chapter 3 showed that disappointingly ligand **2-1** gave poor performance when applied to catalytic systems (Suzuki and Negishi palladium-catalysed cross-coupling reactions). It is believed that the electron-deficient ligand **2-1** stabilises Pd^0 species to such an extent that the Pd^0 complexes generated during the catalytic cycles associated with these transformations do not readily undergo oxidative addition.

However, significant mechanistic understanding of reductive elimination-type processes was gained by applying **2-1** to simpler model systems. The addition of one equivalent of the phosphine-alkene ligand **2-1** to $[\text{PdMe}_2(\text{tmeda})]$ resulted in the formation of *cis*- $[\text{PdMe}_2(\kappa^2\text{-P,C-2-1})]$ (**3-1**). Subsequent reductive elimination of ethane from complex **3-1** is much faster than from the analogous dppe complex *cis*- $[\text{PdMe}_2(\text{dppe})]$ by virtue of the palladium centre being significantly less electron rich in the former.

Importantly, the addition of small amounts of either PPh_3 or propene significantly speed up the reductive elimination of ethane from **3-1**, *via* formation of a 5-coordinate intermediate. In a similar fashion, when two equivalents of P-alkene ligand **2-1** per $[\text{PdMe}_2(\text{tmeda})]$ are used the reductive elimination of ethane is again fast, something that is believed to proceed *via* a 5-coordinate intermediate $[\text{PdMe}_2(\kappa^2\text{-P,C-2-1})(\kappa^1\text{-P-2-1})]$ (**C**). This is the first evidence that an associative mechanism for reductive

elimination from palladium is plausible and thus must be considered alongside both the commonly discussed direct and dissociative mechanisms.

Given the proven ability of phosphine-alkene compound **2-1** promote reductive elimination it was of interest to apply **2-1** to known difficult reductive elimination, e.g. chloromethane from PdCl(Me) fragments. Whilst the reaction of three equivalents of P-alkene **2-1** with [PdCl(Me)(COD)] led to the very rapid formation of [Pd(κ^2 -P,C-**2-1**)₂] (**3-2**) and the methyl phosphonium chloride salt of **2-1**, (**3-3**)Cl, computational studies suggest that the methyl and chloride ligands were not removed from the metal centre by direct chloromethane reductive elimination. Instead, a pathway involving the S_N2 nucleophilic attack of **2-1** on a palladium-methyl group is proposed, with the palladium-methyl group activated by the strongly electrophilic Pd(κ^2 -P,C-**2-1**) fragment. This is the first example of the removal of methyl and chloride ligand from a palladium(II) species and thus constitutes an important new mechanistic pathway in *pseudo* reductive elimination reactions.

In order to prepare a less electron-deficient phosphine-alkene ligand design the synthesis of the monocyclic P-alkene ligand *N*-PPh₂-3-pyrroline (**3-4**) was undertaken. It was hoped that the more flexible structure of **3-4** compared to **2-1** would weaken the strength of the alkene-metal interaction and, hence, potentially give access to complexes that were more labile than those of compound **2-1**. However, there was no evidence of any interaction of the alkene moiety of **3-4** with a palladium centre. Consequently, an alkene moiety with an intermediate metal affinity between **2-1** and **3-4** is required to be used in the catalytic systems described above, a ligand that potentially fits this criteria is presented in Section 3.7.

In contrast to the behaviour of ligand **2-1**, the reaction of compound **3-4** with [PdCl(Me)(COD)] led to the formation of *trans*-[PdCl(Me)(κ^1 -P-**3-4**)₂] (**3-9**) and did not remove the methyl and chloride ligands from the metal centre, clearly signifying that it is the rigid structure of compound **2-1** that is key to its reactivity.

Chapter 4 presented the formation of 1,3-((Cl₂PO)₂C₆H₄) (**4-3**), which opens an important new synthetic route for the synthesis of POCOP ligands containing phosphite and diaminophosphinite moieties. This new synthetic route is similar to that described by Bedford and Pringle (Section 4.1.2), but is a superior route when the presence of bulky *tert*-butyl groups on aromatic backbone are undesirable, for example in the synthesis of ligands for use in aqueous catalysis.

The reactivity of POCOP-type ligands can be fine-tuned by modifying the steric and electronic properties of the donor groups, which is of fundamental interest in catalyst design, in the quest to form catalysts that are more active and/or selective. However, to date, there has been comparatively little modification of the phosphorus donor groups

in known POCOP-containing catalysts (Section 4.1.3), with aryl and alkyl phosphorus substituents being prevalent.

Chapter 4 presents four novel POCOP ligands with significant variation in their steric and electronic properties over commonly used POCOP ligands by using heteroatom atom-substituted phosphorus atoms. The steric and electronic properties of these new POCOP ligands have been quantified by a variety of methods and compared with those of the commonly used ligand 1,3- $\{(\text{tBu}_2\text{PO})_2\text{C}_6\text{H}_4\}$ (**4-1**) demonstrating that all four novel POCOP ligands are both less electron rich and have less steric bulk, with a good correlation between the two parameters.

It would be logical to apply these novel POCOP ligands to catalytic reactions that are known to be catalysed by POCOP complexes, e.g. nickel-catalysed hydroamination or iridium-catalysed alkene transfer dehydrogenation; to study the impact of the steric and electronic properties of the ligand on the reactivity of the catalyst. Unfortunately, time constraints precluded this investigation.

Chapter 5 detailed the synthesis of a novel stable palladium hydride complex $[\text{PdH}(\kappa^3\text{-P,C,P-4-1})]$ (**5-1**). The palladium hydride complex **5-1** was found to be a poor catalyst for both alkene isomerisation and hydrosilylation of aldehydes. However, complex **5-1** was shown to reversibly insert CO_2 into the palladium hydride bond in a facile manner, a reaction that is an important first step in the reduction of the potentially economically and environmentally important C_1 feedstock CO_2 . Initial attempts to regenerate **5-1** from the CO_2 inserted product $[\text{Pd}(\text{OC}(\text{H})\text{O})(\kappa^3\text{-P,C,P-4-1})]$ (**5-4**) by the addition of mild reducing agents were unsuccessful, suggesting that a stronger reducing agent and/or harsher conditions are needed to create a catalytic process for the reduction of CO_2 .

7 Chapter 7: Experimental

7.1 General considerations

Laboratory coat, safety spectacles and gloves were worn at all times, and all experiments were conducted in an efficient fume-hood, following completion of appropriate COSHH assessments. Solvents were disposed of in the appropriate waste solvent container in line with the departmental health and safety policy; precious metal-containing residues were collected and separated according to metal.

All operations were conducted under an atmosphere of dry nitrogen using standard Schlenk and cannula techniques, or in a nitrogen-filled glove box (Saffron Scientific), under ambient laboratory lighting, unless stated otherwise. All NMR-scale reactions were conducted using NMR tubes fitted with J. Young's tap valves. Bulk solvents were purified using an Innovative Technologies SPS facility and degassed prior to use. 1,2-Dimethoxyethane (DME) was distilled from Na/benzophenone and degassed prior to use. NMR solvents (C_6D_6 , d_2 -DCM d_8 -THF and d_8 -toluene) were dried over CaH_2 , distilled and degassed prior to use. $CDCl_3$ was dried over P_2O_5 , passed through a column of alumina, and degassed prior to use.

Palladium, rhodium and iridium salts were used on loan from Johnson Matthey. C_6D_6 , d_2 -DCM, d_8 -THF and d_8 -toluene were purchased from Goss Scientific. All other reagents were purchased from Sigma Aldrich or Alfa Aesar.

Where appropriate, liquid reagents were dried, distilled, and deoxygenated prior to use, while gases were passed through a drying column ($CaCO_3/P_2O_5$).

Solution-phase NMR spectra were collected on a Varian Mercury 200, a Varian Mercury 400, a Bruker Avance 400, a Varian Inova 500, a Varian VNMRS-600, and a Varian VNMRS-700, at ambient probe temperatures (290 K) unless stated otherwise. Chemical shifts were referenced to residual protio impurities in the deuterated solvent (1H), ^{13}C shift of the solvent (^{13}C), or to external aqueous 85% H_3PO_4 (^{31}P). Solvent proton shifts (ppm): $CDCl_3$, 7.26 (s); C_6D_6 , 7.15 (s); CD_2Cl_2 5.32 (t); $(CD_2)_4O$, 1.73 (s), 3.58 (s); C_7D_8 2.08 (m). Solvent carbon shifts (ppm): $CDCl_3$, 77.4 (t); C_6D_6 , 128.6 (t); CD_2Cl_2 , 54.0 (quin); $(CD_2)_4O$, 25.3 (quin), 67.2 (quin); C_7D_8 20.4 (m). Where necessary 1H NMR and ^{13}C NMR spectra were assigned with the aid of COSY, DEPT 135, HMBC and HSQC experiments. Chemical shifts are reported in ppm and coupling constants in Hz.

Solid-state NMR spectra were collected by Dr D. Apperley or Mr F. Markwell of the EPSRC National Solid-state NMR Research Service (Durham University) on a Varian VNMRS instrument: chemical shifts were referenced to H_3PO_4 (^{31}P).

Mass spectra were recorded by the Durham University Mass Spectrometry Service; ESI: Waters TQD equipped with Acquity UPLC and an electrospray ion source, ASAP: Waters LCT Premier XE mass spectrometer equipped with an ASAP ionisation source, and are reported in (m/z). The isotope distributions for all parent ion peaks were verified *via* comparison with the theoretical isotope pattern.

GC-FID analysis was performed on a PerkinElmer Clarus 400, fitted with a PONA (50 m x 0.020 mm x 50 μ m) column. Oven regime: hold 40 °C for 10 mins, ramp 10 °C per min to 320 °C, hold 320 °C for 20 mins. Carrier gas flow = 1 mL/min H₂ flow. 1 μ L injection with 1:100 split.

Elemental analyses were performed by the Analytical Services Department of the Chemistry Department, Durham University or London Metropolitan University elemental analysis service.

Infrared spectra were collected on a Perkin Elmer 1600 spectrophotometer using KBr discs or a solution cell with KBr windows.

Melting points were obtained in sealed glass tubes under N₂ using a Gallenkamp melting point apparatus and are uncorrected.

Single crystal X-ray analysis was performed by the Durham University X-ray service by Dr A. Batsanov.

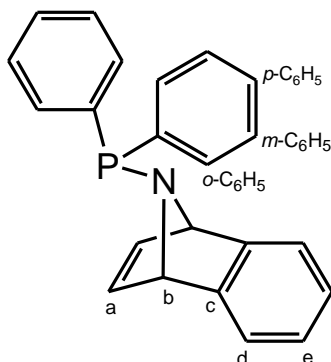
7.2 Chapter 2 experimental

The following compounds were prepared according to literature procedures or slight modifications thereof: $[\text{RhCl}(\text{COD})]_2$,¹ $[\text{RhCl}(\text{CO})_2]_2$,¹ $[\text{IrCl}(\text{COD})]_2$,¹ *N*-BOC-7-aza-benzobicyclo[2.2.1]hept-2-ene,² and 7-aza-benzobicyclo[2.2.1]hept-2-ene.³

General procedure for the synthesis of phosphine selenide compounds

An NMR tube fitted with a J. Young's valve was charged with a small quantity of phosphine (20-50 mg), a slight excess of elemental grey Se and CDCl_3 (0.7 cm³). The system was then heated at 50 °C for 16 h, giving quantitative conversion (according to ³¹P{¹H} NMR spectroscopy) to the required phosphine selenide.

Synthesis of *N*-PPh₂-7-aza-benzobicyclo[2.2.1]hept-2-ene (2-1)



A solution of Ph₂PCl (1.70 cm³, 2.09 g, 9.47 mmol) in CH₂Cl₂ (20 cm³) was added dropwise to a cooled solution (-30 °C) of 7-aza-benzobicyclo[2.2.1]hept-2-ene (1.316 g, 9.19 mmol) and NEt₃ (2.60 cm³, 1.89 g, 18.7 mmol) in CH₂Cl₂ (60 cm³). The reaction was subsequently stirred for 15 mins before being allowed to warm to RT overnight. All volatile components were removed *in vacuo*. Recrystallisation from hot hexane afforded compound **2-1** as an off-white solid (2.085 g, 69%).

¹H NMR (400 MHz, CDCl₃) δ: 4.94 (2H, s, H_b), 6.60-6.62 (2H, m, H_d), 6.77-6.78 (2H, m, H_a), 6.79-6.81 (2H, m, H_e), 7.15-7.21 (10H, m, C₆H₅).

¹³C{¹H} NMR (100 MHz, CDCl₃) δ: 68.1 (d, ²J_{PC} = 10 Hz, C_b), 118.7 (s, C_d), 122.8 (s, C_e), 126.9 (d, J_{PC} = 7 Hz, *o*-/*m*-C₆H₅), 127.3 (s, *p*-C₆H₅), 131.2 (d, J_{PC} = 20 Hz, *o*-/*m*-C₆H₅), 138.2 (d, ¹J_{PC} = 11 Hz, *ipso*-C₆H₅), 143.0 (d, ³J_{PC} = 4 Hz, C_a), 150.0 (d, ³J_{PC} = 3 Hz, C_c).

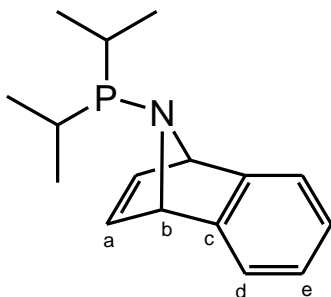
³¹P{¹H} NMR (162 MHz, CDCl₃) δ: 41.6 (s).

CHN: C₂₂H₁₈NP requires: C, 80.72; H, 5.54; N, 4.28%. Found: C, 80.42; H, 5.60; N, 4.33%.

2-1.Se

³¹P{¹H} NMR (162 MHz, CDCl₃) δ: 50.8 (s, + satellites, ¹J_{SeP} = 764 Hz).

Synthesis of *N*-PⁱPr₂-7-aza-benzobicyclo[2.2.1]hept-2-ene (2-2)



A solution of ⁱPr₂PCl (2.70 cm³, 2.59 g, 17.0 mmol) in CH₂Cl₂ (20 cm³) was added dropwise to a cooled solution (−30 °C) of 7-aza-benzobicyclo[2.2.1]hept-2-ene (2.20 g, 15.4 mmol) and NEt₃ (2.40 cm³, 1.74 g, 17.2 mmol) in CH₂Cl₂ (80 cm³). The reaction was subsequently stirred for 15 mins before being allowed to warm to RT overnight. All volatile components were removed *in vacuo* and the resulting residue extracted into hexane (20 cm³). Twice distillation of the resulting oil (bp 120-130 °C at 1.5 x 10⁻¹ mbar) afforded the title compound as a colourless oil. Following cooling (−20 °C) the title compound was isolated as a white solid that did not melt upon warming to RT (1.12 g, 28%).

¹H NMR (600 MHz, C₆D₆) δ: 0.90-0.96 (12H, m, CH(CH₃)), 1.63 (2H, septet, ³J_{HH} = 7.2 Hz, CH(CH₃)), 4.80-4.82 (2H, m, H_b), 6.66-6.69 (2H, m, H_a), 6.71-6.73 (2H, m, H_e), 6.92-6.95 (2H, m, H_d).

¹³C{¹H} NMR (151 MHz, C₆D₆) δ: 19.0-19.4 (m, CH(CH₃)), 26.1 (d, ¹J_{PH} = 15 Hz, CH(CH₃)), 69.2-69.44 (m, C_b), 119.5-119.6 (m, C_d), 123.8-123.9 (m, C_e), 145.1-145.2 (m, C_a), 153.0-153.1 (m, C_c).

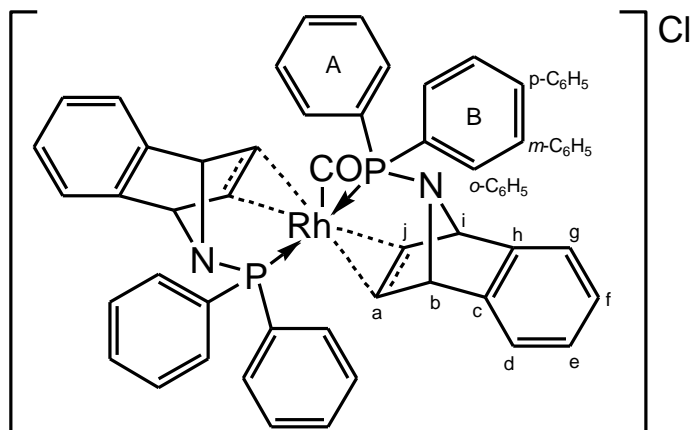
³¹P{¹H} NMR (243 MHz, C₆D₆) δ: 62.7 (s).

CHN: C₁₆H₂₂NP requires: C, 74.10; H, 8.55; N, 5.40%. Found: C, 73.97; H, 8.44; N, 5.49%.

2-2.Se

³¹P{¹H} NMR (81 MHz, CDCl₃) δ: 82.6 (s, + satellites, ¹J_{SeP} = 734 HZ).

Synthesis of $[\text{Rh}(\text{CO})(\kappa^2\text{-P,C-2-1})_2]\text{Cl}$ (**2-3**)



An NMR tube fitted with a J. Young's valve was charged with **2-1** (110 mg, 3.4 mmol), $[\text{RhCl}(\text{CO})_2]_2$ (33 mg, 0.084 mmol) and sealed. CDCl_3 (0.70 cm^3) was added and effervescence observed. Compound **2-3** was obtained quantitatively (according to $^{31}\text{P}\{^1\text{H}\}$ NMR spectroscopy) as a single product.

Complex **2-3** is also obtained when the reaction is undertaken using a Rh:**2-1** ratio of 1:1.

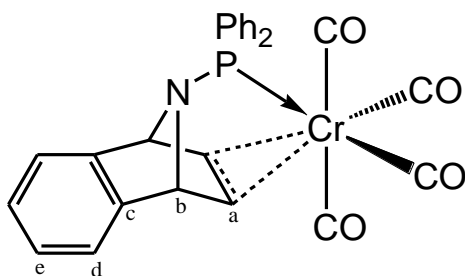
^1H NMR (500 MHz, CDCl_3) δ : 3.98 (2H, bs, $\text{CH}_{a/j}$), 4.98 (2H, s, $\text{CH}_{b/i}$), 5.04 (2H, 2s, $\text{CH}_{b/i}$), 5.51 (2H, bs, $\text{CH}_{a/j}$), 7.01-7.10 (4H, m, $\text{CH}_{e/f}$), 7.15-7.31 (8H, m, $\text{CH}_{d/g}$, $p\text{-C}_6\text{H}_5$ & $o/m\text{-C}_6\text{H}_5$), 7.32-7.47 (12H, m, $\text{CH}_{d/g}$, $p\text{-C}_6\text{H}_5$ & $o/m\text{-C}_6\text{H}_5$), 7.77-7.97 (4H, m, $o/m\text{-C}_6\text{H}_5$).

$^{13}\text{C}\{^1\text{H}\}$ NMR (126 MHz, CDCl_3) δ : 70.6-70.7 (m, $\text{C}_{b/i}$), 71.4-71.5 (m, $\text{C}_{b/i}$), 79.3 (d, $^1J_{\text{RhC}} = 9.0$, $\text{C}_{a/j}$), 82.9 (d, $^1J_{\text{RhC}} = 10.0$ Hz, $\text{C}_{a/j}$), 121.9 (s, $\text{C}_{d/g}$), 122.0 (s, $\text{C}_{d/g}$), 126.9-127.0 (m, $\text{C}_{e/f}$), 128.3-128.9 (m, *ipso*- C_6H_5), 129.3-129.9 (m, $o/m\text{-C}_6\text{H}_5$), 130.2-130.6 (m, *ipso*- C_6H_5), 131.0-131.2 (m, $o/m\text{-C}_6\text{H}_5$), 132.0-132.5 (m, $p\text{-C}_6\text{H}_5$), 142.6-142.7 (m, $\text{C}_{c/h}$), 194.3 (dt, $^1J_{\text{RhC}} = 58.0$, $^2J_{\text{PC}} = 11.0$ Hz, CO).

$^{31}\text{P}\{^1\text{H}\}$ NMR (162 MHz, CDCl_3) δ : 91.4 (d, $^1J_{\text{RhP}} = 89$ Hz).

IR (KBr, CDCl_3 solution) ν (cm^{-1}): 1993, C=O.

Synthesis of $[\text{Cr}(\text{CO})_4(\kappa^2\text{-P,C-2-1})]$ (**2-4**)



A toluene (40 cm³) solution of $[\text{Cr}(\text{CO})_6]$ (350 mg, 1.59 mmol) and **2-1** (393 mg, 1.20 mmol) was heated at reflux for 24 h. The resulting yellow solution was cooled (0 °C) and filtered to remove excess $[\text{Cr}(\text{CO})_6]$. All volatile components were removed *in vacuo* to leave a yellow solid. The title compound was precipitated out of DCM (4 cm³) by the addition of methanol (15 cm³), subsequent isolation by filtration and drying *in vacuo* afforded analytically pure **2-4** (260 mg, 44%).

Crystals suitable for X-ray diffraction were grown by layering a concentrated DCM solution of **2-4** with methanol.

¹H NMR (700 MHz, CDCl₃) δ: 4.33 (2H, bs, H_a), 4.40 (2H, bs, H_b), 7.06 (2H, bs, H_e), 7.24 (2H, bs, H_d), 7.33-7.41 (6H, m, *m*-C₆H₅ and *p*-C₆H₅), 7.77 (4H, bs, *m*-C₆H₅).

¹³C{¹H} NMR (176 MHz, CDCl₃) δ: 70.6 (d, ²J_{CP} = 10 Hz, C_b), 83.2 (s, C_a), 121.6 (s, C_d), 126.5 (s, C_e), 129.0 (d, ³J_{CP} = 10 Hz, *m*-C₆H₅), 130.7 (d, ²J_{CP} = 13 Hz, *o*-C₆H₅), 131.1 (s, *p*-C₆H₅), 135.2 (d, ¹J_{CP} = 39 Hz, C_{ipso}), 145.6 (d, ³J_{CP} = 11 Hz, C_c), 222.6 (d, ²J_{CP} = 4 Hz, CO), 225.5 (d, ²J_{CP} = 14 Hz, CO), 234.1 (d, ²J_{CP} = 11 Hz, CO).

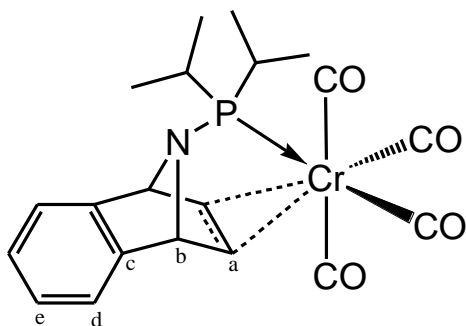
³¹P{¹H} NMR (283 MHz, CDCl₃) δ: 131.7 (s).

CHN: C₂₆H₁₈CrNO₄P requires: C, 63.55; H, 3.69; N, 2.85 %. Found: C, 63.64; H, 3.80; N, 2.91%.

MS (ASAP+): 491.0 (M)⁺, 463.0 (M – CO)⁺, 435.0 (M – 2CO)⁺, 407.1 (M – 3CO)⁺, 379.1 (M – 4CO)⁺, 327.1 (**2-1**)⁺.

IR (Nujol mull) ν (cm⁻¹): 1884, 1915, 1952, 2017, C=O.

Synthesis of $[\text{Cr}(\text{CO})_4(\kappa^2\text{-P,C-2-2})]$ (2-5)



A toluene (20 cm³) solution of $[\text{Cr}(\text{CO})_6]$ (283 mg, 1.29 mmol) and **2-2** (250 mg, 0.96 mmol) was heated at reflux for 24 h. The resulting yellow solution was cooled (0 °C) and filtered to remove excess $[\text{Cr}(\text{CO})_6]$. All volatile components were removed *in vacuo* to leave a yellow solid. The title compound was recrystallized from methanol to give a pale yellow solid (168 mg, 42%).

¹H NMR (700 MHz, CDCl₃) δ: 1.21-1.32 (12H, m, CH(CH₃)₂), 2.10-2.18 (2H, m, CH(CH₃)₂), 4.23-4.27 (2H, m, H_a), 4.41-4.45 (2H, m, H_b), 7.02-7.12 (2H, m, H_e), 7.22-7.27 (2H, m, H_d).

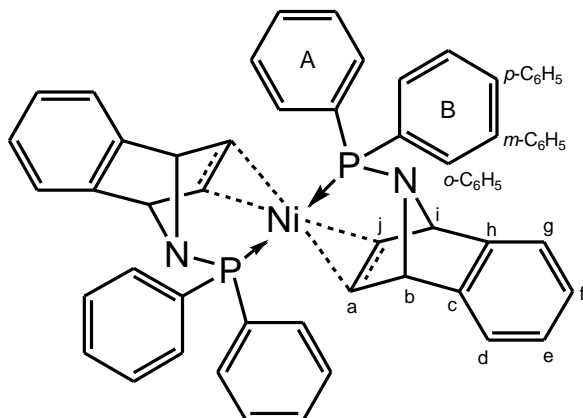
¹³C{¹H} NMR (176 MHz, CDCl₃) δ: 17.9 (d, ²J_{PC} = 5 Hz, CH(CH₃)₂), 18.6 (d, ²J_{PC} = 2 Hz, CH(CH₃)₂), 29.6 (d, ¹J_{PH} = 18 Hz, CH(CH₃)₂), 70.6 (d, ²J_{PC} = 7 Hz, C_b), 82.3-82.5 (bs, C_a), 121.3 (m, C_d), 126.4 (m, C_e), 145.5 (d, ³J_{PC} = 9 Hz, C_c), 222.8 (d, ²J_{PC} = 4 Hz, CO), 227.3 (d, ²J_{PC} = 13 Hz, CO), 234.2 (d, ²J_{PC} = 11 Hz, CO).

³¹P{¹H} NMR (283 MHz, CDCl₃) δ: 150.5 (s).

CHN: C₂₀H₂₂CrNO₄P requires: C, 56.74; H, 5.24; N, 3.31 %. Found: C, 56.62; H, 5.35; N, 3.35%.

IR (Nujol mull) ν (cm⁻¹): 1911 (br), 1921, 2015, C=O.

Synthesis of $[\text{Ni}(\kappa^2\text{-P,C-2-1})_2]$ (**2-6**)



A solution of $[\text{Ni}(\text{COD})_2]$ (294 mg, 1.07 mmol), **2-1** (700 mg, 2.13 mmol) and DCM (10 cm^3) was stirred at RT for 16 h. All volatile components were removed *in vacuo*, the resulting solid was recrystallised by layering a concentrated DCM solution with hexane to give the title complex as a bright yellow solid (465 mg, 61 %).

Crystals suitable for X-ray diffraction were grown by slow diffusion of hexane into a concentrated toluene solution of **2-6**.

^1H NMR (600 MHz, $\text{d}_2\text{-DCM}$) δ : 3.91-3.92 (2H, m, $\text{C}_{a/j}$), 3.95-3.99 (2H, m, $\text{C}_{a/j}$), 4.20 (2H, bs, $\text{C}_{b/i}$), 4.69 (2H, bs, $\text{C}_{b/i}$), 6.96-7.03 (4H, m, $\text{C}_{e/f}$), 7.07-7.09 (2H, d, $^3J_{\text{HH}} = 6.6$ Hz), $\text{C}_{d/g}$), 7.09-7.13 (4H, m, $m\text{-C}_6\text{H}_5$ A), 7.20-7.23 (2H, d, $^3J_{\text{HH}} = 6.8$ Hz, $\text{C}_{d/g}$), 7.26-7.29 (2H, t, $^3J_{\text{HH}}$, $p\text{-C}_6\text{H}_5$ A), 7.36-7.39 (4H, m, $o\text{-C}_6\text{H}_5$ A), 7.41-7.44 (6H, m, $m\text{-C}_6\text{H}_5$ & $p\text{-C}_6\text{H}_5$ B), 7.77-7.81 (4H, m, $o\text{-C}_6\text{H}_5$ B).

$^{13}\text{C}\{^1\text{H}\}$ NMR (151 MHz, $\text{d}_2\text{-DCM}$) δ : 68.8 (s, $\text{C}_{a/j}$), 71.3 (m, $\text{C}_{b/i}$), 72.1 (m, $\text{C}_{a/j}$), 73.6 (m, $\text{C}_{b/i}$), 120.4 (s, $\text{C}_{d/g}$), 120.5 (s, $\text{C}_{d/g}$), 125.5 (s, $\text{C}_{e/f}$), 125.6 (s, $\text{C}_{e/f}$), 128.8 (m, $m\text{-C}_6\text{H}_5$), 128.9 (m, $m\text{-C}_6\text{H}_5$), 129.8 (s, $p\text{-C}_6\text{H}_5$), 130.5 (s, $p\text{-C}_6\text{H}_5$), 132.2 (m, $o\text{-C}_6\text{H}_5$), 133.4 (m, $o\text{-C}_6\text{H}_5$), 136.0 (m, *ipso*- C_6H_5), 137.2 (m, *ipso*- C_6H_5), 146.7 (m, $\text{C}_{c/h}$), 147.5 (m, $\text{C}_{c/h}$).

$^{31}\text{P}\{^1\text{H}\}$ NMR (243 MHz, $\text{d}_2\text{-DCM}$) δ : 99.6 (s).

CHN: $\text{C}_{44}\text{H}_{36}\text{P}_2\text{N}_2\text{Ni}$ requires: C, 74.08; H, 5.09; N, 3.93%. Found: C, 72.30; H, 5.06; N, 3.70%.^{ff}

MS (ASAP+): 712 (M)⁺.

^{ff} Satisfactory elemental analyses were not obtained due to incomplete combustion.

Thermal stability of 2-6

A solution of **2-6** (10 mg, 0.013 mmol) in C₆D₆ (0.7 cm³) was heated at 80 °C in an NMR tube fitted with a J. Young's valve containing a glass capillary enclosing a PPh₃ standard. No decomposition had occurred after 16 h.

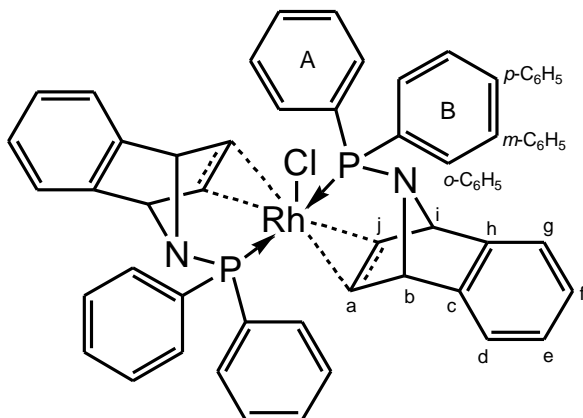
Addition of PPh₃ to 2-6

Complex **2-6** (10 mg, 0.014 mmol), PPh₃ (8 mg, 0.030 mmol) and C₆D₆ (0.7 cm³) were added to an NMR tube fitted with a J. Young's valve and heated at 80 °C for 16 h. Analysis by ¹H and ³¹P{¹H} NMR spectroscopy showed that there was no reaction between **2-6** and PPh₃.

Addition of PhI to 2-6

Complex **2-6** (10 mg, 0.014 mmol), PhI (16 µl, 28 mg, 0.14 mmol) and C₆D₆ (0.7 cm³) were added to an NMR tube fitted with a J. Young's valve and heated at 80 °C for 2 h. Analysis by ¹H and ³¹P{¹H} NMR spectroscopy showed that there was no reaction between **2-6** and PhI.

Synthesis of $[\text{RhCl}(\kappa^2\text{-P,C-2-1})_2]$ (**2-7**)



An NMR tube fitted with a J. Young's valve was charged with **2-1** (100 mg, 0.305 mmol), $[\text{RhCl}(\text{COD})]_2$ (38 mg, 0.076 mmol) and CDCl_3 (0.7 cm³) after standing overnight at RT the title complex was obtained quantitatively (according to $^{31}\text{P}\{^1\text{H}\}$ NMR spectroscopy). Removal of all volatile components *in vacuo* generated the title complex in good yield (103 mg, 94%).

Crystals suitable for X-ray diffraction were grown by layering a concentrated DCM solution of **2-7** with hexane.

Complex **2-7** is also obtained when the reaction is realised with two equivalents of ligand for one equivalent of $[\text{RhCl}(\text{COD})]_2$; the remaining $[\text{RhCl}(\text{COD})]_2$ is observed by ^1H NMR spectroscopy.

^1H NMR (500 MHz, CDCl_3) δ : 3.79 (2H, bs, $\text{CH}_{a/j}$), 4.65 (2H, s, $\text{CH}_{b/i}$), 4.80 (2H, bs, $\text{CH}_{a/j}$), 4.91 (2H, s, $\text{CH}_{b/i}$), 6.97-7.03 (2H, m, $\text{CH}_{e/f}$), 7.04-7.09 (2H, m, $\text{CH}_{e/f}$), 7.12-7.15 (2H, m, $\text{CH}_{d/g}$), 7.15-7.20 (6H, m, *o*-, *p*- C_6H_5 A), 7.22-7.26 (6H, m, *o*-, *p*- C_6H_5 B), 7.26-7.29 (2H, m, $\text{CH}_{d/g}$), 7.41-7.47 (4H, m, *m*- C_6H_5 A), 7.89-7.96 (4H, m, *m*- C_6H_5 B).

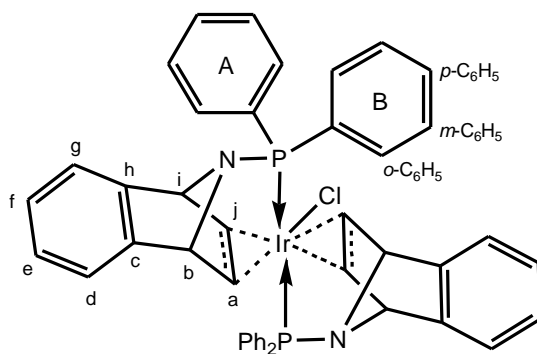
$^{13}\text{C}\{^1\text{H}\}$ NMR (126 MHz, CDCl_3) δ : 70.5 (s, $\text{C}_{b/i}$), 72.1 (s, $\text{C}_{b/i}$), 74.9 (d, $^2J_{\text{PC}} = 8$ Hz, $\text{C}_{a/j}$), 77.4 (d, $^2J_{\text{PC}} = 10$ Hz, $\text{C}_{a/j}$), 120.8 (2s, $\text{C}_{d/g}$), 120.9 (2s, $\text{C}_{d/g}$), 125.9 (2s, $\text{C}_{e/f}$), 126.3 (2s, $\text{C}_{e/f}$), 127.8-128.1 (m, *o*- C_6H_5 B), 128.8-129.0 (m, *o*- C_6H_5 A), 129.7-130.0 (m, *m*- C_6H_5 A), 130.2-130.7 (m, *p*- C_6H_5 A & *ipso*- C_6H_5 & *p*- C_6H_5 B), 132.3-132.7 (m, *m*- C_6H_5 B & *ipso*- C_6H_5), 144.5-144.7 (m, $\text{C}_{c/h}$), 146.5-146.6 (m, $\text{C}_{c/h}$).

$^{31}\text{P}\{^1\text{H}\}$ NMR (81 MHz, CDCl_3) δ : 90.9 (d, $^1J_{\text{PRh}} = 103$ Hz).

CHN: $\text{C}_{44}\text{H}_{36}\text{ClN}_2\text{P}_2\text{Rh}\cdot 2\text{C}_2\text{H}_2\text{Cl}_2$ requires: C, 57.38; H, 4.19; N, 2.91%. Found: C, 57.05; H, 4.28; N, 3.12%.⁹⁹

⁹⁹ DCM visible in molecular structure and ^1H NMR spectrum.

Synthesis of $[\text{IrCl}(\kappa^2\text{-P,C-2-1})_2]$ (**2-8**)



A DCM solution of **2-1** (400 mg, 1.22 mmol) was added drop-wise to a stirred solution of $[\text{IrCl}(\text{COD})]_2$ (202 mg, 0.301); the resulting mixture was stirred for 1 h at RT. All volatile components were removed *in vacuo* to leave an off-white solid. The title complex was precipitated out of DCM (10 cm³) by the addition of hexane (20 cm³), subsequent isolation by filtration and drying *in vacuo* afforded analytically pure **2-8** (351 mg, 66%).

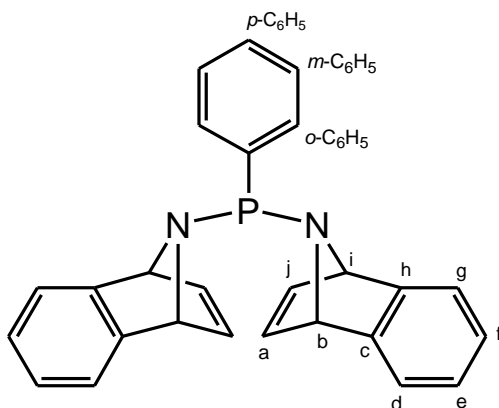
¹H NMR (700 MHz, CDCl₃) δ: 2.98 (2H, m, CH_{a/j}), 3.76 (2H, m, CH_{a/j}), 4.48 (2H, s, CH_{b/i}), 4.80 (2H, s, CH_{b/i}), 7.03-7.06 (2H, m, CH_{e/f}), 7.11-7.14 (2H, m, CH_{e/f}), 7.15-7.17 (2H, m, CH_{d/g}), 7.19-7.23 (6H, m, *o*-, *p*-C₆H₅ A), 7.26-7.29 (6H, m, *o*-, *p*-C₆H₅ B), 7.29-7.31 (2H, m, CH_{d/g}), 7.45-7.49 (4H, m, *m*-C₆H₅ A), 7.87-7.92 (4H, m, *m*-C₆H₅ B).

¹³C{¹H} NMR (176 MHz, CDCl₃) δ: 53.2 (bs, C_{a/j}), 54.6 (bs, C_{a/j}), 69.8 (m, C_{b/i}), 72.0 (m, C_{b/i}), 120.4 (s, C_{d/g}), 120.5 (s, C_{d/g}), 125.9 (s, C_{e/f}), 126.2 (s, C_{e/f}), 127.8-128.1 (m, *o*-C₆H₅ B), 128.7-128.8 (m, *o*-C₆H₅ A), 129.4 (d, ¹J_{PC} = 32 Hz, *ipso*-C₆H₅ A), 129.7-129.8 (m, *m*-C₆H₅ A), 130.4-130.5 (m, *p*-C₆H₅ A), 130.7-130.8 (m, *p*-C₆H₅ B), 131.0 (d, ¹J_{PC} = 28 Hz, *ipso*-C₆H₅ B), 132.1-132.3 (m, *m*-C₆H₅ B), 145.5-145.6 (m, C_{c/h}), 146.5-146.6 (m, C_{c/h}).

³¹P{¹H} NMR (283 MHz, CDCl₃) δ: 61.2 (s).

CHN: C₄₄H₃₆ClN₂P₂Ir requires: C, 59.89; H, 4.11; N, 3.17%. Found: C, 59.73; H, 4.04; N, 3.10%.

Synthesis of *N*-PPh-*bis*-7-aza-benzobicyclo[2.2.1]hept-2-ene (2-9)



A solution of PhPCl_2 (0.68 cm³, 0.90 g, 5.01 mmol) in CH_2Cl_2 (20 cm³) was added dropwise to a cooled solution (−30 °C) of 7-aza-benzobicyclo[2.2.1]hept-2-ene (1.44 g, 10.06 mmol) and NEt_3 (2.80 cm³, 2.03 g, 20.1 mmol) in CH_2Cl_2 (40 cm³). The reaction was subsequently stirred for 15 mins before being allowed to warm to RT and stirred for a further 4 h. All volatile components were removed *in vacuo*. Recrystallisation from hot hexane afforded the title compound as an off-white solid (1.45 g, 74%).

¹H NMR (600 MHz, CDCl_3) δ : 4.96 (2H, bs, $\text{H}_{b/i}$), 5.01 (2H, bs, $\text{H}_{b/i}$), 6.69-6.71 (2H, m, $\text{H}_{a/j}$), 6.77-6.80 (2H, m, $\text{H}_{a/j}$), 6.83-6.88 (4H, m, H_d), 7.05-7.13 (4H, m, H_e), 7.27-7.36 (5H, m, C_6H_5).

¹³C{¹H} NMR (151 MHz, CDCl_3) δ : 67.6 (d, $^2J_{\text{PC}} = 8$ Hz, $\text{C}_{b/i}$), 67.8 (d, $^2J_{\text{PC}} = 12$ Hz, $\text{C}_{b/i}$), 119.5 (s, $\text{C}_{d/g}$), 119.7 (s, $\text{C}_{d/g}$), 123.9 (s, $\text{C}_{e/f}$), 128.1 (d, $J_{\text{PC}} = 6$ Hz, *o*/*m*- C_6H_5), 128.3 (s, *p*- C_6H_5), 131.5 (d, $J_{\text{PC}} = 18$ Hz, *o*/*m*- C_6H_5), 139.6 (d, $^1J_{\text{PC}} = 7$ Hz, *ipso*- C_6H_5), 144.0 (d, $^3J_{\text{PC}} = 2$ Hz, $\text{C}_{a/j}$), 144.4 (d, $^3J_{\text{PC}} = 3$ Hz, $\text{C}_{a/j}$), 151.7 (d, $^3J_{\text{PC}} = 4$ Hz, $\text{C}_{c/h}$), 152.1 (d, $^3J_{\text{PC}} = 4$ Hz, $\text{C}_{c/h}$).

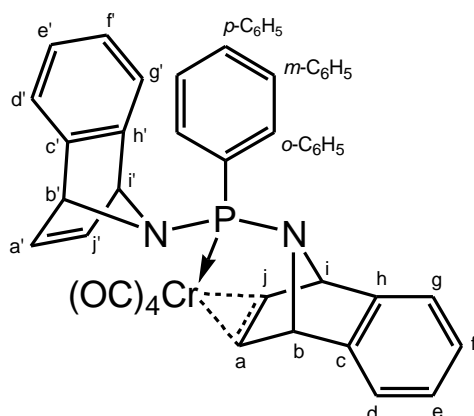
³¹P{¹H} NMR (243 MHz, CDCl_3) δ : 56.9 (s).

CHN: $\text{C}_{26}\text{H}_{21}\text{N}_2\text{P}$ requires: C, 79.58; H, 5.39; N, 7.14%. Found: C, 79.46; H, 5.36; N, 7.23%.

2-9.Se

³¹P{¹H} NMR (162 MHz, CDCl_3) δ : 50.0 (s, + satellites, $^1J_{\text{SeP}} = 791$ Hz).

Synthesis of $[\text{Cr}(\text{CO})_4(\kappa^2\text{-P,C-2-9})]$ (**2-10**)



A toluene (20 cm³) solution of $[\text{Cr}(\text{CO})_6]$ (175 mg, 0.795 mmol) and **2-9** (235 mg, 0.599 mmol) was heated at reflux for 24 h. The resulting yellow solution was cooled (0 °C) and filtered to remove excess $[\text{Cr}(\text{CO})_6]$. All volatile components were removed *in vacuo* to leave a yellow solid. The title complex was dissolved in a minimum amount of DCM and precipitated out by the addition of methanol (5 cm³), subsequent isolation by filtration and drying *in vacuo* afforded **2-10** as a yellow solid (157 mg, 67%).

Crystals suitable for X-ray diffraction were grown by layering a concentrated DCM solution of **2-10** with methanol.

¹H NMR (700 MHz, CDCl₃) δ: 4.17 (1H, s, H_{a/j}), 4.19 (1H, s, H_{b/i}), 4.32 (1H, s, H_{a/j}), 4.66 (1H, s, H_{b/i}), 5.14 (1H, s, H_{b'/i'}), 5.30 (1H, s, H_{b'/i'}), 6.71 (1H, s, H_{a'/j'}), 6.74 (1H, s, H_{a'/j'}), 6.45-7.35 (13H, m, aromatic CH).

¹³C{¹H} NMR (176 MHz, CDCl₃) δ: 67.2 (s, C_{b'/i'}), 67.9 (d, ²J_{PC} = 4 Hz, C_{b'/i'}), 69.3 (d, ²J_{PC} = 15 Hz, C_{b/i}), 69.8 (d, ²J_{PC} = 8 Hz, C_{b/i}), 83.0 (s, C_{a/j}), 83.6 (s, C_{a/j}), 119.9 (s), 120.0 (s), 121.1 (s), 121.6 (s), 123.9 (s), 124.2 (s), 126.1 (d, J = 40 Hz), 128.0 (d, J = 8 Hz), 130.3 (s), 130.4 (s), 133.3 (d, J = 30 Hz), 141.9 (d, ³J_{PC} = 4 Hz, C_{a'/j'}), 144.62 (d, ³J_{PC} = 8 Hz, C_{a'/j'}), 145.2 (d, J = 9 Hz), 145.7 (d, J = 15 Hz), 148.0 (s), 150.7 (d, J = 4 Hz), 222.5 (d, ²J_{PC} = 6 Hz, CO), 224.9 (d, ²J_{PC} = 12 Hz, CO), 226.4 (d, ²J_{PC} = 15 Hz, CO), 234.1 (d, ²J_{PC} = 15 Hz, CO).

³¹P{¹H} NMR (283 MHz, CDCl₃) δ: 156.9 (s).

CHN: C₃₂H₁₉CrN₂O₆P requires: C, 64.75; H, 3.80; N, 5.03%. Found: C, 65.63; H, 3.74; N, 5.14%.^{hh}

MS (ASAP+): 557 (M+H)⁺

IR (Nujol mull) ν (cm⁻¹): 1890, 1919, 1952, 2016, C=O.

^{hh} Satisfactory elemental analysis was not obtained.

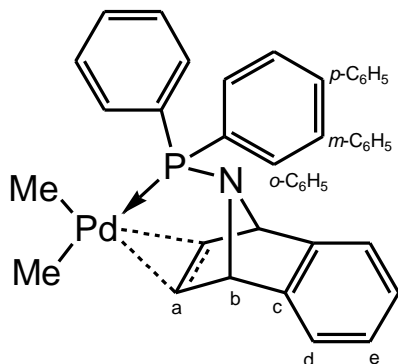
7.3 Chapter 3 experimental

The following compounds were prepared according to literature procedures or slight modifications thereof: $[\text{PdCl}_2(\text{MeCN})_2]$,¹ $[\text{PdMe}_2(\text{tmeda})]$,⁴ $[\text{Pd}(\text{CD}_3)_2(\text{tmeda})]$,⁴ $[\text{PdCl}(\text{Me})(\text{COD})]$,³ and 3-pyrroline.⁵

General procedure for the synthesis of phosphine selenide compounds

An NMR tube fitted with a J. Young's valve was charged with a small quantity of phosphine (20-50 mg), a slight excess of elemental grey Se and CDCl_3 (0.7 cm³). The system was then heated at 50 °C for 16 h, giving quantitative conversion (according to ³¹P{¹H} NMR spectroscopy) to the required phosphine selenide.

Synthesis of [PdMe₂(κ²-P,C-2-1)] (3-1)



A solution of **2-1** (80 mg, 0.24 mmol) in toluene (5 cm³) was added drop-wise to a solution of [PdMe₂(tmeda)] (62 mg, 0.24 mmol) in toluene (5 cm³). The mixture was allowed to stir for 5 mins at RT affording compound **3-1** quantitatively (according to ³¹P{¹H} NMR spectroscopy). All volatile components were removed *in vacuo* and the resultant solid washed with Et₂O (4 cm³) to afford the title complex as a white solid (55 mg, 49%).

Crystals of **3-1** suitable for an X-ray diffraction study were grown by cooling (−30 °C) the concentrated toluene solution

In a separate experiment, an NMR tube fitted with a J. Young's valve was loaded with **2-1** (13 mg, 0.12 mmol), [PdMe₂(tmeda)] (10 mg, 0.12 mmol), d₈-toluene (0.7 cm³), and a sealed capillary tube containing a solution of PPh₃ as a standard. In less than 10 minutes complete consumption of **2-1** was evident, something accompanied by a >99% conversion to **3-1** according to ³¹P{¹H} NMR spectroscopic analysis. Once conversion to **3-2** was complete (5 days) >0.9 mole equivalents of ethane were present in solution according to integration (¹H NMR spectroscopy).

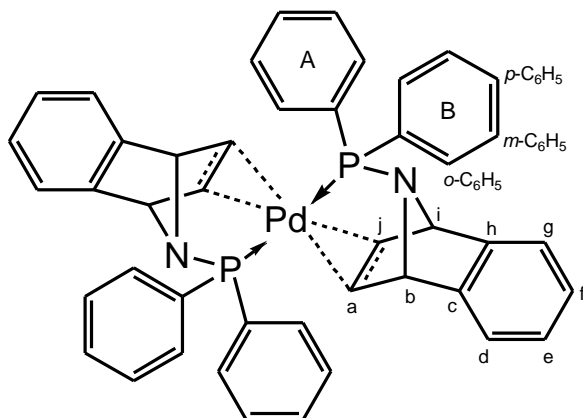
¹H NMR (700 MHz, C₆D₆) δ: 0.97 (3H, d, ³J_{PH} = 7.7 Hz, CH₃), 1.69 (3H, d, ³J_{PH} = 7.5 Hz, CH₃), 4.25 (2H, d, ³J_{HH} = 2.9 Hz, CH_b), 5.78 (2H, bs, CH_a), 6.69-6.74 (4H, m, CH_d and CH_e), 7.01-7.04 (6H, m, *o*- and *p*-C₆H₅), 7.93-7.98 (4H, m, *m*-C₆H₅).

¹³C{¹H} NMR (176 MHz, C₆D₆) δ: 2.6 (d, ²J_{PC} = 8 Hz, CH₃), 5.8 (d, ²J_{PC} = 120 Hz, CH₃), 71.3 (d, ²J_{PC} = 11 Hz, C_b), 119.2 (s, C_a), 121.4 (s, C_d), 125.6 (s, C_e), 128.4 (s, C_c), 129.2 (d, ²J_{PC} = 10 Hz, *o*-C₆H₅), 131.4 (d, ⁴J_{PC} = 2 Hz, *p*-C₆H₅), 133.2 (d, ³J_{PC} = 15 Hz, *m*-C₆H₅), 145.7 (d, ¹J_{PC} = 10 Hz, *ipso*-C₆H₅).

³¹P{¹H} NMR (162 MHz, C₆D₆) δ: 81.3 (s).

Despite repeated attempts, satisfactory elemental analyses for **3-1** could not be obtained since the complex degrades slowly, even in the solid state.

Synthesis of $[\text{Pd}(\kappa^2\text{-P,C-2-1})_2]$, (**3-2**)



A solution of **2-1** (0.15 g, 0.46 mmol) in toluene (15 cm³) was added drop-wise to a solution of $[\text{PdMe}_2(\text{tmeda})]$ (0.057 g, 0.23 mmol) in toluene (10 cm³). The mixture was allowed to stir for 18 h at RT, resulting in the quantitative formation of complex **3-2** (according to $^{31}\text{P}\{^1\text{H}\}$ NMR spectroscopy). Removal of volatile components *in vacuo* and washing with Et₂O (2 x 10 cm³) afforded **3-2** as a dark brown solid, (0.15 g, 87%).

Crystals suitable for an X-ray diffraction study were grown by slow diffusion of hexane into a concentrated toluene solution of **3-2**.

In a separate experiment, an NMR tube fitted with a J. Young's valve was loaded with **2-1** (26 mg, 0.080 mmol), $[\text{PdMe}_2(\text{tmeda})]$ (10 mg, 0.040 mmol) and d₈-toluene (0.7 cm³). The reaction was subsequently monitored by multinuclear NMR spectroscopy until complete formation of **3-2** was achieved (5 h).

^1H NMR (400 MHz, C₆D₆) δ : 4.21 (2H, bs, CH_{b/i}), 4.70-4.74 (2H, m, CH_{a/j}), 4.76 (2H, bs, CH_{b/i}), 4.87-4.92 (2H, m, CH_{a/j}), 6.89-6.95 (6H, m, CH_{d/g} and CH_{e/f}), 7.06-7.08 (2H, m, CH_{d/g}), 7.08-7.19 (12H, m, *o*- and *p*-C₆H₅), 7.94-8.00 (4H, m, *m*-C₆H₅), 8.03-8.09 (4H, m, *m*-C₆H₅).

$^{13}\text{C}\{^1\text{H}\}$ NMR (126 MHz, C₆D₆) δ : 70.7 (m, C_{b/i}), 72.1 (m, C_{b/i}), 75.9 (m, C_{a/j}), 80.7 (m, C_{a/j}), 120.2, 120.4, 125.1 and 125.2 (s, C_{d/g} and C_{e/f}), 128.4 (m, *o*-C₆H₅), 129.8 (s, *p*-C₆H₅), 130.0 (s, *p*-C₆H₅), 132.9 (m, *m*-C₆H₅), 133.2 (m, *m*-C₆H₅), 138.3 (m, *ipso*-C₆H₅), 138.5 (m, *ipso*-C₆H₅); 147.3 (m, C_{c/h}), 148.4 (m, C_{c/h}).

$^{31}\text{P}\{^1\text{H}\}$ NMR (162 MHz, C₆D₆) δ : 82.2 (s).

CHN: C₄₄H₃₆N₂P₂Pd requires: C, 69.43; H, 4.77; N, 3.68%. Found: C, 69.22; H, 4.65; N, 3.71%.

Addition of sub-stoichiometric amount of PPh₃ to 3-1

An NMR tube fitted with a J. Young's valve was loaded with **2-1** (16 mg, 0.049 mmol), [PdMe₂(tmeda)] (12 mg, 0.047 mmol), PPh₃ (1.1 mg, 0.0042 mmol), and d₈-toluene (0.7 cm³). The reaction was followed by ¹H and ³¹P{¹H} NMR spectroscopy until completion.

Addition of sub-stoichiometric amount of propene to 3-1

An NMR tube fitted with a J. Young's valve was loaded with **2-1** (24 mg, 0.073 mmol), [PdMe₂(tmeda)] (20 mg, 0.079 mmol), propene (0.11 mg, 0.0027 mmol) *via* a gas bulb, and d₈-toluene (0.7 cm³). The reaction was followed by ¹H and ³¹P{¹H} NMR spectroscopy until completion.

Variable temperature NMR spectroscopic study of the interaction of 2-1 and 3-1

d₂-DCM (0.5 cm³) was added *via* vacuum transfer into an NMR tube fitted with a J. Young's valve containing **3-1** (19 mg, 0.041 mmol) and **2-1** (13 mg, 0.040 mmol) at -196 °C. The NMR tube was warmed to 0 °C in an ice bath before loading into a NMR machine with the probe pre-cooled to +10 °C. ¹H, ³¹P{¹H} and, ³¹P NMR spectra were obtained at the following temperatures in the following order, +10, 0, -20, -40, -60, -80, -60, -40, -20, 0 and +20°C

Thermal stability of **3-2**

A solution of **3-2** (10 mg, 0.013 mmol) in C₆D₆ (0.7 cm³) was heated at 80 °C in an NMR tube fitted with a J. Young's valve containing a glass capillary enclosing a PPh₃ standard. No decomposition had occurred after 24 h.

Addition of PPh₃ to **3-2**

Complex **3-2** (10 mg, 0.013 mmol), PPh₃ (7 mg, 0.027 mmol) and C₆D₆ (0.7 cm³) were added to an NMR tube fitted with a J. Young's valve and heated at 80 °C for 16 h. Analysis by ¹H and ³¹P{¹H} NMR spectroscopy showed that there was no reaction between **3-2** and PPh₃.

Reaction of **3-2** with PhI

Complex **3-2** (10 mg, 0.013 mmol), PhI (15 µl, 27 mg, 0.13 mmol) and C₆D₆ (0.7 cm³) were added to an NMR tube fitted with a J. Young's valve and heated at 60 °C for 2 mins, which resulted in the precipitation of palladium metal from solution. Analysis of the remaining solution by ¹H and ³¹P{¹H} NMR spectroscopy showed the formation of multiple phosphorus-containing species, none of which could be assigned to a specific compound.

Decreasing the reaction temperature to RT increased the time taken to achieve 100% consumption of **3-2** to 2 weeks.

General procedure for the Suzuki-Miyaura cross-coupling reactions of aryl halides with phenylboronic acid

To an ampule fitted with a J. Young's valve were placed the appropriate amounts of aryl halide (0.5 mmol), phenylboronic acid (91 mg, 0.75 mmol), nonane (89 μ l, 46 mg, 1.0 mmol), K_2CO_3 (138 mg, 1.0 mmol), and toluene (5 cm^3). After stirring for 2 minutes, **3-2** (19 mg, 0.025 mmol) was added from a stock solution in toluene. The mixture was stirred at 80 °C in a sealed system under a nitrogen atmosphere for 20 h. The residual mixture was diluted with H_2O (5 cm^3) and extracted with toluene (2 x 5 cm^3). The combined organic fractions were filtered through Celite and dried ($MgSO_4$). An aliquot of the solution was taken with a syringe and subjected to GC-FID analysis. Yields were calculated with respect to biphenyl product using nonane as an internal standard.

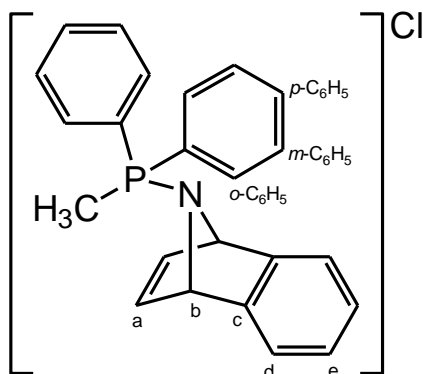
Where mercury poisoning experiments were carried out, 1 drop of Hg was added to the system after 5 minutes stirring at RT.

General procedure for the Negishi cross-coupling reaction of ethyl-2-iodobenzoate with diethylzinc

A small Schlenk was charged with the appropriate amounts of ethyl-2-iodobenzoate (164 μ l, 276mg, 1.0 mmol), nonane (89 μ l, 46 mg, 1.0 mmol), and THF (1.5 cm^3). After stirring for 2 minutes the pre-catalyst (0.050 mmol) was added. Following stirring for a further 2 minutes, Et_2Zn (2.5 cm^3 , 1.0 M in hexane, 2.5 mmol) was added and the system stirred at RT for 2 h. The reaction was quenched with dilute HCl (2 cm^3 , 3 M), separated and then extracted by Et_2O (3 x 2 cm^3). The combined organic layers were filtered through Celite and dried ($MgSO_4$). An aliquot was taken with a syringe and subjected to GC-FID analysis.

Reaction of [PdCl(Me)(COD)] with 2-1 (P:Pd = 3:1) affording 3-2 and [3-3]Cl

To an NMR tube fitted with a J. Young's valve containing **2-1** (35 mg, 0.107 mmol) and CDCl₃ (0.8 cm³) was added [PdCl(Me)(COD)] (9 mg, 0.034 mmol). In under 5 minutes complete consumption of **2-1** was evident by ³¹P{¹H} NMR spectroscopic analysis, with the appearance of two new signals in a 2:1 ratio at $\delta = 82.9$ (**3-2**) and 38.1 ([**3-3**]Cl) ppm, respectively (by integration of the proton-coupled ³¹P NMR spectrum). By integration against a standard present in a sealed capillary tube, the conversion of ligand **2-1** to complex **3-2** was assessed to be 96% and to [**3-3**]Cl was 89%. Subsequently, all volatile components were removed *in vacuo*. Extraction of complex **3-2** into toluene (3 × 1 cm³) afforded phosphonium salt [**3-3**]Cl as a pale yellow solid (10 mg, 80%).

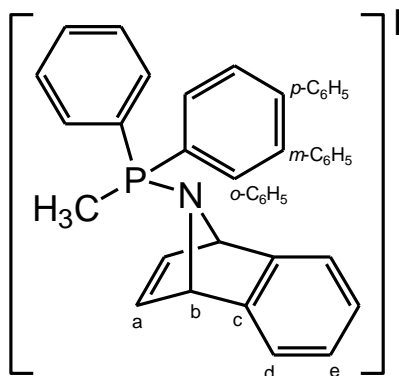
Phosphonium salt [3-3]Cl

¹H NMR (400 MHz, CDCl₃) δ : 2.82 (3H, d, ²J_{PH} = 13.0 Hz, PCH₃), 5.52 (2H, m, CH_b), 6.92-6.94 (2H, m, CH_d), 7.11 (2H, m, CH_a), 7.23-7.25 (2H, m, CH_e), 7.62-7.65 (4H, m, *m*-C₆H₅), 7.73-7.77 (2H, m, *p*-C₆H₅), 7.84-7.89 (4H, m, *o*-C₆H₅).

³¹P{¹H} NMR (162 MHz, CDCl₃) δ : 38.1 (s).

MS (ESI⁺): 342 (M-Cl)⁺.

Synthesis of phosphonium salt [3-3]I



To verify the identity of [3-3]Cl, an authentic sample of the corresponding methyl phosphonium iodide salt [3-3]I was prepared by treating a CDCl₃ (0.7 cm³) solution of 2-1 (25 mg, 0.076 mmol) with MeI (5.0 μL, 0.080 mmol). Standing at RT for 12 h followed by removal of all volatile components *in vacuo* afforded [3-3]I, (31 mg, 87%).

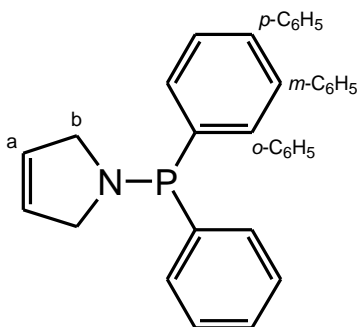
¹H NMR (700 MHz, CDCl₃) δ: 2.70 (3H, d, ²J_{PH} = 13.0 Hz, PCH₃), 5.49 (2H, m, CH_b), 6.87-6.90 (2H, m, CH_d), 7.12 (2H, m, CH_a), 7.24-7.26 (2H, m, CH_e), 7.59-7.62 (4H, m, *m*-C₆H₅), 7.70-7.74 (2H, m, *p*-C₆H₅), 7.77-7.81 (4H, m, *o*-C₆H₅).

¹³C{¹H} NMR (176 MHz, CDCl₃) δ: 11.7 (d, ²J_{CP} = 59 Hz, PCH₃), 67.7 (s, C_b), 119.9 (d, ¹J_{CP} = 100 Hz, *ipso*-C₆H₅), 121.6 (s, C_e), 125.8 (s, C_d), 130.4 (d, ³J_{PC} = 13 Hz, *m*-C₆H₅), 132.6 (d, ²J_{PC} = 11 Hz, *o*-C₆H₅), 135.4 (d, ⁴J_{PC} = 3 Hz, *p*-C₆H₅), 143.7 (d, ³J_{PC} = 6 Hz, C_a), 151.2 (d, ³J_{PC} = 5 Hz, C_c).

³¹P{¹H} NMR (283 MHz, CDCl₃) δ: 37.1 (s).

MS (ESI⁺): 342 (M-I)⁺.

Synthesis of *N*-PPh₂-3-pyrroline (**3-4**)



A solution of Ph₂PCl (13.8 cm³, 74.7 mmol) in DCM (30 cm³) was added drop-wise to a cooled (−30 °C) solution of 3-pyrroline (6.0 cm³, 79 mmol) and NEt₃ (13.2 cm³, 94.7 mmol) in DCM (70 cm³). The resulting mixture was stirred at −30 °C for 15 minutes before being left to warm to room temperature overnight. All volatile components were removed *in vacuo* and the resulting residue was extracted into hexane (60 cm³). After removal of solvent *in vacuo*, vacuum distillation yielded the title compound as a viscous, colourless oil (bp 116-122 °C at 0.15 mbar) in moderate yield (9.1 g, 46%). Following cooling (−20 °C) **3-4** was isolated as a white solid, which did not melt upon warming to RT.

¹H NMR (600 MHz, C₆D₆) δ: 2.89 (4H, d, ²J_{PH} = 3.5 Hz, C_b), 5.38 (2H, bs, C_a), 7.04-7.08 (2H, m, *p*-C₆H₅), 7.09-7.13 (4H, m, *m*-C₆H₅), 7.40-7.44 (4H, m, *o*-C₆H₅).

¹³C{¹H} NMR (151 MHz, C₆D₆) δ: 57.2 (d, ²J_{PC} = 14 Hz, C_b), 127.8 (d, ³J_{PC} = 5 Hz, C_a), 128.6 (s, *p*-C₆H₅), 128.6 (d, ³J_{PC} = 1 Hz, *m*-C₆H₅), 132.5 (d, ²J_{PC} = 18 Hz, *o*-C₆H₅), 139.8 (d, ¹J_{PC} = 13 Hz, *ipso*-C₆H₅).

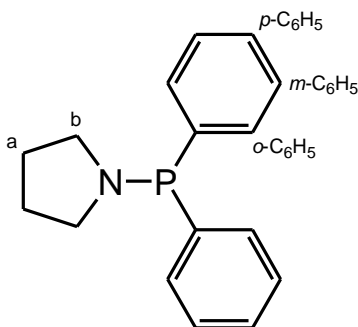
³¹P{¹H} NMR (243 MHz, C₆D₆) δ: 47.4 (s).

CHN: C₁₆H₁₆NP requires: C, 75.87; H, 6.37; N, 5.53%. Found: C, 75.96; H, 6.42; N, 5.61%.

3-4.Se

³¹P{¹H} NMR (162 MHz, C₆D₆) δ: 66.5 (s, + satellites, ¹J_{SeP} = 776 Hz).

Synthesis of N-PPh₂-pyrrolidine (3-5)



A solution of Ph₂PCl (16.2 cm³, 87.7 mmol) in DCM (30 cm³) was added drop-wise to a cooled (−30 °C) solution of pyrrolidine (7.6 cm³, 91 mmol) and NEt₃ (16.0 cm³, 115 mmol) in DCM (150 cm³). The resulting reaction mixture was stirred at −30 °C for 15 minutes before warming to room temperature overnight. All volatile components were removed *in vacuo*. The title compound was extracted into hexane (80 cm³), the solvent was removed *in vacuo*. Vacuum distillation yielded the title compound as a viscous, colourless oil (bp. 115-120 °C at 0.15 mbar) in moderate yield (14.9 g, 66%). Following cooling (−20 °C) the title compound was isolated as a white solid, which did not melt upon warming to RT.

¹H NMR (600 MHz, C₆D₆) δ: 1.39-1.43 (4H, m, C_a), 2.94-2.98 (4H, m, C_b), 7.08-7.11 (2H, m, *p*-C₆H₅), 7.13-7.17 (4H, m, *m*-C₆H₅), 7.45-7.49 (4H, m, *o*-C₆H₅).

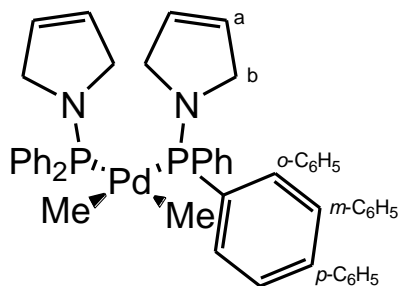
¹³C {¹H} NMR (176 MHz, C₆D₆) δ: 26.5 (d, ³J_{PC} = 5 Hz, C_a), 49.9 (d, ²J_{PC} = 13 Hz, C_b), 128.4 (d, ³J_{PC} = 6 Hz, *m*-C₆H₅), 128.5 (s, *p*-C₆H₅), 132.6 (d, ²J_{PC} = 20 Hz, *o*-C₆H₅), 140.1 (d, ¹J_{PC} = 14 Hz, *ipso*-C₆H₅).

³¹P{¹H} NMR (243 MHz, C₆D₆) δ: 47.4 (s).

CHN: C₁₆H₁₈NP requires: C, 75.27; H, 7.11; N, 5.49%. Found: C, 75.12; H, 7.15; N, 5.49%.

Spectroscopic data are in good agreement with the literature.⁶

Synthesis of *cis*-[PdMe₂(κ¹-P-3-4)₂] (3-6)



A Schlenk was loaded with [PdMe₂(tmeda)] (100 mg, 0.40 mmol), **3-4** (200 mg, 0.79 mmol) and DCM (5 cm³), the resulting colourless solution was then stirred for 5 minutes. All volatile components were removed *in vacuo*, before the resulting solid was washed with hexane (3 x 4 cm³). The title complex was dried *in vacuo* and was isolated as a white solid (160 mg, 62%).

¹H NMR (600 MHz, C₆D₆) δ: 1.03 (6H, dd, ²J_{PH} = 3.9 Hz, ²J_{PH} = 6.5 Hz, PdCH₃), 4.03-4.07 (8H, m, H_b), 5.38 (4H, s, H_a), 6.95-7.00 (12H, m, *m*-C₆H₅ + *p*-C₆H₅), 7.38-7.42 (8H, m, *o*-C₆H₅).

¹³C{¹H} NMR (151 MHz, C₆D₆) δ: 9.7 (dd, ¹J_{PC} = 15 Hz, ¹J_{PC} = 109 Hz, PdCH₃), 58.7 (t, ²J_{PC} = 4 Hz, C_b), 127.2 (t, ³J_{PC} = 3 Hz, C_a), 127.8 (t, ³J_{PC} = 4 Hz, *m*-C₆H₅), 129.1 (s, *p*-C₆H₅), 133.2 (t, ²J_{PC} = 7 Hz, *o*-C₆H₅), 137.2-137.6 (m, *ipso*-C₆H₅).

³¹P{¹H} NMR (243 MHz, C₆D₆) δ: 70.8 (s).

CHN: C₃₄H₃₈N₂P₂Pd requires: C, 63.50; H, 5.96; N, 4.36%. Found: C, 63.63; H, 5.84; N, 4.48%.

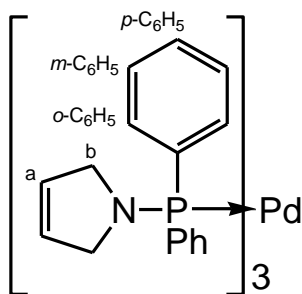
Conversion of 3-6 into 3-7 in solution

An NMR tube fitted with a J. Young's valve was charged with **3-6** (40 mg, 0.062 mmol) and C₆D₆ (0.8 cm³). The reaction mixture was sonicated for 10 minutes. The reaction was then followed by ¹H and ³¹P{¹H} NMR spectroscopy until completion.

Deuterium cross-over experiment

An NMR tube fitted with a J. Young's valve was charged with [PdMe₂(tmeda)] (10 mg, 0.040 mmol), [Pd(CD₃)₂(tmeda)] (10 mg, 0.039 mmol), **3-4** (40 mg, 0.158 mmol) and C₆D₆ (0.7 cm³). The reaction mixture was sonicated for 10 minutes, before all volatile compounds were removed *in vacuo* (>0.1 mbar, 24 h). The resulting mixture was redissolved in C₆D₆ (0.7 cm³). The reaction was followed by ¹H and ³¹P{¹H} NMR spectroscopy until completion.

Synthesis of $[\text{Pd}(\kappa^1\text{-P-3-4})_3]$ (**3-7**)



A solution of $[\text{PdMe}_2(\text{tmeda})]$ (200 mg, 0.791 mmol) in toluene (20 cm³) was added *via* cannula to a solution of **3-4** (601 mg, 2.27 mmol) in toluene (10 cm³). The resulting pale yellow solution was stirred at RT for 30 mins before being heated at 80 °C for 15 mins. The resulting orange solution was filtered to remove any insoluble material, before being washed with hexane (2 x 10 cm³). The title complex was isolated in moderate yield (452 mg, 62%).

Crystals suitable for X-ray diffraction were grown by slow diffusion of hexane into a concentrated toluene solution of **3-7**.

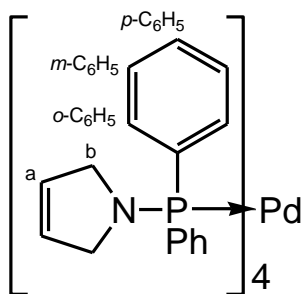
^1H NMR (600 MHz, C₆D₆) δ : 3.92 (12H, s, H_b), 5.39 (6H, s, H_a), 7.05-7.08 (18H, m, *m*-C₆H₅ + *p*-C₆H₅), 7.49-7.52 (12H, m, *o*-C₆H₅).

$^{13}\text{C}\{^1\text{H}\}$ NMR (151 MHz, C₆D₆) δ : 57.6 (s, C_b), 127.5-127.6 (m, C_a), 127.9-128.0 (m, *m*-C₆H₅), 128.3-128.4 (m, *p*-C₆H₅), 132.3-132.6 (m, *o*-C₆H₅), 141.4-141.7 (m, *ipso*-C₆H₅).

$^{31}\text{P}\{^1\text{H}\}$ NMR (243 MHz, C₆D₆) δ : 66.9 (bs, FWHM = 16 Hz).

CHN: C₄₈H₄₈N₃P₃Pd requires: C, 66.55; H, 5.59; N, 4.85%. Found: C, 66.32; H, 5.46; N, 4.91%.

Synthesis of $[\text{Pd}(\kappa^1\text{-P-3-4})_4]$ (**3-8**)



An NMR tube fitted with a J. Young's valve was charged with $[\text{PdMe}_2(\text{tmeda})]$ (20 mg, 0.079 mmol), **3-4** (80 mg, 0.32 mmol) and C_6D_6 (0.8 cm^3). The resulting colourless solution was sonicated for 10 minutes. Subsequent heating (80 °C) for 30 minutes resulted in the formation of a yellow solution containing the title complex. All volatile components were removed *in vacuo* leaving the title complex as an orange solid (82 mg, 93%).

^1H NMR (600 MHz, C_6D_6) δ : 3.92-3.94 (16H, m, H_b), 5.40 (8H, s, H_a), 7.06-7.13 (24H, m, $m\text{-C}_6\text{H}_5 + p\text{-C}_6\text{H}_5$), 7.46-7.51 (16H, m, $o\text{-C}_6\text{H}_5$).

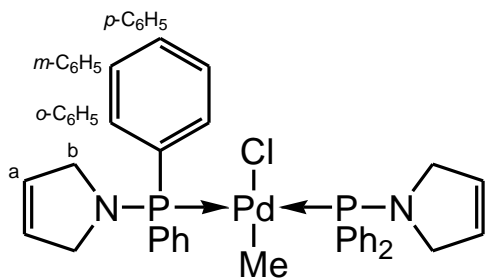
$^{13}\text{C}\{^1\text{H}\}$ NMR (151 MHz, C_6D_6) δ : 57.4 (d, $^2J_{\text{PC}} = 12$ Hz, C_b), 127.7 (d, $^3J_{\text{PC}} = 5$ Hz, C_a), 128.2-128.3 (m, $m\text{-C}_6\text{H}_5$), 128.3-128.4 (m, $p\text{-C}_6\text{H}_5$), 132.5 (d, $^2J_{\text{PC}} = 19$ Hz, $o\text{-C}_6\text{H}_5$), 140.5-140.7 (m, *ipso*- C_6H_5).

$^{31}\text{P}\{^1\text{H}\}$ NMR (243 MHz, C_6D_6) δ : 53.1 (vbs, FWHM = 385 Hz).

CHN: $\text{C}_{64}\text{H}_{64}\text{N}_4\text{P}_4\text{Pd}$ requires: C, 68.66; H, 5.76; N, 5.00%. Found: C, 68.52; H, 5.68; N, 4.85%.

Solid-State $^{31}\text{P}\{^1\text{H}\}$ NMR (162 MHz) δ : 60.7 ppm (s).

Synthesis of *trans*-[PdCl(Me)(κ¹-P-3-4)₂] (**3-9**)



An NMR tube fitted with a J. Young's valve was charged with [PdCl(Me)(COD)] (20 mg, 0.079 mmol), **3-4** (38 mg, 0.15 mmol) and CDCl₃ (0.7 cm³), the resulting pale yellow solution was sonicated for 10 minutes. All volatile components were removed *in vacuo* and the resulting solid washed with pentane (3 x 1 cm³). The title compound was recrystallised by layering a concentrated DCM solution with hexane, yielding a pale yellow crystalline solid (34 mg, 65 %).

Crystals of **3-9** suitable for X-ray diffraction were grown by layering a concentrated DCM solution with hexane.

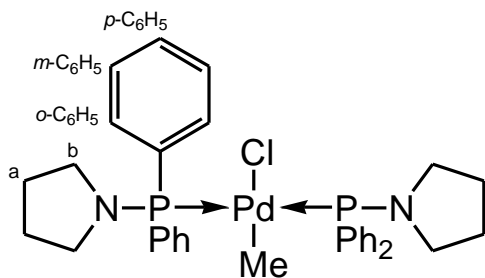
¹H NMR (600 MHz, CDCl₃) δ: -0.19 (3H, t, ³J_{PH} = 6.2 Hz, PdCH₃), 4.26-4.29 (8H, m, H_b), 5.78-5.80 (4H, m, H_a), 7.36-7.41 (12H, m, *m*-C₆H₅ + *p*-C₆H₅), 7.62-7.67 (8H, m, *o*-C₆H₅).

¹³C{¹H} NMR (151 MHz, CDCl₃) δ: 4.2 (t, ¹J_{PC} = 3 Hz, PdCH₃), 58.6 (t, ²J_{PC} = 4 Hz, C_b), 127.0 (t, ³J_{PC} = 3 Hz, C_a), 129.0 (t, ³J_{PC} = 5 Hz, *m*-C₆H₅), 130.0 (s, *p*-C₆H₅), 133.1 (t, ¹J_{PC} = 24 Hz, *ipso*-C₆H₅), 133.6 (t, ²J_{PC} = 6 Hz, *o*-C₆H₅).

³¹P{¹H} NMR (243 MHz, CDCl₃) δ: 69.4 (s).

CHN: C₃₃H₃₅ClN₂P₂Pd requires: C, 59.74; H, 5.32; N, 4.22%. Found: C, 59.83; H, 5.25; N, 4.16%.

Synthesis of *trans*-[PdCl(Me)(κ^1 -P-3-5)₂] (3-10)



An NMR tube fitted with a J. Young's valve was charged with [PdCl(Me)(COD)] (20 mg, 0.079 mmol), **3-5** (39 mg, 0.15 mmol) and d₂-DCM (0.7 cm³), the resulting pale yellow solution was sonicated for 10 minutes. All volatile components were removed *in vacuo* and the resulting solid washed with pentane (3 x 1 cm³). The title complex was recrystallised by layering a concentrated DCM solution with hexane, yielding a pale yellow solid (39 mg, 74 %).

Crystals suitable for X-ray diffraction were grown by layering a concentrated DCM solution of **3-10** with hexane.

¹H NMR (700 MHz, CDCl₃) δ: -0.17 (3H, t, ³J_{PH} = 6.1 Hz, PdCH₃), 1.80-1.83 (8H, m, H_a), 3.29-3.32 (8H, m, H_b), 7.34-7.38 (12H, m, *m*-C₆H₅ + *p*-C₆H₅), 7.61-7.65 (8H, m, *o*-C₆H₅).

¹³C{¹H} NMR (176 MHz, CDCl₃) δ: 3.5 (t, ¹J_{PC} = 3 Hz, PdCH₃), 26.7 (t, ³J_{PC} = 3 Hz, C_a), 51.0 (t, ²J_{PC} = 3 Hz, C_b), 127.8 (t, ³J_{PC} = 5 Hz, *m*-C₆H₅), 129.8 (s, *p*-C₆H₅), 133.3 (t, ¹J_{PC} = 24 Hz, *ipso*-C₆H₅), 133.4 (t, ²J_{PC} = 7 Hz, *o*-C₆H₅).

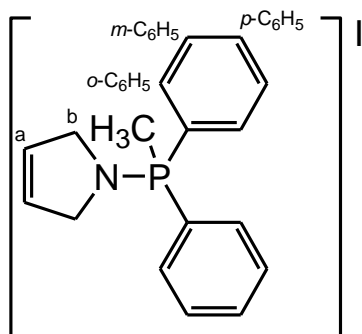
³¹P{¹H} NMR (162 MHz, CDCl₃) δ: 65.8 (s).

CHN: C₃₃H₃₉ClN₂P₂Pd requires: C, 59.38; H, 5.89; N, 4.20%. Found: C, 59.27; H, 5.80; N, 4.20%.

Reaction of [PdCl(Me)(COD)] with **3-4** (P:Pd = 3:1) affording **3-4** and **3-9**

An NMR tube fitted with a J. Young's valve was charged with [PdCl(Me)(COD)] (20 mg, 0.079 mmol), **3-4** (57 mg, 0.23 mmol) and CDCl₃ (0.7 cm³). Analysis of the resulting pale yellow solution by multinuclear NMR spectroscopy showed the formation of **3-9** and unreacted **3-4** in a 1:1 ratio. Heating the mixture at 80 °C for 2 h resulted in the formation of palladium metal and multiple unidentified products in solution, none of which was [3-11]Cl.

Synthesis of (3-4)MeI ([3-11]I)



To a solution of **3-4** (40 mg, 0.16 mmol) in CDCl₃ (0.7 cm³) in an NMR tube fitted with a J. Young's valve was added MeI (10 µl, 0.16 mmol). After shaking for 1 minute all volatile components were removed *in vacuo* to leave the title compound as a brown oil in excellent yield (58 mg, 92%).

¹H NMR (600 MHz, CDCl₃) δ: 2.84 (3H, d, ²J_{PH} = 13 Hz, PdCH₃), 4.12 (4H, d, ²J_{PH} = 3.5 Hz, C_b), 5.81 (2H, bs, C_a), 7.61-7.65 (4H, m, *m*-C₆H₅), 7.70-7.74 (2H, m, *p*-C₆H₅), 7.74-7.79 (4H, m, *o*-C₆H₅).

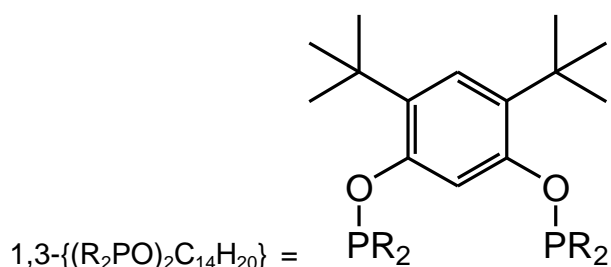
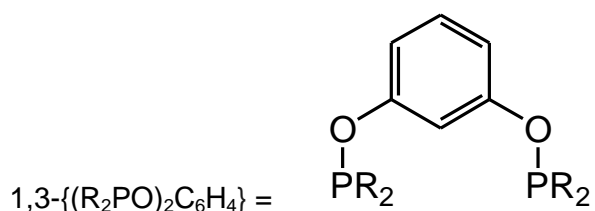
¹³C{¹H} NMR (151 MHz, CDCl₃) δ: 12.9 (d, ¹J_{PC} = 70 Hz, PdCH₃), 56.4 (d, ²J_{PC} = 5 Hz, C_b), 120.3 (d, ¹J_{PC} = 105 Hz, *ipso*-C₆H₅), 125.8 (d, ³J_{PC} = 8 Hz, C_a), 130.4 (d, ³J_{PC} = 13 Hz, *m*-C₆H₅), 132.4 (d, ²J_{PC} = 12 Hz, *o*-C₆H₅), 135.2 (d, ⁴J_{PC} = 3 Hz, *p*-C₆H₅).

³¹P{¹H} NMR (243 MHz, CDCl₃) δ: 43.2 (s).

MS (ESI+): 268 (M-I)⁺.

7.4 Chapter 4 experimental

The following compounds were prepared according to literature procedures or slight modifications thereof: 1,3- $\{({}^t\text{Bu}_2\text{PO})_2\text{C}_6\text{H}_4\}$ (**4-1**),⁷ $\text{ClP}(\text{N}^i\text{Pr}_2)_2$,⁸ $[\text{PdCl}_2(\text{MeCN})_2]$,¹ $\text{ClP}(\text{N-pyrrole})_2$,⁹ 1,3- $\{(\text{Cl}_2\text{PO})_2\text{C}_{14}\text{H}_{20}\}$ (**4-6**),¹⁰ 1,3- $\{({}^t\text{Bu}_2\text{PO})_2\text{C}_{14}\text{H}_{20}\}$ (**4-7**).¹¹



General procedure for the synthesis of phosphine selenide compounds

An NMR tube fitted with a J. Young's valve was charged with a small quantity of phosphine (20-50 mg), a slight excess of elemental grey Se and CDCl_3 (0.7 cm^3). The system was then heated at 50 °C for 16 h, giving quantitative conversion (according to $^{31}\text{P}\{^1\text{H}\}$ NMR spectroscopy) to the required phosphine selenide.

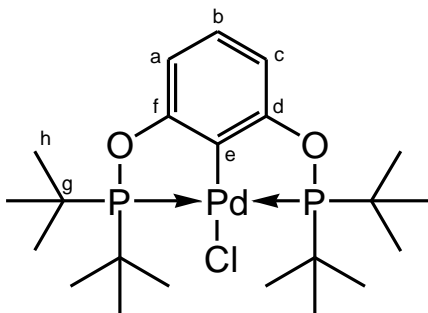
4-1.Se

$^{31}\text{P}\{^1\text{H}\}$ NMR (162 MHz, CDCl_3) δ : 139.1 (s + satellites, $^1J_{\text{SeP}} = 797$ Hz).

4-7.Se

$^{31}\text{P}\{^1\text{H}\}$ NMR (162 MHz, CDCl_3) δ : 131.3 (s + satellites, $^1J_{\text{SeP}} = 806$ Hz).

Synthesis of $[\text{PdCl}(\kappa^3\text{-P,C,P-4-1})]$ (**4-2**)



$[\text{PdCl}_2(\text{MeCN})_2]$ (0.605 g, 2.332 mmol), **4-1** (1.020 g, 2.560 mmol) and 1,1,2,2-tetrachloroethane (TCE) (60 cm³) were heated at 125 °C for 3 days with no observable colour change. Subsequently, volatile components were removed *in vacuo* to give a beige solid, which was washed with hexane (2 × 40 cm³). The resulting solid was recrystallized by layering a concentrated CHCl_3 solution with hexane, yielding the title compound (0.89 g, 71%).

Crystals suitable for X-ray diffraction were grown by layering a concentrated DCM solution of **4-2** with hexane.

¹H NMR (400 MHz, CDCl_3) δ : 1.18 (36H, vt, $J = 7.5$ Hz, H_h), 6.47 (2H, d, $^3J_{\text{HH}} = 8.0$ Hz, $\text{H}_{a/c}$), 6.88 (1H, t, $^3J_{\text{HH}} = 8.0$ Hz, H_b).

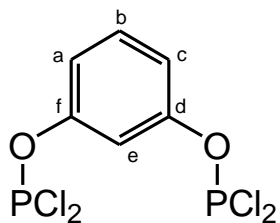
¹³C{¹H} NMR (176 MHz, CDCl_3) δ : 27.7 (vt, $J = 15$ Hz C_h), 39.6 (vt, $J = 30$ Hz, C_g), 105.6 (vt, $J = 41$ Hz, $\text{C}_{a/c}$), 127.5 (s, C_b), 129.9 (t, $^2J_{\text{PC}} = 2$ Hz, C_e), 167.1 (vt, $J = 24$ Hz, $\text{C}_{d/f}$).

³¹P{¹H} NMR (202 MHz, CDCl_3) δ : 192.2 (s).

CHN: $\text{C}_{22}\text{H}_{39}\text{P}_2\text{O}_2\text{ClPd}$ requires C, 48.99; H, 7.29; N, 0.00%. Found: C, 49.02; H, 7.21; N, 0.00%.

MS (ASAP+): 538 (M)⁺, 503 (M-Cl)⁺.

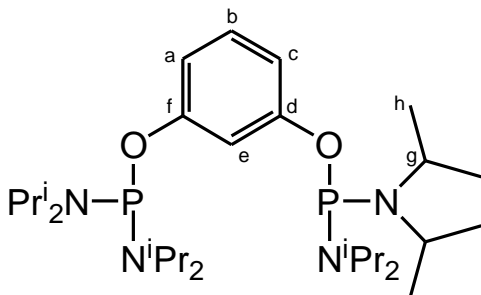
After this compound was first synthesised as part of this thesis work an alternative route became available in the literature; the spectroscopic data for products from both methods are consistent.¹²

***In situ* synthesis of 1,3- $\{(\text{Cl}_2\text{PO})_2\text{C}_6\text{H}_4\}$ (4-3)**

To a cooled solution (-78°C) of **4-4** (0.500 g, 0.876 mmol) in Et_2O (20 cm^3) was added a solution of HCl (4.7 cm^3 , 2M in Et_2O , 9.4 mmol) in Et_2O (10 cm^3), dropwise over a period of 1 hour. The reaction mixture was allowed to warm to RT overnight.

$^{31}\text{P}\{^1\text{H}\}$ NMR (162 MHz, Et_2O , C_6D_6 capillary locktube) δ : 179.2 (s).

Synthesis of 1,3-(((ⁱPr₂N)₂PO)₂C₆H₄) (4-4)



A solution of $\text{ClP}(\text{N}^i\text{Pr}_2)_2$ (1.714 g, 6.42 mmol) in Et_2O (30 cm^3) was added dropwise to a cooled solution ($-40\text{ }^\circ\text{C}$) of resorcinol (0.345 g, 3.13 mmol), NEt_3 (1.10 cm^3 , 0.799 g, 7.89 mmol) and Et_2O (60 cm^3). The resulting mixture was stirred for an additional 15 minutes then allowed to warm to RT overnight. A white solid was removed by filtration, and the residue washed with Et_2O (2 x 20 cm^3). The washings were combined and the solvent removed *in vacuo*. The product was extracted into hexane (40 cm^3) and the volatile components removed under reduced pressure to leave the desired compounds as a white solid (1.68 g, 94 %).

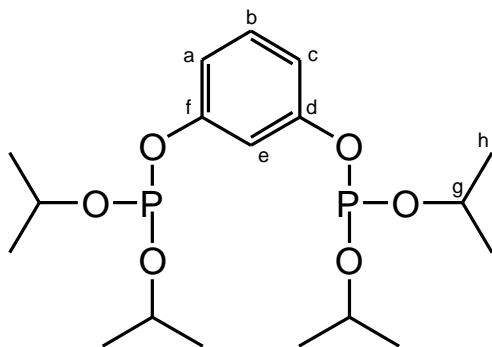
¹H NMR (700 MHz, CDCl_3) δ : 1.17 (24H, $^3J_{\text{HH}} = 6.7\text{ Hz}$, H_h), 1.21 (24H, $^3J_{\text{HH}} = 7.0\text{ Hz}$, H_h), 3.58-3.66 (8H, m, H_g), 6.65 (2H, t, $^3J_{\text{HH}} = 8.2\text{ Hz}$, $\text{H}_{a/c}$), 6.79-6.81 (1H, m, H_e), 7.06 (1H, t, $^3J_{\text{HH}} = 8.2\text{ Hz}$, H_b).

¹³C{¹H} NMR (176 MHz, CDCl_3) δ : 23.9 (d, $^3J_{\text{PC}} = 4\text{ Hz}$, C_h), 24.2 (d, $^3J_{\text{PC}} = 9\text{ Hz}$, C_h), 44.82 (d, $^2J_{\text{PC}} = 12\text{ Hz}$, C_g), 109.4 (t, $^3J_{\text{PC}} = 11\text{ Hz}$, C_e), 111.1 (d, $^3J_{\text{PC}} = 12\text{ Hz}$, $\text{C}_{a/c}$), 128.8 (s, H_b), 156.8 (d, $^2J_{\text{PC}} = 10\text{ Hz}$, $\text{C}_{d/f}$).

³¹P{¹H} NMR (161 MHz, CDCl_3) δ : 119.4 (s).

CHN: $\text{C}_{30}\text{H}_{60}\text{N}_4\text{O}_2\text{P}_2$ requires C, 63.13; H, 10.60; N, 9.82%. Found: C, 62.96; H, 10.77; N, 9.73%.

Synthesis of 1,3-(((ⁱPrO)₂PO)₂C₆H₄) (4-5)



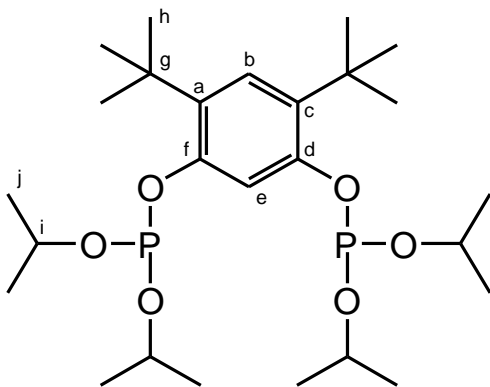
A solution of HCl (4.7 cm³, 2M in Et₂O, 9.4 mmol) in Et₂O (10 cm³) was added dropwise to a cooled solution (-78°C) of **4-4** (0.500 g, 0.876 mmol) in Et₂O (20 cm³). The reaction mixture was allowed to warm to RT overnight. The subsequent mixture was diluted with Et₂O (70 cm³) and cooled (-78 °C). NEt₃ (1.30 cm³, 9.33 mmol) and ⁱPrOH (0.27 cm³, 3.53 mmol) was added *via* syringe, the reaction mixture was allowed to reach RT over 4 h. A white solid was separated from solution by filtration, and the residue washed with Et₂O (2 x 20 cm³). The volatile components were removed *in vacuo*, the product was extracted into hexane (20 cm³) and the solvent removed under reduced pressure to produce the title compound as a pale yellow oil (0.26 g, 73%).

¹H NMR (400 MHz, CDCl₃) δ: 1.26 (24H, dd, ³J_{HH} = 6.4 Hz, ⁴J_{PH} = 1.5 Hz, H_h), 4.54-4.63 (4H, m, H_g) 6.75-6.84 (3H, m, H_{a/c/e}), 7.15 (1H, t, ³J_{HH} = 8.3 Hz, H_b).

¹³C{¹H} NMR (101 MHz, CDCl₃) δ: 24.5 (d, ³J_{PC} = 3 Hz, C_h), 67.0 (d, ²J_{PC} = 10 Hz, C_g) 112.0 (t, ³J_{PC} = 9 Hz, C_e), 114.5 (d, ³J_{PC} = 9 Hz, C_{a/Cc}), 129.7 (s, C_b), 153.9 (d, ²J_{PC} = 7 Hz, C_{d/Cf}).

³¹P{¹H} NMR (162 MHz, CDCl₃) δ: 135.2 (s).

Synthesis of 1,3-(((ⁱPrO)₂PO)₂C₁₄H₂₀) (4-8)



A solution of ⁱPrOH (3.3 cm³, 2.6 g, 43 mmol) in Et₂O (50 cm³) was added dropwise to a cooled (−40 °C) solution of **4-6** (4.000 g, 9.43 mmol) and NEt₃ (7.9 cm³, 5.7 g, 57 mmol) in Et₂O (150 cm³). The resulting mixture was stirred overnight at RT. All insoluble material was removed by filtration and all volatile components were removed *in vacuo*. Extraction in hexane (20 cm³) and subsequent removal of solvent resulted in the formation of the title compound as a pale yellow solid (3.52 g, 72%).

¹H NMR (700 MHz, CDCl₃) δ: 1.29-1.33 (24H, m, H_j), 1.40 (18H, s, H_h), 4.62-4.68 (4H, m, H_i), 7.08 (1H, ³J_{PH} = 2.0 Hz, H_e), 7.25 (1H, s, H_b).

¹³C{¹H} NMR (176 MHz, CDCl₃) δ: 24.8 (d, ²J_{PC} = 3 Hz, C_j), 24.9 (d, ²J_{PC} = 3 Hz, C_i), 30.3 (s, C_h), 34.7 (s, C_g), 67.2 (d, ²J_{PC} = 10 Hz, C_i), 110.6 (t, ³J_{PC} = 19 Hz, C_e), 125.3 (s, C_b), 132.8 (s, C_{a/c}), 150.3 (d, ²J_{PC} = 8 Hz, C_{d/f}).

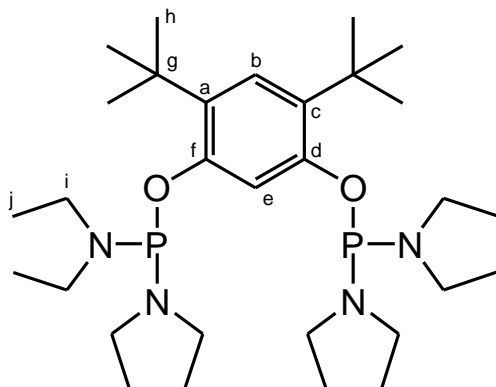
³¹P{¹H} NMR (283 MHz, CDCl₃) δ: 134.9 (s).

CHN: C₂₆H₄₈O₆P₂ requires C, 60.22; H, 9.33; N, 0.00%. Found: C, 60.09; H, 9.43; N, 0.00%.

4-8.Se

³¹P{¹H} NMR (162 MHz, CDCl₃) δ: 58.9 (s + satellites, ¹J_{SeP} = 965 Hz).

Synthesis of 1,3-(((Et₂N)₂PO)₂C₁₄H₂₀) (4-9)



A solution of HNEt₂ (9.8 cm³, 6.9 g, 95 mmol) in Et₂O (50 cm³) was added dropwise to a cooled (−40 °C) solution of **4-6** (4.000 g, 9.43 mmol) in Et₂O (150 cm³). The resulting mixture was stirred overnight at RT. Subsequently, all insoluble material was removed by filtration and all volatile components were removed *in vacuo*. Extraction into hexane (20 cm³) and subsequent removal of solvent resulted in the formation of the title compound as a yellow oil that slowly solidified into a yellow solid (3.88 g, 72%).

¹H NMR (600 MHz, CDCl₃) δ: 1.08 (24H, ³J_{HH} = 7.3 Hz, H_i), 1.39 (18H, s, H_h), 3.15-3.24 (16H, m, H_i), 6.86 (1H, ³J_{PH} = 3.0 Hz, H_e), 7.16 (1H, s, H_b).

¹³C{¹H} NMR (151 MHz, CDCl₃) δ: 14.7-14.9 (m, C_i), 30.3 (s, C_h), 34.6 (s, C_g), 39.5 (d, ²J_{PC} = 19 Hz, C_i), 108.2 (t, ³J_{PC} = 23 Hz, C_e), 124.3 (s, C_b), 130.1 (d, ³J_{PC} = 1 Hz, C_{a/c}), 153.0 (d, ²J_{PC} = 9 Hz, C_{d/f}).

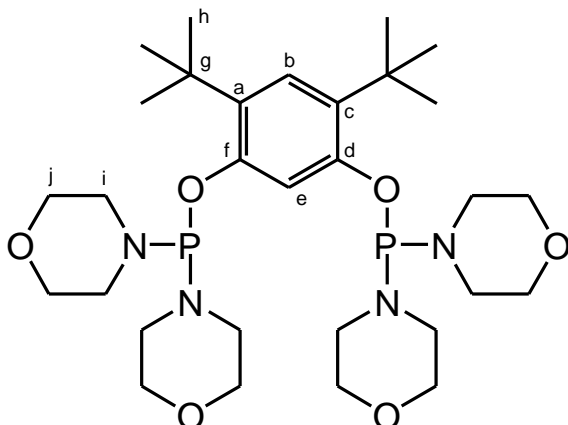
³¹P{¹H} NMR (243 MHz, CDCl₃) δ: 126.2 (s).

CHN: C₃₀H₆₀N₄O₂P₂ requires C, 63.13; H, 10.60; N, 9.82%. Found: C, 63.01; H, 10.49; N, 9.74%.

4-9.Se

³¹P{¹H} NMR (162 MHz, CDCl₃) δ: 71.1 (s + satellites, ¹J_{SeP} = 855 Hz).

Synthesis of 1,3-(((OH₈C₄N)₂PO)₂C₁₄H₂₀) (4-10)



A solution of morpholine (8.2 cm³, 8.2 g, 94 mmol) in Et₂O (50 cm³) was added dropwise to a cooled (−40 °C) solution of **4-6** (4.000 g, 9.43 mmol) in Et₂O (150 cm³). The resulting mixture was stirred overnight at RT. Next, all insoluble material was removed by filtration and all volatile components were removed *in vacuo*. Washing the resulting solid with hexane (2 × 20 cm³) resulted in the isolation of the title compound as a white solid (2.24 g, 38%).

¹H NMR (600 MHz, CDCl₃) δ: 1.38 (18H, s, H_h), 3.10-3.18 (16H, m, H_i), 3.64-3.69 (16H, m, H_j), 7.02 (1H, ³J_{PH} = 2.8 Hz, H_e), 7.22 (1H, s, H_b).

¹³C{¹H} NMR (151 MHz, CDCl₃) δ: 30.2 (s, C_h), 34.7 (s, C_g), 45.4-45.6 (m, C_i), 67.7-68.1 (m, C_j), 107.5 (t, ³J_{PC} = 21 Hz, C_e), 125.2 (s, C_b), 131.1 (d, ³J_{PC} = 2 Hz, C_{a/c}), 152.2 (d, ²J_{PC} = 8 Hz, C_{d/f}).

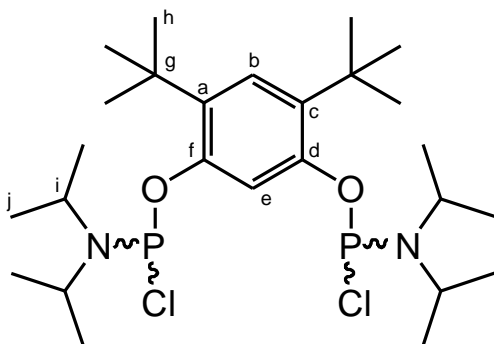
³¹P{¹H} NMR (243 MHz, CDCl₃) δ: 121.4 (s).

CHN: C₃₀H₅₂N₄O₆P₂ requires C, 57.49; H, 8.36; N, 8.94%. Found: C, 57.57; H, 8.44; N, 9.07%.

4-10.Se

³¹P{¹H} NMR (162 MHz, CDCl₃) δ: 73.2 (s + satellites, ¹J_{SeP} = 881 Hz).

Synthesis of 1,3-(((ⁱPr₂N)Cl)PO)₂C₁₄H₂₀ (4-11)



A solution of HNⁱPr₂ (4.0 cm³, 2.9 g, 29 mmol) in Et₂O (20 cm³) was added drop-wise to a cooled (−40 °C) solution of **4-6** (2.000 g, 4.72 mmol) in Et₂O (60 cm³). The resulting mixture was stirred overnight at RT. Then, all insoluble material was removed by filtration and all volatile components were removed *in vacuo*. Extraction into hexane (40 cm³) and subsequent removal of solvent resulted in the formation of a pale yellow solid (2.025 g).

Analysis by ¹H and ³¹P NMR spectroscopy revealed the formation of the di-substituted species **4-11**. ¹H NMR spectroscopy indicated that two diastereoisomers had formed in a 1:0.8 (**4-11a**:**4-11b**) ratio.

All efforts to separate the two isomers failed.

CHN: C₂₆H₄₈Cl₂N₂O₂P₂ requires C, 56.42; H, 8.74; N, 5.06%. Found: C, 56.59; H, 8.66; N, 4.96%.

Diastereoisomer 1 (**4-11a**):

¹H NMR (600 MHz, CDCl₃) δ: 0.90 (12H, d, ³J_{HH} = 6.9 Hz, H_j), 0.93 (12H, d, ³J_{HH} = 6.8 Hz, H_i), 1.26 (18H, s, H_h), 3.44-3.63 (4H, m, H_i), 7.25 (1H, s, H_b), 7.62 (1H, t, ⁴J_{PH} = 3.0 Hz, H_e).

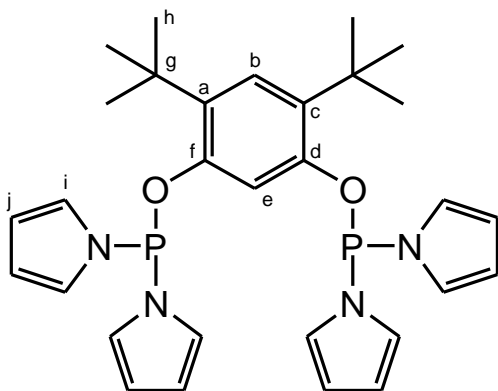
³¹P{¹H} NMR (243 MHz, CDCl₃) δ: 164.8 (s).

Diastereoisomer 2 (**4-11b**):

¹H NMR (600 MHz, CDCl₃) δ: 0.88 (12H, d, ³J_{HH} = 6.9 Hz, H_j), 0.92 (12H, d, ³J_{HH} = 6.8 Hz, H_i), 1.25 (18H, s, H_h), 3.44-3.63 (4H, m, H_i), 6.91 (1H, s, H_b), 7.74 (1H, t, ⁴J_{PH} = 2.6 Hz, H_e).

³¹P{¹H} NMR (243 MHz, CDCl₃) δ: 165.0 (s).

Synthesis of 1,3-(((pyr)₂PO)₂C₁₄H₂₀) (4-12)



A solution of 4,6-di-tert-butylresorcinol (3.440 g, 15.5 mmol) in THF (50 cm³) was added dropwise to a cooled (−40 °C) stirred solution of ClP(*N*-pyrrole)₂ (6.14 g, 31 mmol) and NEt₃ (10 cm³, 6.5 g, 65 mmol); the reaction mixture was allowed to warm to RT and stirred for 1h. Subsequent removal of all volatile components *in vacuo* and recrystallization from hexane allowed the isolation of the title compound in good yield, (6.67 g, 79%).

¹H NMR (600 MHz, CDCl₃) δ: 1.30 (18H, s, H_h), 6.20 (1H, ³J_{PH} = 2.0 Hz, H_e), 6.38-6.40 (8H, m, H_i), 7.06-7.09 (8H, m, H_i), 7.35 (1H, s, H_b).

¹³C{¹H} NMR (151 MHz, CDCl₃) δ: 30.1 (s, C_h), 34.6 (s, C_g), 109.0 (t, ³J_{PC} = 18 Hz, C_e), 112.9 (d, ³J_{PC} = 5 Hz, C_i), 121.7 (d, ²J_{PC} = 16 Hz, C_i), 126.3 (s, C_b), 135.0 (d, ³J_{PC} = 3 Hz, C_{a/c}), 150.9 (d, ²J_{PC} = 12 Hz, C_{d/f}).

³¹P{¹H} NMR (243 MHz, CDCl₃) δ: 104.6 (s).

CHN: C₃₀H₃₆N₄O₂P₂ requires C, 65.92; H, 6.64; N, 10.25%. Found: C, 65.84; H, 6.73; N, 10.16%.

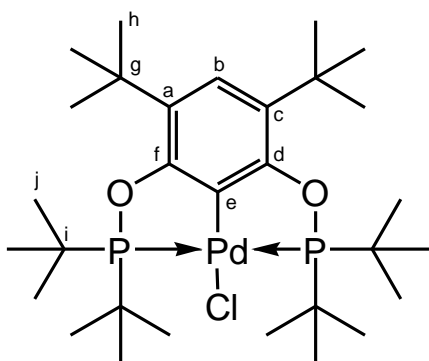
4-12.Se

³¹P{¹H} NMR (162 MHz, CDCl₃) δ: 50.8 (s + satellites, ¹J_{SeP} = 993 Hz).

General procedure for the synthesis of $[\text{PdCl}(\kappa^3\text{-P,C,P-L})]$, L = 4-7 to 4-10, 4-12

A solution of each ligand (1.000 g) and an equimolar quantity of $[\text{PdCl}_2(\text{MeCN})_2]$ in DCE (20 cm^3) is stirred for 15 mins before 1.5 equivalents of NEt_3 are added and the system heated at $80 \text{ }^\circ\text{C}$ for 2 h. All volatile components are removed *in vacuo* and appropriate work-up performed, detailed below.

Synthesis of $[\text{PdCl}(\kappa^3\text{-P,C,P-4-7})]$ (4-13)



Using the general procedure described above, with the following work-up: the resulting solid residue was recrystallized from hot ($60 \text{ }^\circ\text{C}$) hexane to give the title complex as a white solid (0.80 g, 63%).

^1H NMR (700 MHz, CDCl_3) δ : 1.38 (18H, s, H_h), 1.47 (36H, vt, $J = 7.5 \text{ Hz}$, H_j), 6.96 (1H, s, H_b).

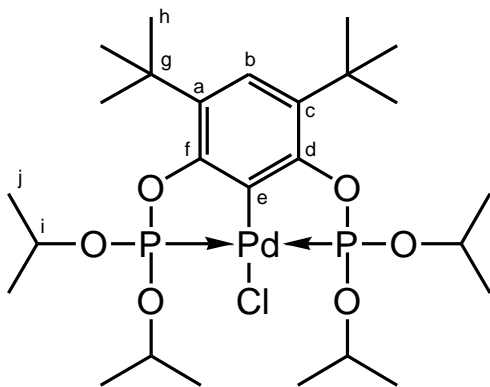
$^{13}\text{C}\{^1\text{H}\}$ NMR (176 MHz, CDCl_3) δ : 28.1 (vt, $J = 4 \text{ Hz}$, C_j), 30.5 (s, C_h), 34.6 (s, C_g), 39.9 (vt, $J = 8 \text{ Hz}$, C_i), 123.1 (s, C_b), 127.2 (t, $^3J_{\text{PC}} = 6 \text{ Hz}$, C_e), 134.4 (s, $\text{C}_{a/c}$), 162.5 (vt, $J = 6 \text{ Hz}$, $\text{C}_{d/f}$).

$^{31}\text{P}\{^1\text{H}\}$ NMR (283 MHz, CDCl_3) δ : 191.3 (s).

CHN: $\text{C}_{30}\text{H}_{55}\text{ClO}_2\text{P}_2\text{Pd}$ requires C, 55.30; H, 8.51; N, 0.00%. Found: C, 55.18; H, 8.65; N, 0.00%.

MS (ASAP+): 652 (M) $^+$, 617 ($\text{M}-\text{Cl}$) $^+$.

Synthesis of $[\text{PdCl}(\kappa^3\text{-P,C,P-4-8})]$ (4-14)



Using the general procedure described above, with the following work-up: the resulting solid residue was recrystallized twice from hot (60 °C) hexane to give the title complex as a pale beige solid (0.76 g, 76%).

$^1\text{H NMR}$ (700 MHz, CDCl_3) δ : 1.34 (12H, d, $^3J_{\text{PC}} = 6.3$ Hz, H_j), 1.45 (12H, d, $^3J_{\text{PC}} = 6.3$ Hz, H_i), 1.35 (18H, s, H_h), 4.94-4.99 (4H, m, H_i), 7.11 (1H, s, H_b).

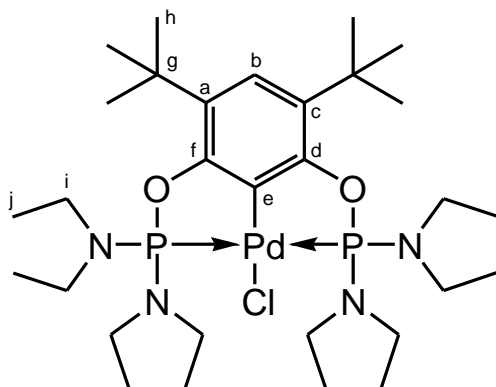
$^{13}\text{C}\{^1\text{H}\}$ NMR (176 MHz, CDCl_3) δ : 24.1 (vt, $J = 2$ Hz, C_j), 24.3 (vt, $J = 2$ Hz, C_i), 30.0 (s, C_h), 34.8 (s, C_g), 73.0 (m, C_i), 124.9 (s, C_b), 129.1 (t, $^3J_{\text{PC}} = 8$ Hz, C_e), 131.8 (vt, $J = 5$ Hz, $\text{C}_{a/c}$), 152.8 (vt, $J = 10$ Hz, $\text{C}_{d/f}$).

$^{31}\text{P}\{^1\text{H}\}$ NMR (283 MHz, CDCl_3) δ : 140.6 (s).

CHN: $\text{C}_{26}\text{H}_{47}\text{ClO}_6\text{P}_2\text{Pd}$ requires C, 47.35; H, 7.18; N, 0.00%. Found: C, 47.37; H, 7.26; N, 0.00%.

MS (ASAP+): 660 (M) $^+$, 625 ($\text{M}-\text{Cl}$) $^+$.

Synthesis of [PdCl(κ^3 -P,C,P-4-9)] (4-15)



Using the general procedure described above, with the following work-up: the resulting solid residue was recrystallized from hot (60 °C) hexane to give the title complex as a pale yellow solid (0.70 g, 70%).

^1H NMR (600 MHz, CDCl_3) δ : 1.12 (24H, $^3J_{\text{HH}} = 7.3$ Hz, H_j), 1.34 (18H, s, H_h), 3.20-3.36 (16H, m, H_i), 7.02 (1H, s, H_b).

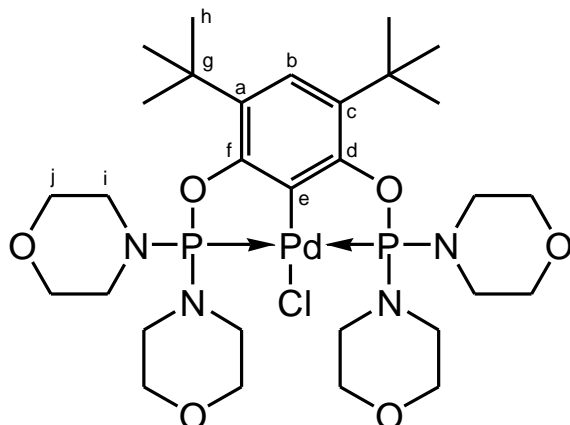
$^{13}\text{C}\{^1\text{H}\}$ NMR (151 MHz, CDCl_3) δ : 14.2 (bs, C_j), 30.3 (s, C_h), 34.8 (s, C_g), 39.5 (vt, $J = 6$ Hz, C_i), 123.7 (s, C_b), 127.4 (t, $^3J_{\text{PC}} = 8$ Hz, C_e), 132.6 (vt, $J = 4$ Hz, $\text{C}_{a/c}$), 155.6 (vt, $J = 10$ Hz, $\text{C}_{d/f}$).

$^{31}\text{P}\{^1\text{H}\}$ NMR (243 MHz, CDCl_3) δ : 147.4 (s).

CHN: $\text{C}_{30}\text{H}_{59}\text{ClN}_4\text{O}_2\text{P}_2\text{Pd}$ requires C, 50.63; H, 8.36; N, 7.87%. Found: C, 50.71; H, 8.46; N, 7.84%.

MS (ASAP+): 712 (M) $^+$, 677 ($\text{M}-\text{Cl}$) $^+$.

Synthesis of $[\text{PdCl}(\kappa^3\text{-P,C,P-4-10})]$ (4-16)



Using the general procedure described above, with the following work-up: the resulting solid residue was extracted into toluene (20 cm³), removal of the solvent and washing with Et₂O (2 × 10 cm³) resulted in the isolation of the title complex as a white solid (0.72 g, 72%).

¹H NMR (600 MHz, CDCl₃) δ: 1.33 (18H, s, H_h), 3.28-3.36 (16H, m, H_i), 3.67-3.75 (16H, m, H_j), 7.07 (1H, s, H_b).

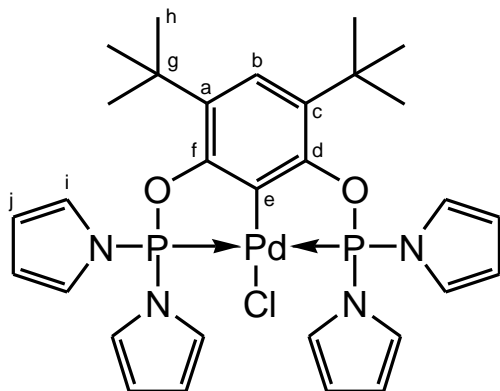
¹³C{¹H} NMR (151 MHz, CDCl₃) δ: 30.2 (s, C_h), 34.9 (s, C_g), 45.5-45.6 (m, C_i), 67.2-67.3 (m, C_j), 124.7 (s, C_b), 128.3 (t, ³J_{PC} = 8 Hz, C_e), 131.8 (vt, J = 5 Hz, C_{a/c}), 155.5 (vt, J = 9 Hz, C_{d/f}).

³¹P{¹H} NMR (243 MHz, CDCl₃) δ: 142.9 (s).

CHN: C₃₀H₅₁ClN₄O₆P₂Pd requires C, 46.94; H, 6.70; N, 7.30%. Found: C, 47.09; H, 6.82; N, 7.15%.

MS (ASAP+): 768 (M)⁺, 733 (M-Cl)⁺.

Synthesis of [PdCl(κ^3 -P,C,P-4-12)] (4-17)



Using the general procedure described above, with the following work-up: the resulting solid residue was extracted into hexane (80 cm³), removal of the solvent and washing with very cold (−78 °C) hexane (2 × 10 cm³) resulted in the isolation of the title complex as a brown solid (0.35 g, 28%).

¹H NMR (700 MHz, CDCl₃) δ: 1.33 (18H, s, H_h), 6.45-6.47 (8H, m, H_i), 7.23 (1H, s, H_b), 7.27-7.30 (8H, m, H_i).

¹³C{¹H} NMR (176 MHz, CDCl₃) δ: 30.2 (s, C_h), 35.1 (s, C_g), 115.5 (vt, *J* = 4 Hz, C_i), 122.9 (vt, *J* = 5 Hz, C_i), 126.1 (s, C_b), 131.1 (t, ³*J*_{PC} = 8 Hz, C_e), 133.3 (vt, *J* = 5 Hz, C_{a/c}), 155.7 (vt, *J* = 9 Hz, C_{d/f}).

³¹P{¹H} NMR (283 MHz, CDCl₃) δ: 126.3 (s).

CHN: C₃₀H₃₅ClN₄O₂P₂Pd requires C, 52.41; H, 5.13; N, 8.15%. Found: C, 52.57; H, 5.23; N, 8.25%.

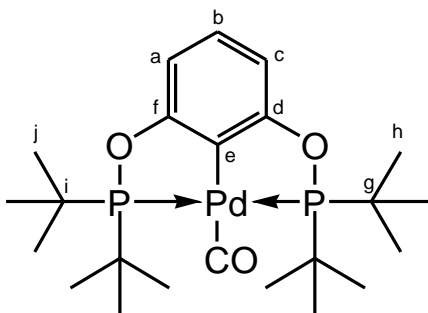
MS (ASAP+): 688 (M)⁺, 653 (M-Cl)⁺.

General procedure for the for the synthesis of $[\text{Pd}(\text{CO})(\kappa^3\text{-P,C,P-L})]\text{BF}_4$, L = 4-1, 4-7 to 4-10

AgBF_4 (5 mg, 0.03 mmol) is added to a solution of an equimolar amount of each palladium chloride complex in $\text{d}_2\text{-DCM}$ (0.8 cm^3), located in a NMR tube. The reaction mixture was stood for 15 mins with rigorous exclusion of light and occasional shaking. The solution was isolated by filtration through Celite into a NMR tube fitted with a J. Young's valve, the NMR tube was then degassed by freeze-pump-thaw method and back-filled with CO (1 atm), yielding the carbonyl adduct.

CO release from the palladium carbonyl complexes was observed under reduced pressure, hence elemental analysis was not obtained.

Synthesis of $[\text{Pd}(\text{CO})(\kappa^3\text{-P,C,P-4-1})]\text{BF}_4$ (4-18)



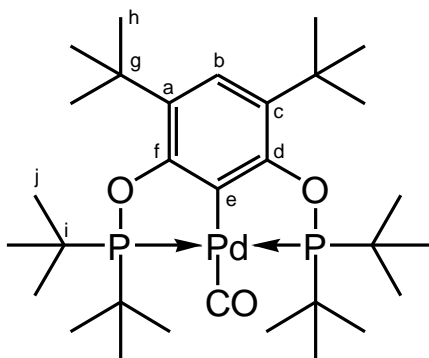
$^1\text{H NMR}$ (700 MHz, $\text{d}_2\text{-DCM}$) δ : 1.41-1.45 (36H, m, $\text{H}_{\text{h/j}}$), 6.81 (2H, d, $^3J_{\text{HH}} = 8.2 \text{ Hz}$, $\text{H}_{\text{a/c}}$), 7.25 (1H, t, $^3J_{\text{HH}} = 8.2 \text{ Hz}$, H_{b}).

$^{13}\text{C}\{^1\text{H}\}$ NMR (176 MHz, $\text{d}_2\text{-DCM}$) δ : 28.1 (vt, $J = 3 \text{ Hz}$ $\text{C}_{\text{h/j}}$), 41.5 (vt, $J = 9 \text{ Hz}$, $\text{C}_{\text{g/i}}$), 108.0 (vt, $J = 7 \text{ Hz}$, $\text{C}_{\text{a/c}}$), 133.2 (s, C_{b}), 136.3 (t, $^3J_{\text{PC}} = 2 \text{ Hz}$, C_{e}), 168.6 (vt, $J = 4 \text{ Hz}$, $\text{C}_{\text{d/f}}$), 183.0 (t, $^3J_{\text{PC}} = 11 \text{ Hz}$, CO).

$^{31}\text{P}\{^1\text{H}\}$ NMR (202 MHz, $\text{d}_2\text{-DCM}$) δ : 213.7 (s).

IR (KBr, $\text{d}_2\text{-DCM}$ solution): 2119 cm^{-1} , C=O.

Synthesis of $[\text{Pd}(\text{CO})(\kappa^3\text{-P,C,P-4-7})]\text{BF}_4$ (4-19)



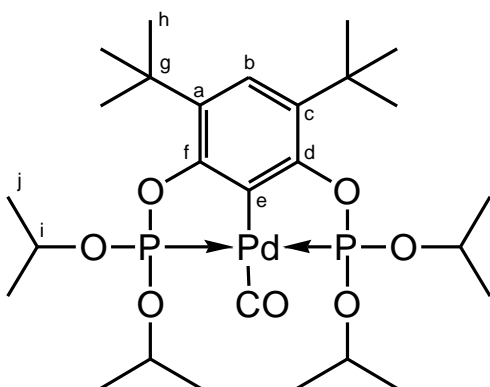
$^1\text{H NMR}$ (700 MHz, $\text{d}_2\text{-DCM}$) δ : 1.40 (18H, s, H_h), 1.45-1.48 (36H, H_j), 7.27 (1H, s, H_b).

$^{13}\text{C}\{^1\text{H}\}$ NMR (176 MHz, $\text{d}_2\text{-DCM}$) δ : 28.4 (vt, $J = 3$ Hz, C_j), 30.5 (s, C_h), 35.4 (s, C_g), 41.6 (vt, $J = 9$ Hz, C_i), 128.6 (s, C_b), 130.0 (t, $^3J_{\text{PC}} = 6$ Hz, C_e), 141.5 (s, $\text{C}_{a/c}$), 164.0 (vt, $J = 4$ Hz, $\text{C}_{d/f}$), 183.4 (t, $^3J_{\text{PC}} = 12$ Hz, CO).

$^{31}\text{P}\{^1\text{H}\}$ NMR (283 MHz, $\text{d}_2\text{-DCM}$) δ : 212.5 (s).

IR (KBr, $\text{d}_2\text{-DCM}$ solution): 2116 cm^{-1} , C=O.

Synthesis of $[\text{Pd}(\text{CO})(\kappa^3\text{-P,C,P-4-8})]\text{BF}_4$ (4-20)



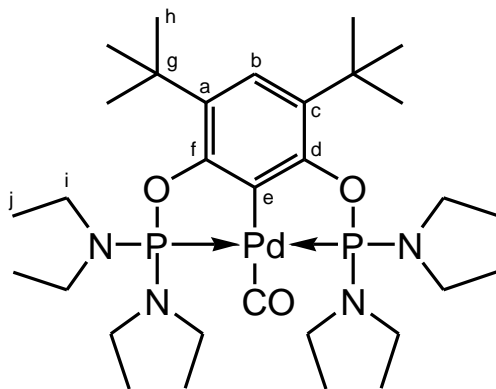
$^1\text{H NMR}$ (700 MHz, $\text{d}_2\text{-DCM}$) δ : 1.37 (18H, s, H_h), 1.44-1.47 (12H, m, H_j), 4.90-4.95 (4H, m, H_i), 7.38 (1H, s, H_b).

$^{13}\text{C}\{^1\text{H}\}$ NMR (176 MHz, $\text{d}_2\text{-DCM}$) δ : 24.4 (vt, $J = 2$ Hz, C_j), 24.5 (vt, $J = 2$ Hz, C_j), 30.1 (s, C_h), 35.6 (s, C_g), 77.1 (m, C_i), 128.7 (s, C_b), 129.5 (s, $\text{C}_{a/c}$), 130.0 (bs, CO), 131.6 (t, $^3J_{\text{PC}} = 9$ Hz, C_e), 152.9 (vt, $J = 10$ Hz, $\text{C}_{d/f}$).

$^{31}\text{P}\{^1\text{H}\}$ NMR (283 MHz, $\text{d}_2\text{-DCM}$) δ : 128.1 (s).

IR (KBr, $\text{d}_2\text{-DCM}$ solution): 2145 cm^{-1} , C=O.

Synthesis of $[\text{Pd}(\text{CO})(\kappa^3\text{-P,C,P-4-9})]\text{BF}_4$ (4-21)



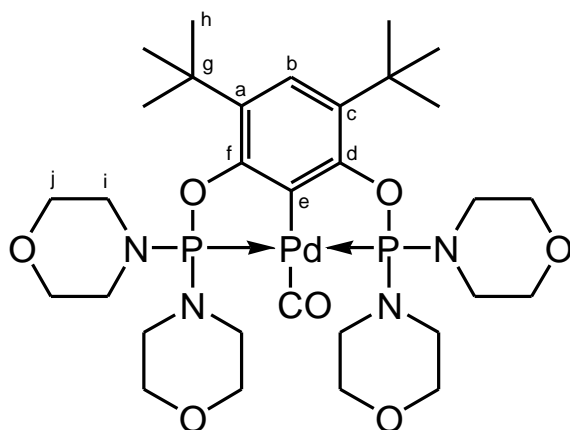
$^1\text{H NMR}$ (700 MHz, $\text{d}_2\text{-DCM}$) δ : 1.16 (24H, $^3J_{\text{HH}} = 7.1$ Hz, H_i), 1.36 (18H, s, H_h), 3.18-3.29 (16H, m, H_i), 7.31 (1H, s, H_b).

$^{13}\text{C}\{^1\text{H}\}$ NMR (176 MHz, $\text{d}_2\text{-DCM}$) δ : 14.3 (bs, C_i), 30.4 (s, C_h), 35.5 (s, C_g), 40.8 (vt, $J = 5$ Hz, C_i), 129.3 (s, C_b), 130.4 (vt, $J = 8$ Hz, $\text{C}_{a/c}$), 138.2 (t, $^3J_{\text{PC}} = 4$ Hz, C_e), 155.4 (vt, $J = 9$ Hz, $\text{C}_{d/f}$), 181.9 (t, $^3J_{\text{PC}} = 15$ Hz, CO).

$^{31}\text{P}\{^1\text{H}\}$ NMR (283 MHz, $\text{d}_2\text{-DCM}$) δ : 142.5 (s).

IR (KBr, $\text{d}_2\text{-DCM}$ solution): 2116 cm^{-1} , C=O.

Synthesis of $[\text{Pd}(\text{CO})(\kappa^3\text{-P,C,P-4-10})]\text{BF}_4$ (4-22)

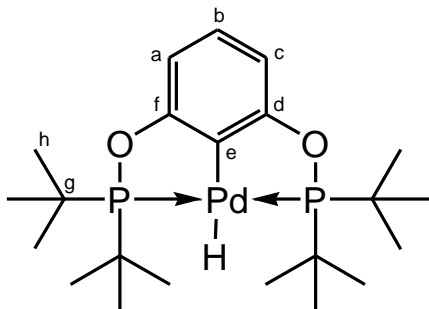


$^1\text{H NMR}$ (400 MHz, $\text{d}_2\text{-DCM}$) δ : 1.36 (18H, s, H_h), 3.20-3.33 (16H, m, H_i), 3.70-3.77 (16H, m, H_j), 7.31 (1H, s, H_b).

$^{31}\text{P}\{^1\text{H}\}$ NMR (162 MHz, $\text{d}_2\text{-DCM}$) δ : 140.0 (s).

IR (KBr, $\text{d}_2\text{-DCM}$ solution): 2136 cm^{-1} , C=O.

7.5 Chapter 5 experimental

Synthesis of $[\text{PdH}(\kappa^3\text{-P,C,P-4-1})]$ (5-1)

To a cooled ($-78\text{ }^{\circ}\text{C}$) suspension of **4-2** (0.500 g, 0.927 mmol) in Et_2O (60 cm^3) was added dropwise a solution of LiAlH_4 (1.80 cm^3 , 1 M in Et_2O , 1.80 mmol) in Et_2O (20 cm^3). The reaction mixture was allowed to warm to RT overnight. Extraction into toluene (20 cm^3) followed by hexane (30 cm^3) and recrystallization from hexane resulted in the isolation of the title complex as a white solid (0.37 g, 78%).

$^1\text{H NMR}$ (700 MHz, C_6D_6) δ : -2.49 (1H, t, $^2J_{\text{PH}} = 18.5\text{ Hz}$, Pd-H) 1.28 (36H, vt, $J = 7.5\text{ Hz}$, H_h), 6.87 (2H, dd, $^3J_{\text{HH}} = 7.9\text{ Hz}$, $^3J_{\text{PH}} = 1.2\text{ Hz}$, $\text{H}_{a/c}$), 7.01 (1H, t, $^3J_{\text{HH}} = 7.9\text{ Hz}$, H_b).

$^{13}\text{C}\{^1\text{H}\}$ NMR (176 MHz, C_6D_6) δ : 28.3 (vt, $J = 5\text{ Hz}$, C_h), 38.2 (vt, $J = 9\text{ Hz}$, C_g), 105.3 (vt, $J = 7\text{ Hz}$, $\text{C}_{a/c}$), 128.4 (s, C_b), 145.1 (t, $^2J_{\text{PC}} = 6\text{ Hz}$, C_e), 166.8 (vt, $J = 7\text{ Hz}$, $\text{C}_{d/f}$).

$^{31}\text{P}\{^1\text{H}\}$ NMR (283 MHz, C_6D_6) δ : 213.5 (s).

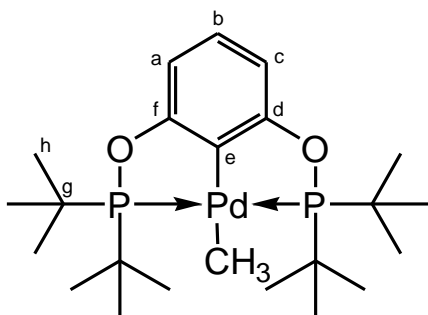
CHN: $\text{C}_{22}\text{H}_{40}\text{P}_2\text{O}_2\text{Pd}$ requires C, 52.33; H, 7.98; N, 0.00%. Found: C, 52.33; H, 8.02; N, 0.00%.

Attempted insertion of ethylene into Pd-H bond of 5-1

To a solution of **5-1** (10 mg, 0.020 mmol) in d_8 -toluene (0.7 cm³) in an NMR tube fitted with a J. Young's valve was added 1 equivalent of ethylene *via* a gas bulb.

No new products were detected by ¹H or ³¹P{¹H} NMR spectroscopy.

Synthesis of [PdMe(κ^3 -P,C,P-4-1)] (**5-2**)



MeLi (0.60 cm³, 1.6M in Et₂O, 0.96 mmol) was added dropwise to a cooled (−78 °C) solution of **4-2** (0.500 g, 0.927 mmol) in THF (20 cm³). The resulting mixture was stirred for 30 mins before being left to warm to RT and then stirred for 1 h. Extraction into toluene (20 cm³) and recrystallization from Et₂O resulted in the isolation of **5-2** as a white solid (0.24 g, 50%).

Subsequently, crystals of [PdMe(κ^3 -P,C,P-4-1)] (**5-2**) suitable for X-ray diffraction were grown by slow evaporation of Et₂O.

¹H NMR (400 MHz, CDCl₃) δ : −0.02 (3H, t, ³J_{PH} = 5.0 Hz, PdCH₃), 1.32 (36H, vt, *J* = 7.3 Hz, H_h), 6.56 (2H, d, ³J_{HH} = 8.0 Hz, H_{a/c}), 6.91 (1H, t, ³J_{HH} = 8.0 Hz, H_b).

¹³C{¹H} NMR (100 MHz, CDCl₃) δ : −17.8 (t, ²J_{PC} = 10 Hz, PdCH₃), 28.0 (vt, *J* = 4 Hz C_h), 39.4 (vt, *J* = 8 Hz, C_g), 104.4 (vt, *J* = 7 Hz, C_{a/c}), 126.7 (s, C_b), 143.1 (s, C_e), 165.9 (vt, *J* = 7 Hz, C_{d/f}).

³¹P{¹H} NMR (162 MHz, CDCl₃) δ : 193.1 (s).

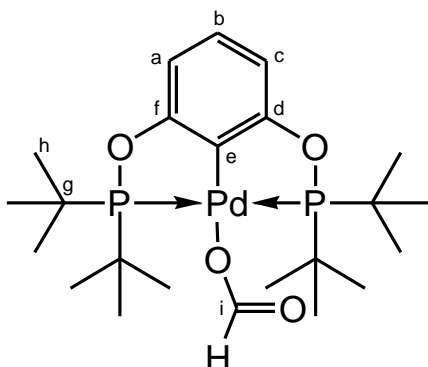
CHN: C₂₃H₄₂O₂P₂Pd requires C, 53.23; H, 8.16; N, 0.00%. Found: C, 53.38; H, 8.06; N, 0.00%.

Addition of acetone to 5-1

To a solution of **5-1** (10 mg, 0.020 mmol) in C₆D₆ (0.7 cm³) was added acetone (15 μl, 12 mg, 0.20 mmol) in a NMR tube fitted with a J. Young's valve. No reaction had taken place after 1 h heating at 60 °C. After 4 days heating at 80 °C, multiple unidentified phosphorus-containing compounds had formed in solution, and there were a few pale yellow crystals, which were subsequently isolated.

The crystals were identified as [μ-(**4-1**)Pd]₂.C₆D₆ (**5-3**) by single crystal X-ray diffraction analysis.

Synthesis of $[\text{Pd}(\text{OC}(\text{H})\text{O})(\kappa^3\text{-P,C,P-4-1})]$ (**5-4**) by insertion of CO_2 into Pd-H bond of **5-1**



An NMR tube fitted with a J. Young's valve was charged with **5-1** (20 mg, 0.040 mmol) and d_8 -THF (0.7 cm^3) to form a colourless solution. The NMR tube was then degassed by three freeze-pump-thaw cycles and back-filled with CO_2 (1 atm). Within minutes a powdery white solid had precipitated from solution. Analysis by multinuclear NMR spectroscopy revealed all starting material had been consumed and that the title complex had formed in quantitative yield. Complex **5-4** was only sparingly soluble in d_8 -THF, d_8 -toluene and insoluble in C_6D_6 .

Crystals of **5-4** suitable for X-ray diffraction were grown by slow cooling of a hot toluene solution.

The exposure of **5-4** to vacuum (1×10^{-2} mbar, 24h) resulted in the loss of CO_2 and the formation of **5-1** in quantitative yield.ⁱⁱ

^1H NMR (400 MHz, d_8 -THF) δ : 1.40 (36H, vt, $J = 7.5 \text{ Hz}$, H_h), 6.48 (2H, d, $^3J_{\text{HH}} = 7.9 \text{ Hz}$, $\text{H}_{a/c}$), 6.91 (1H, t, $^3J_{\text{HH}} = 7.9 \text{ Hz}$, H_b), 8.22 (1H, t, $^4J_{\text{PH}} = 1.6 \text{ Hz}$, H_i).

$^{13}\text{C}\{^1\text{H}\}$ NMR (100 MHz, d_8 -THF) δ : 27.7 (vt, $J = 4 \text{ Hz}$, C_h), 40.2 (vt, $J = 7 \text{ Hz}$, C_g), 106.5 (vt, $J = 7 \text{ Hz}$, $\text{C}_{a/c}$), 126.1 (s, C_b), 128.6 (s, C_e), 167.1 (s, C_i), 168.4 (vt, $J = 6 \text{ Hz}$, $\text{C}_{d/f}$).

$^{31}\text{P}\{^1\text{H}\}$ NMR (162 MHz, d_8 -THF) δ : 188.4 (s).

Alternative synthesis of **5-4**

To a solution of **5-1** (10 mg, 0.020 mmol) in C_6D_6 (0.7 cm^3) was added formic acid (8 μl , 10 mg, 0.21 mmol). Quantitative conversion to **5-4** and H_2 was achieved in less than 30 minutes, as confirmed by a ^1H and $^{31}\text{P}\{^1\text{H}\}$ NMR spectroscopy.

^1H NMR (400 MHz, C_6D_6) δ : 4.47 (s, H_2).

ⁱⁱ Due to CO_2 loss under reduced pressure elemental analyses were not obtained.

Addition of hydrogen to 5-4

An NMR tube fitted with a J. Young's valve was charged with **5-1** (10 mg, 0.020 mmol) and d_8 -toluene (0.7 cm^3). The tube was then degassed by three freeze-pump-thaw cycles and back-filled with CO_2 (1 atm). The tube then frozen (77 K) and back-filled with H_2 (1 atm).^{jj} The system was heated to 65 °C for 12 h.

No new products were detected by ^1H or $^{31}\text{P}\{^1\text{H}\}$ NMR spectroscopy.

Addition of triisopropylsilane to 5-4

An NMR tube fitted with a J. Young's valve was charged with **5-1** (10 mg, 0.020 mmol) and d_8 -toluene (0.7 cm^3). Under a flow of CO_2 , triisopropylsilane (81 μl , 63 mg, 0.40 mmol) was added *via* microsyringe. The system was heated to 60 °C for 1 h.

No new products were detected by ^1H or $^{31}\text{P}\{^1\text{H}\}$ NMR spectroscopy.

^{jj} Melting point CO_2 is 195 K and thus is not lost during the addition of H_2 .

Isomerisation of *cis*-stilbene catalysed by 5-1

An NMR tube fitted with a J. Young's valve was charged with **5-1** (5 mg, 0.010 mmol), *cis*-stilbene (18 μ l, 18 mg, 0.10 mmol), C₆D₆ (0.7 cm³). Toluene (10 μ l, 8.7 mg, 0.094 mmol) was used as an internal standard. Heating at 80 °C for 48 h resulted in 26% *cis*-stilbene being consumed, according to ¹H NMR spectroscopy.

¹H NMR (400 MHz, C₆D₆) δ : 6.45 (s, *cis*-stilbene alkene CH).

A control experiment under the same conditions, but with the omission of **5-1** resulted in no *cis*-stilbene being consumed over the same time period.

Hydrosilylation of benzaldehyde with phenylsilane catalysed by 5-1

An NMR tube fitted with a J. Young's valve was charged with **5-1** (5 mg, 0.010 mmol), benzaldehyde (12 μ l, 12 mg, 0.12 mmol), phenylsilane (33 μ l, 29 mg, 0.27 mmol) and C₆D₆ (0.7 cm³). Toluene (10 μ l, 8.7 mg, 0.094 mmol) was used as an internal standard. Heating at 80 °C for 2 h resulted in 36% benzaldehyde being consumed, according to ¹H NMR spectroscopy.

¹H NMR (400 MHz, C₆D₆) (hydrosilylation products) δ : 5.19 (s, OCH₂Ph, PhSi(OCH₂Ph)₃), 4.72 (s), 4.58 (s), 4.47 (s), 4.21 (s, free, PhSiH₃).

A control experiment under the same conditions in which **5-1** was omitted resulted in no benzaldehyde being consumed over the same time period.

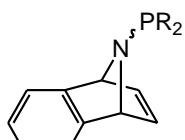
7.6 References

1. S. Komiya, *Synthesis of Organometallic Compounds - A Practical Guide* Wiley-Interscience, New York, 1998.
2. M. Lautens, K. Fagnou and V. Zunic, *Org. Lett.*, 2002, **4**, 3465-3468.
3. A. Prenzel, N. Deppermann and W. Maison, *Org. Lett.*, 2006, **8**, 1681-1684.
4. W. De Graaf, J. Boersma, W. J. J. Smeets, A. L. Spek and G. Van Koten, *Organometallics*, 1989, **8**, 2907-2917.
5. D. F. Burdi, R. Hunt, L. Fan, T. Hu, J. Wang, Z. Guo, Z. Huang, C. Wu, L. Hardy, M. Detheux, M. A. Orsini, M. S. Quinton, R. Lew and K. Spear, *J. Med. Chem.*, 2010, **53**, 7107-7118.
6. M. N. Chevykalova, L. F. Manzhukova, N. V. Artemova, Y. N. Luzikov, I. E. Nifant'ev and E. E. Nifant'ev, *Russ. Chem. Bull.*, 2003, **52**, 78-84.
7. I. Gottker-Schnetmann, P. White and M. Brookhart, *J. Am. Chem. Soc.*, 2004, **126**, 1804-1811.
8. R. B. King and P. M. Sundaram, *J. Org. Chem.*, 1984, **49**, 1784-1789.
9. R. Jackstell, H. Klein, M. Beller, K.-D. Wiese and D. Röttger, *Eur. J. Org. Chem.*, 2001, 3871-3877.
10. R. A. Baber, R. B. Bedford, M. Betham, M. E. Blake, S. J. Coles, M. F. Haddow, M. B. Hursthouse, A. G. Orpen, L. T. Pilarski, P. G. Pringle and R. L. Wingad, *Chem. Commun.*, 2006, 3880-3882.
11. A. Brück, D. Gallego, W. Wang, E. Irran, M. Driess and J. F. Hartwig, *Angew. Chem. Int. Ed.*, 2012, **51**, 11478-11482.
12. A. V. Polukeev, S. A. Kuklin, P. V. Petrovskii, S. M. Peregudova, A. F. Smol'yakov, F. M. Dolgushin and A. A. Koridze, *Dalton Trans.*, 2011, **40**, 7201-7209.

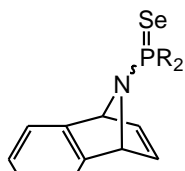
8 Appendix

8.1 Appendix 1: List of compound numbers

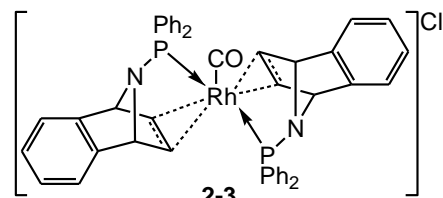
8.1.1 Chapter 2



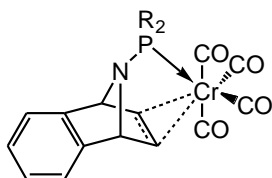
2-1 R = Ph
2-2 R = *i*Pr₂



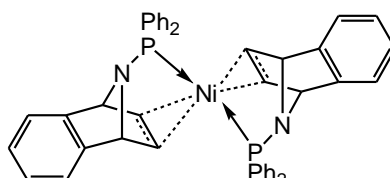
2-1.Se R = Ph
2-2.Se R = *i*Pr₂



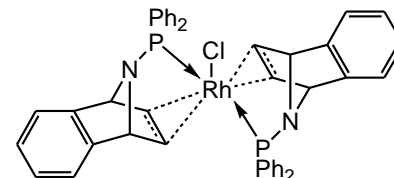
2-3



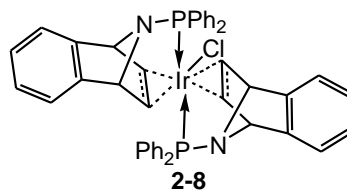
2-4 R = Ph
2-5 R = *i*Pr₂



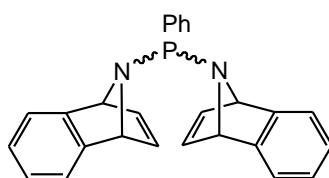
2-6



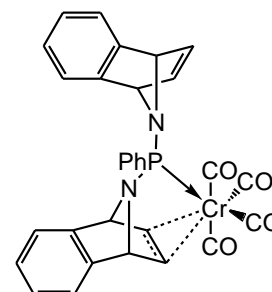
2-7



2-8

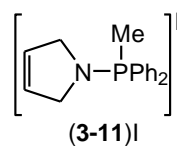
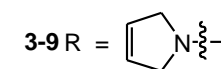
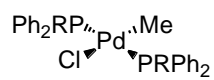
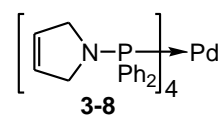
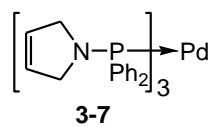
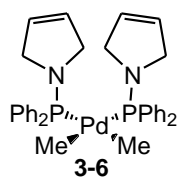
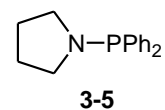
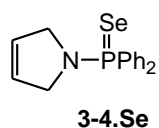
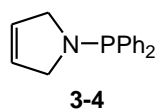
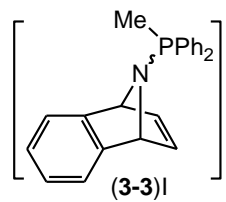
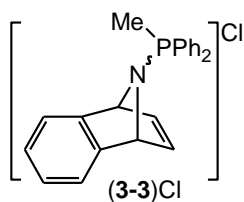
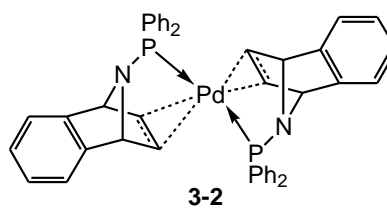
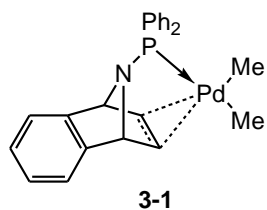


2-9

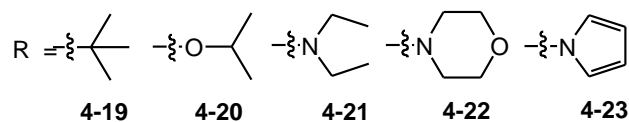
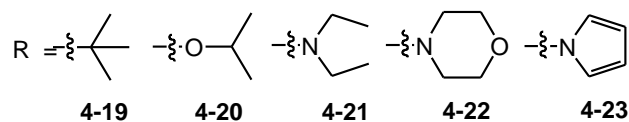
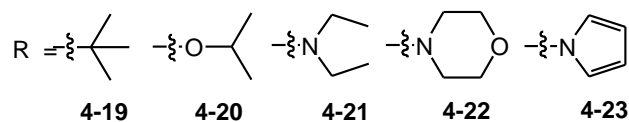
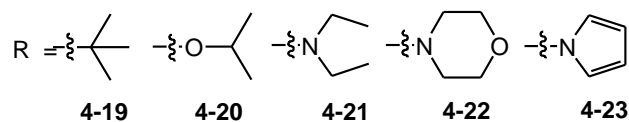
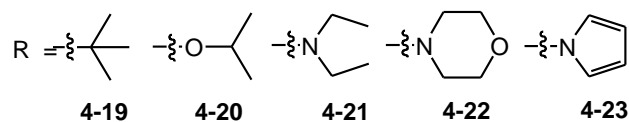
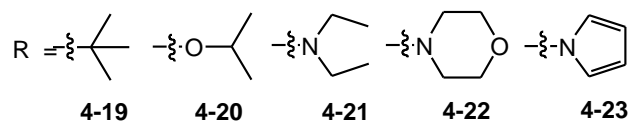
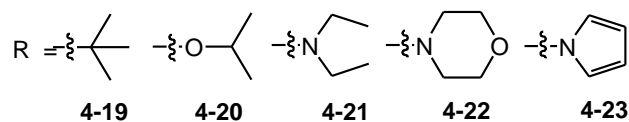
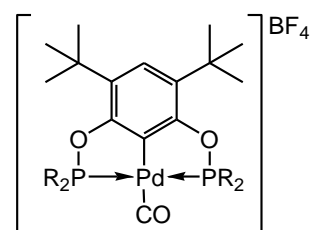
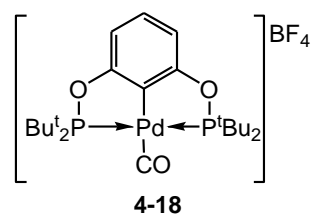
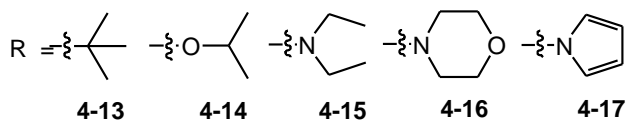
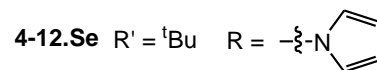
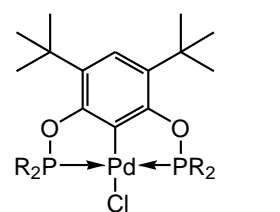
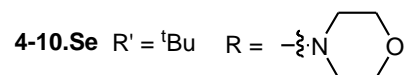
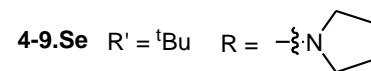
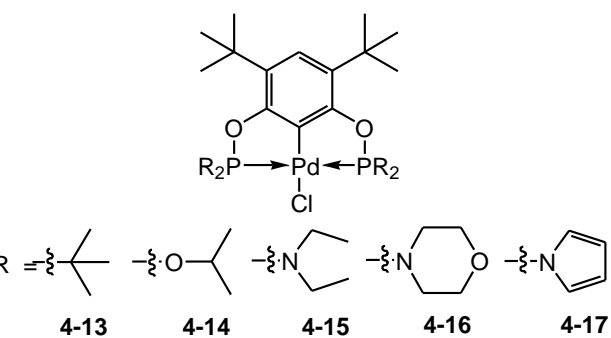
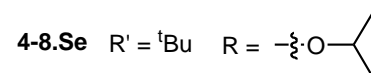
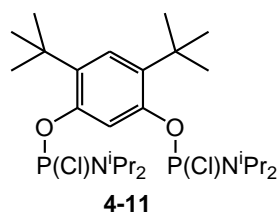
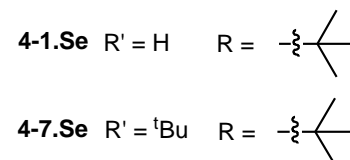
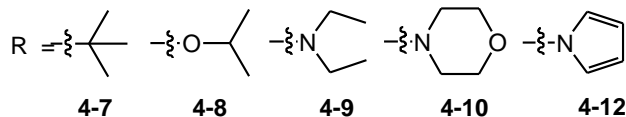
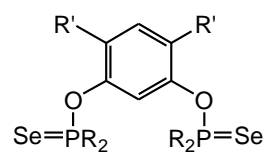
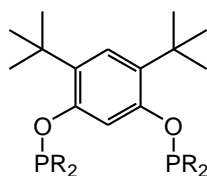
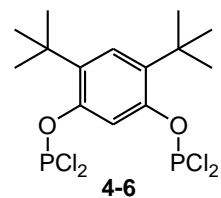
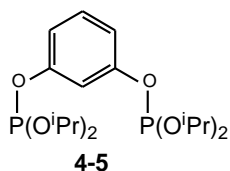
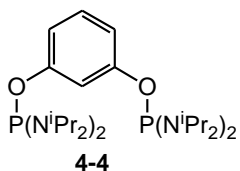
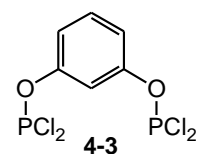
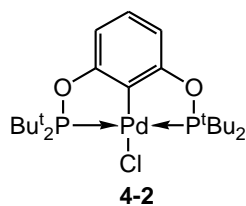
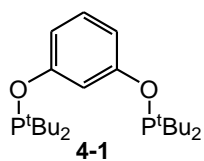


2-10

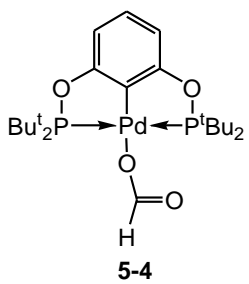
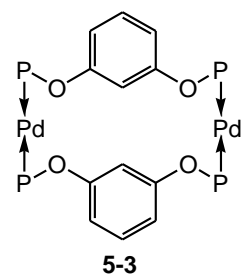
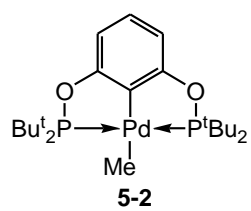
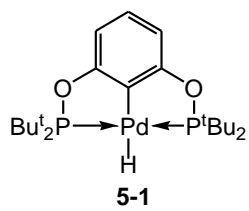
8.1.2 Chapter 3



8.1.3 Chapter 4



8.1.4 Chapter 5



8.2 Appendix 2: Crystallographic data

Complex	2-4	2-6	2-7
Empirical formula	C ₂₆ H ₁₈ NO ₄ PCr	C ₄₄ H ₃₆ N ₂ P ₂ Ni	C ₄₆ H ₄₀ Cl ₅ N ₂ P ₂ Rh
Formula weight	491.38	713.40	962.90
Temperature/K	120	120	120
Crystal system	monoclinic	triclinic	monoclinic
Space group	P2 ₁ /n	P-1	C2/c
a/Å	7.6622(3)	11.5708(8)	22.7492(11)
b/Å	16.3488(6)	12.4653(8)	11.3028(5)
c/Å	18.1159(8)	13.4651(10)	17.8360(9)
α/°	90	69.835(8)	90
β/°	94.071(13)	73.455(8)	111.466(8)
γ/°	90	80.278(8)	90
Volume/Å ³	2263.61(12)	1742.2(2)	4268.0(4)
Z	4	2	4
ρ _{calc} mg/mm ³	1.442	1.360	1.499
m/mm ⁻¹	0.610	0.684	0.824
F(000)	1008.0	744.0	1960.0
Crystal size/mm ³	0.18 × 0.08 × 0.06	0.47 × 0.23 × 0.14	0.4 × 0.3 × 0.2
Radiation	MoKα (λ = 0.71073)	MoKα (λ = 0.71073)	MoKα (λ = 0.71073)
2θ range for data collection	3.36 to 49.998 °	3.32 to 69.96 °	3.848 to 70.032 °
Index ranges	-9 ≤ h ≤ 9 -19 ≤ k ≤ 19 -21 ≤ l ≤ 21	-18 ≤ h ≤ 18 -19 ≤ k ≤ 19 -20 ≤ l ≤ 20	-36 ≤ h ≤ 36 -17 ≤ k ≤ 18 -27 ≤ l ≤ 28
Reflections collected	23621	40256	53497
Independent reflections	3985 [R _{int} = 0.0668]	14431 [R _{int} = 0.0255]	9171 [R _{int} = 0.0462]
Data/restraints/parameters	3985/97/302	14431/0/474	9171/0/260
Goodness-of-fit on F ²	0.932	1.042	1.069
Final R indexes [I ≥ 2σ (I)]	R ₁ = 0.0384 wR ₂ = 0.0802	R ₁ = 0.0358 wR ₂ = 0.0930	R ₁ = 0.0374 wR ₂ = 0.0902
Final R indexes [all data]	R ₁ = 0.0703 wR ₂ = 0.0900	R ₁ = 0.0463 wR ₂ = 0.0991	R ₁ = 0.0476 wR ₂ = 0.0965
Largest diff. peak/hole / e Å ⁻³	0.42/-0.29	1.13/-0.33	1.43/-0.97

Complex	2-8	2-10
Empirical formula	C ₄₆ H ₄₀ Cl ₅ IrN ₂ P ₂	C ₃₀ H ₂₁ CrN ₂ O ₄ P
Formula weight	1052.19	556.46
Temperature/K	150	120.0
Crystal system	monoclinic	triclinic
Space group	C2/c	P-1
a/Å	22.6894(16)	8.4949(4)
b/Å	11.2587(8)	11.7134(6)
c/Å	18.1243(17)	14.3091(7)
α/°	90	71.765(11)
β/°	111.890(11)	74.002(11)
γ/°	90	70.784(10)
Volume/Å ³	4296.1(7)	1253.09(15)
Z	4	2
ρ _{calc} mg/mm ³	1.627	1.475
m/mm ⁻¹	3.529	0.561
F(000)	2088.0	572.0
Crystal size/mm ³	0.2 × 0.15 × 0.12	0.16 × 0.1 × 0.1
Radiation	MoKα (λ = 0.71073)	MoKα (λ = 0.71073)
2θ range for data collection	3.87 to 59.992°	3.054 to 70.042°
Index ranges	-24 ≤ h ≤ 31 -15 ≤ k ≤ 11 -25 ≤ l ≤ 25	-13 ≤ h ≤ 13 -18 ≤ k ≤ 18 -22 ≤ l ≤ 22
Reflections collected	18098	53269
Independent reflections	6267 [R _{int} = 0.0518]	10464 [R _{int} = 0.0420]
Data/restraints/parameters	6267/0/282	10464/6/361
Goodness-of-fit on F ²	1.032	1.053
Final R indexes [I ≥ 2σ (I)]	R ₁ = 0.0392 wR ₂ = 0.0898	R ₁ = 0.0395 wR ₂ = 0.1049
Final R indexes [all data]	R ₁ = 0.0535 wR ₂ = 0.0972	R ₁ = 0.0480 wR ₂ = 0.1110
Largest diff. peak/hole / e Å ⁻³	1.93/-1.88	1.00/-0.32

Complex	3-1	3-2	3-7
Empirical formula	C ₄₈ H ₄₈ N ₂ P ₂ Pd ₂	C ₄₄ H ₃₆ N ₂ P ₂ Pd	C ₄₈ H ₄₈ N ₃ P ₃ Pd
Formula weight	927.62	761.09	866.20
Temperature/K	120	120	120
Crystal system	monoclinic	triclinic	monoclinic
Space group	P2 ₁ /c	P-1	P2 ₁ /c
a/Å	10.2185(3)	11.9327(3)	9.1707(5)
b/Å	10.6113(4)	12.2787(3)	18.3478(8)
c/Å	19.2717(7)	13.2937(3)	24.8596(10)
α°	90.00	70.0570(10)	90
β°	104.176(14)	74.1200(10)	97.990(7)
γ°	90.00	81.5170(10)	90
Volume/Å ³	2026.03(12)	1757.92(7)	4142.3(3)
Z	2	2	4
ρ _{calc} mg/mm ³	1.521	1.438	1.389
m/mm ⁻¹	1.003	0.654	0.602
F(000)	944.0	780.0	1792.0
Crystal size/mm ³	0.13 × 0.05 × 0.02	0.2 × 0.15 × 0.08	0.4 × 0.11 × 0.08
Radiation	MoKα (λ = 0.71073)	MoKα (λ = 0.71073)	MoKα (λ = 0.71073)
2θ range for data collection	4.12 to 60 °	3.36 to 69.98 °	2.768 to 60.002°
Index ranges	-14 ≤ h ≤ 14 -14 ≤ k ≤ 14 -27 ≤ l ≤ 27	-19 ≤ h ≤ 18 -19 ≤ k ≤ 19 -21 ≤ l ≤ 20	-12 ≤ h ≤ 12 -25 ≤ k ≤ 25 -34 ≤ l ≤ 34
Reflections collected	26057	40929	75101
Independent reflections	5912 [R _{int} = 0.0606]	14631 [R _{int} = 0.0394]	12078 [R _{int} = 0.0595]
Data/restraints/parameters	5912/0/340	14631/0/466	12078/0/508
Goodness-of-fit on F ²	0.883	1.001	1.038
Final R indexes [I ≥ 2σ (I)]	R ₁ = 0.0310 wR ₂ = 0.0557	R ₁ = 0.0355 wR ₂ = 0.0838	R ₁ = 0.0414 wR ₂ = 0.0988
Final R indexes [all data]	R ₁ = 0.0545 wR ₂ = 0.0607	R ₁ = 0.0481 wR ₂ = 0.0883	R ₁ = 0.0606 wR ₂ = 0.1109
Largest diff. peak/hole / e Å ⁻³	0.71/-0.54	1.75/-0.57	1.66/-0.77

Complex	3-9	3-10
Empirical formula	C ₃₄ H ₃₆ Cl ₃ N ₂ P ₂ Pd	C ₃₃ H ₃₉ ClN ₂ P ₂ Pd
Formula weight	747.34	667.45
Temperature/K	120	120
Crystal system	monoclinic	monoclinic
Space group	P2 ₁ /m	P2 ₁ /n
a/Å	11.2333(5)	11.6096(6)
b/Å	14.0327(7)	23.2868(13)
c/Å	11.8483(5)	12.0414(6)
α/°	90	90
β/°	117.125(5)	113.002(6)
γ/°	90	90
Volume/Å ³	1662.27(15)	2996.6(3)
Z	2	4
ρ _{calc} mg/mm ³	1.493	1.479
m/mm ⁻¹	0.922	0.841
F(000)	762.0	1376.0
Crystal size/mm ³	0.15 × 0.12 × 0.1	0.68 × 0.21 × 0.14
Radiation	MoKα (λ = 0.71073)	MoKα (λ = 0.71073)
2θ range for data collection	3.862 to 65.996°	3.498 to 69.948 °
Index ranges	-17 ≤ h ≤ 17 -21 ≤ k ≤ 21 -18 ≤ l ≤ 18	-18 ≤ h ≤ 18 -36 ≤ k ≤ 36 -19 ≤ l ≤ 19
Reflections collected	35272	69135
Independent reflections	6490 [R _{int} = 0.0292]	12767 [R _{int} = 0.0368]
Data/restraints/parameters	6490/60/213	12767/0/362
Goodness-of-fit on F ²	1.042	1.059
Final R indexes [I ≥ 2σ (I)]	R ₁ = 0.0372 wR ₂ = 0.0887	R ₁ = 0.0377 wR ₂ = 0.0919
Final R indexes [all data]	R ₁ = 0.0483 wR ₂ = 0.0970	R ₁ = 0.0502 wR ₂ = 0.0986
Largest diff. peak/hole / e Å ⁻³	1.41/-0.71	2.20/-0.74

Complex	4-2	4-13	4-14
Empirical formula	C ₂₂ H ₃₉ ClO ₂ P ₂ Pd	C ₃₀ H ₅₅ ClO ₂ P ₂ Pd	C ₂₆ H ₄₇ O ₆ P ₂ ClPd
Formula weight	539.32	651.53	659.43
Temperature/K	120	120	120
Crystal system	triclinic	monoclinic	monoclinic
Space group	P-1	P2/c	P2 ₁ /n
a/Å	8.2862(4)	11.4884(3)	9.0088(3)
b/Å	12.0042(5)	11.6968(2)	38.5884(12)
c/Å	13.3401(5)	13.2762(3)	9.0585(3)
α/°	100.322(6)	90	90.00
β/°	96.148(6)	111.603(3)	99.5630(10)
γ/°	103.855(6)	90	90.00
Volume/Å ³	1251.75(11)	1658.71(8)	3105.29(17)
Z	2	2	4
ρ _{calc} mg/mm ³	1.431	1.304	1.410
m/mm ⁻¹	0.991	0.760	6.878
F(000)	560.0	688.0	1376.0
Crystal size/mm ³	0.32 × 0.16 × 0.15	0.433 × 0.3573 × 0.1193	0.104 × 0.097 × 0.059
Radiation	MoKα (λ = 0.71073)	MoKα (λ = 0.7107)	CuKα (λ = 1.54178)
2θ range for data collection	3.58 to 60 °	6.292 to 64.124 °	6.88 to 140 °
Index ranges	-11 ≤ h ≤ 11 -16 ≤ k ≤ 16 -18 ≤ l ≤ 18	-16 ≤ h ≤ 16 -16 ≤ k ≤ 17 -19 ≤ l ≤ 19	-9 ≤ h ≤ 10 -44 ≤ k ≤ 46 -9 ≤ l ≤ 10
Reflections collected	22956	20882	20168
Independent reflections	7291 [R _{int} = 0.0299]	5396 [R _{int} = 0.0313]	5743 [R _{int} = 0.0325]
Data/restraints/parameters	7291/0/277	5396/0/183	5743/6/340
Goodness-of-fit on F ²	1.086	1.075	1.141
Final R indexes [I ≥ 2σ (I)]	R ₁ = 0.0315 wR ₂ = 0.0801	R ₁ = 0.0273 wR ₂ = 0.0618	R ₁ = 0.0378 wR ₂ = 0.0850
Final R indexes [all data]	R ₁ = 0.0355 wR ₂ = 0.0826	R ₁ = 0.0344 wR ₂ = 0.0668	R ₁ = 0.0416 wR ₂ = 0.0866
Largest diff. peak/hole / e Å ⁻³	1.43/-0.87	0.92/-0.81	2.11/-0.41

Complex	4-15	4-16	4-17
Empirical formula	C ₃₀ H ₅₉ ClN ₄ O ₂ P ₂ Pd	C ₃₀ H ₅₁ ClN ₄ O ₆ P ₂ Pd	C ₃₀ H ₃₅ ClN ₄ O ₂ P ₂ Pd
Formula weight	711.60	767.54	687.41
Temperature/K	120.0	120.0	120.0
Crystal system	monoclinic	orthorhombic	monoclinic
Space group	P2 ₁ /c	Pca2 ₁	P2 ₁ /n
a/Å	17.4846(3)	23.9712(9)	12.1743(11)
b/Å	9.52106(16)	8.7778(3)	19.3567(18)
c/Å	21.8231(4)	32.7838(11)	13.8867(13)
α/°	90	90	90
β/°	97.2077(16)	90	108.458(10)
γ/°	90	90	90
Volume/Å ³	3604.23(11)	6898.2(4)	3104.1(5)
Z	4	8	4
ρ _{calc} mg/mm ³	1.311	1.478	1.471
m/mm ⁻¹	0.708	0.755	0.821
F(000)	1504.0	3200.0	1408.0
Crystal size/mm ³	0.2667 × 0.2016 × 0.0997	0.42 × 0.09 × 0.08	0.25 × 0.22 × 0.16
Radiation	MoKα (λ = 0.71073)	MoKα (λ = 0.71073)	MoKα (λ = 0.71073)
2θ range for data collection	5.98 to 64.02 °	2.484 to 58.102 °	3.74 to 62.998 °
Index ranges	-25 ≤ h ≤ 23 -13 ≤ k ≤ 14 -32 ≤ l ≤ 29	-32 ≤ h ≤ 32 -11 ≤ k ≤ 11 -44 ≤ l ≤ 44	-17 ≤ h ≤ 17 -28 ≤ k ≤ 28 -20 ≤ l ≤ 20
Reflections collected	45817	95159	56545
Independent reflections	11597 [R _{int} = 0.0518]	18378 [R _{int} = 0.0585]	10329 [R _{int} = 0.0534]
Data/restraints/parameters	11597/46/410	18378/14/799	10329/0/373
Goodness-of-fit on F ²	1.038	1.036	1.036
Final R indexes [I ≥ 2σ (I)]	R ₁ = 0.0407 wR ₂ = 0.0780	R ₁ = 0.0400 wR ₂ = 0.0852	R ₁ = 0.0372 wR ₂ = 0.0847
Final R indexes [all data]	R ₁ = 0.0637 wR ₂ = 0.0889	R ₁ = 0.0515 wR ₂ = 0.0913	R ₁ = 0.0561 wR ₂ = 0.0960
Largest diff. peak/hole / e Å ⁻³	0.52/-0.53	0.82/-0.50	1.40/-0.67

Complex	5-2	5-3	5-4
Empirical formula	C ₂₃ H ₄₂ O ₂ P ₂ Pd	C ₂₄ H ₄₂ O ₂ P ₂ Pd	C ₂₃ H ₄₀ O ₄ P ₂ Pd
Formula weight	518.91	532.92	548.89
Temperature/K	120	120.0	120
Crystal system	triclinic	trigonal	triclinic
Space group	P-1	R-3	P-1
a/Å	8.3462(4)	40.257(5)	8.3363(3)
b/Å	11.9438(5)	40.257(5)	11.9802(5)
c/Å	13.4184(5)	8.5291(9)	13.5358(5)
α/°	100.422(6)	90	100.647(7)
β/°	95.926(6)	90	97.667(7)
γ/°	103.725(6)	120	103.692(7)
Volume/Å ³	1262.94(9)	11971(3)	1268.39(8)
Z	2	18	2
ρ _{calc} mg/mm ³	1.365	1.331	1.437
m/mm ⁻¹	0.877	0.834	0.883
F(000)	544.0	5004.0	572.0
Crystal size/mm ³	0.33 × 0.24 × 0.06	0.37 × 0.14 × 0.08	0.18 × 0.15 × 0.06
Radiation	MoKα (λ = 0.71073)	MoKα (λ = 0.71073)	MoKα (λ = 0.71073)
2θ range for data collection	3.12 to 59.98 °	3.504 to 59.994 °	3.12 to 59.98 °
Index ranges	-11 ≤ h ≤ 11 -16 ≤ k ≤ 16 -18 ≤ l ≤ 18	-55 ≤ h ≤ 56 -56 ≤ k ≤ 56 -11 ≤ l ≤ 11	-11 ≤ h ≤ 11 -16 ≤ k ≤ 16 -19 ≤ l ≤ 19
Reflections collected	23229	42310	23357
Independent reflections	7366 [R _{int} = 0.0420]	7659 [R _{int} = 0.0496]	7388 [R _{int} = 0.0315]
Data/restraints/parameters	7366/15/290	7659/0/268	7388/0/295
Goodness-of-fit on F ²	1.089	1.082	1.036
Final R indexes [I >= 2σ (I)]	R ₁ = 0.0312 wR ₂ = 0.0789	R ₁ = 0.0320, wR ₂ = 0.0727	R ₁ = 0.0269 wR ₂ = 0.0636
Final R indexes [all data]	R ₁ = 0.0363 wR ₂ = 0.0817	R ₁ = 0.0517, wR ₂ = 0.0782	R ₁ = 0.0331 wR ₂ = 0.0663
Largest diff. peak/hole / e Å ⁻³	1.38/-0.68	0.75/-0.39	1.26/-0.57

8.3 Appendix 3: Example percent buried volume (% V_{bur}) calculation

SambVca @ MoLNaC

Results page

Molecule from input :

11srv017 (Complex **4-2**)

Number of atoms : 66
 Atom that is coordinated : 1
 Atoms that define the axis : 3
 ID of these atoms : 2 3 6

Radius of sphere (Å) : 3.500
 Distance from sphere (Å) : 0.000
 Mesh step (Å) : 0.050
 H atoms omitted in the V_{bur} calculation

Cartesian coordinates from input :

H	-3.36807	1.95675	3.55204
P	-2.24801	-0.02073	3.20768
P	-4.14703	4.08645	3.19757
O	-1.39654	0.22523	1.80707
O	-3.38925	4.58608	1.81278
C	-2.40605	2.39918	1.85775
C	-1.56635	1.48108	1.23366
C	-0.88354	1.76616	0.06079
H	-0.32045	1.11681	-0.34477
C	-1.04167	3.02712	-0.50666
H	-0.57397	3.24054	-1.30651
C	-1.87564	3.98341	0.07466
H	-1.98673	4.84165	-0.31755
C	-2.53995	3.63869	1.24792
C	-3.28385	-1.48466	2.74159
C	-4.17936	-0.98674	1.61369
H	-3.62388	-0.68128	0.86711
H	-4.76003	-1.71603	1.31169
H	-4.73018	-0.24358	1.93772
C	-4.13338	-1.91678	3.93248
H	-4.55905	-1.12934	4.33169

H	-4.82368	-2.54379	3.63177
H	-3.56366	-2.35398	4.59869
C	-2.49614	-2.67932	2.22158
H	-1.98590	-3.07987	2.95519
H	-3.11483	-3.34415	1.85347
H	-1.87947	-2.38343	1.51907
C	-0.87461	-0.39132	4.39649
C	-0.14412	0.93437	4.54814
H	-0.75838	1.60787	4.90847
H	0.61293	0.82251	5.15992
H	0.18525	1.22806	3.67325
C	0.12789	-1.40838	3.88841
H	0.37393	-1.19141	2.96426
H	0.92875	-1.38890	4.45352
H	-0.27128	-2.30413	3.91822
C	-1.44984	-0.79636	5.72892
H	-1.78704	-1.71493	5.67060
H	-0.75267	-0.74739	6.41587
H	-2.18454	-0.19258	5.96482
C	-5.92209	4.19277	2.67678
C	-6.14931	2.92661	1.83014
H	-5.95885	2.13299	2.37193
H	-7.08076	2.89923	1.52685
H	-5.55291	2.94162	1.05246
C	-6.82919	4.13140	3.90902
H	-6.79041	4.98556	4.38742
H	-7.75213	3.95584	3.62789
H	-6.52681	3.41185	4.50148
C	-6.25285	5.42306	1.82496
H	-5.62537	5.47878	1.07450
H	-7.16747	5.34612	1.48148
H	-6.17753	6.23030	2.37452
C	-3.61714	5.39966	4.39922
C	-4.04134	6.80884	4.00260
H	-5.01361	6.89377	4.08542
H	-3.60526	7.45972	4.59221
H	-3.77567	6.98042	3.07443
C	-2.08990	5.31330	4.41853

H	-1.74047	5.53316	3.52938
H	-1.73472	5.94828	5.07437
H	-1.81663	4.40492	4.66220
C	-4.16286	5.05503	5.79049
H	-4.02402	4.10114	5.97000
H	-3.69235	5.58659	6.46642
H	-5.12113	5.25825	5.82613

Atoms and radius in the parameter file

H	1.29
C	1.99
N	1.81
O	1.78
F	1.72
Si	2.45
P	2.11
S	2.10
Cl	2.05
Br	2.16
I	2.31

Coordinates scaled to put the metal at the origin

H	0.00000	0.00000	0.00000
P	1.12006	-1.97748	-0.34436
P	-0.77896	2.12970	-0.35447
O	1.97153	-1.73152	-1.74496
O	-0.02118	2.62933	-1.73926
C	0.96202	0.44242	-1.69428
C	1.80172	-0.47568	-2.31837
C	2.48453	-0.19059	-3.49125
H	3.04763	-0.83994	-3.89681
C	2.32641	1.07037	-4.05870
H	2.79410	1.28378	-4.85854
C	1.49243	2.02666	-3.47738
H	1.38135	2.88489	-3.86959
C	0.82812	1.68194	-2.30412
C	0.08422	-3.44142	-0.81045
C	-0.81129	-2.94349	-1.93835

H	-0.25581	-2.63803	-2.68492
H	-1.39196	-3.67278	-2.24035
H	-1.36211	-2.20033	-1.61431
C	-0.76531	-3.87354	0.38044
H	-1.19098	-3.08610	0.77965
H	-1.45561	-4.50055	0.07974
H	-0.19559	-4.31073	1.04666
C	0.87193	-4.63608	-1.33046
H	1.38217	-5.03662	-0.59685
H	0.25325	-5.30090	-1.69856
H	1.48860	-4.34019	-2.03296
C	2.49347	-2.34807	0.84446
C	3.22395	-1.02239	0.99611
H	2.60969	-0.34888	1.35643
H	3.98100	-1.13424	1.60788
H	3.55332	-0.72869	0.12121
C	3.49596	-3.36514	0.33637
H	3.74200	-3.14816	-0.58777
H	4.29683	-3.34565	0.90149
H	3.09680	-4.26088	0.36618
C	1.91823	-2.75312	2.17689
H	1.58103	-3.67168	2.11856
H	2.61540	-2.70414	2.86384
H	1.18353	-2.14933	2.41278
C	-2.55402	2.23602	-0.87526
C	-2.78124	0.96986	-1.72189
H	-2.59078	0.17624	-1.18011
H	-3.71269	0.94247	-2.02519
H	-2.18484	0.98487	-2.49957
C	-3.46112	2.17464	0.35698
H	-3.42234	3.02880	0.83539
H	-4.38406	1.99909	0.07585
H	-3.15874	1.45510	0.94945
C	-2.88478	3.46631	-1.72708
H	-2.25730	3.52203	-2.47754
H	-3.79940	3.38937	-2.07055
H	-2.80946	4.27355	-1.17751
C	-0.24906	3.44291	0.84718

C	-0.67327	4.85209	0.45056
H	-1.64553	4.93702	0.53339
H	-0.23719	5.50297	1.04017
H	-0.40760	5.02367	-0.47760
C	1.27817	3.35654	0.86649
H	1.62760	3.57641	-0.02266
H	1.63335	3.99153	1.52234
H	1.55144	2.44816	1.11017
C	-0.79479	3.09828	2.23845
H	-0.65595	2.14439	2.41797
H	-0.32428	3.62983	2.91439
H	-1.75306	3.30150	2.27410
XX	0.00000	0.00000	0.00000

Results : Volumes in Å³

N of voxels examined :	1436277
Volume of voxel :	0.125E-03

V Free	V Buried	V Total	V Exact
52.665	126.869	179.535	179.594

%V_Free	%V_Bur	% Tot/Ex
29.334	70.666	99.967

The %V_Bur of your molecule is: 70.7

8.4 Appendix 4: Seminars attended

Ligands with strongly donating character

Yves Canac (Laboratoire de Chimie de Coordination, Toulouse)

26th October 2010

Following Function in Real Time: New NMR and Diffraction Methods for Studying Structure and Dynamics in Batteries and Fuel Cells

Clare Grey (University of Cambridge)

3rd November 2010

Controlling Emissions from Cars - Chemistry, Successes, and Challenges

Martyn Twigg (Johnson Matthey)

10th November 2010

Pincer-type Complexes of Divalent and Trivalent Ni: Redox Chemistry and Catalytic Reactivities

Davit Zargarian (University of Montreal)

26th November 2010

Highly Reactive Nitrogen Heterocycles - Synthesis and Properties

John Murphy (University of Strathclyde)

18th January 2011

Making light work of it – process analysis within petrochemicals

Andrew Poole (BP)

18th January 2011

Local Structure and Dynamics in Functional Framework Materials

Andrew Goodwin (University of Oxford)

26th January 2011

Spectroelectrochemical Studies of CO₂ Reducing Systems

Franstisek Hartl (University of Reading)

2nd February 2011

**Magnetism and Chemistry of Layered Transition Metal Oxychalcogenides and
Pnictides**

Simon Clarke (University of Oxford)

9th February 2011

Green Chemistry and Supercritical Fluids

Martyn Poliakoff (University of Nottingham)

23rd February 2011

**Ambiphilic Metal Ligand Activation from Stoichiometric to Catalytic CH
Activation**

Dai Davies (University of Leicester)

25th May 2011

The reactivity of divalent complexes of the heavier group 14 elements

Robin Fulton (University of Sussex)

30th June 2011

**Organoboron in synthetic methodology and chemical biology application in
disrupting protein-RNA interactions**

Webster Santos (Virginia Tech)

21st July 2011

Chemoselective catalytic reduction of nitriles, pyridine and acyl chlorides

Georgii Nikonov (Brock University)

16th August 2011

Molecular wires made from Fe(Cp*)(dppe) endgroups

Frederic Paul (University of Rennes)

19th October 2011

Harvesting solar energy in photo-electrochemical cells

Leone Spiccia (Monash University)

9th November 2011

Catalysis on the edge

Bob Tooze (SASOL UK)

23rd November 2011

360 Degree chemistry – Using tubes in synthesis

Ian Baxendale (University of Cambridge)

29th November 2011

Phosphine-borane-stabilised carbanions – bulky ligands of the future

Keith Izod (Newcastle University)

6th December 2011

Metal-organo cooperative catalysis: Asymmetric hydrogenation with achiral metal catalysts

Jainlaing Xiao (Liverpool University)

7th December 2011

Catalysts made from earth-abundant elements for making C-C and C-H bonds

Xile Hu (Ecole Polytechnique Federale de Lausanne (EPFL))

17th January 2012

New copper-catalyzed reactions

Matthew Gaunt (University of Cambridge)

1st February 2012

Functional Nanomaterials via living self-assembly

Ian Manners (University of Bristol)

21st February 2012

Chiral metal compounds in catalysis and medicine

Peter Scott (University of Warwick)

28th February 2012

The status of catalyst design: Case studies on C-N bond formation

John Hartwig (University of California, Berkeley)

14th May 2012

Catalytic functionalization of aryl and alkyl C-H bonds

John Hartwig (University of California, Berkeley)

15th May 2012

Making sense of copper-catalysed coupling

John Hartwig (University of California, Berkeley)

16th May 2012

Catalytic activation of carbon dioxide for polymer synthesis

Charlotte Williams (Imperial College London)

7th November 2012

Organometallic chemistry in the solid-state

Andrew Weller (University of Oxford)

16th January 2013

The physical chemistry of heterogeneous catalysis

Ken Waugh (University of Manchester)

5th March 2013

A trio of challenges: reactivity, stereocontrol and region-control in asymmetric catalysis

Matt Clarke (University of St Andrews)

26th March 2013

The Durham Lecture 2013

Peter Seeberger (Free University Berlin)

14th May 2013

Designing Heterogeneous catalysts for sustainable chemistry

Karen Wilson (Aston University)

26th November 2013

8.5 Appendix 5: Conferences attended

Northern Sustainable Chemistry (NORSC) 2010

- University of York, 28th October 2010

8th European Workshop on Phosphorus Chemistry

- Poster presented
- Westfälische Wilhelms-Universität Münster, 28-29th March 2011

RSC Main Group Chemistry Interest Group 2011

- Poster presented
- Burlington House, London, 15th July 2011

Northern Sustainable Chemistry (NORSC) 2011

- Poster presented
- University of York, 25th October 2011

9th European Workshop on Phosphorus Chemistry

- Poster presented
- Université de Rennes 1, 22-23rd March 2012

RSC Main Group Chemistry Interest Group 2012

- Poster presented
- Burlington House, London, 21st September 2012

RSC-ACG / SURCAT Dennis Dowden Commemoration: Catalysis - from fundamentals to application

- Durham University, 3-4th April 2013

10th European Workshop on Phosphorus Chemistry

- Oral presentation
- Universität Regensburg, 18-20th March 2013